



Precipitation, runoff and water balance regimes variability along the Peruvian Pacific slope and coast: ENSO influence and sensitivity to hydroclimatic change.

Pedro Rau Lavado

► To cite this version:

Pedro Rau Lavado. Precipitation, runoff and water balance regimes variability along the Peruvian Pacific slope and coast: ENSO influence and sensitivity to hydroclimatic change.. Continental interfaces, environment. Université Toulouse 3 Paul Sabatier (UT3 Paul Sabatier), 2017. English. NNT : . tel-01627597

HAL Id: tel-01627597

<https://theses.hal.science/tel-01627597>

Submitted on 2 Nov 2017

HAL is a multi-disciplinary open access archive for the deposit and dissemination of scientific research documents, whether they are published or not. The documents may come from teaching and research institutions in France or abroad, or from public or private research centers.

L'archive ouverte pluridisciplinaire **HAL**, est destinée au dépôt et à la diffusion de documents scientifiques de niveau recherche, publiés ou non, émanant des établissements d'enseignement et de recherche français ou étrangers, des laboratoires publics ou privés.



THÈSE

En vue de l'obtention du

DOCTORAT DE L'UNIVERSITÉ DE TOULOUSE

Délivré par :

Université Toulouse 3 Paul Sabatier (UT3 Paul Sabatier)

Présentée et soutenue par :

Pedro RAU LAVADO

le jeudi 28 septembre 2017

Titre :

Variabilité du régime des précipitations, des débits et des bilans hydriques le long du Versant Pacifique Péruvien : influence du phénomène ENSO et sensibilité au changement hydroclimatique

École doctorale et discipline ou spécialité :

ED SDU2E : Surfaces et interfaces continentales, Hydrologie

Unité de recherche :

Géosciences Environnement Toulouse (GET) UMR 5563, UPS-CNRS-IRD-OMP-CNES

Directeur/trice(s) de Thèse :

David LABAT – Professeur des universités UPS (GET, Toulouse) – Directeur de thèse

Luc BOURREL – Chargé de recherche IRD (GET, Toulouse) – Co-directeur de thèse

Boris DEWITTE – Directeur de recherche IRD (LEGOS, Toulouse) – Co-directeur de thèse

Jury :

Roger MOUSSA – Directeur de recherche INRA (LISAH, Montpellier)

– Rapporteur / Président du jury

Benjamin POHL – Chargé de recherche CNRS (CRC, Dijon) – Rapporteur

Denis RUELLAND – Ingénieur de recherche CNRS (HSM, Montpellier) – Examineur

Isabelle BRAUD – Directeur de recherche IRSTEA (IRSTEA, Lyon-Villeurbanne) – Examinatrice

*This thesis is dedicated to my mother
For teaching me the endless love of God and His revelation in nature*

ACKNOWLEDGMENTS

All this time, there have been many people and institutions to whom I must thank for the motivation and support towards me, which covered all possible areas in order to start, develop and end this thesis.

First of all, my deepest thanks to my three thesis supervisors: *David Labat*, *Luc Bourrel* and *Boris Dewitte*, with whom it has been a great pleasure to work for almost seven years since an initial subject which introduced me to “El Niño phenomenon” in my master's studies. Thank you for the constant motivation, for having formed me with a scientific spirit in the field of hydroclimatology, for your advices as supervisors and as friends. Also my gratitude to *Denis Ruelland* for his help in the last part of the thesis, with whom I was able to understand a little more about hydrology, that branch of earth sciences and environment that I thought I understood. Special thanks to *Waldo Lavado* for his advice and motivation.

A special recognition to the institutions that made this work possible. This thesis is funded by PRONABEC (National Program of Scholarships from the Ministry of Education of Peru) and has two institutional partners: SENAMHI (National Service of Meteorology and Hydrology of Peru) and IRD (French Institute for Research for Development). This agreement made possible the development of the thesis within the GET laboratory (Géosciences Environnement Toulouse) in association with the LEGOS laboratory (Laboratoire d'Etudes en Géophysique et Océanographie Spatiales) in Toulouse-France and the collaboration with the HSM laboratory (Hydrosciences Montpellier) in Montpellier-France.

This thesis comes to light after 4 years of hard work; however the constancy and overcoming of adversities would not have been possible without the emotional support of very special people: *Guadalupe* (my mother), *Pedro* (my father) and the *Lavado* family, thank you for always motivating me. I also thank the great company of friends and the great moments shared in the GET laboratory and during my stay in France.

My gratitude to all professionals, scientists, engineers and institutions in Peru, who in one way or another became interested in the subject of my research since 2010 and who contributed with their appreciations, recommendations, facilitated its diffusion and offered some funding.

Precipitation, runoff and water balance regimes variability along the Peruvian Pacific slope and coast: ENSO influence and sensitivity to hydroclimatic change.

Abstract

Climate variability and associated extreme events as El Niño phenomenon (ENSO) represent the most difficult episodes to deal with along the Peruvian Pacific slope and coast. In addition, a growing water concern takes place since seventies.

In-depth documentation of precipitation and runoff regimes becomes a key part in any water management plan and this research offers the first hydroclimatic variability study at monthly and annual time step in the study area over the last four decades (1970–2010 period). First, an exhaustive database treatment was carried out overcoming some limitations due to Andean geographical conditions. Second, precipitation regime was studied with a regionalization approach under non-stationary time-series conditions. A combined process consisting in k-means clustering and regional vector methodology was proposed. Nine regions were identified with a homogeneous precipitation regime following a latitudinal and altitudinal gradient. Third, a hydroclimatic balance is done at catchment-scale addressing the issue of climate and anthropogenization and their potential influences over hydroclimatic time series. The theoretical Budyko-Zhang framework was used and allowed identifying 11 out of 26 catchments with both low climate and anthropogenization influence (i.e. unimpaired conditions). This hypothesis was verified with the use of land use and land cover remote sensing products as MODIS and LBA imagery. Then, runoff regime was studied under unimpaired conditions and an extension over 49 catchments of the Peruvian Pacific drainage was done. A regional runoff model is proposed via two conceptual lumped models at annual and monthly time scale (GR1A and GR2M respectively). A Differential Split-Sample Test (DSST) was used to cope with modelling robustness over contrasted climate conditions as dry and wet years according to the semi-arid conditions. These results also showed an increasing regional discharge from arid Peruvian Pacific coast towards the Pacific Ocean.

Finally, the scope of the thesis covers (1) a revisitation of ENSO/precipitation relationship considering the regionalized precipitation and several ENSO indices in order to discriminate the influence of the two types of El Niño (the eastern Pacific (EP) El Niño and the central Pacific (CP) El Niño) as well as the influence of large-scale atmospheric variability associated with the Madden and Julian Oscillation, and of regional oceanic conditions. The proposed methodology consisting in principal component analysis, wavelets and coherence, running correlations and spatial covariance analysis, highlights the significant decadal modulation with the larger ENSO impact in particular in the 2000s, ENSO/precipitation relationship reverses compared to the previous decade. The two dominant co-variability modes between sea surface temperature in the tropical Atlantic and Pacific oceans and the nine regions show salient features of the ENSO influence: increased precipitation over downstream regions in northern Peru during EP El Niño and decreased precipitation over upstream regions along the Pacific slope during CP El Niño events. (2) The sensitivity to hydroclimatic change is explored by hydroclimatic trend analysis as changes indicators of regional hydroclimatology. According to significant upward trends in annual temperature found in all catchments, results showed a significant warming in the study area with a mean of 0.2°C per decade. Also, changes in trajectories in the Budyko space (i.e. direction and magnitude) over the 11 selected catchments revealed that six catchments were shown to be sensitive to climate variability (i.e. likely with high sensitivity to future climate) and land use changes, where precipitation and temperature are the main drivers of these environments changes.

Key words: Peruvian Pacific slope and coast, precipitation, runoff, hydroclimatic balance, ENSO, hydroclimatic change.

Variabilité du régime des précipitations, des débits et des bilans hydriques le long du Versant Pacifique Péruvien : influence du phénomène ENSO et sensibilité au changement hydroclimatique.

Résumé

La variabilité climatique et les événements extrêmes associés comme le phénomène El Niño (ENSO) représentent les épisodes les plus difficiles à gérer dans le Versant Pacifique Péruvien. En outre, une préoccupation croissante sur la disponibilité en eau a lieu depuis les années 1970s.

Une documentation approfondie des régimes de précipitations et des débits est un élément clé de tout plan de gestion de l'eau et notre recherche est la première étude sur la variabilité hydroclimatique à l'échelle mensuelle et annuelle dans la zone d'étude au cours des quatre dernières décennies (période 1970-2010). Tout d'abord, un traitement de base de données exhaustif a été effectué pour surmonter certaines limitations et notamment celles liées aux conditions géographiques des Andes. Deuxièmement, le régime des précipitations a été étudié avec une approche de régionalisation liée aux conditions de séries temporelles non stationnaires. Une méthode mixte associant la méthode des clusters k-means et la méthode du vecteur régional a été proposée. Neuf régions ont été identifiées avec des régimes homogènes de précipitation tenant compte d'un gradient latitudinal et altitudinal. Un bilan hydroclimatique a ensuite été fait à l'échelle de bassin versant, abordant la problématique du climat et de l'anthropisation et leurs influences potentielles sur les séries chronologiques hydroclimatiques. Le cadre théorique de Budyko-Zhang a été utilisé et a permis d'identifier 11 des 26 bassins versants à faible influence climatique et anthropique (i.e. des conditions quasi-naturelles). Le régime des débits a ensuite été étudié pour ces conditions et une extension pour l'ensemble des 49 bassins versants de la zone d'étude a été effectuée. Un modèle hydrologique régional est proposé via deux modèles conceptuels agrégés à l'échelle de temps annuelle et mensuelle (GR1A et GR2M respectivement). Un test d'échantillonnage différentiel (DSST) a été utilisé pour améliorer la robustesse de la modélisation par rapport aux conditions climatiques contrastées entre années sèches et humides dans les conditions semi-arides.

Enfin, la portée de la thèse couvre (1) une revisite de la relation ENSO/précipitation en prenant en compte les neuf régions identifiées et de plusieurs indices ENSO afin de discriminer l'influence des deux types d'El Niño (El Niño du Pacifique Est EP et du Pacifique Central CP) ainsi que l'influence de la variabilité atmosphérique (i.e. l'oscillation Madden et Julian) et aux conditions océaniques régionales. La méthodologie proposée consiste en l'analyse des composantes principales, ondelettes et de cohérence, les corrélations glissantes et l'analyse de la covariance spatiale afin de mettre en évidence la modulation décennale significative du phénomène ENSO ainsi que sa croissance à partir des années 2000s où la relation ENSO/précipitations s'inverse par rapport à la décennie précédente. Les deux modes de co-variabilité dominants entre la température superficielle de la mer dans le Pacifique tropical et les neuf régions montrent des caractéristiques dominantes de l'influence de l'ENSO: une augmentation des précipitations sur les régions aval dans le nord pendant El Niño EP et une diminution des précipitations sur les régions amont le long des Andes lors des événements El Niño CP. (2) La sensibilité au changement hydroclimatique est explorée via l'analyse des tendances hydroclimatiques comme indicateurs de changement de l'hydroclimatologie régionale. Les résultats montrent un réchauffement important dans la zone d'étude avec une moyenne de 0,2°C par décennie. En outre, les changements dans les trajectoires dans l'espace de Budyko (i.e. direction et amplitude) ont révélé que six bassins versants étaient sensibles à la variabilité du climat (i.e. probablement avec une grande sensibilité au climat futur) et aux changements d'utilisation du sol et où les précipitations et la température sont les facteurs prépondérants du changement de ces environnements.

Mots clés : Versant Pacifique Péruvien, précipitations, débits, bilan hydrique, ENSO, changement hydroclimatique.

Table of contents

Chapter 1

Introduction	17
1.1. General context	17
1.2. Motivation	20
1.3. Main and specific objectives	23
1.4. Organization	24
Introduction (version française)	27

Chapter 2

Study area and data	37
2.1. Hydroclimatic context of the Peruvian Pacific drainage	37
2.1.1. Climate variability	37
a. Mean climatic conditions in the South East Pacific	37
b. Modes of variability	38
El Niño phenomenon (ENSO) and its diversity	38
Decadal variability	41
Intraseasonal variability (MJO and oceanic Kelvin waves)	41
2.1.2. Physical landscape	42
a. Topography	42
b. Geology	43
c. Vegetation	43
2.1.3. Hydrological context	46
a. Arid and semi-arid conditions	46
b. Anthropogenization	48
2.2. Data	50
2.2.1. Precipitation	50
2.2.2. Temperature and evapotranspiration	51
2.2.3. Streamflow	52
2.2.4. Climatic indices	54
a. ENSO indices	54
b. MJO index and Kelvin waves	54

Chapter 3

Precipitation regime	57
3.1. Theoretical background	57
3.2. Methods	58
3.2.1. Data homogenization and validation	59
3.2.2. Classification and Regionalization Process	60
a. K-means clustering technique	60
b. Regionalization Analysis	61

c. Precipitation data interpolation	62
3.3. Results and discussion	62
3.3.1. Precipitation Classification	62
3.3.2. Regionalization	64
3.3.3. Regions Characterization	70
3.4. Conclusions	74
Chapter 4	
Hydroclimatic balance	77
4.1. Theoretical background	77
4.2. Methods	78
4.2.1. Catchment water balance disparity	78
4.3. Results and discussion	79
4.3.1. Hydroclimatic time series	79
4.3.2. Catchment water balance disparity	83
4.4. Conclusions	88
Chapter 5	
Runoff regime	89
5.1. Theoretical background	89
5.1.1. Hydrological lumped conceptual modelling	90
5.1.2. Regional runoff	90
5.2. Methods	91
5.2.1. Runoff simulation based on conceptual lumped models	91
5.2.2. Performance and efficiency of conceptual lumped models	92
5.2.3. Regional runoff model (RRM) and freshwater estimates	93
5.3. Results and discussion	94
5.3.1. Efficiency of the GR1A and GR2M models	94
5.3.2. Regional runoff model evaluation	98
5.3.3. Freshwater runoff estimation	102
5.4. Conclusions	105
Chapter 6	
Impacts of climate variability and hydroclimatic change on precipitation and runoff	107
6.1. Precipitation and runoff variability associated with ENSO	108
6.1.1. Theoretical background	108
6.1.2. Methods	109
a. Principal Component Analysis (PCA)	109
b. The wavelets and coherence analysis	109
c. Correlation analysis	111
d. Covariance analysis	111
6.1.3. Results and discussion	111
a. PCA analysis of ENSO indices	111

b. Coherence between ENSO indices and precipitation series	112
c. Low frequency modulation of ENSO and precipitation regime	115
d. Precipitation variability and sea surface temperature anomalies	120
e. Low frequency modulation of ENSO and runoff regime	123
6.1.4. Conclusions	125
6.2. Trends and hydroclimatic change disparity over catchments	127
6.2.1. Theoretical background	127
6.2.2. Methods	127
a. Characterization of hydroclimatic time series	127
b. Hydroclimatic change disparity	128
6.2.3. Results and discussion	129
a. Characterization of hydroclimatic time series	130
b. Hydroclimatic change disparity	131
6.2.4. Conclusions	134
Chapter 7	
General conclusions and perspectives	137
7.1. Conclusions	137
7.2. Perspectives	141
7.2.1. Impact of climate variability over seasonal hydrological regime as a forecasting tool	141
7.2.2. Impact of climate and catchment change over the hydrological regimes ...	142
Conclusions générales et perspectives (version française)	143
References	151
Annex A	
List of scientific articles made throughout the thesis	165
Annex B	
List of scientific collaborations, communications and vulgarizations made throughout the thesis	166
Annex A.1	167
Annex A.2.....	185
Annex A.3.....	203
Annex A.4.....	251

List of tables

Chapter 2

Table 2.1. General characteristics of the 7 selected studied catchments at their outlets gauging stations for the indicated period (Min Alt: Minimum altitude; Max Alt: Maximum altitude; A: drainage area; L: main channel length; p: perimeter; S: mean slope; P: Mean annual precipitation; PET: Mean annual evapotranspiration; R: Mean annual runoff)	48
Table 2.2. General characteristics of the 26 studied catchments at their outlets gauging stations for the 1970-2008 period (Lat: latitude; Long: longitude; A: drainage area; Min Alt: minimum altitude; Max Alt: maximum altitude S: mean slope; Mean annual values of Q: streamflow; Qsp: specific runoff)	52
Table 2.3. Description of ENSO indices used in the study	56

Chapter 3

Table 3.1. Results of the k-means analysis for number of clusters varying from 3 to 10	63
Table 3.2. Geographical features and annual precipitation values for the nine identified regions	74

Chapter 4

Table 4.1. Hydroclimatic conditions over the 1970-2008 period and 2008 land cover types in the 26 studied catchments. Mean annual values of precipitation (P), temperature (T), potential evapotranspiration (PET), actual evapotranspiration (AET), runoff (R) and aridity index (P/PET). Land cover percentage from MODIS (2008) of Open schrubland (OS), Grasslands (GL), Croplands (CL) and Bare ground (BG)	81
Table 4.2. Budyko-Zhang curve adjustment values. w: Budyko-Zhang coefficient; r: correlation coefficient between AET estimated by Budyko-Zhang and water balance; RSE: relative standard error from the curve adjustment. Catchments with low disparity in water balance are shaded in grey rows	86

Chapter 5

Table 5.1. GR1A performance and mean annual runoff values for dry (DY) and wet (WY) years following the DSST scheme $DY \leftrightarrow WY$. Observed runoff at gauging station (Robs); Simulated runoff (Rsim). Satisfactory results are shaded in grey rows	95
Table 5.2. GR2M parameters set and efficiencies over dry (DY) and wet (WY) years following the DSST scheme $DY \leftrightarrow WY$. Satisfactory results are shaded	97

in grey rows	
Table 5.3. Mean monthly values of S' and R' reservoirs for dry (DY) and wet (WY) years following the DSST scheme DY↔WY. Valid results are shaded in grey rows according to Table 5.2	97
Table 5.4. Mean values of regional discharge (SD: Standard deviation)	105
 Chapter 6	
Table 6.1. Summary of maximal coherences for each region (in all cases, coherences correspond to quasi-decadal frequency)	115
Table 6.2. Mean annual change (Δ) in precipitation (P), temperature (T), potential evapotranspiration (PET), actual evapotranspiration (AET) and runoff (R). Values with significant trends at 95% of confidence level are shown in bold. Years of significant change-point at 95% of confidence level are indicated between parentheses. Catchments with low disparity in water balance are shaded in grey rows	130
Table 6.3. Budyko trajectories defined by direction (α) and magnitude (β) values across the selected catchments. Catchments with major sensitivity to climate variability and land use changes are shaded in grey rows. Errors expressed in (%) were obtained via a 10-year moving window	133

List of figures

Chapter 1

Figure 1.1. Main hydrographic system of the Peruvian Pacific drainage. Andes mountain elevation and rivers flowing into the Pacific Ocean	18
--	----

Chapter 2

Figure 2.1. Idealized schematic diagram reflecting the ENSO Phenomenon. Normal non-ENSO conditions are shown above, while the climax of an ENSO event is pictured below. In either cases both the slope of the sea level as well as the thermocline change considerably. Source: Madl (2000)	40
Figure 2.2. Anomalies of climatologic SST (1900–2009) of the Eastern Pacific El Niño (EP El Niño or classical ENSO, shown above) and Central Pacific El Niño (CP El Niño or ENSO Modoki, shown below) for the HadISST data (Rayner et al., 2003). Source: Gutierrez et al. (2011)	40
Figure 2.3. Physical landscape of the Peruvian Pacific drainage. a) Topography map from SRTM digital elevation model. b) Geological framework (Gilboa, 1971) and the 7 selected studied catchments location. c) Vegetation map from land cover MODIS types and the 26 studied catchment location	45
Figure 2.4. Mean seasonal lumped runoff, precipitation and evapotranspiration (left) and precipitation-runoff anticlockwise hysteresis plot in a bi-logarithmic scale of monthly data (right). Colour classification is scaled for a hydrological year (September - August)	47
Figure 2.5. Location of major cities and main large hydraulic infrastructures (names of hydraulic systems in italic blue) built between 1970 and 2008	49
Figure 2.6. Spatial distribution of hydrometeorological stations over a SRTM digital elevation model	53

Chapter 3

Figure 3.1. Schematic of the methodological steps for the regionalization of the precipitation time series	59
Figure 3.2. Clusters spatial distribution (a) cluster 3 group and (b) cluster 6 group obtained with the k-means process. Silhouette value for each cluster group is provided in the bottom panels	64
Figure 3.3. Spatial distribution and range of coefficient of variation (CV) for all of the pluviometric stations of the Pd	66
Figure 3.4. The nine homogeneous precipitation regions after the regionalization process of clustering and RVM. Interpolated surface of annual precipitation (isohyets obtained using co-kriging method) is also shown to demonstrate precipitation differences between regions	67

Figure 3.5. Relationship between mean interannual precipitation and latitude for the nine identified regions grouped in upstream and downstream regions. Representation for upstream regions is significant at the 90% level using a Student t-test	68
Figure 3.6. Coefficient of correlation related to the regional vector recalculated for each final region. A global value of correlation is also showed by region in bold as well as spatial distribution of correlation with the regional vector	69
Figure 3.7. Monthly precipitation regime (1964-2011) for the nine identified regions. A precipitation time series is shown by region. Regions 4 and 7 are shown in a different precipitation scale	73
Figure 3.8. Boxplot of monthly precipitation for the nine identified regions	74

Chapter 4

Figure 4.1. Long term variations of annual mean time series of precipitation (P), potential evapotranspiration (PET) and runoff (R) for eleven selected catchments over the 1970-2008 period	82
Figure 4.2. Comparison of two catchments with low (Piura up n°1) and high (Rimac n°15) water balance disparity according to the Budyko-Zhang framework. (a) and (c) black lines represent the energy limit (diagonal) and the water limit (horizontal). (b) and (d) scatter plot for correlation of annual AET obtained from water balance equation 4.1 and AET estimated by using equation 4.2	84
Figure 4.3. Budyko space over the 1970-2008 period over the 26 studied catchments. The black lines represent the energy limit (horizontal) and the water limit (diagonal). Black (Grey) points represent the association of yearly values from catchments showing a low (high) water balance disparity via the Budyko-Zhang framework. Red dashed curves represent the theoretical adjustment range for “w” parameter (“ $w_{min} = 0.1$ ”; “ $w_{max} = 2$ ”)	85
Figure 4.4. Evolution of land cover (%) with LBA and MODIS products over catchments grouped by (a) Low and high water balance disparity. (b) Latitudinal gradient: northern catchments (n°1 to n°6), central catchments (n°7 to n°18) and southern catchments (n°19 to n°26)	87

Chapter 5

Figure 5.1. Scheme of the GR2M model with the parameters $X1$ and $X2$ (modified from Mouelhi et al., 2006a)	92
Figure 5.2. Evaluation of the performance of GR2M model (catchments in numbers) via parameter transposability (DSST). (a) NSE for the calibration over dry (DY) years. (b) Idem for the bias. (c) NSE for the validation over wet (WY) years. (d) Idem for the bias. (e) GR2M parameters values ($X1$ and $X2$) within the calibration envelope over DY and WY	96

Figure 5.3. Linear associations between physical catchments characteristics (A: Area, L: Main channel length, p: Perimeter) using a natural bi-logarithmic scale (a) for the <i>X1</i> parameter; (b) for the <i>X2</i> parameter	99
Figure 5.4. Performance of the Regional Runoff Model (catchments in numbers) via parameter transposability (DSST). (a) NSE for the calibration over dry years (DY). (b) Idem for the bias. (c) NSE for the validation over wet years (WY). (d) Idem for the bias	99
Figure 5.5. Mean seasonal runoff (observed, uncertainty by DSST, simulated by the regional runoff model) and precipitation over dry (DY) and wet (WY) years for each catchment. Calibration over DY and validation over WY considering a hydrological year (September to August)	101
Figure 5.6. Runoff simulations along dry (DY) and wet (WY) years. Observed and simulated monthly runoff by GR2M and the regional runoff model. Runoff uncertainty via DSST	102
Figure 5.7. Spatial distribution of ungauged freshwater runoff (1970–2010) estimated by the RRM over 49 main catchments of the Pd: (a) Mean annual specific runoff by catchment. (b) to (f) Annual time series grouped in function of the regime characteristics. (g) Total annual discharge reaching 709 m ³ /s ...	104
 Chapter 6	
Figure 6.1. Projection of ENSO indices into a Principal Component Analysis (PCA). Note that the E and C indices are by construction orthogonal based on the monthly averaged data. For the PCA, averaged data from September to February were used	112
Figure 6.2. (a) Wavelet of R1 precipitation; (b) Wavelet of R1 precipitation not considering strong El Niño events; (c) Wavelet of R6 precipitation; (d) Wavelet of E index; (e) Wavelet coherence between E index and R1 precipitation; (f) Mean coherence peaks for wavelet coherence between E index and R1	114
Figure 6.3. Correlation coefficients between precipitation and ENSO indices for 4 periods: 1964-1976, 1977-1999, 1977-1999 without ENSO (not considering strong El Niño events of 1982/1983 and 1997/1998) and 2000-2011. For Akm1 and Akm2 the last period correspond to 2000-2007 (a) For E index; (b) For C index; (c) For MJO index; (d) For Akm1 index and (e) For Akm2 index. Maximal significance of 95% obtained for the shorter periods 2000-2011 and 2000-2007	117

Figure 6.4. 11-year running correlation coefficients between precipitation and (a) the E index and within each region (R1 to R9) not considering the ENSO strong events of 1982/1983 and 1997/1998. The plot on the right hand side displays the slope of the linear trend of the running correlation (red dots indicates that the trend is significant at the 90% level using a t-student test). The white dashed lines indicate the significance level of the correlation at the 90% level; (b) <i>Idem</i> for E index but considering the ENSO strong events of 1982/1983 and 1997/1998; (c) <i>Idem</i> for C index not considering the ENSO strong events of 1982/1983 and 1997/1998	119
Figure 6.5. 11-year running correlation coefficients between precipitation and (a) Akml index within each region (R1 to R9) not considering the ENSO strong events of 1982/1983 and 1997/1998. The plot on the right hand side displays the slope of the linear trend of the running correlation (red dots indicates that the trend is significant at the 90% level using a t-student test). The white dashed lines indicate the significance level of the correlation at the 90% level. (b) <i>Idem</i> for MJO index	120
Figure 6.6. Dominant SVD mode between precipitation in DJFMA over the 9 regions and SST anomalies in DJF over the tropical Pacific and Atlantic: a) Mode pattern for precipitation; b) Mode pattern for SST (contour interval is every 0.2°C); c) Associated SVD time series for precipitation (red colour) and SST (blue colour). The percentage of variance of the modes is indicated in panels a) and b), whereas the percentage of covariance (covar) is indicated in panel c). The correlation (r) between the SVD time series is also indicated in panel c). The contour in thick black line in panel b) indicates the zero-contour. The shading (red) colour in panel b) (a) respectively, indicates where the mode pattern is statistically significant at the 90% level	122
Figure 6.7. Same as Figure 6.6, but for the second SVD mode	122
Figure 6.8. 11-year running correlation coefficients between unimpaired runoff and E index within each catchment (1 to 49) considering the ENSO strong events of 1982/1983 and 1997/1998. The plot on the right hand side displays the slope of the linear trend of the running correlation (red dots indicates that the trend is significant at the 90% level using a t-student test). The white dashed lines indicate the significance level of the correlation at the 90% level.	123
Figure 6.9. <i>Idem</i> as previous Figure 6.8 but not considering the ENSO strong events of 1982/1983 and 1997/1998	124
Figure 6.10. <i>Idem</i> as previous Figure 6.8 but for C index and not considering the ENSO strong events of 1982/1983 and 1997/1998	125
Figure 6.11. Grouping of Budyko trajectories defined by their direction (a) and the magnitude (b) of change for the 11 selected catchments in the Budyko space over the 1970-2008 period	132

Figure 6.12. Budyko trajectories defined by their direction (a) and magnitude (b) plotted across catchments. Red/orange, yellow and green arrows in Figure 6.12a show the three regions grouped by their hydroclimatic change adaptation. Purple and red points in Figure 6.12b show the catchments with major sensitivity to climate variability and land use changes 134

Chapter 1

Introduction

1.1. General context

The Peruvian Pacific slope and coast (see location map in Figure 1.1) covers nearly 25% of the South American Pacific drainage surface and presents strong climate variability as extreme opposite climate events like floods and droughts mainly caused by El Niño phenomenon (ENSO) (Tapley and Waylen, 1990; Lagos et al., 2008). Climate and topographic features over this very narrow area define one of the driest places in the earth as the Peruvian desert (Nicholson, 2011) located in lowlands of this arid and semi-arid region.

A growing water concern has taken place in this region since the seventies. On the one hand this region presents a very high population density (50% of Peruvian total population) being the most important economical region of Peru and on the other hand this region is characterized by a very low freshwater availability (2% of Peruvian national total) (ANA, 2012). This means a challenge for any water management plan, which should be based on an in-depth analysis of hydroclimatic processes. This analysis has not yet been satisfied from a scientific approach, mainly in both subjects of climate variability and surface water availability.

Climate variability and precipitation

Climate variability and associated extreme events as ENSO represent the most difficult episodes to deal with for an emerging Peruvian economy. Their impacts and economical losses continue to be repeated since ancient times. Not surprisingly, the first documentations in the Peruvian Pacific drainage revealed to the world the Spanish name of “El Niño” (or “Christ child”) as a warming oceanic counter current in the northern area which started to manifest at “Christmas” time causing strong precipitation and floods (Carranza, 1892; Pezet, 1896). Until now, the societal consequences of these events have highlighted the strong vulnerability of this region. For instance, the last strong ENSO event of 1997/1998 induced a 12% significant reduction of the gross domestic product (GDP) of Peru (OPS, 2000). Difficulties in understanding ENSO impacts in Peru are related to the fact that it is a non-stationary phenomenon (Boucharel *et al.*, 2009) with a significant modulation of its characteristics (amplitude, frequency, asymmetry) at decadal timescales (Torrence and Compo, 1998; Guilderson and Schrag, 1998). Some impact studies focused on precipitation offer an overview about the evolution of ENSO/precipitation relationship (Tapley and

Waylen, 1990; Lagos et al, 2008; Lavado and Espinoza, 2014) whereas others studies focused on the ocean-atmosphere-continent physical processes (Takahashi, 2004).

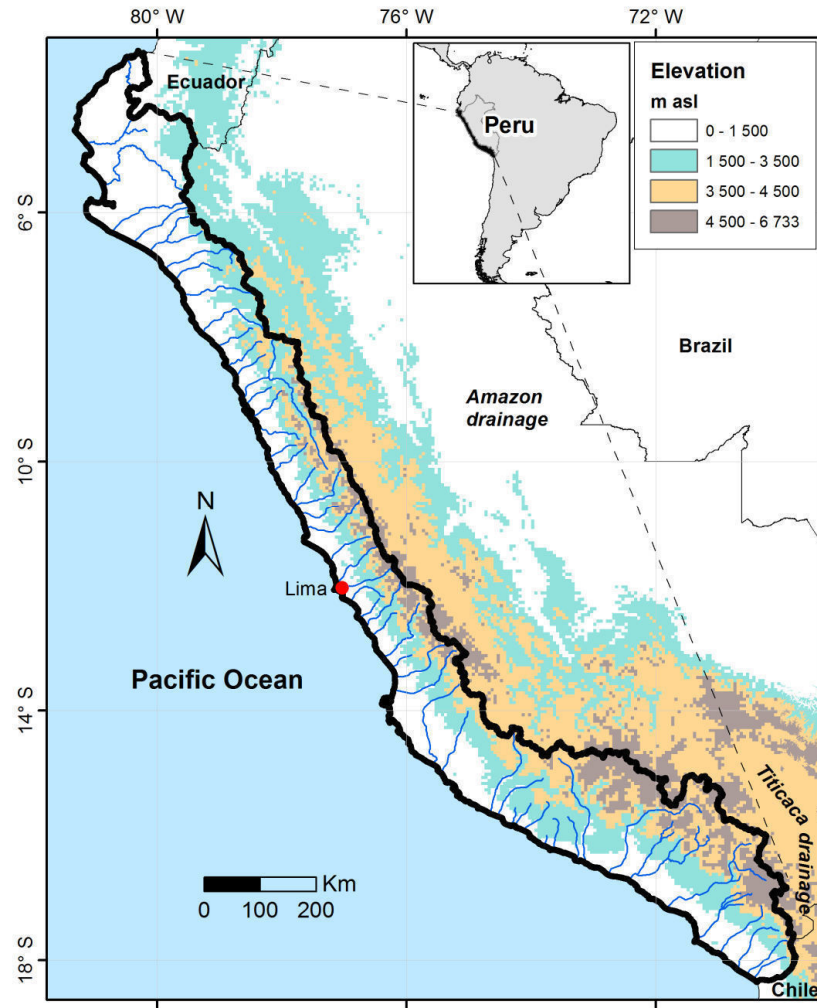


Figure 1.1. Main hydrographic system of the Peruvian Pacific slope and coast.

Two types of El Niño events have been documented to date: El Niño of the Eastern Pacific, corresponding to warm sea surface temperature (SST) anomalies in the eastern equatorial Pacific (EP El Niño) and El Niño of the Central Pacific (or Niño Modoki) corresponding to warm SST anomalies in the central equatorial Pacific (CP El Niño, as the variability of moderate events or La Niña) (see Ashok et al. 2007, Takahashi et al., 2011).

In addition, there has been a climate shift in the 1970s from when EP El Niño events became stronger (Miller *et al.*, 1994). The 1980s and 1990s are in fact the decades over which the relationship between ENSO and hydrology (precipitations and discharges) in Peru (Lagos *et al.*, 2008; Lavado *et al.*, 2013) is the most significant due to the strong signature on the regional circulation of the two extremes events of 1982/83 and 1997/98. Also, over the last two decades, the CP El Niño appears to be more frequent relatively to the EP El Niño (Yeh *et al.*, 2009; Lee and McPhaden, 2010; Takahashi *et al.*, 2011).

Such change in the ENSO characteristics modify features of the equatorial oceanic and atmospheric circulation in the Pacific, that is the oceanic equatorial Kelvin waves (Dewitte et al., 2012) and the intraseasonal atmospheric variability (Gushchina and Dewitte, 2012) including the Madden and Julian Oscillation (MJO) (Madden and Julian, 1972). All these aspects of the change in ENSO properties have been somewhat overlooked in studies addressing the impact of ENSO on the precipitations along the Peruvian Pacific slope and coast, although they can provide guidance for refining current forecasting strategies aimed at improving resource management (agriculture, water resources). Therefore, ENSO impact on precipitation regime at a regional scale clearly needs to be revisited in light of the recent studies pointing out a so called ENSO diversity. It becomes essential to update and obtain high quality information about precipitation regime over the last four decades from 1970 up to 2010 and in particular to address the potential non-linearity behaviour of the time series.

Surface freshwater, climate and human activities

As a response of water scarcity, there exists a strong human activity along the 54 main catchments of the Peruvian Pacific drainage to supply water to the main cities and their economic activities. For instance the catchment where is located the Peruvian capital city of Lima with nearby 10 millions of inhabitants (called Rimac catchment) is considered into an absolute water shortage per capita scenario with less than 500 m³/year and the whole Peruvian Pacific drainage is considered into a water stress per capita scenario with less than 1700 m³/year (ANA, 2012; White, 2012; MINAM, 2016). Detailed regulated river system of Rimac catchment and its evolution since 1920s can be found in Vega et al. (2017). However the 53 remaining catchments along the study area have still not been deeply studied with regards to water availability.

Quantifying and deciphering the effects of climate variability and human activities on hydrological regime represent a major challenge, especially at short scales in time and space (Donohue et al. 2007; Wagener et al. 2010). The degree of anthropogenic influence can be determined using two types of influence on runoff changes: human activity with direct influence (soil conservation, water control works, increasing water demand) and human activity with indirect influence (land use and land cover (LULC) changes) (Wang et al. 2013). They constitute descriptive elements to understand the behaviour of hydroclimatic data series and to identify the catchments presenting a low level of anthropogenization. Therefore, we emphasize the need to obtain high quality information about the hydroclimatological regime to address the issue of anthropogenization and climate variability influence and their susceptible interference over runoff time series.

Despite the social and economical importance of the region, there is not yet dedicated scientific works that address the influence of hydroclimatic change over freshwater availability. This calls for understanding the variability of precipitation and its relation to natural climatic variability (ENSO and decadal variability) as a prerequisite for carrying out water resources studies. It can only be mentioned the monographic works of de Reparaz (2013) which covers the 1920–1960 period and a general documentation about runoff regime

until 2011 made by Lavado et al (2012). This context also calls for formulating several assumptions and methodologies which are developed in the next sections.

1.2. Motivation

Validation of a hydroclimatological in-situ database

Peruvian economic and social context in development does not offer yet the conditions to have a high quality hydroclimatological in-situ database. Such a database is however essential to understand both regionalizations of climate variability and hydroclimatic changes, which are the two main topics covered in this thesis. As a result, there is a need for collecting and deeply analysing the main hydro-climatic in-situ observations (precipitation, temperature, evapotranspiration and streamflow) over a multi-decadal period. Homogenization and validation processes should take into account climate variability conditions reflected on time series with high peaks and low values. In these conditions, it becomes necessary to define a procedure for dealing with missing data and doing a selection of appropriate stations. From a hydrological perspective the analysis of streamflow time series is a very interesting case for poor gauged and ungauged conditions over the numerous small catchments along the study area with a significant degree of anthropogenization, which is not well known until now.

Despite these limitations, several methodologies throughout the thesis are proposed to deal with the representativeness of in-situ stations without using non in-situ measurements or products (e.g. remote sensing and climate reanalysis). At catchment scale it becomes mandatory to make a correction by elevation gradients of interannual precipitation and temperature variables (e.g. Valéry et al., 2010; Ruelland et al., 2014; Hublart et al., 2015) because of high Andean mean slopes. Also the streamflow time series at hydrological stations, which represent the discharges outputs of lumped catchments, need to be differentiated into those catchments with strong climatic and anthropogenic influence that disturb a natural streamflow signal and those with quasi-natural conditions. For this purpose, we propose the use of a Budyko framework (Budyko et al., 1958; 1974) which is resumed in the paragraphs below.

The scope of the thesis covers the analysis of the influence of climate variability and hydroclimatic change over precipitation and runoff regime with a regionalization approach; however it would not be possible to reach without all the previous steps described above, mainly with the database treatment in view of providing high quality hydroclimatic time series.

Precipitation regime variability

At regional scale, documenting precipitation regime can be reached by an approach of regionalization. The goal is to achieve a regionalized precipitation product in order to reveal how precipitation is distributed or grouped into significant homogeneous regions. Each region

could be represented by a precipitation time-series ready to use for a climate variability analysis. We highlight the advantage of using a cluster analysis in the regionalization procedure of the precipitations which time series are non-stationary and/or non-Gaussian due to the complex of influence of climate phenomena (Takahashi and Dewitte, 2015). For instance, the ENSO has a strong positive asymmetry resulting from the fact that strong extreme events are warm events (An and Jin, 2004; Boucharel *et al.*, 2011), resulting in a non-Gaussian distribution of most historical indices (Boucharel *et al.*, 2009). Such non-linearity in the large scale circulation over the tropical Pacific is likely to influence the precipitation over the Peruvian Pacific slope and coast, which calls for refining regionalization procedures just based on linear techniques.

Climate and human activities influences on water balance

At catchment scale, the previous application of an elevation gradient correction in the spatialization of climate variables made it possible to work properly in a lumped way, thus offering realistic information for analyzing water balance under semi-arid conditions. The proposed water balance brings up for the first time evapotranspiration estimations over the Peruvian Pacific drainage catchments. A detailed analysis about catchments with low and high water balance disparity via the Budyko framework is provided. This method relates the interannual evaporative index (ratio between actual evapotranspiration and precipitation) with the interannual dryness index (ratio between potential evapotranspiration and precipitation) in a global description called the “Budyko space”. Thereby, all interactions through the hydrological cycle between vegetation, soil and atmosphere create an empirical equilibrium represented by the Budyko curve (van der Velde *et al.* 2013). To emphasize the impact of other factors on the water balance such as vegetation, an emerging general relationship proposed by Zhang (Zhang *et al.* 2001) known as the Budyko-Zhang framework is used. This equilibrium is related to catchments with natural conditions, low anthropogenization and low climate variability conditions especially droughts (Wang *et al.*, 2011; Jones *et al.*, 2012; Coron *et al.*, 2015). Additionally, we attempted to establish a relationship between the water balance disparity degree and dynamics in land use and land cover as a comparison source.

Runoff regime variability

The numerous small catchments can be reduced into a set of selected catchments with quasi-natural conditions or with low anthropogenization at annual scale via the Budyko framework, offering high quality time-series for its use in a regional approach, in climate variability and hydroclimatic change analysis. Also at catchment scale, we propose to study hydrological semi-arid conditions through hydrological modelling as a mean to simulate the runoff regime over quasi-natural selected catchments.

Runoff estimates take into account historical observations of streamflow, which reflect the changes in environmental conditions such as climate and land use. Conceptual modelling is regularly criticized for oversimplifying the physics of catchments and leading to unreliable simulations when conditions shift beyond the range of prior experience (Hublart *et al.*, 2015). The usual sources of uncertainty in hydrological modelling under stationary conditions

(concerning the climate and the physical characteristics of the catchment) are linked to the structure of the model, the calibration procedures and erroneous data used for calibration and validation (e.g. Liu and Gupta, 2007; Brigode et al., 2013). Under non-stationary conditions, such as climate variability or change, an additional source of uncertainty arises from parameters instability due to possible changes in the physical characteristics of the catchment and in the main processes at play (e.g. Coron et al., 2012; Thompson et al., 2013; Dakhlaoui et al., 2017). For this reason, it appears necessary to evaluate the modelling robustness and notably the transferability of the calibrated parameters to contrasted climate and/or anthropogenic conditions. We propose the use of the Differential Split-Sample Test (DSST; Klemeš, 1986). For instance, Thirel et al. (2015) suggested a calibration and evaluation protocol for dealing with changing catchments, highlighting the advantages of the DSST.

About regional approach, one of the major obstacles in estimating regional and continental freshwater runoff is the lack of gauging records. Some methods have been applied to account for the contribution from poorly gauged regions in estimating long-term mean discharge as a simple sum of available streamflow records. However, those methods would contain discontinuities, which are a major issue in long term climate data analyses (Milliman and Farnsworth, 2011).

Moreover, there is a need to account for the numerous non-gauged catchments in the study area. For this purpose, a regional runoff model was proposed, built from the GR1A and GR2M conceptual model (Mouelhi et al., 2006a; 2006b) to simulate natural runoff over ungauged and poorly gauged catchments at outlet points towards the Pacific Ocean. This will offer an updated result about river discharges from arid Peruvian coast as a regional approach over the last four decades.

Influence of climate variability over precipitation and hydroclimatic sensitivity at regional and catchment scale

As already mentioned, the influence of climate variability (i.e. ENSO and also intraseasonal modes of variability as MJO and Kelvin waves) over precipitation need to be revisited. We first propose to use the regionalized precipitation product and apply the methodology proposed in Bourrel et al. (2015). That study was focused in the northern to central part of the study area and used a variety of ENSO indices categorized as classical, atmospheric, oceanic and the new ENSO variations (e.g. El Niño Modoki). This allowed interpreting this complex climate phenomenon and its relationship with precipitation.

In that sense our contribution extends the ones by Lagos *et al.* (2008) and Lavado and Espinoza (2014). Due to the interplay between large scale and regional oceanic conditions, such relationship is thought to result from the non-linear interaction between local and remote influences, which a study based on a diversity of indices, may help to disentangle. Former studies focused on extreme El Niño events that caused large economic losses for Peru but little has been said on moderate events. In a context of climate change, there is also a clear need to better understand the natural low-frequency of the teleconnection patterns. Here we take advantage of a long-term data record and a revisited interpretation of the ENSO variability over the last four decades, where ENSO is viewed as two distinct and independent regimes, one associated with extreme events, that is the case of the 1982/83 and 1997/98

strong El Niño events, and the other one associated with moderate warm event and La Niña events (Takahashi *et al.*, 2011). In addition we explore for the first time the ENSO/runoff relationship with the use of the quasi-natural time series found along the Peruvian Pacific drainage.

About the influence of hydroclimatic change, there is a dramatic lack of studies and outdated information about hydroclimatological trends in the last decades related to precipitation, streamflow and mainly with evapotranspiration. We propose the first complete hydroclimatological trend analysis at catchment scale. Until now only is known a regional warming trend scenario found in Vuille *et al.* (2015) over the Peruvian Andes. Hydroclimatic variables trends are considered as changes indicators of regional hydroclimatology over the last four decades and we propose to study them into the Budyko framework following the methodology proposed in van der Velde *et al.* (2013). This methodology can highlight catchment sensitivity in terms of Budyko trajectories (i.e. direction and magnitude) with respect to climate change (e.g. future conditions mainly) and catchment change (e.g. land use mainly). Regions consisting of several catchments following the same change trajectory, present a common water balance adaptation to regional climatic and/or anthropogenic forcings (van der Velde *et al.* (2013).

Overall, the present thesis outlines the Peruvian Pacific slope and coast hydroclimatology over the last four decades, being the main motivation to deal with the limitations and needs explained and being possible to do a study with scientific approach, which will be of great relevance for water resources planning.

1.3. Main and specific objectives

Given the high vulnerability of this region in terms of climate variability and water availability (MINAM, 2016), the main objective is to improve our understanding of the relationship between precipitation and variability (and extreme events) and the Tropical Pacific variability at interannual and decadal timescales taking into account recent progresses in ENSO (e.g. its diversity). The thesis aims also at addressing the influence of hydroclimatic change over precipitation, evapotranspiration, water balance and runoff regime, covering the issue of anthropogenization of the Peruvian Pacific drainage and its large number of catchments.

The specific objectives are presented as five questions as follows:

1) What is the spatio-temporal variability of interannual precipitation?

A regionalization approach is proposed to characterize the interannual variability of precipitation along the Peruvian Pacific slope and coast.

2) How to address the issue of climate variability and anthropogenization as well as their potential interferences over hydroclimatic time series?

Hydroclimatic annual cycles at catchment scale are explored through water and energy balances. Catchments with quasi-natural conditions are identified.

3) What is the spatio-temporal variability of unimpaired interannual runoff? Hydrological modelling is used to generate and characterize quasi-natural or unimpaired runoff interannual variability along Peruvian Pacific drainage.

4) What is the influence of climate variability as El Niño phenomenon and intra-seasonal variability over precipitation and runoff modulation?

The computation and analysis of various climate indices are used to study the relationship between ENSO and precipitation and runoff during the last four decades.

5) What is the influence of hydroclimatic change on the precipitation and runoff regimes?

Hydroclimatic trends are explored as the basis of hydroclimatic changes. Sensitivity of catchments to those changes is analyzed.

1.4. Organization

The thesis is organized as follows:

After an introductory chapter (Chapter 1), Chapter 2 presents a complete description of the study area and data used along the research, mainly related to the hydroclimatic context of the Peruvian Pacific drainage. It covers ocean-atmospheric conditions as mean climatic conditions and modes of variability as the El Niño phenomenon, decadal and intraseasonal variability. Then, we describe the physical landscape (i.e. topography, geology and vegetation) and the hydrological characteristics with a focus on arid conditions and anthropogenization degree. About database, a complete description of hydroclimatological in-situ datasets is done. Then proposed methodologies for dealing with database limitations is described which includes validation and homogenisation processes.

Chapter 3 describes precipitation regime from a statistical perspective along the entire study area. For that purpose, a methodology for its regionalization under non-stationary time-series condition is proposed. This methodology consists of a combined approach of clustering and regional vector methods. We present a regionalized precipitation product consisting in nine homogenous regions.

Chapter 4 reports the hydroclimatological regimes at lumped catchment scale, thus distinguishing between catchments with low and high water balance disparity. This distinction is based on the Budyko framework, which allows identifying a catchment set with quasi-

natural conditions related to low climate and anthropogenization influence and its relationship with land use and land cover over the last four decades.

Chapter 5 describes the quasi-natural or unimpaired runoff regime of selected catchments with a regional extension over poorly gauged and ungauged catchments through a hydrological modelling framework. This analysis also offers an updated estimate of river discharge to coastal Pacific Ocean.

Finally, after obtaining a consistent understanding of precipitation and runoff regimes with a homogenized and validated database, Chapter 6 introduces a study of ENSO/precipitation relationship over the Peruvian Pacific drainage based on a homogenized regions and a first attempt to study ENSO/runoff relationship at catchment scale. Also we explore catchments sensitivities to hydroclimatic change over unimpaired selected catchments.

Chapter 7 presents the general conclusions, summarising the main results of the thesis and discussing prospects for future research.

(This page has been left blank intentionally)

Introduction

(Version française)

1.1. Contexte général

Le versant Pacifique du Pérou (voir la carte de localisation de la Figure 1.1) couvre près de 25 % du versant Pacifique de l'Amérique du Sud et présente une forte variabilité climatique induisant des événements climatiques extrêmes opposés tels que les inondations et les sécheresses causées principalement par le phénomène ENSO (El Niño – La Niña) (Tapley et Waylen, 1990 ; Lagos et al., 2008). Les conditions climatiques et orographiques de cette zone très étroite caractérisent cette région comme aride et semi-aride, génèrent notamment l'un des endroits les plus secs de la terre connu comme le désert péruvien située dans les basses terres (Nicholson, 2011).

Depuis les années 1970, les ressources en eau constituent une préoccupation croissante dans cette région. Cette région, économiquement la plus importante du Pérou, présente d'une part une densité de population très élevée (50 % de la population totale péruvienne) et d'autre part une très faible disponibilité en eau douce (2 % du total national péruvien) (ANA, 2012). Ces conditions constituent un défi permanent pour tout plan de gestion de l'eau, qui doit être basé sur une analyse approfondie des processus hydroclimatiques. A ce jour, cette analyse ne s'appuie pas encore sur une approche scientifique que ce soit en termes de variabilité climatique ou de disponibilité en eaux de surface.

Variabilité climatique et précipitations

La variabilité climatique (et principalement celle liée au phénomène ENSO) et les événements extrêmes qui y sont associés représentent les épisodes les plus difficiles à gérer pour une économie péruvienne émergente. Leurs impacts et les pertes économiques continuent de se répéter depuis les temps anciens. Les premières documentations concernant ce phénomène affectant la côte Pacifique péruvienne ont été révélées au monde sous le nom espagnol de "El Niño" (ou "enfant Jésus") et le décrivent comme un contre-courant océanique chaud situé dans la zone nord de l'océan Pacifique qui commence à se manifester à la période de "Noël" et qui provoque des fortes précipitations et inondations (Carranza, 1892 ; Pezet, 1896). Jusqu'à présent, les conséquences socio-économiques catastrophiques de ces événements ont mis en évidence la forte vulnérabilité de cette région. A titre d'exemple, le dernier événement ENSO extrême qui s'est produit en 1997/1998 a entraîné une réduction significative de 12 % du produit intérieur brut (PIB) du Pérou (OPS, 2000). Les difficultés de compréhension des impacts de l'ENSO au Pérou sont liées au fait qu'il s'agit d'un phénomène

non stationnaire (Boucharel et al., 2009) avec une modulation significative de ses caractéristiques (amplitude, fréquence, asymétrie) aux échelles décennales (Torrence et Compo, 1998 ; Guilderson et Schrag, 1998). Certaines études d'impact axées sur les précipitations offrent un aperçu de l'évolution de la relation ENSO / précipitation (Tapley et Waylen, 1990 ; Lagos et al, 2008 ; Lavado et Espinoza, 2014) alors que d'autres études portent sur les processus physiques océan-atmosphère-continent (Takahashi, 2004).

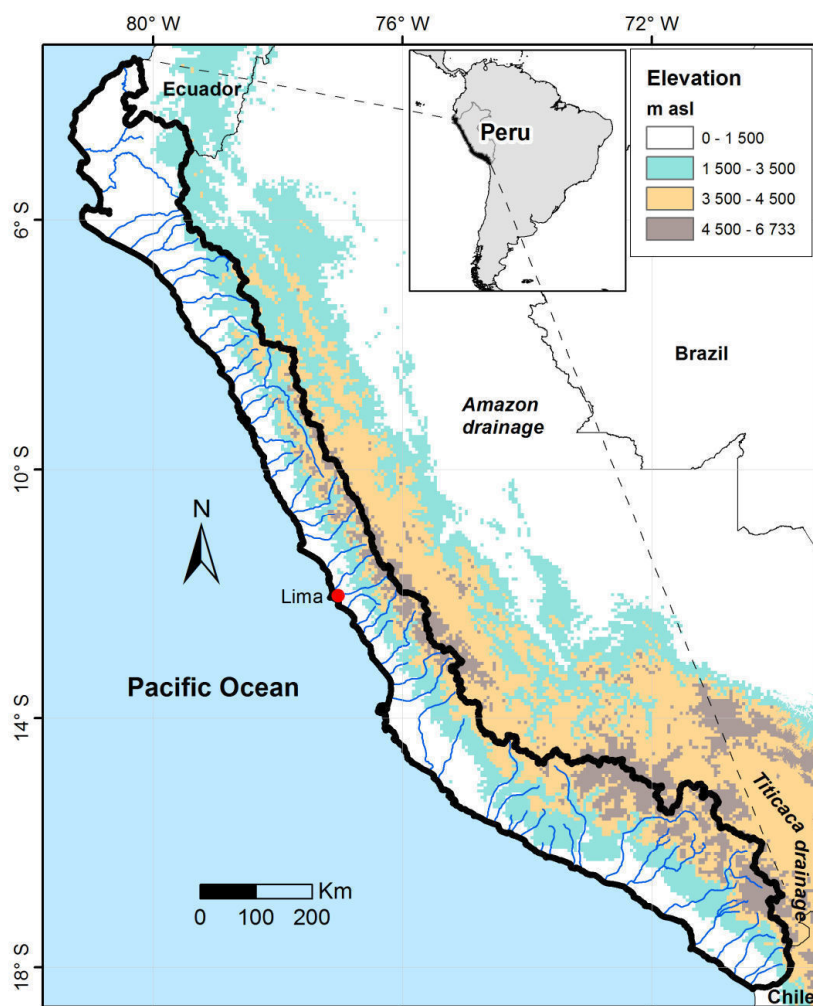


Figure 1.1. Système hydrographique principal du versant Pacifique péruvien.

Deux types d'événements El Niño ont été documentés à ce jour : El Niño du Pacifique Est, correspondant aux anomalies de la température de surface de la mer (SST) dans le Pacifique équatorial oriental (El Niño EP) et El Niño du Pacifique Central (ou Niño Modoki) correspondant à des anomalies SST chaudes dans le Pacifique équatorial central (El Niño CP représentant la variabilité des événements modérés ou des phases La Niña) (Ashok et al., 2007, Takahashi et al., 2011).

En outre, un changement climatique s'est opéré dans les années 1970 entraînant une recrudescence des événements El Niño EP qui sont devenus plus forts (Miller et al., 1994). Les années 1980 et 1990 sont de ce fait les décennies pour lesquelles la relation entre l'ENSO et l'hydrologie (précipitations et débits) au Pérou (Lagos et al., 2008 ; Lavado et al., 2013) est

la plus marquée en raison de la forte signature sur la circulation régionale des deux événements extrêmes de 1982/83 et 1997/98. Par contre, au cours des deux dernières décennies, le Niño CP semble être plus fréquent par rapport au El Niño EP (Yeh et al., 2009 ; Lee et McPhaden, 2010 ; Takahashi et al., 2011).

Un tel changement dans les caractéristiques de l'ENSO modifie les caractéristiques de la circulation océanique et atmosphérique équatoriale dans le Pacifique, c'est-à-dire les ondes océaniques équatoriales dites de Kelvin (Dewitte et al., 2012) et la variabilité atmosphérique saisonnière (Gushchina et Dewitte, 2012), ainsi que l'Oscillation de Madden et Julian (MJO) (Madden et Julian, 1972). Tous ces aspects du changement dans les propriétés de l'ENSO ont été quelque peu négligés dans les études portant sur l'impact de l'ENSO sur les précipitations le long du versant Pacifique, alors qu'elles sont susceptibles de fournir des conseils précieux pour affiner les stratégies actuelles de prévision de ces phénomènes extrêmes et l'amélioration de la gestion des ressources en eau (irrigation, approvisionnement en eau potable). Par conséquent, l'impact de l'ENSO sur le régime des précipitations à l'échelle régionale doit être revisité à la lumière des études récentes soulignant une diversité de l'ENSO. Il devient donc essentiel de mettre à jour et d'obtenir des informations de haute qualité sur le régime des précipitations au cours des quatre dernières décennies (1970 à 2010) de manière à étudier le comportement non-linéaire de ces séries chronologiques.

Eau superficielle, climat et activités humaines

Il existe une forte activité humaine le long des 54 principaux bassins versants constituant le versant Pacifique péruvien qui crée un fort déficit en eau pour approvisionner les principales villes et leurs activités économiques. A titre d'exemple, le bassin versant du Rimac dans lequel est située la capitale péruvienne de Lima (près de 10 millions d'habitants) est déjà reconnu être dans un scénario absolu de déficit en eau par habitant avec moins de 500 m³/an alors que la moyenne de l'ensemble du versant Pacifique péruvien est considérée être dans un scénario de stress hydrique par habitant avec moins de 1700 m³/an (ANA, 2012 ; White, 2012 ; MINAM, 2016). Le système fluvial détaillé du bassin de Rimac et son évolution depuis les années 1920 pour la ville de Lima a été présenté par Vega et al. (2017). Cependant, à ce jour, la majorité des 54 bassins versants constituant le versant Pacifique péruvien n'ont toujours pas été étudiés de manière approfondie en ce qui concerne la disponibilité en eau.

La quantification et la compréhension des effets de la variabilité climatique et des activités humaines sur le régime hydrologique représentent un défi majeur, en particulier à des échelles de temps pluri-annuelles (le décennale) et d'espace (l'échelle des bassins versants) (Donohue et al., 2007 ; Wagener et al., 2010). Le degré d'influence anthropique peut être déterminé en utilisant deux types d'influence sur les écoulements : activité humaine avec influence directe (conservation du sol, travaux de contrôle de l'eau, augmentation de la demande en eau) et activité humaine avec influence indirecte (modification de l'utilisation et de la couverture des sols (LULC)) (Wang et al. 2013). Ils constituent des éléments descriptifs pour comprendre le comportement des séries de données hydroclimatiques et pour identifier

les bassins versants présentant un faible niveau d'anthropisation. Par conséquent, nous soulignons ici la nécessité d'obtenir des informations de haute qualité sur le régime hydroclimatologique pour aborder la question de l'anthropisation et de la variabilité climatique et de leur influence sur les séries temporelles des variables hydrologiques (ruissellements, débits).

Malgré l'importance sociale et économique de la région d'étude, il n'existe pas encore de travaux scientifiques dédiés qui traitent de l'influence du changement hydroclimatique sur la disponibilité en eau superficielle. Cela nécessite tout d'abord une compréhension de la variabilité des précipitations et de leur relation avec la variabilité climatique naturelle (ENSO et variabilité décennale) comme condition préalable à la réalisation des études sur les ressources en eau. Concernant ces aspects il n'existe à ce jour que l'œuvre monographique de Reparaz (2013) qui couvre la période 1920 – 1960 et une documentation générale sur le régime de ruissellement jusqu'en 2011 réalisée par Lavado et al. (2012). Ce contexte initial appelle donc à formuler plusieurs hypothèses et méthodologies qui sont développées dans les sections suivantes.

1.2. Motivation

Validation d'une base de données hydroclimatologique in-situ

Le contexte économique et social dans un pays en voie de développement tel que le Pérou n'offre pas encore les conditions d'existence d'une base de données hydroclimatologique in-situ de haute qualité. Une telle base de données est cependant essentielle pour comprendre à la fois les régionalisations de la variabilité climatique et les changements hydroclimatiques, qui sont les deux principaux sujets abordés dans cette thèse. En conséquence, il a été nécessaire de collecter et d'analyser en profondeur les principales observations hydroclimatiques in-situ disponibles (précipitations, température, évapotranspiration et débits) au cours des 4 dernières décades (1970 – 2010). Les processus d'homogénéisation et de validation que nous avons utilisés devaient tenir compte des conditions de variabilité du climat reflétées dans les séries chronologiques avec présence de pics élevés et de valeurs très faibles. Dans ces conditions, il a été nécessaire de définir une méthodologie pour traiter les données manquantes et effectuer une sélection de stations appropriées à notre étude. D'un point de vue hydrologique, l'analyse des séries chronologiques de débits est un cas très intéressant car la zone d'étude du versant Pacifique péruvien est constituée de nombreux petits bassins présentant des conditions de bassins non jaugés ou insuffisamment jaugés et qui présentent de plus un degré significatif d'anthropisation qui n'a pas été quantifié jusqu'à présent.

Malgré ces limites, plusieurs méthodologies sont proposées tout au long de la thèse pour utiliser la représentativité des variables hydroclimatologiques par des observations in-situ plutôt que par des sources externes (par exemple, issues de la télédétection et de produits de réanalyses climatiques). À l'échelle du bassin versant et en raison des hautes altitudes et des fortes pentes de la Cordillère des Andes, il a été nécessaire de procéder à une correction

par des gradients d'élévation des précipitations interannuelles et des variables de température en s'appuyant sur des méthodes proposées dans la littérature (Valéry et al., 2010 ; Ruelland et al., 2014 ; Hublart et al., 2015). En outre, les séries chronologiques des stations d'hydrologie, qui représentent les sorties de débits des bassins versants, ont dû être différenciées entre les bassins versants ayant une influence climatique et anthropique forte qui perturbent le signal de débit naturel et ceux qui ont des conditions quasi naturelles. À cette fin, nous proposons l'utilisation de la méthode de Budyko (Budyko et al., 1958 ; 1974) qui est détaillée dans les paragraphes ci-dessous.

Les objectifs de la thèse sont l'analyse de l'influence de la variabilité climatique et du changement hydroclimatique sur les régimes de précipitations et de débits avec une approche de régionalisation de la zone d'étude. Mais il ne serait pas possible d'atteindre cet objectif sans toutes les étapes préliminaires indispensables décrites ci-dessus, c'est-à-dire le traitement de la base de données in-situ en vue de disposer des séries chronologiques hydroclimatiques fiables et de haute qualité.

Variabilité du régime des précipitations

À l'échelle de l'ensemble du versant Pacifique péruvien, la manière de décrire le régime de précipitations peut être atteinte via une approche de régionalisation des pluies. L'objectif est de réaliser un produit de précipitation régionalisé afin de révéler comment les précipitations sont réparties ou distribuées au sein de régions homogènes. Chaque région pourra être ainsi représentée par une série temporelle de précipitations « prête à l'emploi » pour une analyse de la variabilité climatique. Nous cherchons à mettre en évidence l'avantage d'utiliser une analyse de classification statistique par cluster k-means dans la procédure de régionalisation des précipitations pour prendre en compte le fait que les séries chronologiques sont non stationnaires et/ou non gaussiennes en raison de l'influence des phénomènes complexes climatiques (Takahashi et Dewitte, 2015). A titre d'exemple, l'ENSO présente une forte asymétrie positive résultant du fait que les événements extrêmes sont des événements chauds (An et Jin, 2004 ; Boucharel et al., 2011), ce qui entraîne une distribution non gaussienne de la plupart des indices historiques (Boucharel et Al., 2009). Une telle non-linéarité dans la circulation à grande échelle dans le Pacifique tropical est susceptible d'influencer la précipitation sur la côte Pacifique et sur les pentes de la Cordillère des Andes, ce qui appelle à raffiner les procédures de régionalisation basées uniquement sur des techniques linéaires.

Influence du climat et des activités humaines sur le bilan hydrique

À l'échelle du bassin versant, l'application d'une correction de gradient d'élévation dans la spatialisation des variables climatiques permet de travailler correctement de manière agrégée, offrant ainsi des informations réalistes pour l'analyse du bilan hydrique dans des conditions semi-arides. Le bilan hydrique proposé cherche à présenter les premières estimations de l'évapotranspiration sur les bassins hydrographiques du versant Pacifique péruvien. Une analyse détaillée des bassins versants avec une disparité faible et élevée du

bilan hydrique via le cadre de Budyko est ainsi utilisée. Cette méthode analyse le rapport entre l'indice d'évaporation interannuelle (rapport entre l'évapotranspiration réelle et la précipitation) et l'indice de sécheresse interannuelle (rapport entre l'évapotranspiration potentielle et les précipitations) dans un cadre global appelé «espace Budyko». Cet espace représente toutes les interactions entre la végétation, le sol et l'atmosphère qui constituent le cycle hydrologique et qui créent un équilibre empirique représenté par la courbe de Budyko (van der Velde et al., 2013). Pour souligner l'impact d'autres facteurs sur le bilan hydrique tels que la végétation, nous cherchons à tester une relation générale émergente proposée par Zhang (Zhang et al., 2001), et connue sous le nom de cadre de Budyko-Zhang. Cette courbe à l'équilibre représente les bassins versants présentant des conditions naturelles, soumis à une faible anthropisation et à une faible variabilité climatique, en particulier les sécheresses (Wang et al., 2011 ; Jones et al., 2012 ; Coron et al., 2015). Enfin, nous avons aussi essayé d'établir une relation entre le degré de disparité de l'équilibre hydrique identifié et la dynamique de l'utilisation et de la couverture des sols avec l'utilisation de données satellitales MODIS et LBA.

Variabilité du régime des débits

Nous avons réduit les nombreux petits bassins versants (54) qui constituent l'ensemble du versant Pacifique péruvien à un ensemble de bassins versants qui montrent des conditions quasi naturelles ou avec une faible anthropisation à l'échelle annuelle via le cadre Budyko, offrant ainsi des séries chronologiques de haute qualité pour leur utilisation dans une approche régionale, dans le cadre de l'analyse de la variabilité climatique et du changement hydroclimatique. A l'échelle du bassin versant, nous avons aussi étudié les conditions hydrologiques semi-arides via la modélisation hydrologique comme moyen de simuler le régime de ruissellement sur ces bassins versants quasi naturels sélectionnés.

Les estimations des écoulements (observations historiques des débits) reflètent les changements dans les conditions environnementales telles que le climat et l'utilisation des terres. La modélisation conceptuelle est régulièrement critiquée car elle simplifie la physique des processus qui se déroulent au sein des bassins versants et conduit à des simulations peu fiables lorsque les conditions changent au-delà de la portée de l'expérience antérieure (Hublart et al., 2015). Les sources habituelles d'incertitude dans la modélisation hydrologique dans des conditions stationnaires (concernant le climat et les caractéristiques physiques du bassin) sont liées à la structure du modèle, aux procédures d'étalonnage et aux données erronées utilisées pour l'étalonnage et la validation (Liu et Gupta, 2007 ; Brigode et al., 2013). Dans des conditions non stationnaires, telles que la variabilité ou le changement climatique, une source d'incertitude supplémentaire provient de l'instabilité des paramètres en raison des changements possibles des caractéristiques physiques du bassin versant et des principaux processus en jeu (Coron et al., 2012 ; Thompson et al., 2013 ; Dakhlaoui et al., 2017). Pour cette raison, il apparaît nécessaire d'évaluer la robustesse de la modélisation et notamment la transférabilité des paramètres calibrés à des conditions climatiques et/ou anthropiques contrastées. Nous proposons donc l'utilisation du test différentiel d'échantillonnage partitionné (DSST) selon Klemes (1986) et Thirel et al. (2015).

Concernant l'approche régionale, l'un des principaux obstacles à l'estimation de l'écoulement régional et continental d'eau douce est l'absence et la non continuité de données de jaugeage. Certaines méthodes ont été appliquées pour compenser la contribution de régions mal jaugées en estimant le débit moyen à long terme comme une simple somme des enregistrements de débits disponibles. Cependant, ces méthodes contiendraient des discontinuités, ce qui est un problème majeur dans les analyses de données climatiques à long terme (Milliman et Farnsworth, 2011).

Il était nécessaire de tenir compte des nombreux bassins versants non jaugés constituant notre zone d'étude et d'estimer leur écoulement. À cette fin, nous proposons et testons un modèle d'écoulement régional, construit à partir du modèle conceptuel GR1A et GR2M (Mouelhi et al., 2006a ; 2006b) pour simuler l'écoulement naturel sur ces bassins hydrographiques soit non jaugés ou soit insuffisamment jaugés aux points de sortie vers l'océan Pacifique. Nous cherchons aussi à générer le premier produit régional qui permet de disposer des séries chronologiques de débits de l'ensemble de la côte péruvienne au cours des quatre dernières décennies, ainsi que de proposer les premières estimations des apports d'eau douce du versant Pacifique péruvien à l'océan.

Influence de la variabilité climatique sur les précipitations et la sensibilité hydroclimatique à l'échelle régionale et à l'échelle du bassin versant

Comme il a déjà été mentionné, l'étude de l'influence de la variabilité climatique (c'est-à-dire l'ENSO et les modes de variabilité saisonnières comme les ondes de MJO et Kelvin) sur les précipitations doit être revisitée. Pour cela, nous proposons d'abord d'utiliser le produit de précipitation régionalisé que nous avons généré et d'appliquer la méthodologie proposée dans Bourrel et al. (2015). Cette étude était centrée dans la partie nord et centre de la zone d'étude et utilisait une variété d'indices ENSO classés comme classiques, atmosphériques, océaniques et nouveaux indices ENSO (E et C). Cela a permis d'interpréter ce phénomène climatique complexe et sa relation avec les précipitations.

En ce sens, notre contribution est l'extension des résultats préliminaires présentés par Lagos et al. (2008) et Lavado et Espinoza (2014). En raison de l'interaction entre les conditions océaniques à grande échelle et régionales, nous faisons l'hypothèse que cette relation résulte de l'interaction non linéaire entre les influences locales et éloignées et qu'une étude basée sur une diversité d'indices peut aider à comprendre cette interaction. D'anciennes études ont porté sur des événements extrêmes El Niño qui ont causé de grandes pertes économiques pour le Pérou, mais peu a été dit sur des événements modérés. Dans un contexte de changement climatique, il est également nécessaire de mieux comprendre la basse fréquence naturelle des modèles de téléconnexion. Ici, nous profitons d'un enregistrement de données à long terme et d'une interprétation revisitée de la variabilité de l'ENSO au cours des quatre dernières décennies, où l'ENSO présente deux régimes distincts et indépendants, l'un associé à des événements extrêmes El Niño tels que ceux de 1982/83 et 1997/98, et l'autre associé aux événements chauds modérés et à La Niña (Takahashi et al., 2011). En outre, nous

explorons pour la première fois la relation ENSO/débits avec l'utilisation des séries chronologiques régionales quasi naturelles que nous avons générées le long du versant Pacifique péruvien.

À propos de l'influence du changement hydroclimatique, il existe un manque dramatique d'études et d'informations non actualisés concernant les tendances hydroclimatologiques (des précipitations, aux débits en passant par l'évapotranspiration) au cours des dernières décennies. Nous proposons la première analyse complète des tendances hydroclimatologiques à l'échelle des bassins constituant l'ensemble du versant Pacifique péruvien. Jusqu'à présent, seul un constat de réchauffement régional a été mis en évidence dans Vuille et al. (2015) sur les Andes péruviennes. Les tendances des variables hydroclimatiques sont considérées comme des indicateurs de changement de l'hydroclimatologie régionale au cours des quatre dernières décennies et nous proposons de les étudier dans le cadre Budyko suivant la méthodologie proposée dans van der Velde et al. (2013). Les régions regroupant plusieurs bassins versants suivant la même trajectoire de changement présentent une adaptation commune de l'équilibre hydrique aux forçages climatiques et/ou anthropiques régionaux. Cette méthodologie permet de mettre en évidence la sensibilité du bassin versant en termes de trajectoires de Budyko (c'est-à-dire la direction et la magnitude) en ce qui concerne le changement hydroclimatique (par exemple, l'influence des changements dans le contexte des conditions futures principalement) et le changement des paramètres physiques du bassin (en termes d'utilisation et d'occupation des sols principalement).

Dans l'ensemble, la présente thèse décrit l'hydroclimatologie du versant Pacifique du Pérou au cours des quatre dernières décennies, qui constitue la principale motivation pour faire face aux limites et aux besoins exposés et de façon à rendre possible des études avec une approche scientifique qui seront d'une grande importance pour la planification des ressources d'eau.

1.3. Objectifs principaux et spécifiques

Compte tenu de la forte vulnérabilité de cette région en termes de variabilité climatique et de disponibilité en eau (MINAM, 2016), l'objectif principal est d'améliorer notre compréhension de la relation entre la précipitation et sa variabilité (et les événements extrêmes) et la variabilité du Pacifique tropical aux échelles de temps interannuel et décennal en tenant compte des progrès récents dans l'étude du phénomène ENSO (i.e. sa diversité). La thèse vise également à aborder l'influence du changement hydroclimatique sur les précipitations, l'évapotranspiration, le bilan hydrique et le régime de l'écoulement en intégrant les questions de l'anthropisation du versant Pacifique péruvien et du grand nombre de bassins versants qui le constituent.

Les objectifs spécifiques peuvent être présentés sous la forme des cinq questions suivantes :

1) Quelle est la variabilité spatio-temporelle des précipitations interannuelles ? Une approche de régionalisation est proposée pour caractériser la variabilité interannuelle des précipitations le long du versant Pacifique péruvien.

2) Comment aborder la problématique de la variabilité climatique et de l'anthropisation ainsi que de leurs influences potentielles sur les séries chronologiques hydroclimatiques ?

Les cycles annuels hydroclimatiques sont explorés à l'échelle du bassin versant via les bilans d'eau et d'énergie selon le modèle Budyko permettant ainsi d'identifier les bassins versants présentant des conditions quasi-naturelles.

3) Quelle est la variabilité spatio-temporelle de l'écoulement interannuel quasi-naturel ?

La modélisation hydrologique est utilisée pour générer et caractériser la variabilité interannuelle de l'écoulement quasi-naturel ou naturel le long des nombreux petits bassins versants constituant le versant Pacifique péruvien.

4) Quelle est l'influence de la variabilité climatique interannuelle (notamment celle de liée au phénomène El Niño) et la variabilité saisonnière sur les régions homogènes des précipitations et des débits des bassins identifiés constituant l'ensemble du versant Pacifique péruvien ?

Le calcul et l'analyse de divers indices climatiques sont utilisés pour étudier la relation entre l'ENSO et les précipitations et les débits au cours des quatre dernières décennies.

5) Quelle est l'influence du changement hydroclimatique sur les régimes de précipitation et de l'écoulement ?

Les tendances des variables hydroclimatiques sont identifiées au sein de la période des 4 dernières décennies dans un contexte de changement hydroclimatique.

1.4. Organisation

La thèse est organisée comme suit :

Après un chapitre introductif (chapitre 1), le chapitre 2 présente une description complète de la zone d'étude et des données utilisées tout au long de la recherche, principalement liées au contexte hydroclimatique du versant Pacifique péruvien. Il couvre les conditions atmosphériques océaniques comme les conditions climatiques moyennes et les modes de variabilité tels que le phénomène ENSO (El Niño – La Niña), la variabilité décennale et saisonnière. Ensuite, nous décrivons le paysage physique (topographie, géologie et végétation) et les caractéristiques hydrologiques axées sur les conditions arides et semi-

arides, et le degré d'anthropisation. Une description complète de l'ensemble des données hydroclimatologiques in-situ est ensuite présentée ainsi que les méthodologies utilisées pour traiter les limitations des bases de données existantes (y compris les processus de validation et d'homogénéisation) afin d'obtenir des séries chronologiques fiables et de haute qualité au cours des quatre dernières décennies pour mener à bien notre recherche.

Le chapitre 3 décrit le régime des précipitations dans une perspective statistique sur l'ensemble de la zone d'étude. À cette fin, une méthodologie pour sa régionalisation sous la condition de série temporelle non stationnaire est proposée. Cette méthodologie consiste en une approche combinée des méthodes du cluster k-means et du vecteur régional. Nous présentons ainsi un produit de précipitations régionalisées composé de neuf régions homogènes.

Le chapitre 4 étudie les régimes hydroclimatologiques à l'échelle du bassin versant, afin de distinguer les bassins versants avec une faible et une forte disparité du bilan hydrique. Cette distinction est basée sur le cadre du modèle Budyko, qui permet d'identifier un ensemble de bassins avec des conditions quasi-naturelles, c'est-à-dire avec une faible influence du climat et de l'anthropisation (notamment sa relation avec l'utilisation et l'occupation du sol).

Le chapitre 5 décrit le régime de l'écoulement quasi-naturel ou naturel des bassins versants sélectionnés avec une extension régionale sur les bassins versants non jaugés ou insuffisamment jaugés au travers de l'utilisation de la modélisation hydrologique. Cette analyse propose également une première estimation fiable des apports d'eau douce des fleuves de l'ensemble du versant Pacifique péruvien vers l'Océan Pacifique.

Enfin, après avoir obtenu une compréhension cohérente des régimes des précipitations et de ruissellement avec une base de données homogénéisée et validée, le chapitre 6 présente une étude de la relation ENSO/précipitations sur le versant Pacifique péruvien basée sur les régions homogénéisées identifiées et une première tentative d'étude de la relation ENSO/débits à l'échelle des bassins versants. De plus, nous explorons la sensibilité des bassins versants quasi-naturels sélectionnés aux changements hydroclimatiques.

Le chapitre 7 présente les conclusions générales, résumant les principaux résultats de la thèse ainsi que les perspectives de recherches futures.

Chapter 2

Study area and data

2.1. Hydroclimatic context of the Peruvian Pacific slope and coast

This section describes some features about the main components of the Peruvian Pacific slope and coast climate system and the influence of its variability over main hydroclimatic variables, as well as the description of physical landscape.

2.1.1. Climate variability

Climate variability is defined by the World Meteorological Organization (WMO) as “variations in the mean state and other statistics of the climate on all temporal and spatial scales, beyond individual weather events”. This can influence patterns of precipitation, temperature and other hydroclimatological variables on timescales anywhere from a few weeks to a few decades. Here we provide an emphasis on climate variability influence over precipitation, considered as the main source of nearly all freshwater in the hydrologic cycle.

a. Mean climatic conditions in the South East Pacific

On the one hand, under normal conditions, the Peruvian Pacific drainage region (hereafter Pd) is influenced by the Southern Pacific Anticyclone (hereafter SPA) in combination with the Humboldt current characterized by cold Sea Surface Temperatures (hereafter SST) which produces dry and stable conditions to the western central Andes, with moist air trapped below the inversion zone at about 900 hPa ~ 1000 m.asl (Vuille *et al.*, 2000; Garreaud *et al.*, 2002), conditions that produce extreme aridity until about that altitude (Lavado *et al.*, 2012). Over this altitudinal limit, it is known that there is an influence of the southward displacement of the Inter Tropical Convergence Zone (hereafter ITCZ) and is supposed that other mechanisms influencing over the Peruvian Andes, also influence over the Peruvian Pacific slope (i.e. humidity transport from the Amazon, Bolivian High, etc) (Nickl, 2007; Lagos *et al.*, 2008), nevertheless this has not been studied to date. On the other hand, this region exhibits greater seasonal and interannual precipitation variability than the two main others hydrological regions of Peru: the Amazon and the endorheic Titicaca drainage areas (Lavado *et al.*, 2012), mainly caused by the El Niño Southern Oscillation (hereafter ENSO) influence in the northern areas during the rainy season, with no clear evidence of the ENSO influence for central and southern areas (Lagos *et al.*, 2008; Lavado *et al.*, 2012; Lavado and Espinoza, 2014).

Precipitation along the Pacific drainage of South America is characterized by a complex pattern of spatial and seasonal variability related to its meridional extension and the prominent topography of the Andes Cordillera (Waylen and Poveda, 2002; Garreaud *et al.*, 2009). The Pd region is located at tropical latitudes and precipitation is mainly influenced by orographic conditions, ocean and atmosphere. The region is characterized by a steep topography that inhibits cross-shore atmospheric flow and disrupt a geotropically balanced zonal wind, inducing a northward sea level pressure gradient along the coast that accelerate the wind northward (Muñoz and Garreaud, 2005). Such a low-level northward mean circulation is associated with cool SST through inducing upwelling and evaporation, which makes this region persistently free of convective precipitation year-around (Takahashi and Battisti, 2007). The Pacific coast of Peru is thus mostly a “dry zone” that only episodically experiences precipitation events. At interannual timescales, those precipitation events are associated with ENSO phenomenon that is the main climatic influence over precipitation over the Peruvian Pacific coast (Lagos *et al.*, 2008). A rainy season can also be developed owed to a slight weakening of the southeast Pacific anticyclone and the southward displacement of the Pacific ITCZ (Lavado *et al.*, 2012).

b. Modes of variability

El Niño phenomenon (ENSO) and its diversity

The ocean-atmosphere interactions in the Pacific Ocean produce a large-scale phenomenon known as the El Niño Southern Oscillation (ENSO). It is attributed to irregular variations in atmospheric pressure and sea surface temperature of the tropical Pacific Ocean (see Figure 2.1). This phenomenon is decomposed into two phases: El Niño phase is a hot event (positive sea surface temperature anomalies of the ocean) while La Niña phase is a cold event (negative sea surface temperature anomalies of the ocean). These climatic changes can severely disrupt the climate of the tropical regions on both sides of the Pacific Ocean (see Figure 2.1) and in particular the Pacific coast of South America (Aceituno, 1993).

El Niño in Peru is often associated with heavy rain along the coastal fringe of the country due to the intrusion of warm tropical waters along the coast that allows deep convection in a region where cold upwelled waters and semi-arid to arid climate usually prevails (Tapley, 1990; Lagos and Buizer, 1992). Over the last decades, two extreme El Niño events (1982/1983 and 1997/1998) took place and led to large socio-economical consequences because of the disasters caused by the floods and droughts. Considering the societal concern, recent studies have thus been devoted to inferring precipitation in Peru based on seasonal forecast products from climate models (Lagos *et al.*, 2008). The approach consists of building a statistical model between local precipitation as inferred from observations and

climate indices as derived from SST of the tropical Pacific predicted by the seasonal forecast systems (ex. NCEP). The skill of the forecast system is also highly dependent on the selected predictors and statistical method. For instance, the linear assumption, often used for the statistical approach, is certainly not the most appropriate for predicting precipitation in Peru, because ENSO has a strong positive asymmetry (evidenced by the extreme warm events) reflecting the non-linearity in the system (An and Jin, 2004). Recent studies have revealed that there is also different types of El Niño events that have distinct characteristics in terms of atmospheric teleconnections (Yeh *et al.*, 2009), frequency (Kim and Yu, 2012), and oceanographic manifestations off Peru (Dewitte *et al.*, 2012). Two types of El Niño events have been documented so far in the literature (Ashock *et al.*, 2007; Kug *et al.*, 2009): the so-called Cold Tongue El Niño or Eastern Pacific El Niño (hereafter EP El Niño) that corresponds to extreme warm events developing strong SST anomalies in the eastern equatorial Pacific, and the Warm Pool El Niño or Central Pacific El Niño (hereafter CP El Niño) that corresponds to standing warm SST anomaly development in the central equatorial Pacific, within the so-called Warm Pool region (see Figure 2.2). In a recent study, Takahashi *et al.* (2011) suggest that the dominant mode of variability in the equatorial Pacific is in fact associated with a regime that encompasses the CP El Niño and that the EP El Niño events are extreme events, which are by definition much rarer than CP El Niño events. This view has of course implications for the study of the ENSO teleconnection pattern over Peru for precipitation because CP El Niño are characterized by weak anomalous SST conditions off Peru compared to EP El Niño (Dewitte *et al.*, 2012).

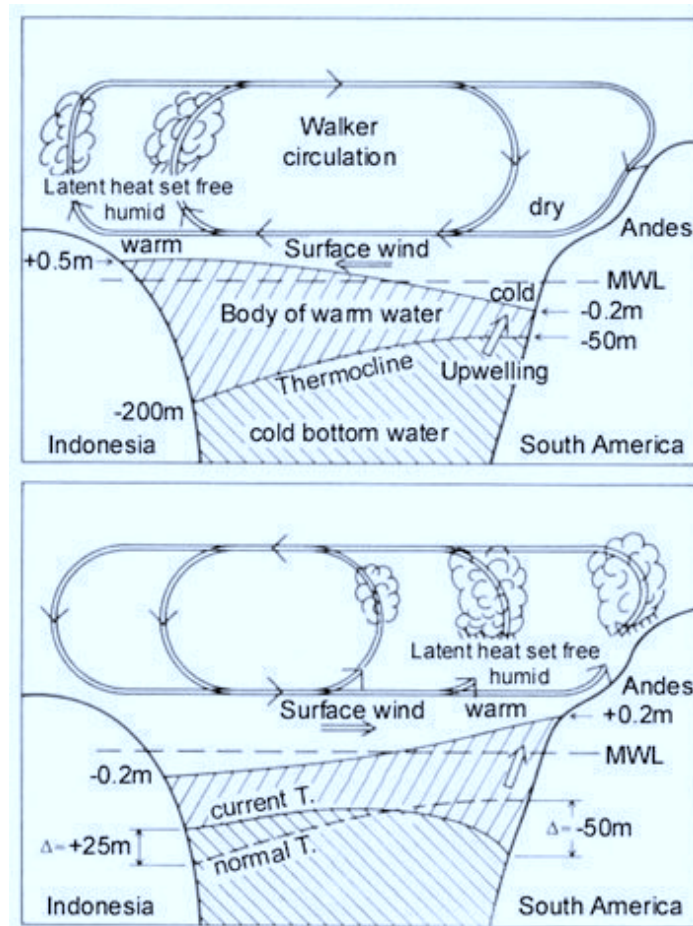


Figure 2.1. Idealized schematic diagram reflecting the ENSO Phenomenon. Normal non-ENSO conditions are shown above, while the climax of an ENSO event is pictured below. In either cases both the slope of the sea level as well as the thermocline change considerably. Source: Madl (2000).

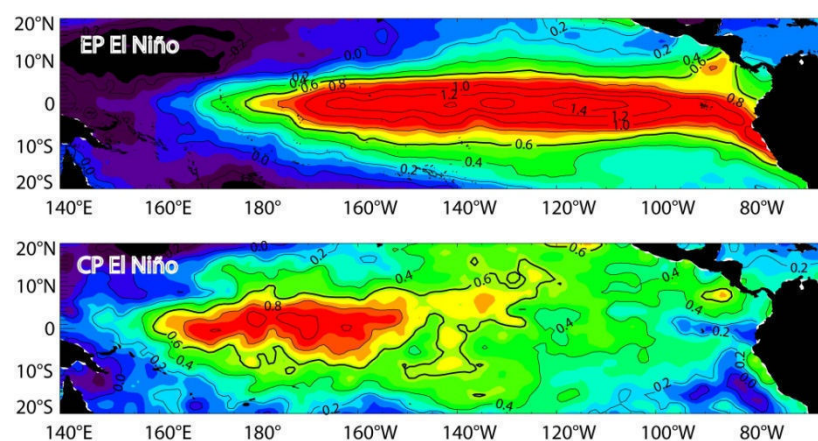


Figure 2.2. Anomalies of climatologic SST (1900–2009) of the Eastern Pacific El Niño (EP El Niño or classical ENSO, shown above) and Central Pacific El Niño (CP El Niño or ENSO Modoki, shown below) for the HadISST data (Rayner et al., 2003). Source: Gutierrez et al. (2011).

Decadal variability

Hydrometeorological variations at timescales of a few days to a few decades and longer can cause persistent dry and wet periods, being one of the first sources of documenting decadal hydrological cycles. The most pertinent cause of decadal hydrological cycles is the ocean-atmosphere interactions resulting in natural decadal climate variability (Mehta, 2017). There are major decadal climate variability phenomena as the Pacific Decadal Oscillation (PDO) and Interdecadal Pacific Oscillation (IPO). At regional scale, there is some influence of positive phase of PDO over extreme warm and wet events in Bolivia (Seiler et al., 2013). Also, a recent study (Segura et al., 2016) evidence decadal and interdecadal hydroclimatic variability over South American Central Andes related to central-western Tropical Pacific influencing low frequency variability of zonal wind at 200 hPa (U200) over this region. Until now, there is a clear need for in-depth analysis of decadal natural variability over the Peruvian Pacific slope and coast.

Intraseasonal variability (MJO and oceanic Kelvin waves)

The motivation for studying these phenomena lies in part to the possibility that different regime of atmospheric circulation may take place over the different regions due to their distinct elevation. In particular the western coast of Peru is embedded in the large-scale subsidence zone corresponding to the descending branch of the Walker circulation, leading a shallow marine boundary layer propitious to the development of low level clouds. Thus, conversely to the region over the Andes where deep convection and advection of humidity from the Amazon basin can take place, the coastal region is characterized by a relatively stable air column, implying dry mean conditions. Still, at 2000 m above sea level, deep convection associated with large scale disturbances (e.g. MJO) or/and orographic-induced circulation can take place, which is associated with precipitation. On the other hand, where SST near the coast reaches a threshold from which deep convection can occur, local precipitation events can be generated. Such events may be thus triggered by SST anomalies induced by the crossing of equatorial Kelvin waves.

MJO activity index

Atmospheric circulation in the region of Peru is also influenced by atmospheric conditions not necessarily directly related to ENSO but to local ocean conditions in the central-western Pacific. The Madden and Julian Oscillation (MJO, Madden and Julian, 1972) is a tropical global scale atmospheric disturbance and the dominant tropical intraseasonal mode. It is a key source of untapped predictability in both the tropics and extratropics (Wheeler and Kiladis, 1999; Waliser *et al.*, 2003; Waliser, 2005; Wheeler and Weickmann, 2001; Gottschalck and Higgins, 2008). The MJO can propagate from the western Pacific to the South America continent which can

alter the tropospheric circulation all over the tropical band, with a potential impact on precipitation over the South American continent. Because MJO is a circumnavigating wave, it can modify the regional atmospheric circulation in northern Peru by altering the well stratified air above a shallow inversion zone in this region due to the coastal upwelling. In particular the inversion zone near the coast lies around the 900hPa isobar below which low clouds (stratocumulus) generally develop. MJO-related variability is also found in the mid-latitudes of the Southern Hemisphere, and modulates the South-Pacific anticyclone, which variability is influential on the atmospheric circulation off central Peru (Dewitte *et al.*, 2011). At last MJO is tightly linked to ENSO (Roundy and Kiladis, 2006) and its activity may also reflect ENSO property changes (Gushchina and Dewitte, 2012).

Oceanic regional indices

The MJO is also associated with the formation of Westerly Wind Burst (Vecchi and Harrison, 2000) in the equatorial western-central Pacific that can trigger planetary oceanic waves, called equatorial Kelvin wave. The energy of these planetary oceanic waves is within the intraseasonal frequency band, that is $\sim [2-120] \text{ days}^{-1}$ (Dewitte *et al.*, 2008). We referred to these intraseasonal Kelvin waves as intraEKW hereafter. They should not be confused with the interannual Kelvin waves that are forced when El Niño develops, that is when the atmospheric circulation in the tropics interacts with the warm SST anomalies, leading to energetic westerlies at interannual timescales. The interannual Kelvin waves, named interEKW hereafter, are tightly linked to ENSO in the tropical Pacific and therefore do not convey more information than say the E and C indices. The intraEKW is active also during ENSO but presents a seasonal modulation depending on the nature of ENSO (Gushchina and Dewitte, 2012). It propagates from the central Pacific to the coast of Ecuador and locally can modify the oceanographic conditions along the coast of Peru (Dewitte *et al.*, 2012). For instance a downwelling intraEKW (i.e. which deepens the thermocline) can produce a warming event along the coast of Peru (see Mosquera *et al.* (2013) for the 2002 El Niño), that in turn may favor local convection leading to intense precipitation events (Woodman, 1985). Therefore change in intraEKW activity can be reflected in the precipitation fluctuations at interannual timescales through its impacts on coastal SST. The IntraEKW may be associated with episodic warm/cold events along the coast that are not related in a straight-forward manner to ENSO

2.1.2. Physical landscape

a. Topography

The study area comprises the Peruvian Pacific drainage (hereinafter Pd) region that covers an area of ~280,500 km². This area is characterized by a significant altitudinal gradient ranging from 0 to ~ 6,500 m asl and includes 54 main river catchments covering near 90% of this region. The rivers generally flows from east to west from the Andes towards the Pacific Ocean (see Figure 2.3) with bare and steep slopes from 4 to 9% within small and medium catchment areas from 500 to 16,000 km² that favour significant rising, flooding and erosion during huge precipitation episodes.

To characterize the topography, we used a digital elevation model showed in Figure 2.3a. It was obtained from the 90 x 90 m grid SRTM data (Shuttle Radar Topography Mission, NASA-NGA, USA available from <http://srtm.csi.cgiar.org>). It allowed the orographic corrections to be applied for the climate forcing interpolation (see section 3.1) and the 26 main studied river catchments to be delineated.

b. Geology

The western flank of the Andes is composed of igneous rock following the next distribution, until ~8°S lithology is composed of Palaeozoic to Cretaceous formations; from 8°S to 16°S geological formations are dominated by the continuous Andean batholith while from 16°S they are made of young volcanic cover, vast Tertiary pampas and coastal range. These conditions do not favour underflow through the Andes in some regions, mainly because of the continuous batholith acting as a barrier upper 2,000 to 4,000 m asl (see Figure 2.3b), limiting the precipitation drainage through the canyons and main channels in catchments (Gilboa, 1971).

c. Vegetation

Pd region is characterized mainly by 4 types of land cover: bare ground, open shrublands, grasslands and croplands. These different types of vegetation are directly related to the different climates observed following altitudinal and latitudinal range and were obtained from four land cover maps based on remotely sensed images acquired between 1984 and 2008. They are based on multispectral images from different sensors with a spatial resolution increasing against time. The LBA (Large Scale Biosphere-Atmosphere Experiment in Amazonia) Regional Land Cover products for 1984 (DeFries et al. 1998; 8 x 8 km grid) and 1992/1993 (Hansen et al. 2000; 1 x 1 km grid) were derived from acquisitions from the Advanced Very High Resolution Radiometer (AVHRR) for comparative purposes. The land cover of 2001 and 2008 were derived from acquisitions from the Moderate Resolution Imaging Spectroradiometer (MODIS). These products, made available by the Global Land Cover Facility (GLCF, <http://glcf.umd.edu/data/lc>) on

10 x 10 km grid, have a spatial resolution of 5'. The land cover map used in Figure 2.3c is the MODIS land cover type for 2008.

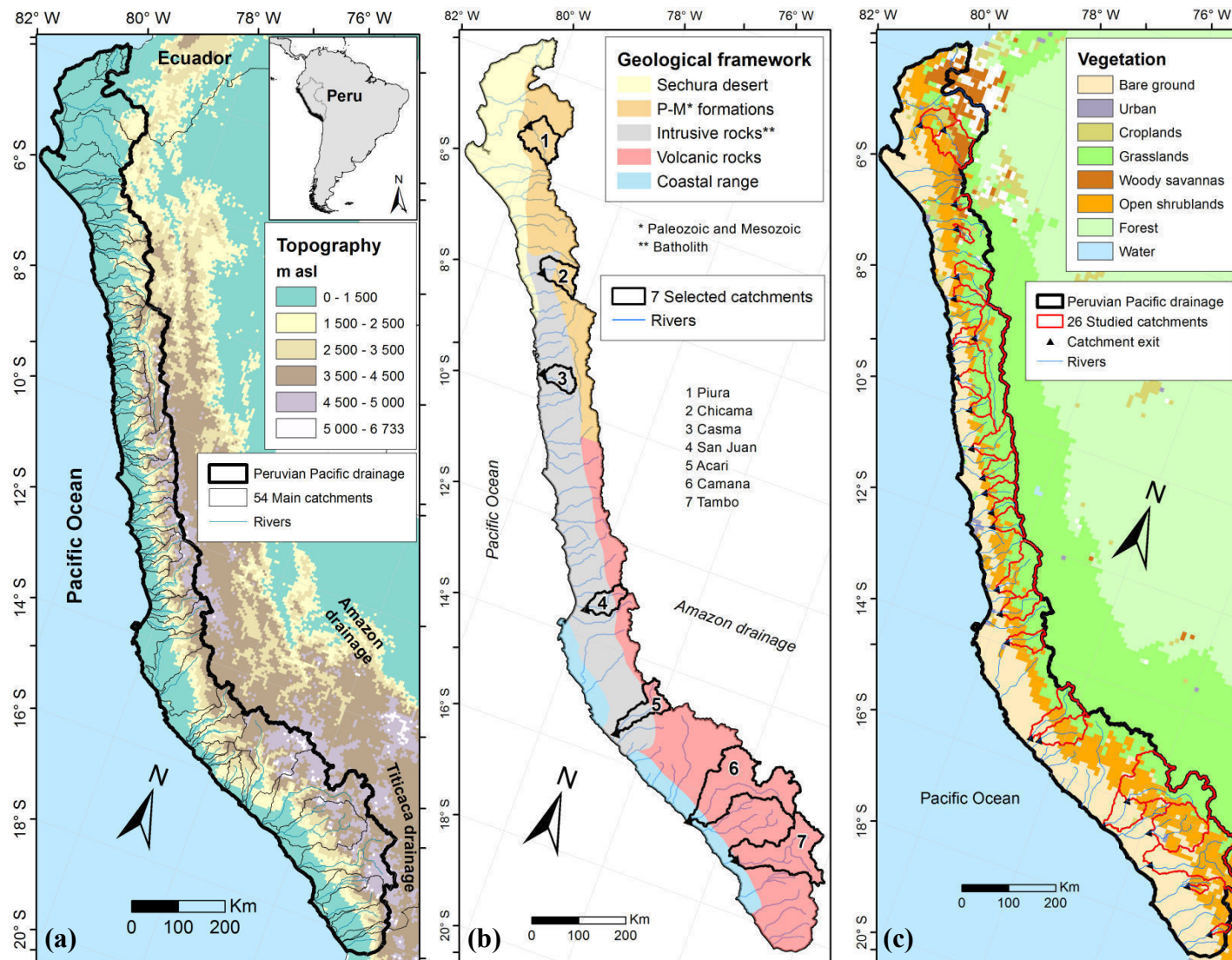


Figure 2.3. Physical landscape of the Peruvian Pacific drainage. a) Topography map from SRTM digital elevation model. b) Geological framework (Gilboa, 1971) and the 7 selected studied catchments location. c) Vegetation map from land cover MODIS types and the 26 studied catchment location.

2.1.3. Hydrological context

a. Arid and semi-arid conditions

Causes of aridity in the Pd have been widely explained in section 1.1 featuring in particular the low lands known as “Peruvian desert”, one of the driest places in the Earth (Nicholson, 2011). Aridity degree and its classification become unclear as the many numerical definitions for this term. However, depending on space and time scales it is generally accepted that dryland conditions occurred when evapotranspiration exceeds precipitation (Maliva and Missimer, 2012). It is worth to mention that dryland regions encompass hyper-arid, arid, semi-arid and dry sub-humid areas (Brouwer and Heibloem 1986; Mortimore et al. 2009). Under these conditions, here we described precipitation, evapotranspiration and streamflow regimen over the Pd at basin scale.

Monthly precipitation and runoff at basin scale for seven selected studied catchments (see location of these catchments in Figure 2.3b and its characteristics in Table 2.1), highlight a considerable scatter within the 40-year datasets (see scatter plots in Figure 2.4) and a seasonal regional behaviour (see mean seasonal hydrographs in Figure 2.4). Nevertheless, the chronology of the data exhibits a well-defined annual cycle, showing an increase of runoff with increasing precipitation during wet months from November to May and a slight decrease during the dry months of July and August. The data consequently show an annual anticlockwise hysteresis loop in all studied catchments regardless of the geology, glaciers or snow cover. This implies that precipitation is temporarily stored within the basins and not transferred directly to the river during the wet period whereas the storage compartment is drained during the dry period.

The mechanisms explaining the hysteresis effect are not enough documented over the study area and we suggested here some relationships between hydrologic variables. Snow and ice melt runoff represents ~14% and less than 1% respectively of annual mean distributed runoff located mainly over central and southern latitudes of the upper Pd (Mernild et al., 2016). Release of water by snowmelt generally reaches its peaks over wet months, which is not consistent with the anticlockwise nature of the hysteresis. Release of water by ice melt peaks over dry months (Condom et al., 2012; Mernild et al., 2016) and is consistent with the hysteresis effect. However given the low representativeness of ice melt runoff, it can be considered as negligible. This suggests that snow and ice melt runoff could be discarded as the main mechanisms explaining hysteresis. We also note that hysteresis occurs even over non-glacierized and non-snow covered catchments as Piura (n°1), and Chicama (n°2). In the same way, evapotranspiration reaches maximum values in the wet months from December to March and could qualitatively explain the hysteresis effect mainly in the catchments of Piura (n°1) and San Juan (n°4) identified by Rau et al. (2017b) as catchments with a water

balance sensitive to both precipitation and evapotranspiration. Finally, the main mechanism explaining the hysteresis effect is probably associated with a transient storage of water in a groundwater unit during the wet months and its release during dry months. It makes sense in the light of the mean seasonal hydrological behaviour of catchments (see the mean seasonal hydrographs in Figure 2.4) and lithologic composition in Figure 2.3b. Catchments located outside of the quasi impervious batholith reasonably present the hysteresis effect (catchments n°1, n°2, n°6 and n°7) which is corroborated with the extension of their recession limbs above zero runoff. Catchments located mainly inside the batholith (n°3, n°4 and n°5) also present the hysteresis effect, bringing out the relevance of the transient storage, which at unimpaired conditions is the main source of recharge of alluvial coastal aquifers at lowlands by way of infiltration from river beds (Gilboa, 1971).

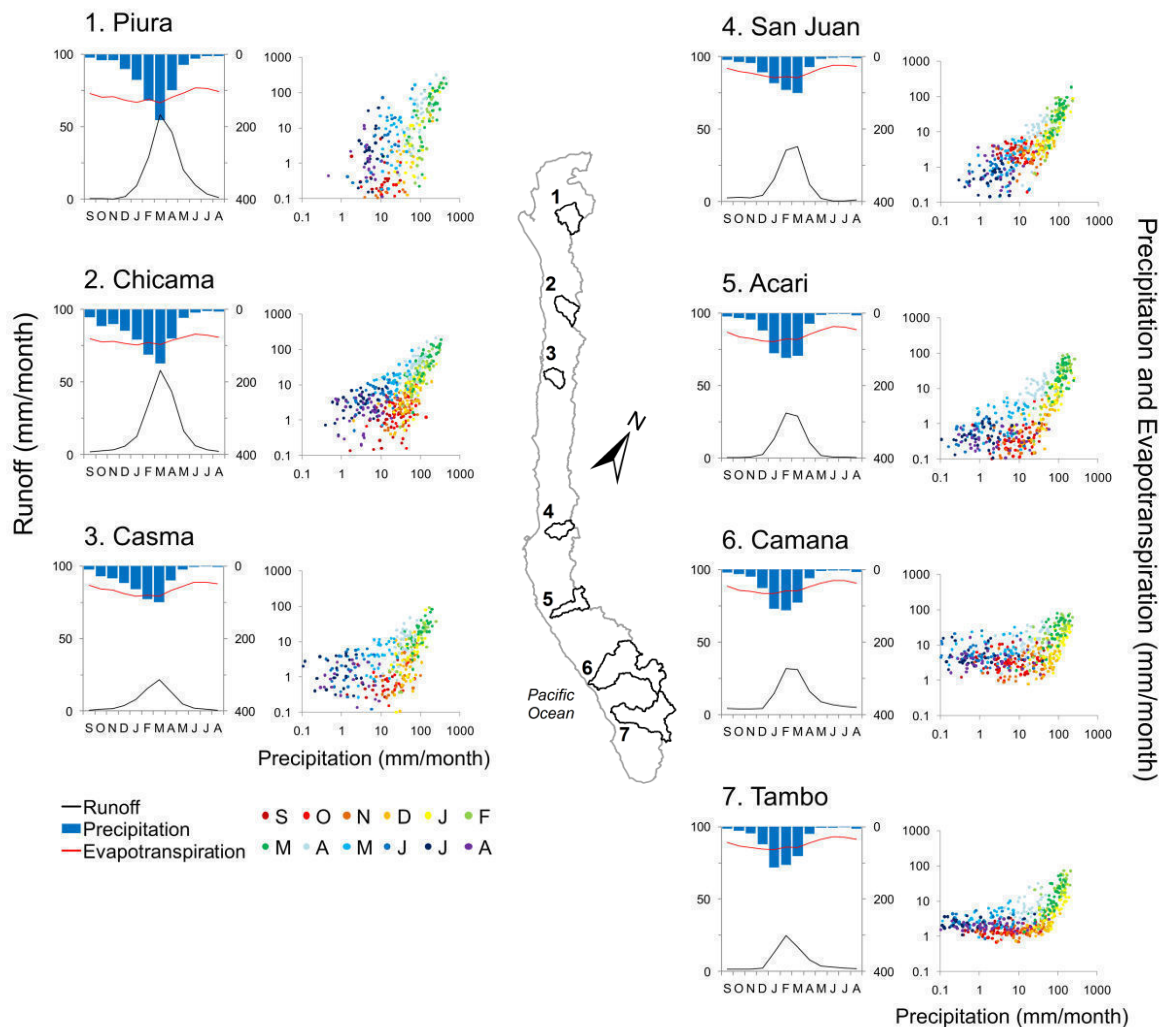


Figure 2.4. Mean seasonal lumped runoff, precipitation and evapotranspiration (left) and precipitation-runoff anticlockwise hysteresis plot in a bi-logarithmic scale of monthly data (right). Colour classification is scaled for a hydrological year (September - August).

Table 2.1. General characteristics of the 7 selected studied catchments at their outlets gauging stations for the indicated period (Min Alt: Minimum altitude; Max Alt: Maximum altitude; A: drainage area; L: main channel length; p: perimeter; S: mean slope; P: Mean annual precipitation; PET: Mean annual evapotranspiration; R: Mean annual runoff).

n°	Catchment	Gauging Station (data period)	Min Alt m asl	Max Alt m asl	A (km ²)	L (km)	p (km)	S %	P mm/yr	PET mm/yr	R mm/yr
1	Piura	Pte. Nacara (1970–2005)	119	3526	4762	96	363	5.7	613	1376	181
2	Chicama	Salinar (1970–2008)	350	4217	3684	98	323	8.5	643	1013	211
3	Casma	S. Tutuma (1970–2005)	71	4769	2567	86	241	9.1	430	769	75
4	San Juan	Conta (1970–2006)	350	5049	3057	116	293	6.9	393	496	119
5	Acari	Bella Union (1970–2008)	70	4620	4242	158	471	6.1	486	715	92
6	Camana	Pte Camana (1970–2006)	122	6300	16238	360	1060	5.4	441	593	137
7	Tambo	Chucarapi (1970–2008)	281	5554	13063	254	820	5.0	418	566	82

b. Anthropogenization

Catchments in the Pd are characterized mainly by arid and semi-arid areas, implying water shortage issues for human consumption in major cities located in arid lowlands and agriculture and industrial activities located throughout catchment. Water supply for economic activities (agriculture, mining, industrial and livestock) and domestic use is about 87% of the national total consumption and agriculture represents the greatest demand (86% of the Pd total consumption), which is based entirely on irrigation infrastructure systems because of little precipitation over arid lands (ANA, 2012). Besides, they are likely to be affected by the devastating effects of floods (ANA, 2012).

This hydraulic infrastructure was built along main catchments since the beginning of the seventies. This development implies the presence of ten large hydraulic systems with irrigation purposes (see their location and names in grey italic in Figure 2.5) and two systems mainly used for population supply and hydroelectricity purposes for the major cities of Lima and Arequipa. Figure 2.5 shows the large hydraulic infrastructure predominant in the studied period, where one system can present only lakes intakes and diversions (not shown for a reason of scale) as in the case of “Tacna” located around latitude 17.5°S; present diversion channels only as in the case of “Chavimochic” and “Chinecas” located around latitude 9°S; present two mega-reservoirs of 1000 Hm³ and 250 Hm³ capacity as in the case of “Chira-Piura” located around latitude 5°S, and present only one mega-reservoir as the general case of around 300 Hm³ capacity. These mega-reservoirs located in

highlands and midlands, and diversion channels are responsible in many cases of huge water transfer from the Atlantic to the Pacific drainage basins (see Figure 2.5 for the cities of Lima and Ica). However, in some cases, this infrastructure has an influence restricted to areas located downstream of the hydrological stations and does not have relevant impacts over the water balance upstream of these stations.

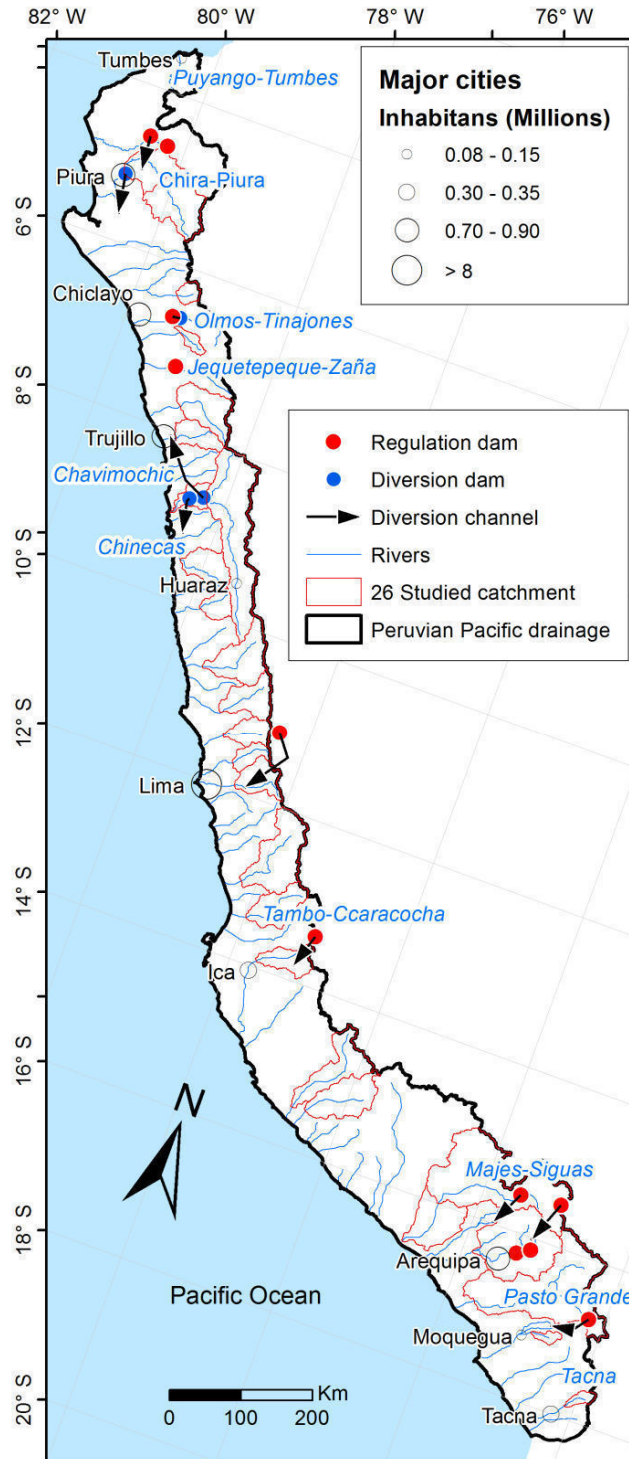


Figure 2.5. Location of major cities and main large hydraulic infrastructures (names of hydraulic systems in italic blue) built between 1970 and 2008.

2.2. Data

The database covers in general the 1964–2011 period and includes monthly precipitation, temperature and streamflow observations. The period differs from one variable to another because of availability. Here it is explained, as well as the methods for database homogenization and validation. All analyses have been carried out considering the hydrological year over the Pd from September to August.

2.2.1. Precipitation

The database includes monthly precipitation records from 139 meteorological stations managed by the SENAMHI (National Meteorological and Hydrological Service of Peru) and 6 meteorological stations managed by the INAMHI (National Meteorological and Hydrological Institute of Ecuador). It was necessary to extend the area into the foothills of the northern Andes, which cover bi-national river watersheds between Peru and Ecuador. Monthly precipitation data are available over 1964–2011 period. Over the 145 stations, 124 stations are located in the Pd region (see Figure 2.6) and 11 belong to the Peruvian Atlantic drainage and 4 to the Titicaca drainage. Because of this latitudinal and altitudinal dispersion (see Figure 2.6), we proposed a standard process for data quality assessment, data completion and homogenization processes.

A careful quality check of this data was performed using the Regional Vector Methodology (Brunet-Moret, 1979), which consists in assuming that for the same climatic zone under the same precipitation regime, the annual precipitation is proportional in-between stations, with a little random variation due to rain distribution in the zone (Espinoza *et al.*, 2009), defining a homogenous region. Then, it was completed the series and obtained a representative time series for each region. The algorithm is briefly described below:

- 1) Identification of Regional Vectors by considering the statistical and hydrographic criteria (elevation, watershed boundaries, latitude). Here, we used a linear correlation between the Regional Vector obtained and the series of months to complete.
- 2) If a significant correlation is not reached, we conducted an analysis of linear correlation between the stations of a region for a given month.
- 3) If a significant correlation is not reached at level 2, the monthly hyetographs between neighboring stations of a region are compared and the missing monthly data are gap-filled.
- 4) Finally, in the case of a normal event (i.e. not El Niño event), we reconstructed the series replacing each monthly precipitation value by the corresponding interannual mean monthly value calculated for all the period (including an arbitrary small noise on the mean and standard deviation of the value).
- 5) Otherwise, it is not recommended to complete the missing months.

In this dataset containing 145 stations records, 76% of them present more than 45 years of continuous records, 20% of them between 20 and 45 years of continuous records and only 4% of them between 15 and 20 years of continuous records (see Figure 2.6).

For water and energy balance analysis over the Pd catchments (see Chapter 4), lumped precipitation time series at basin-scale were computed. Precipitation was interpolated to a 5 x 5 km grid using the inverse distance weighting technique. Orographic effects on precipitation were accounted for using the SRTM digital elevation model in a similar way as described in Ruelland et al. (2014). These effects on precipitation were considered using the approach proposed by Valéry et al. (2010) with a correction factor of $4 \times 10^{-4} \text{ m}^{-1}$ (estimated from the observed data), which corresponds to a 20% increase in local precipitation with an elevation of 500 m.

2.2.2. Temperature and evapotranspiration

Temperature series were obtained from 59 meteorological stations (see Figure 2.6) managed by the SENAMHI for the 1970–2008 available period. A careful quality check of these data was performed. Mean monthly temperature data were homogenized and validated following Lavado et al. (2013). Missing values were filled by monthly average and by a multiple correlation method based on nearby geographical stations data.

Also lumped temperature time series were computed at basin-scale for water and energy balance analysis over the Pd catchments. Temperature data were interpolated to a 5 x 5 km grid using the inverse distance weighting technique. Orographic effects on temperature are notorious and they were accounted for using the SRTM digital elevation model in a similar way as described in Ruelland et al. (2014). These effects on precipitation were considered using the approach proposed by Valéry et al. (2010) with a constant lapse rate of $-6.5^\circ\text{C}/\text{km}$ (estimated from the observed data). Finally, since the only data available for calculating potential evapotranspiration (PET) were temperature data, a formula relying on clear monthly sky solar radiation and mean monthly air temperature was selected (Oudin et al. 2005):

$$\begin{aligned} PET &= \frac{R_e T + K_2}{\lambda \rho K_1} \text{ if } T + K_2 > 0 \\ PET &= 0, \text{ otherwise} \end{aligned} \quad (2.1)$$

where PET is the rate of potential evapotranspiration (mm/d), R_e is the extraterrestrial radiation ($\text{MJ}/\text{m}^2/\text{d}$), λ is the latent heat flux ($2.45 \text{ MJ}/\text{kg}$), ρ is the density of water (kg/m^3), T is the mean daily air temperature ($^\circ\text{C}$) and K_1 and K_2 are fitted parameters (for a general case: $K_1 \sim 100$ and $K_2 \sim 5$). Equation 2.1 was applied at monthly time step. The Oudin formula is a temperature-based evapotranspiration model, which is adapted to arid and semi-arid regions limited by scarcity of in-situ climate data (see e.g. Hublart et al. 2015; 2016). Indeed, Oudin et al. (2005) showed that from an operational point of view, this model is as efficient as more complex models such as the Penman model (Penman, 1948) and its variants.

2.2.3. Streamflow

Monthly streamflow were obtained from 35 hydrological stations managed by the SENAMHI. Monthly streamflow data were homogenized and validated considering the approaches of regionalization between neighbouring catchments (Lavado et al. 2012). Missing values (less than 5% of total) were filled by monthly average considering also the points 4 and 5 of Section 2.1 about the occurrence of ENSO events. Finally, for a basin scale analysis the study was restricted to 26 catchments (see Figure 2.6) characterized by a valuable and confident complete dataset of monthly precipitation, temperature and streamflow series over 1970–2008.

Table 2.2. General characteristics of the 26 studied catchments at their outlets gauging stations for the 1970–2008 period (Lat: latitude; Long: longitude; A: drainage area; Min Alt: minimum altitude; Max Alt: maximum altitude S: mean slope; Mean annual values of Q: streamflow; Qsp: specific runoff).

n°	Catchment	Gauging Station	Lat °S	Long °W	A (km ²)	Min Alt m asl	Max Alt m asl	S %	Q m ³ /s	Qsp l/s/km ²
1	Piura up	Pte. Ñacara	5.11	80.17	4762	119	3526	5.7	27.4	5.7
2	Piura	Pte. Sanchez Cerro	5.18	80.62	7622	23	3547	3.6	51.3	6.7
3	La Leche	Puchaca	6.38	79.47	771	355	3982	9.3	6.1	7.9
4	Zaña	Batan	6.8	79.29	664	260	3799	7.9	7.7	11.6
5	Chicama	Salinar	7.67	78.97	3684	350	4217	8.5	24.7	6.7
6	Moche	Quirihuac	8.08	78.87	1883	200	4238	9.2	8.1	4.3
7	Santa up	Condorcerro	8.65	78.25	1041	450	6567	8.1	142.2	13.7
8	Santa	Pte. Carretera	8.97	78.63	1166	18	6567	7.7	200.1	17.2
9	Casma	Sector Tutuma	9.48	78.3	2567	71	4769	9.1	6.1	2.4
10	Huarmey	Puente Huamba	9.97	77.87	1329	555	4742	8.3	5.4	4.0
11	Pativilca	Yanapampa	10.67	77.58	4196	800	5941	8.4	41.6	9.9
12	Huaura	Sayan	11.12	77.18	2893	650	5348	7.0	28.1	9.7
13	Ch. Huaral	Santo Domingo	11.38	77.05	1856	697	5122	7.7	17.8	9.6
14	Chillon	Larancocha	11.68	76.8	1207	1200	5099	8.6	6.3	5.2
15	Rimac	Chosica	11.93	76.69	2352	906	5370	7.2	31.5	13.4
16	Cañete	Socsi	13.03	76.2	5845	330	5632	6.7	54.5	9.3
17	San Juan	Conta	13.45	75.98	3057	350	5049	6.9	11.5	3.8
18	Ica	La Achirana	13.97	75.68	2119	500	4591	5.7	7.2	3.4
19	Acari	Bella Union	15.48	74.63	4242	70	4620	6.1	12.4	2.9
20	Yauca	Puente Jaqui	15.48	74.45	4140	214	4923	6.8	9.7	2.3
21	Majes	Huatiapa	16.0	72.47	13414	699	6300	5.4	85.5	6.4
22	Camana	Pte. Camana	16.6	72.73	16238	122	6300	5.4	70.7	4.4
23	Chili	Puente del diablo	16.42	71.87	8393	2360	5954	4.3	13.3	1.6
24	Tambo	Chucarapi	16.99	71.64	13063	281	5554	5.0	33.9	2.6
25	Moquegua	Chivaya	17.13	70.83	469	2000	5279	5.8	1.0	2.0
26	Caplina	Aguas Calientes	17.85	70.12	548	130	5522	7.7	0.8	1.5

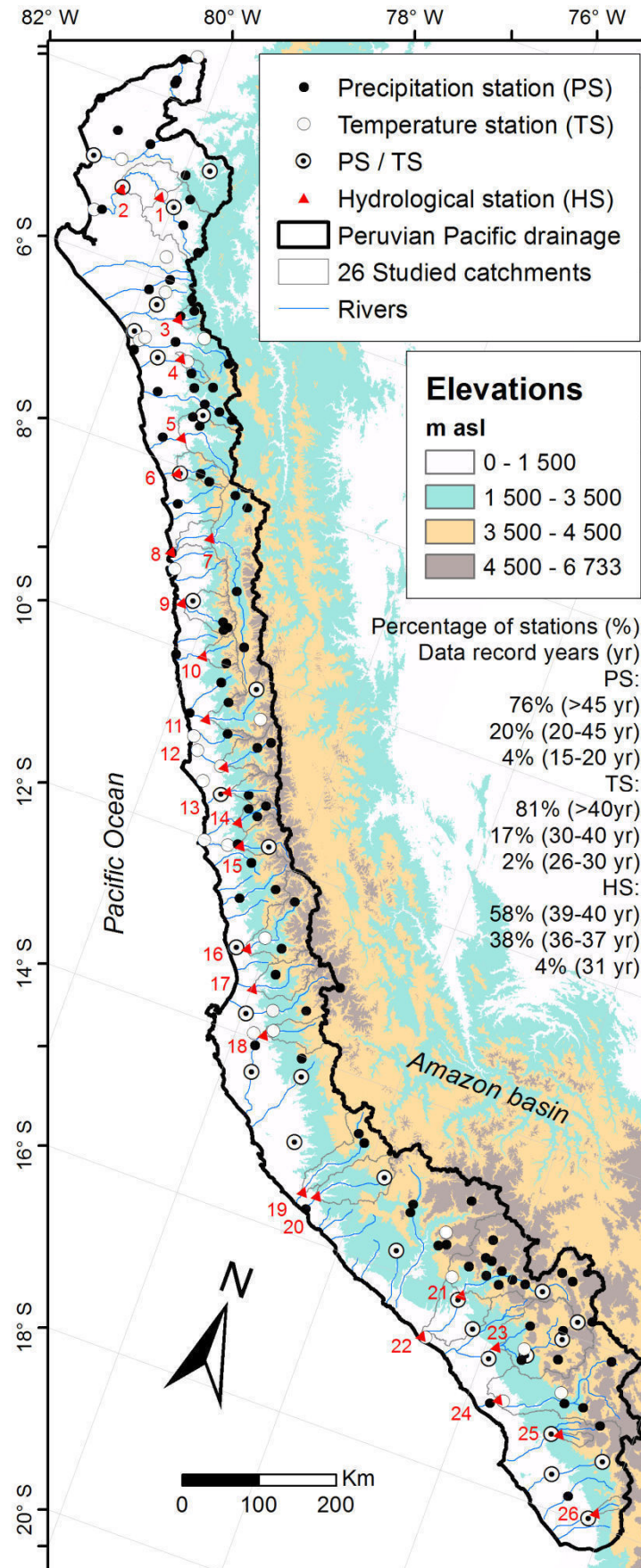


Figure 2.6. Spatial distribution of hydrometeorological stations over a SRTM digital elevation model.

2.2.4. Climatic indices

a. ENSO indices

We used classical monthly ENSO indices (Kiem and Franks, 2001) derived from databases of the NOAA (Climate Prediction Center): SST 1+2 (NINO 1+2), SST 3 (NINO 3), SST 4 (NINO 4), SST 3.4 (NINO 3.4) and SOI (Southern Oscillation Index). Non-standardized monthly anomalies were computed. Former studies showed that there is a close relationship between the development of El Niño and a SOI fall (negative values) and an increase (positive values) of SST indices (Lagos et Buizer, 1992; Lagos *et al.*, 2008; Lavado *et al.*, 2013). Kiem and Franks (2001) mention two methods for identifying ENSO events. The first method consists in identifying the years when the SOI is above or below its average value for a minimum period of 5 consecutive months. The second method is the same as the first method but using indices based on SST anomalies instead of the SOI index.

Whereas these indices are commonly used for ENSO impact studies, they are not completely appropriate for characterizing the different types of El Niño that has been documented in recent years (Ashock *et al.*, 2007; Kug *et al.*, 2009). In a recent study (Takahashi *et al.*, 2011), two new indices were proposed, the so-called E and C indices that can describe two regimes of variability accounting for extreme warm events (or EP El Niño) and moderate events (La Niña and CP El Niño). These indices are by construction independent (orthogonal) and they are comparable to the SST1+2 and SST4 indices respectively (see Figure 2.2). The E index accounts for the SST variability in the far eastern Pacific and captures very clearly the two strong El Niño over the data record used in this study, namely the 1982/1983 and 1997/98 extreme El Niño. Therefore correlation analysis using this index will emphasize the relationship for extreme events.

Also, we used global values of *in-situ* monthly SST obtained from the Hadley Centre Global Sea Ice and Sea Surface Temperature (HadISST) data set (Rayner *et al.*, 2003) over 1964–2011 time interval at 150°E–0°, 25°S–25°N of the Pacific and Atlantic basins (<http://www.metoffice.gov.uk/hadobs/hadisst/data/download.html>) available on a 1°x1° grid. The evaluation of the relationship between precipitation variability and Tropical Pacific SST was conducted by using the two oceanic indices explained (the E and C indices).

b. MJO index and Kelvin waves

In this study, we used an MJO activity index following the method by Wheeler and Kiladis (1999) which consists in extracting the energy bivariate space–time spectral analysis (Hayashi, 1982) of outgoing long wave radiation (OLR) in the frequency-space domain of the MJO over the tropical belt. The MJO-filtered time series are then used to define a MJO activity index by taking the variance over a 3-month running

window and averaging over the region where its variability peaks. Typically, a MJO activity index is defined by averaging over the western central Pacific along the equator (5°S–5°N; 120°–180°E) (McPhaden *et al.*, 2006; Gushchina and Dewitte, 2012). It was chosen here to remove the annual cycle by a wavelet multiresolution filtering (Labat *et al.*, 2000). Summarizing the MJO activity index used in the paper accounts for the periods when there is an enhanced or reduced variability of the MJO. When this index is larger than usual (positive anomaly), this means that more high-frequency fluctuations of tropical Pacific origin may reach the Peru coast and lead to precipitation anomalies on average along the coast.

In this study, an IntraEKW cumulative index is defined that is aimed at quantifying the integrated effect of an IntraEKW along the coast. The concept is similar to cumulative upwelling index defined by Bograd *et al.* (2009) but for the oceanic Kelvin wave is based on the idea that, whereas a downwelling IntraEKW will favor a warming along the coast, the opposite phase (upwelling) will induce cooler conditions along the coast, not favorable for precipitation. Over a year, the cumulative effect of the IntraEKW can be estimated by considering the integration of the skewness of the IntraEKW over the period that encompasses the Austral summer season (i.e. when IntraEKW activity usually peaks, cf. Dewitte *et al.* (2011)). This index is therefore defined as:

$$C_{EKW}^n(y) = \int_{D-6}^{D+6} \left(\text{IntraEKW}^n(x = 90^\circ W, t) \right)^3 .dt \quad (2.2)$$

where D is the month of December of the year y, t is in days and n refers to the type of the waves. Two types of waves will be considered here that differs from their vertical structure and phase speeds along the equator. These waves, that are the most energetic waves in the equatorial Pacific, will be referred to as n=1 or n=2 waves (i.e. EKW1 and EKW2). Note that the C_{EKW}^1 (hereafter Akm1) and C_{EKW}^2 (hereafter Akm2) indices also reflects the ENSO amplitude and evolution at basin scale because intraEKW is linked to ENSO (Hendon *et al.*, 2007; Gushchina and Dewitte, 2012).

The intraEKWs are derived from an oceanic Reanalysis (SODA) over the period 1958–2008. The method consists in projecting the zonal current and pressure anomaly field on the theoretical wave structures as estimated from the mean stratification of the oceanic Reanalysis. Details on the method can be found in Dewitte *et al.* (2008).

We work with the 10 indices described above (see table 2.3 for a summary). However considering the inter-relationship between indices, we focused on 5 indices that exhibit significant correlation with precipitation fluctuations. Please note that many of the results presented in this thesis correspond to the yearly-averaged data, from September to February for the ENSO indices.

Table 2.3. Description of ENSO indices used in the study

Name	Methods	Aims	Data sources	References
SST1+2 SST3 SST3.4 SST4	Averaged SST over Tropical Pacific sectors	Characterizing the El Niño with classical indices	ERSST.V3B	Kiem A. and Franks S (2001)
SOI	Based on pressure level differences between Tahiti and Darwin locations in the Tropical Pacific.	Characterizing the El Niño Canonical	NOAA	Rasmusson and Carpenter (1982)
E/C	Based on the first two EOF modes of SST in the tropical Pacific	Characterizing the two types of El Niño	HadiSST	Takahashi <i>et al.</i> (2011)
MJO	Wavelength-frequency (w-k) decomposition and recomposition in the MJO w-k domain	Characterizing regional atmospheric circulations related to MJO	NCEP/NCAR Reanalysis	Wheeler and Kiladis (1999)
Akm1/Akm2	Two baroclinic modes, Akm1 and Akm2 are considered as the most energetic Kelvin waves	Characterizing oceanographic conditions related to El Niño and coastal SST anomalous conditions	Simple Ocean Data Assimilation (SODA) Reanalysis	Dewitte <i>et al.</i> (2008)

Chapter 3

Precipitation regime

This chapter presents the results obtained in the first part of the published paper entitled: “Regionalization of rainfall over the Peruvian Pacific slope and coast” submitted to *International Journal of Climatology* in January 16, 2015, accepted in January 21, 2016 (<http://dx.doi.org/10.1002/joc.4693>) and published in an issue in January 2, 2017 (Rau et al., 2017a, see Annex A.1).

This chapter is organized as follows: it starts by a theoretical background in section 3.1, a methodology part in section 3.2, results and discussion in section 3.3 and conclusions in section 3.4.

Chapter highlights:

- A proposed methodology for regionalization of precipitation under non-stationary and/or non-Gaussian time-series condition based on k-means clustering and regional vector methodologies.
 - Nine identified regions of homogeneous precipitation regimes following a latitudinal and altitudinal gradient over the study area.
 - Generation and characterization of the interannual precipitation regime for the first time over the Peruvian Pacific drainage.
-

3.1. Theoretical background

Documenting the heterogeneity of precipitation regimes is a prerequisite for water resources management, mitigation of risks associated with extremes weather events and for impact studies. Although the Peruvian Pacific drainage (hereafter Pd) concentrates more than 50 % of population of Peru, it remains poorly documented in terms of precipitation regionalization. Recent works (Suarez, 2007; Lavado *et al.*, 2012; Ochoa *et al.*, 2014; Bourrel *et al.*, 2015) mostly focused on principal stations or major watersheds. In 1999, a technical report (BCEOM, 1999) proposed a previous precipitation regionalization for the Pd based on the Regional Vector Method - RVM (Brunet-Moret, 1979, see section 2.2.1 in chapter 2 for more

details). In that report, nine regions were delineated mainly located over the northern coastal region.

Multivariate analysis techniques have proved their efficiency to delineate homogeneous regions based on climatic features such as precipitation data. Many authors have used factor analysis, principal components, clustering techniques or a mixture of all these techniques, to define more precisely climatic zones or precipitation regions (e.g. Ünal *et al.*, 2003; Razei *et al.*, 2008), to classify precipitation stations (e.g. Stooksbury and Michaels, 1991; Jackson and Weinand, 1995) and to analyze precipitation variability or distribution patterns (Sneyers *et al.*, 1989; Ramos, 2001; Muñoz-Díaz and Rodrigo, 2004; Dezfuli, 2010). Recently Sönmez and Kömüscü (2011) proposed a precipitation reclassification for Turkey based on k-means methodology highlighting the benefit over prior techniques as regionalization based on topographic and climatic parameters, long-term seasonal precipitation patterns (Türkeş *et al.*, 2002) and hierarchical clustering (Ünal *et al.*, 2003). Sönmez and Kömüscü (2011) in particular indicate that their method is efficient in grasping shifts in time periods. The advantage of using a cluster analysis in the regionalization procedure stands in the fact that precipitation time series may be non-stationary and/or non-Gaussian due to the complex influence of climate phenomena (Takahashi and Dewitte, 2015). For instance, the ENSO has a strong positive asymmetry resulting from the fact that strong extreme events are warm events (An and Jin, 2004; Boucharel *et al.*, 2011), resulting in a non-Gaussian distribution of most historical indices (Boucharel *et al.*, 2009). Such non-linearity in the large scale circulation over the tropical Pacific is likely to influence the precipitation over the Pd, which calls for refining regionalization procedures just based on linear techniques (e.g. RVM).

The main motivation in this chapter is to estimate the improvement brought to precipitation regionalization by applying a hybrid procedure consisting of a combination of two widely used techniques: k-means clustering (Hartigan and Wong, 1979) to obtain a coarse regionalization that is used as first guess in the regionalization using the Regional Vector Method (RVM). The identified regions are also aimed at being used for ecological and water resources management and easing the interpretation of the manifestation of the main climatic modes in the region as described in Muñoz-Díaz and Rodrigo (2004), Sönmez and Kömüscü (2011) and Parracho *et al.* (2015).

3.2. Methods

The regionalization methodology is composed of three steps summarized in Figure 3.1. The first one corresponds to the reviewing of precipitation data, their homogenization by RVM, and the filling of missing monthly precipitation data; the second one corresponds to the regionalization process including k-means clustering and RVM analysis using an iterative process by trial and error with the goal of searching regions that present similar annual precipitation amount and interannual variability; and the last one corresponds to a detailed characterization of the precipitation regime in each region in response to climate variability at seasonal and interannual time scales.

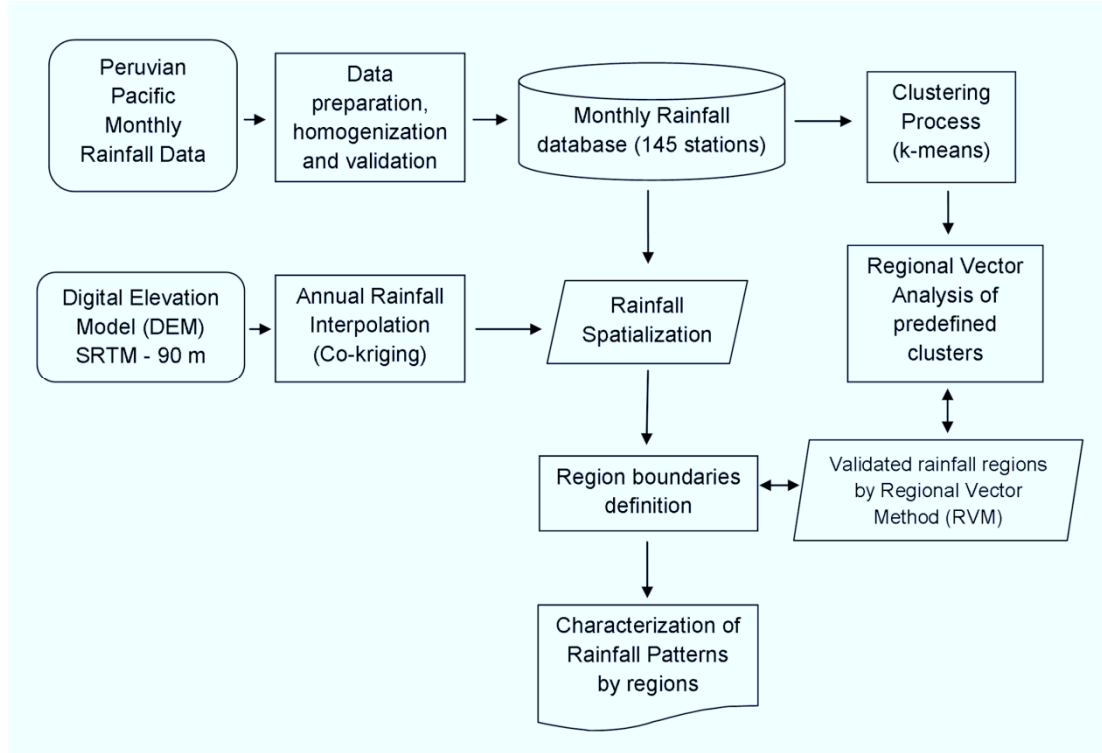


Figure 3.1. Schematic of the methodological steps for the regionalization of the precipitation time series.

3.2.1. Data homogenization and validation

It was carried out in three steps:

1) The analysis period was chosen to be as long as possible for a significant number of stations over the Pd and complementary stations presented in data section. We also impose that the selected stations should have at least continuous records longer than 15 years.

2) To evaluate the homogeneity of datasets for identifying inconsistent information in terms of quality issues as: station microenvironment, instrumentation, variations in time and position (Changnon and Kenneth, 2006); we used here the RVM. It relies on the principle of annual precipitation proportionality between neighbouring stations represented as precipitation indexes which characterize the precipitation pattern of a predetermined area. The RVM is based on the calculation of an extended precipitation vector within the study period. This concept refers to the calculation of a weighted average of precipitation anomalies for each station, overcoming the effects of stations with extreme and low values of precipitation. Then, the regional annual pluviometric indices Z_i and the extended average precipitation P_j are found by using the least squares technique. This could be obtained by minimizing the sum of Equation 3.1.

$$\sum_{i=1}^N \sum_{j=1}^M \left(\frac{P_{ij}}{P_j} - Z_i \right) \quad (3.1)$$

Where i is the year index, j the station index, N the number of years, and M the number of stations. P_{ij} stands for the annual precipitation in the station j , year i ; P_j is the extended average precipitation period of N years; and finally, Z_i is the regional pluviometric index of year i . The complete set of Z_i values over the entire period is known as “regional annual pluviometric indexes vector”. Being an iterative process, this method allows to calculate the vector of each of the predefined regions, then provides a stations - vector interannual variability comparison, for finally discards those that are not consistent with the regional vector (RV). This process is repeated as much as necessary. See more details of this method in Espinoza *et al.* (2009).

3) For the stations that were selected during the homogenization process and also had missing monthly data, once their spatial representation proved significant, were subjected to a process of information completion. In this case, this procedure was performed using the values of precipitation index calculated from the RV and the mean value of precipitation monthly data of the concerned station. A more detailed description can be found in Bourrel *et al.* (2015).

Through these three stages, 145 pluviometric stations were validated. The geographical location of the 124 stations over the Pd is depicted in Figure 2.3.

3.2.2. Classification and Regionalization Process

In this section, we describe the regionalization process using the RVM approach, which required a first guess to initialize the process. In this study, this first guess is obtained performing a k-means clustering as a classification of precipitation data from the stations selected in 3.1.

a. K-means clustering technique

K-means clustering is a statistical technique designed to assign objects to a fixed number of groups (clusters) based on a set of specified variables. One of the principal advantages of k-means technique consists in its cluster's identifying performance which allows ranking the obtained clusters as a function of their representativeness. The process involves a partitioning schema into k different clusters previously defined. Objects that are within those k clusters must be as similar as possible to those that belongs to its own group and completely dissimilar to the objects that are in the other clusters. Similarity depends on correlation, average difference or another type of metrics. By definition each cluster is characterized by its own centroid with the cluster members located all around it. The algorithm used at annual precipitation timescale was the Hartigan-Wong which adopts the squared Euclidean distance as a dissimilarity measurement. See more details of this method in Hartigan and Wong (1979).

A key part of the k-means application is to define an optimum number of clusters. In order to succeed in the definition of partitioning groups, an estimation of the

silhouette number must be performed for each desired number of groups. The silhouette width is used to evaluate the statistical significance of each identified cluster (Rousseeuw, 1987). The silhouette value is obtained following Rousseeuw (1987) as:

$$S(i) = \frac{\min\{b(i,k)\} - a(i)}{\max\{a(i), \min\{b(i,k)\}\}} \quad (3.2)$$

Where: $a(i)$ corresponds to the average similarity between the i th object and the other objects of the same group and $b(i,k)$ is the average similarity between the i th object and the members of the k th clusters. The range of variation for this silhouette index is between -1 and +1, when the silhouette value is close to +1 means that there is a better member correspondence to its own cluster, while a negative value represents the object this is not well located in the appropriate cluster. Meanwhile the value of 0 means that objects could belong to any k cluster. We also computed an average silhouette width for the whole k clusters which represents the mean of $S(i)$, and it can be used to choose the best number of clusters, by taking the value of k for which $S(i)$ is maximal.

b. Regionalization Analysis

There are classical ways to predefine regions; it can be based on stations proximity and homogeneity, physiographic patterns or topographical constraints related to isohyets (Espinoza *et al.*, 2009; Bourrel *et al.*, 2015). Here, precipitation stations grouped by k-means clustering are set up as predefined regions. The criteria for using k-means clustering as first step of regionalization is based on the advantages in time solving and the preset number of groups at the beginning of the process whilst RVM requires defining the stations grouped into a predefined region, being a long and exhaustive methodology if it is not provided an accurate number of groups.

Regionalization was performed using the RVM, which is generally oriented to: a) assess precipitation data quality based on the homogeneity within a predetermined region (Espinoza *et al.*, 2009) and b) achieve precipitation regionalization processes (establishment of representative vectors of homogeneous precipitation zones) to gather the stations exhibiting the same interannual variability. The process for regionalization is similar to the process explained in section 3.2.1 (item 2). It depends on the computation of a “mean station” or “vector” from all data involved in the study area that will be compared with each pluviometric station (Brunet-Moret, 1979). Prior to the use of the RVM, it is necessary to group stations into predefined regions.

Once calculated, the RV is compared iteratively with data station for discarding those stations whose data are not consistent with the RV and reprise the process. The rejection of a given station could mean that this station belongs to a

neighbouring region that could present greater consistency. Therefore in many cases, stations or areas are re-grouped or divided in order to obtain regions that show homogeneous features. The main statistical criteria for regrouping stations into homogeneous regions are based on thresholds applied to the standard deviation of the differences between annual pluviometric indices of stations and the RV indices; and to the correlation coefficient between RV and annual pluviometric values of stations. These thresholds are fixed to the standard deviation lower than 0.4 and correlation coefficient greater than 0.7. Precipitation database management and RVM were carried out using the HYDRACCESS software (Vauchel, 2005).

c. Precipitation data interpolation

After regionalization based on punctual information (i.e. precipitation stations), we did a precipitation spatialization by isohyets allowing to delimit polygonal regions. Annual precipitation was interpolated incorporating elevation data using the co-kriging classical geostatistical approach, which is widely used in the hydrometeorological field (Goovaerts, 2000; Diodato, 2005; Buytaert *et al.*, 2006). Co-kriging, which is a multivariate version of kriging technique, took into account the digital elevation model (DEM) SRTM - 90 m data as correlated secondary information based on a spherical variogram (Goovaerts, 2000; Mair *et al.*, 2011). This precipitation interpolation map was used as a background raster guide for delineating polygonal regions involving the station points grouped with regionalization analysis. These polygons follow the isohyets shape with geometrical approach (perpendicular and bisector criteria of boundaries of regions traversing isohyets and stations) and a statistical approach (revalidation of new defined areas with the RVM with proper fit of stations inside each region).

Finally, representative monthly precipitation time series of each region were obtained with the co-kriging methodology because of better performance than other techniques (e.g. Thiessen Polygons, Inverse Distance Weighted and Kriging) over mountains areas (Hevesi *et al.*, 1992a, 1992b; Goovaerts, 2000; Diodato *et al.*, 2005). Time series were assigned to centroids as representative points for obtain mean latitude, longitude and altitude of each region.

3.3. Results and discussion

3.3.1. Precipitation Classification

A cluster analysis of the annual precipitation data was performed by applying k-means technique on the 124 precipitation stations previously selected. The optimal value for the cluster numbers was determined by an average silhouette value and a negative silhouette number for a number of clusters varying from 3 to 10 (see Table 3.1).

Maximum silhouette values are obtained for cluster-three (0.64), cluster-four (0.60) and cluster-six (0.55), considering as a reasonable structure a cluster having a silhouette value greater than 0.50 and as a weak structure a silhouette value less than 0.50 following Kononenko and Kukar (2007). The number of negative silhouette values is minimal for cluster-three (6), cluster-four (4) and cluster-six (6). After plotting the cluster groups into a map showing their spatial distribution, we selected the cluster-three and cluster-six among them, as these two clusters show certain arrangement of precipitation stations according to topographical and latitudinal variation (see Figures 3.2a and 3.2b). Cluster-four was an intermediate group that corresponds to one sub-region in the north.

Table 3.1. Results of the k-means analysis for number of clusters varying from 3 to 10.

Number of Clusters	3	4	5	6	7	8	9	10
Average Silhouette Value	0.64	0.60	0.54	0.55	0.54	0.54	0.46	0.45
Negative Silhouette Number	6	4	9	6	8	6	11	9

The two cluster groups (cluster-three and six) exhibit a similar spatial distribution. Pluviometric stations from both groups present an altitudinal distribution along the Pd, defining three regions: the stations located in lowlands (green triangles), in middle altitude basin (white circles) and in highlands (black points). Cluster-six group presents three additional regions, two of them closely related to northern precipitation features for the middle altitude basin (cluster 4 represented by red triangles) and highlands (cluster 6 represented by yellow circles). Two stations are considered as isolated (cluster 5 represented by blue circles).

Even if the cluster-six group is less representative than the cluster-three one in terms of silhouette value, cluster-six group is considered acceptable to represent correctly the variability of northern precipitation, offering an initial classification of precipitation or initial approach of precipitation regionalization over the Pd.

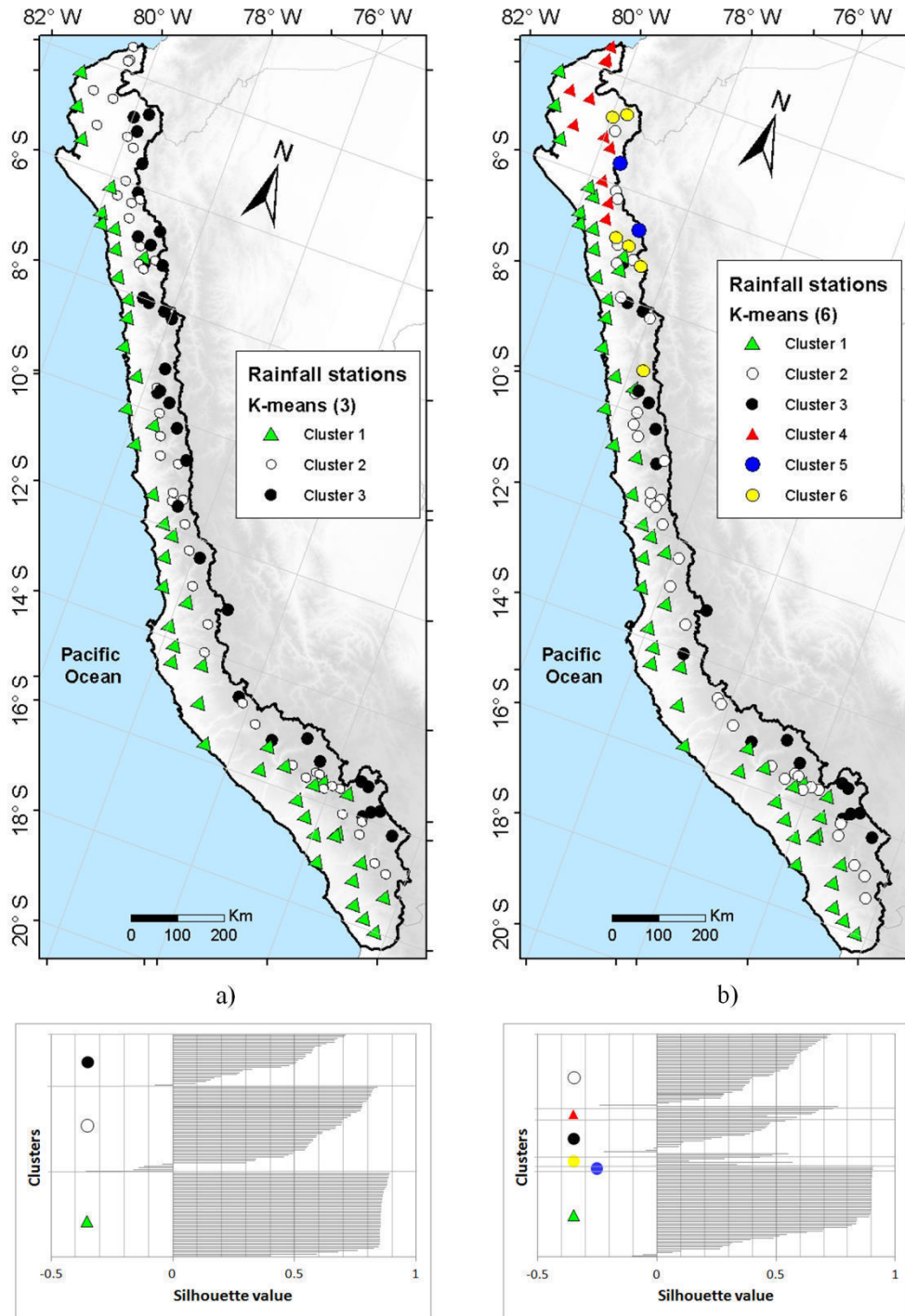


Figure 3.2. Clusters spatial distribution (a) cluster 3 group and (b) cluster 6 group obtained with the k-means process. Silhouette value for each cluster group is provided in the bottom panels.

3.3.2. Regionalization

After cluster definition, the RVM was performed over these preliminary regions using an iterative process by trial and error, which adds and deletes stations from neighbouring

regions considering the criteria described in section 3.2.2b. This process could be also verified by their interannual coefficient of variation (CV). In Figure 3.3, the stations located in the western area of the coast (lowlands) present greater values of CV (> 1.8) than those located in middle altitude basin and in highlands. Northern region presents higher CV values in lowlands and in the middle altitude basin. Highlands present lower CV values (< 0.8) along the Pacific slope independently of the latitude.

High CV values in the northern region correspond to strong interannual precipitation variability with anomalies greater than 1000 mm/yr. High CV values are also observed along southern latitude which are mostly caused by small values around the near zero annual average. These values are due to the large-scale mid tropospheric subsidence over the southeastern subtropical Pacific Ocean, enhanced by the coastal upwelling of cold water (Virji, 1981; Enfield, 1981; Vuille *et al.*, 2000; Garreaud *et al.*, 2002; Lavado *et al.*, 2012).

Based on the iterative process of the RVM, we identified nine homogeneous precipitation patterns (see Figure 3.4). Comparing with the initial cluster groups derived from k-means, precipitation stations from clusters 1, 2 and 4 located in the coastal zone and northern Andes (see Figure 3.2b) exhibit higher coefficients of variation in coastal proximity (see Figure 3.3). Cluster 1 includes the regions 1, 4 and 7 along the coastal zone. Cluster 4 defines region 2: in this case, clustering process successfully assigned each station as well as RV reported them as separate from other regions. Cluster 5 and 6 are regrouped into region 3. Finally, Cluster 3 defines regions 5, 6, 8 and 9: in this case, the low variability, their high altitude as the latitudinal extension, defines these four regions.

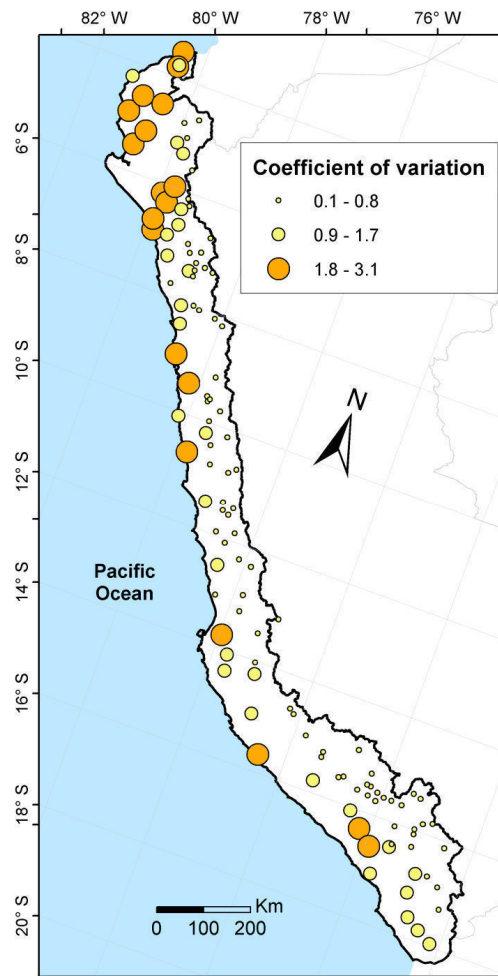


Figure 3.3. Spatial distribution and range of coefficient of variation (CV) for all of the pluviometric stations of the Pd.

K-means methodology and RVM did not provide a final regionalization by their own. For clustering method, some groups are not well defined because of isolated stations to be included in other groups, associated with low silhouette values (see cluster 2 from cluster-three group in Figure 3.2a and cluster 2, 3 and 6 from cluster-six group in Figure 3.2b). This can be explained by the characteristics of the annual precipitation database used, related to the presence of non-globular clusters with a chainlike shape or with not well defined centres (see regions 3, 8 and 9 in Figure 3.4), which are one of the principal disadvantages using this technique (Kaufman and Rousseeuw, 1990). For the RVM, it is possible to obtain grouped regions following only the statistical criteria with the thresholds presented in section 3.2.2b. However there is the risk of increasing computing time and obtaining unrealistic groups because of using only a statistical criteria and not an initial arrangement inferred in this case from the k-means clustering. K-means inferred 3 regions for lowlands, middle altitude basin and highlands (see Figure 3.2b) as a first guess to the final regionalization by the RVM in the north (see regions 1, 2 and 3 in Figure 3.4) and in the south (see regions 7, 8 and 9 in Figure 3.4), which it not was possible to identify using only the RVM. The two-step methodology (k-means and RVM) has also presented a slight improvement in the thresholds of section 3.2.2b with respect to

the thresholds obtained with RVM only, with about +6% for the standard deviation of the differences between annual pluviometric indices of stations and the RV indices (from 0.39 to 0.42); and about +0.5% for the correlation coefficient between RV and annual pluviometric values of stations (from 0.78 to 0.79).

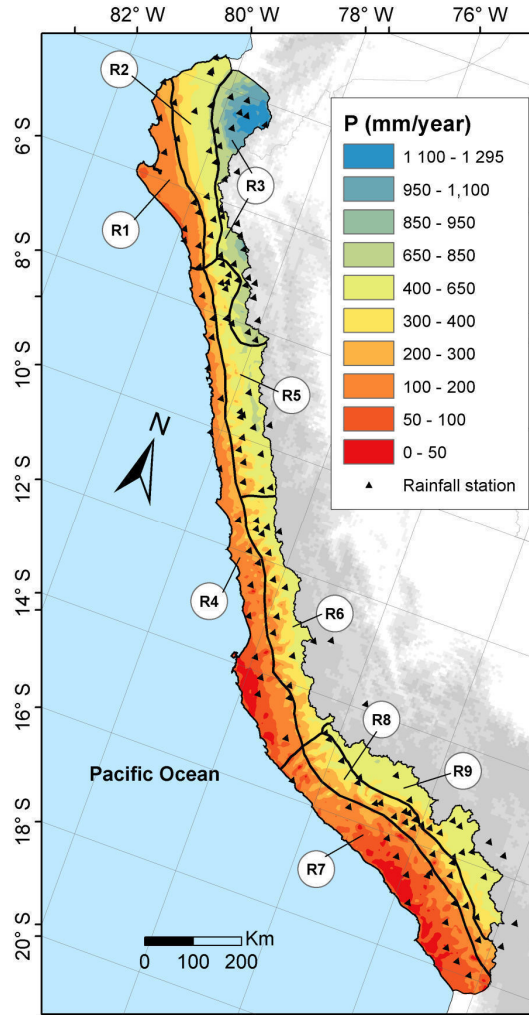


Figure 3.4. The nine homogeneous precipitation regions after the regionalization process of clustering and RVM. Interpolated surface of annual precipitation (isohyets obtained using co-kriging method) is also shown to demonstrate precipitation differences between regions.

Following the approach summarized in the flow chart presented in Figure 3.1 and applying the methodology described in section 3.2.2c; the nine regions were well delineated taking into account the precipitation interpolation map as shown in Figure 3.4. Annual precipitation in each region exhibits a relationship with altitude and latitude, precipitation is higher at low latitudes and at southern latitudes in high altitudes as shown in Figures 3.4 and 3.5.

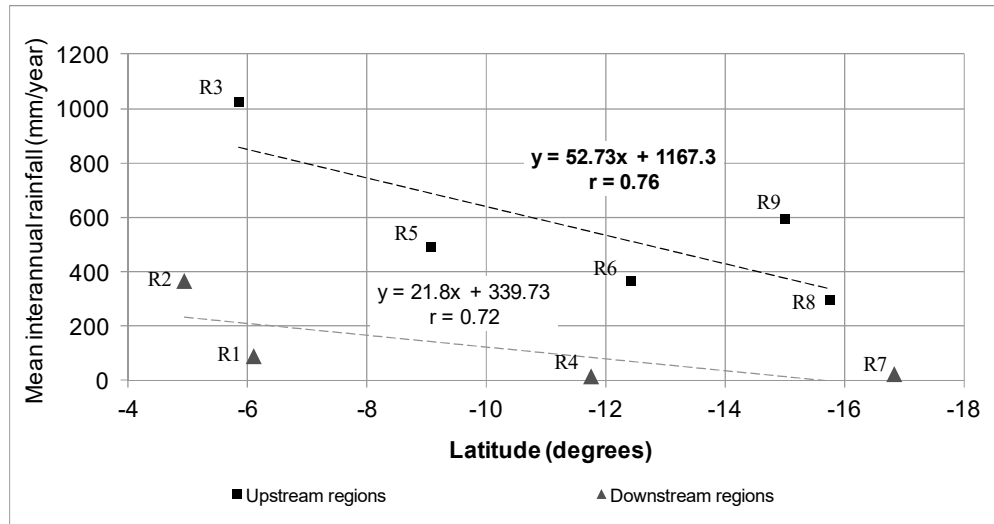


Figure 3.5. Relationship between mean interannual precipitation and latitude for the nine identified regions grouped in upstream and downstream regions. Representation for upstream regions is significant at the 90% level using a Student t-test.

Correlation coefficients between the stations and the regional vector of each region was calculated separately and the spatial distribution of these correlation coefficients is shown in Figure 3.6. The purpose of this analysis is to emphasize the level of representation of the regional vector and identify locally the areas within a region where this vector is more representative. Considering regions 4 and 7, the coefficient of correlation is less than 0.7 and greater than 0.5. These coefficients are considered as acceptable considering the dryer conditions with more than 90% of the precipitation records near zero throughout the year due to hydroclimatic features, where any value greater than zero causes a strong variability reducing the relationship with its RV. For the northern regions 1 and 2, the mean correlation is more than 0.9 being a very good representation of RV and the more representative areas are shown in red coloration. The strong correlation values are due to extreme precipitation events related to ENSO strong events increasing the association level between stations and RV. Regions 3, 5, 6, 8 and 9 located in highlands, have correlations greater than 0.7 being a good representation of the RV with the more representatives areas in orange coloration.

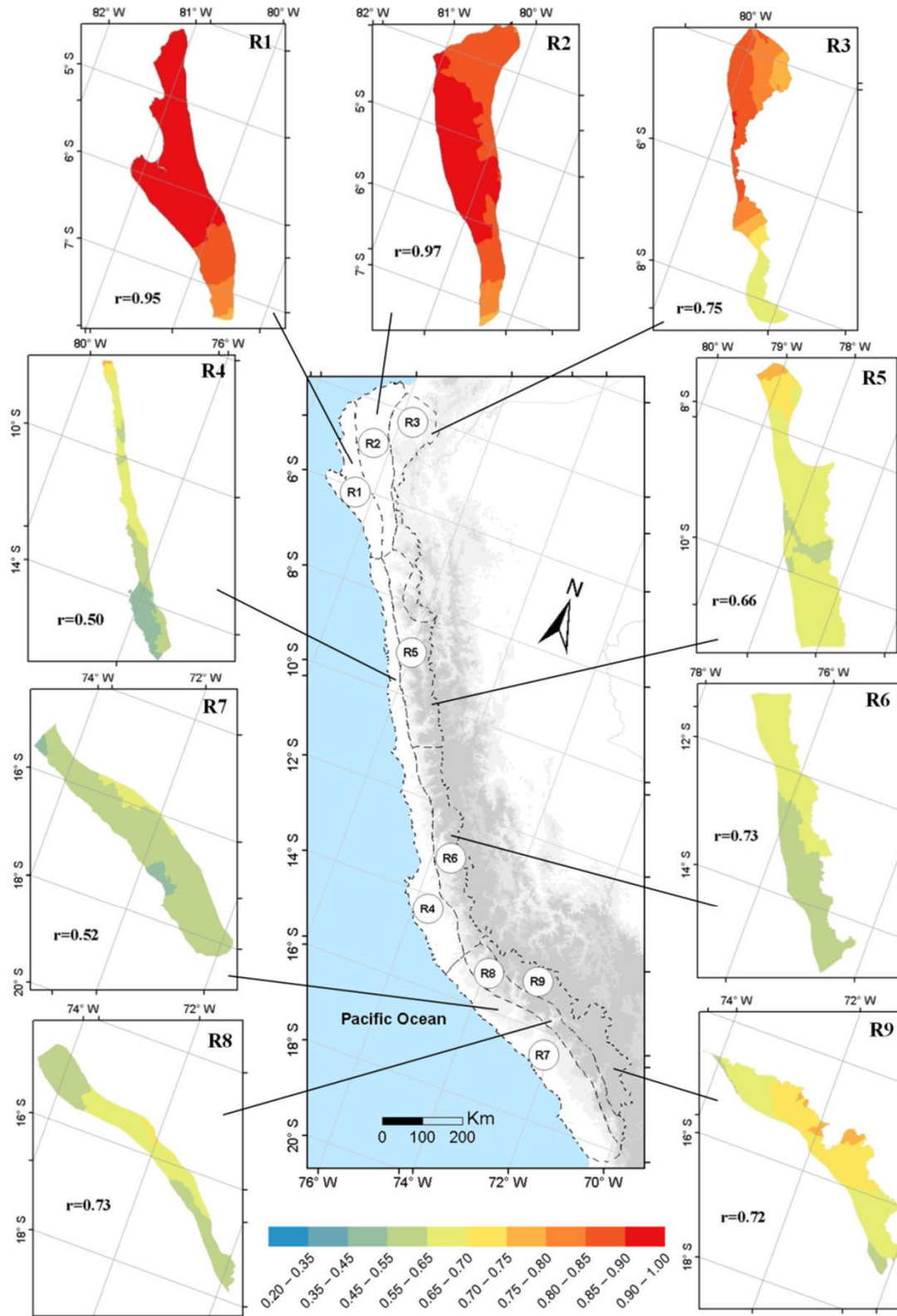


Figure 3.6. Coefficient of correlation related to the regional vector recalculated for each final region. A global value of correlation is also showed by region in bold as well as spatial distribution of correlation with the regional vector.

3.3.3. Regions Characterization

In this section, we documented the precipitation seasonal distribution and interannual variability over the nine identified regions. Some of geographical features (area, latitudinal and altitudinal ranges) are presented in Table 3.2. All regions present a unimodal precipitation seasonal distribution (see Figure 3.7) and differ from their peak calendar month, intensity and duration of the rainy season.

Region 1 extends over northern lowlands including drier areas as the Sechura desert (79°W to 81°W and 5.5°S to 6.5°S) where the average interannual precipitation is about 90 mm/yr. A maximum seasonal precipitation is observed in March (see Figure 3.7a1) with a rainy season from January to May (JFMAM) with values less than 50 mm.month⁻¹ which represent near to 90% of the annual precipitation. The rest of the year is considered as dry due to values near or equal to zero, corroborating the irregularity in the seasonal precipitation pattern (see Figure 3.7a1) and in the interannual variability of monthly precipitation (see Figure 3.7a2) at the coast (Garreaud *et al.*, 2002; Lavado *et al.*, 2012).

Region 2 comprises a large part that belongs to the foothills of the northern Andes covering bi-national river watersheds of Peru and Ecuador. This zone exhibits an irregular seasonal precipitation pattern (see Figure 3.7b1) and an irregular interannual variability of monthly precipitation (see Figure 3.7b2). Average interannual precipitation value is around 370 mm/yr. The wettest period occurs between January and April (JFMA) cumulating near to 90% of total precipitation.

Northern coastal regions as regions 1 and 2 are significantly affected by strong events represented by two peaks reaching 413 mm.month⁻¹ in March 1983 and 299 mm.month⁻¹ in March 1998 for region 1 (see Figure 3.7a2); and 746 mm.month⁻¹ in March 1983 and 708 mm.month⁻¹ in March 1998 for region 2 (see Figure 3.7b2). A summary of precipitation statistics is given in Table 3.2 and a box plot representation of monthly precipitation in Figure 3.8. Outliers from Figure 3.8, represented by small circles, correspond to values exceeding 1.5 times the interquartile range (IQR). All regions have observations that exceed $Q3 + 1.5(IQR)$, however northern coastal regions 1 and 2 differs from the rest for having greater number of outliers values (14% and 17% respectively) with the largest precipitation anomalies reaching 56 and 25 times of mean monthly precipitation for region 1 and 2 respectively. Most of the interannual variability in precipitation, reflected as well in higher CV values (see Table 3.2), is directly due to the occurrence of the strong El Niño events indicating also a high intensity of interannual variability than other regions. This is particularly obvious for region 1 where three extreme precipitation events are observed corresponding to the year 1972, 1982 and 1997, known as strong El Niño years. Interestingly the more inland region 2 exhibits interannual variations of precipitation that does not necessarily corresponds to the strong El Niño years. These events may correspond to local convective events associated with coastal warm oceanic conditions related mainly to Kelvin waves and the Madden and Julian Oscillation (MJO) (Woodman, 1985; Bourrel *et al.*, 2015).

Region 3 covers bi-national river watersheds of Peru and Ecuador bordering with the Amazon Basin by the east. This is also the wettest region (see Figure 3.7c1, 3.7c2 and Figure 3.8). On the other hand, precipitation amount decreases southward with precipitation regularity in the seasonal pattern (see Figure 3.7c1) and in the interannual variability of monthly precipitation (see Figure 3.7c2), with a rainy season from January to April (JFMA) that represents almost 70% of the annual precipitation. Mean interannual precipitation reaches 1024 mm/yr, representing eleven times of the mean interannual precipitation of region 1 and three times of region 2 (see Table 3.2). The precipitation interannual variations are weakly associated with the extreme El Niño events (the correlation between the E index and precipitation is 0.2) but is negatively correlated to the C index ($r=-0.4$) indicating that the R3 region is sensitive to cool enhanced coastal conditions during Central Pacific El Niño events (Bourrel *et al.*, 2015). The inter-events fluctuations are also noticeable which are related to local convective events not related to ENSO but mostly by the ITCZ and the large-scale atmospheric variability associated with the MJO (Tapley and Waylen, 1990; Takahashi, 2004; Bourrel *et al.*, 2015). Also noteworthy, there is an increase of precipitation peaks frequency over the last two decades (see Figure 3.7c2).

Region 4 is the longest region located between the coastal plain and the foothills of the western Andes and contains some of the major coastal cities as the capital Lima. This region corresponds to a zone influenced by the large-scale mid tropospheric subsidence of the southeastern subtropical Pacific Ocean, enhanced by the coastal upwelling of cold water (Vuille *et al.*, 2000; Garreaud *et al.*, 2002; Lavado *et al.*, 2012) without presenting a relationship between strong precipitation peaks and strong ENSO events. Then, mean interannual precipitation reaches a value of 16 mm/yr defining the driest region in the country (see Table 3.2) with precipitation irregularity in the seasonal pattern (see Figure 3.7d1) and in the interannual variability of monthly precipitation (see Figure 3.7d2) very common in coastal regions (see Figure 3.8). The wet period from January to March (JFM) represents near to 75% of the annual precipitation. In the southern part, drier areas are found like the Nazca desert (74.5°W to 75.5°W and 14.5°S to 15.5°S).

Region 5 comprises a border with region 3 and the Amazon Basin by the east. The mean interannual precipitation reaches 492 mm/yr and the wet period occurs between December and April (DJFMA) cumulating near to 80% of total precipitation. No precipitation peaks were identified during strong El Niño events (see Figure 3.7e2) as those in regions 1 and 2, suggesting that precipitation in regions 4 and 5 are likely to be affected by others processes, either local (e.g. coastal SST) or non-local (e.g., dry air transport from the southern region that reduce the precipitation), resulting in a heterogeneous interannual variability of monthly precipitation (see Figure 3.7e2) with a low value of coefficient of variation around 0.3 (see Table 3.2).

Region 6 borders with the Amazon Basin by the east and shows a heterogeneous precipitation pattern without distinguishing any peak corresponding to the strong El Niño events (see Figure 3.7f2). Precipitation distribution is well defined with a rainy season

from December to March (DJFM) that represents near to 85% of the annual precipitation (see Figure 3.7f1) and with a mean interannual precipitation reaching 366 mm/yr.

Region 7 is characterized by lower precipitation regime with a rainy season from January to March (JFM) accounting for 65% of the annual precipitation. Furthermore, this region is one of the driest areas in the country where the interannual precipitation (23 mm/yr) presenting precipitation irregularity in the seasonal pattern (see Figure 3.7g1) and in the interannual variability of monthly precipitation (see Figure 3.7g2). This region could be considered as an extension of region 4, also influenced by the large-scale mid tropospheric subsidence of the southeastern subtropical Pacific Ocean but differing in the increase of precipitation peaks frequency in the last decade unlike region 4 as can be seen in Figure 3.7g2.

Region 8 comprises an area thus belongs to the foothills of the southern Andes. This zone exhibits irregular precipitation in the seasonal pattern (see Figure 3.7h1) and in the interannual variability of monthly precipitation (see Figure 3.7h2). The mean interannual precipitation presents a higher value than region 7, reaching 296 mm/yr. The wettest period occurs between December and March (DJFM) cumulating near to 90% of total precipitation (see Figure 3.7h1).

Finally, region 9 borders with the Titicaca Basin in the south and east and with the Amazon Basin by the east. The mean interannual precipitation reaches 594 mm/yr and the wet period occurs between December and March (DJFM) cumulating near to 80% of total precipitation. Like region 8, region 9 presents a deficit in precipitation during strong El Niño events (see Figure 3.7h2 and 3.7i2). However, unlike region 8, it presents precipitation regularity in the seasonal pattern (see Figure 3.7i1) and in the interannual variability of monthly precipitation (see Figure 3.7i2) associate with a low value of coefficient of variation around 0.2 (see Table 3.2) indicating also the lowest intensity of interannual variability.

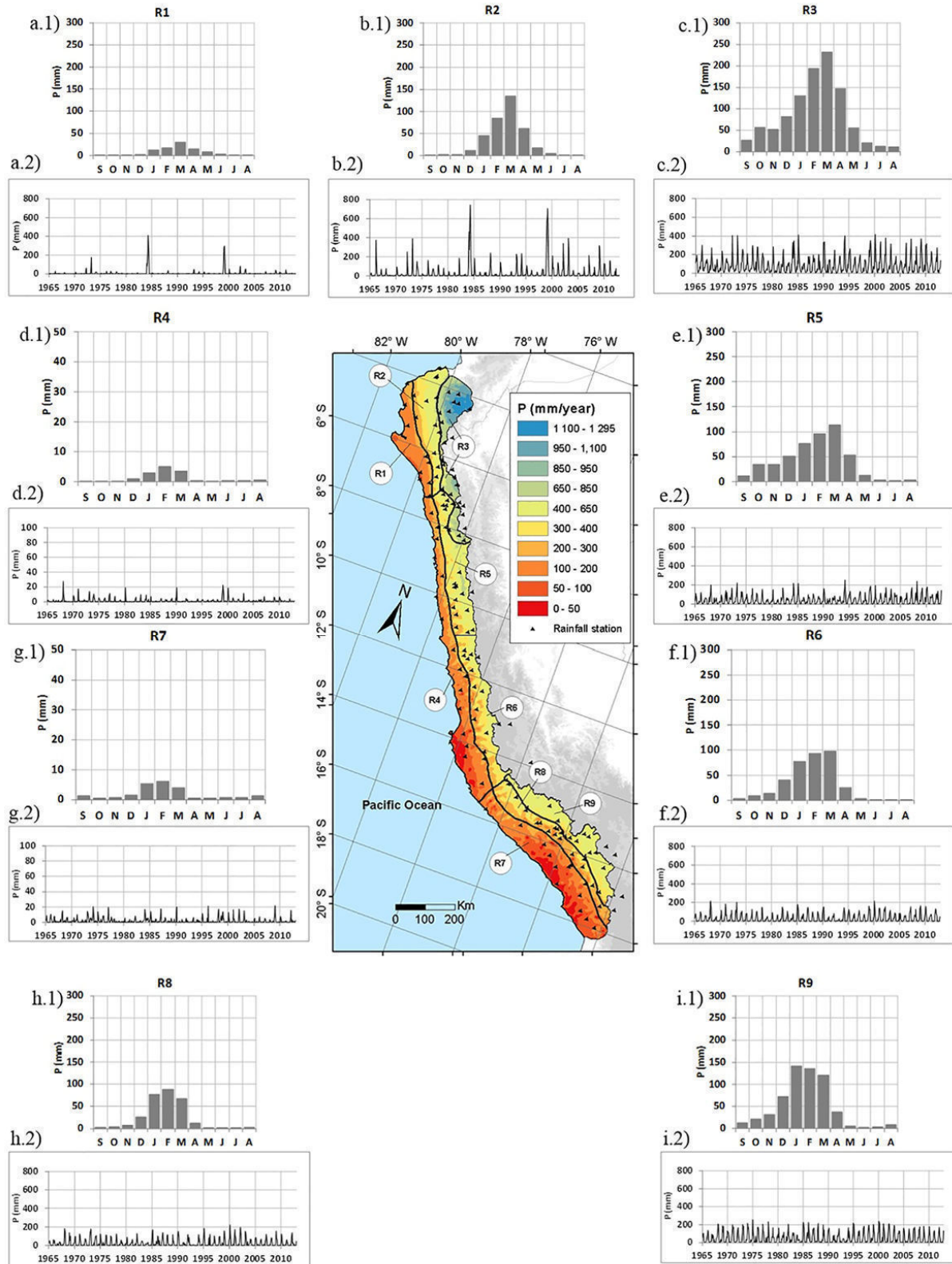


Figure 3.7. Monthly precipitation regime (1964-2011) for the nine identified regions. A precipitation time series is shown by region. Regions 4 and 7 are shown in a different precipitation scale.

Table 3.2. Geographical features and annual precipitation values for the nine identified regions.

Region	Area (km ²)	Altitudinal range (m.asl)	Latitudinal range (°S)	Annual minimum precipitation (mm/yr)	Annual maximum precipitation (mm/yr)	Annual Average precipitation (mm/yr)	CV	Std Dev. (mm/yr)
1	20 300	0-500	4.2-7.3	3.2	1345.2	89.7	2.6	233.3
2	27 600	0-1500	3.4-7.3	17.3	2772.2	366.5	1.5	534.2
3	27 200	1500-3500	3.6-8.3	533.0	1812.9	1023.7	0.3	294.4
4	48 600	0-1500	7.3-15.5	1.6	62.2	15.5	0.7	11.4
5	32 500	1000-5000	7-11	174.1	825.8	492.4	0.3	145.8
6	30 400	2000-5000	11-15	75.0	693.5	365.9	0.4	133.3
7	49 300	0-2500	15.5-18.4	5.1	54.9	23.2	0.6	13.5
8	25 400	2500-4000	14.6-17.8	23.2	528.8	296.1	0.4	111.8
9	30 100	3500-5500	14.4-17.7	220.5	833.2	594.0	0.2	143.2

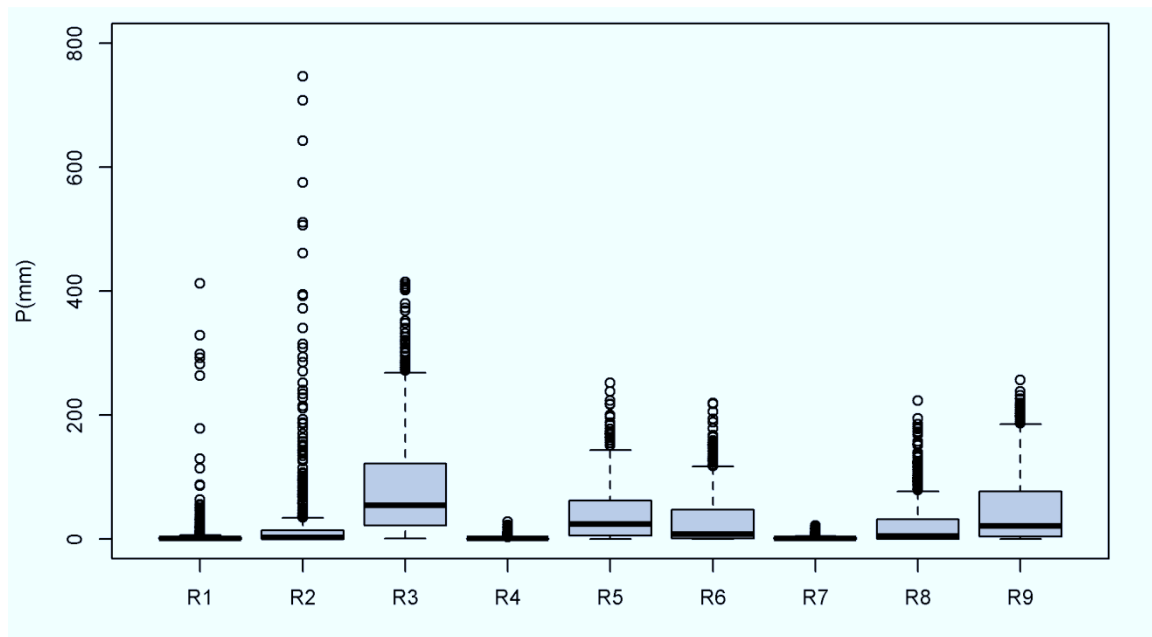


Figure 3.8. Boxplot of monthly precipitation for the nine identified regions.

3.4. Conclusions

This chapter proposes a method for the regionalization of the precipitation in the Pd that consists in a two-step procedure: a preliminary cluster analysis (k-means) followed by the regional vector method (RVM) analysis. Using this procedure, 9 regions were identified so as to depict synthetically the relationship between precipitation variability and altitude and latitude. In particular, precipitation variability is higher at the northern latitudes and decreases to the south in high altitudes. The motivation for performing a classification using cluster analysis prior to the regionalisation by RVM stands in the complex of processes influencing

precipitation variability over this region. In particular, previous studies (Lavado and Espinoza, 2014; Bourrel *et al.*, 2015) have shown that precipitation along the Pd experiences the influence of both type of El Niño, and due to the strong positive skewness of strong El Niño events, the distribution of precipitation data is not Gaussian, limiting to some extents the linear analysis approach (i.e. RVM).

It was verified that the proposed approach leads to a different definition of the regions than an approach based only on RVM; we inferred 3 regions for lowlands, middle altitude basin and highland in the northern and southern Pd, which was not possible to identify using the method based on the RVM only. The k-means clustering analysis allows for a preliminary grouping of station data that is used as a first guess for the RVM and this step constrains to a large extend the regionalization procedure. The proposed two-step methodology also leads to a slight improvement in the thresholds estimate for evaluating the RVM quality.

This product will provide valuable information for hydrological sensitivity analysis over Peruvian Pacific watersheds (through hydrological modelling) for quantifying the effects of climate variability and human activities on runoff with the aim of improving ecological and water resources management. The ENSO/precipitation relationship based on the nine identified regions is discussed in Chapter 6 incorporating other atmospheric and oceanic key indices (cf. Bourrel *et al.*, 2015).

(This page has been left blank intentionally)

Chapter 4

Hydroclimatic balance

This chapter presents the results obtained in the first part of the paper entitled: “Hydroclimatic change disparity of Peruvian Pacific drainage catchments” submitted to *Theoretical and Applied Climatology* in February 12, 2016, accepted in August 23, 2017 (<http://dx.doi.org/10.1007/s00704-017-2263-x>) and published online in September 5, 2017 (Rau et al., 2017b, see Annex A.2).

The chapter is organized as follows: it starts by a theoretical background in section 4.1, a methodology part in section 4.2, results and discussion in section 4.3 and conclusions in section 4.4.

Chapter highlights:

- Identification of 11 from 26 catchments with low water balance disparity based on a hydroclimatic balance with the Budyko theory.
- A first approach of the relationship between anthropogenization, evolution of land cover and low/high water balance disparity.
- Documentation of the annual hydroclimatological regime (i.e. precipitation, temperature, evapotranspiration and runoff) at basin scale for the first time of Peruvian Pacific drainage catchments.

4.1. Theoretical background

Quantifying and deciphering the effects of climate variability and human activities on hydrological regime represent a major challenge, especially at short scales of time and space (Donohue et al. 2007; Wagener et al. 2010). In order to decipher climate variability and anthropogenic influence on water balance, this chapter is based on the Budyko theory (Budyko 1958, 1974). This theory is widely used and is a well-established global empirical framework within the hydrological community (Donohue et al. 2011; Coron et al. 2015; Greve et al. 2015). This method relates the interannual evaporative index (ratio between actual evapotranspiration and precipitation) and the interannual dryness index (ratio between potential evapotranspiration and precipitation) in a global description called the “Budyko

space”. Thereby, all interactions through the hydrological cycle between vegetation, soil and atmosphere create an empirical equilibrium represented by the Budyko curve (van der Velde et al. 2013). To emphasize the impact of other factors on the water balance such as vegetation, an emerging general relationship proposed by Zhang (Zhang et al. 2001) known as the Budyko-Zhang framework has been used. This empirical framework comes from an evaluation of 250 catchments worldwide including dryland regions (Zhang et al. 2001). It has been applied to single catchments and specific areas until nowadays, considering different approaches as the assessment of their sensitivity to climate change (Donohue et al. 2011; Renner et al. 2012; van der Velde et al. 2013). In order to answer properly to the issues raised by the effects of climate change on water resources (Sivapalan et al. 2011), the Budyko curve is recognized “as a much valuable tool to back to the basics, it means, the physical basis of catchment water balance” (Coron et al. 2015).

The degree of anthropogenic influence can be determined using two types of influence on runoff change: human activity with direct influence (soil conservation, water control works, increasing water demand) and human activity with indirect influence (land use and land cover changes) (Wang et al. 2013). They constitute descriptive elements to understand the behaviour of hydroclimatic data series at interannual scale and to identify the catchments presenting a low level of anthropogenization. This selection can be performed through an analysis of water balance disparity by catchment via the Budyko-Zhang framework, which assumes that catchments do not present changes in basin water storage over long-term averages (≥ 10 year) (Zhang et al. 2001). This steady-state assumption is related to a closed land water balance, which is expected to maintain over catchments with a low water balance disparity.

A general hydroclimatic description of the Pd is achieved based on the available time series of precipitation, temperature, evapotranspiration and streamflow. Then the Budyko-Zhang framework is applied to this dataset in order to identify catchments with a low (high) water balance disparity, which are associated with environments with less (more) climatic and human activity influence.

4.2. Methods

4.2.1. Catchment water balance disparity

The water balance for a catchment can be basically described in a general form at annual scale as:

$$P = AET + R + \Delta S \quad (4.1)$$

where P is precipitation (mm/yr), AET is the actual evapotranspiration (mm/yr), R is runoff (mm/yr) and ΔS is the change in basin water storage (mm/yr). At the annual scale, ΔS can be neglected especially for long periods (≥ 10 years) (Zhang et al. 2001).

Based on the Budyko theory (Budyko 1974) which considers that the available energy and water are the primary factors for determining the rate of actual evapotranspiration, the approach developed by Zhang et al. (2001) is used here. It is called the Budyko-Zhang curve, which estimates the AET based on a simple model (see equation 4.2) that writes as follows:

$$\frac{AET}{P} = \frac{1 + w \left(\frac{PET}{P} \right)}{1 + w \left(\frac{PET}{P} \right) + \frac{P}{PET}} \quad (4.2)$$

where PET (mm/yr) is the potential evapotranspiration and w (non-dimensional) is the plant-available water coefficient related to vegetation type. The details of the relationship can be found in Zhang et al. (2001). The very sensitive parameter “ w ” is calibrated over the long-term interannual AET from Equation 4.2. The use of the Budyko-Zhang curve over the Pd appears as a valuable method for the interpretation of the water balance considering the importance of vegetation (Donohue et al. 2007) over arid and semi-arid areas. It has been used previously in comparable studies such as Yang et al. (2009), Zhao et al. (2013) and Chen et al. (2013).

Low disparity of a water balance was evaluated in terms of three criteria: a) the shape of the association of points between dryness index (PET/P) and evaporative index (AET/P), must follows a Budyko-Zhang curve with a positive value of “ w ”, b) the correlation coefficient “ r ” between the AET estimated using the Budyko-Zhang framework and estimated using the water balance ($P-R$) must be higher than 0.7 and c) the relative standard error (%RSE) from the curve adjustment should be less than 15%. Any catchment outside these three criteria falls off the Budyko curve and is considered as a catchment with a high water balance disparity. According to Wang et al. (2011), Jones et al. (2012) and Coron et al. (2015), such a catchment is interpreted as being strongly influenced by anthropogenization, a catchment under strong climatic variability conditions especially droughts, a catchment with missing other components of the water balance (such as water demands, groundwater flows alteration) or in the worst case, a catchment where there were inadequate measures of the hydroclimatic variables.

4.3. Results and discussion

4.3.1. Hydroclimatic time series

Based on the processing of the original monthly time step database, a complete monthly hydroclimatic dataset of precipitation (P), temperature (T), potential evapotranspiration (PET) and streamflow (Q), over the 1970–2008 period was computed, over the 26 catchments in a lumped way. The series of annual PET, annual runoff (R) by the ratio between Q and catchment area, and annual actual evapotranspiration (AET) by water-balance ($P - R$) following the hydrological year (September – August) were determined. Observed annual P , estimated PET and R series from eleven catchments (mostly covering

the 1970–2008 period) are presented for displaying purposes in Figure 4.1 (the choice of these 11 catchments among the whole of the 26 studied catchments is discussed in section 4.3.2).

Mean annual values of hydroclimatic series are given in Table 4.1. For mean annual precipitation, catchments located in northern areas generally present higher values above 600 mm/yr than southern areas with values under around 400 mm/yr. This is because of the influence of the ENSO phenomenon over northern catchments that clearly appears in peaks during 1982/1983 and 1997/1998 events known as years of extreme El Niño events (see Figure 4.1a, 4.1b, 4.1c and 4.1d).

This influence is also present in the runoff variability, decreasing towards southern latitudes in general, but showing high values above 400 mm/yr in catchments located at central areas as Santa upstream (n°7), Santa (n°8) and Rimac (n°15), associated with the relationship of water availability and catchment size. For mean annual temperature, PET and AET, they decrease in general towards southern latitudes. Mean annual PET variability follows the same behaviour of the mean annual temperature variability along the Pd because of the empirical nature of the Oudin method. However, there is a slight increase over arid catchment located in the south where there is a predominance of bare ground and open shrubland areas.

Table 4.1. Hydroclimatic conditions over the 1970–2008 period and 2008 land cover types in the 26 studied catchments. Mean annual values of precipitation (P), temperature (T), potential evapotranspiration (PET), actual evapotranspiration (AET), runoff (R) and aridity index (P/PET). Land cover percentage from MODIS (2008) of Open shrubland (OS), Grasslands (GL), Croplands (CL) and Bare ground (BG).

n°	Catchment	Gauging Station	P mm/yr	T °C/yr	PET mm/yr	AET mm/yr	R mm/yr	P/PET	OS %	GL %	CL %	BG %
1	Piura up	Pte. Ñacara	613	20	1376	432	181	0.45	27	11	13	0
2	Piura	Pte. Sanchez Cerro	551	22	1456	355	212	0.38	34	12	20	0
3	La Leche	Puchaca	640	10	831	391	249	0.77	0	75	0	0
4	Zaña	Batan	817	12	933	450	367	0.88	0	50	12	0
5	Chicama	Salinar	643	14	1013	432	211	0.63	23	69	4	2
6	Moche	Quirihuac	645	8	703	509	136	0.92	26	74	0	0
7	Santa up	Condorcero	936	2	400	505	431	2.34	13	86	0	1
8	Santa	Pte. Carretera	854	3	473	381	541	1.80	17	76	0	7
9	Casma	Sector Tutuma	430	9	769	354	75	0.56	10	63	0	27
10	Huarmey	Puente Huamba	580	6	576	453	127	1.01	14	86	0	0
11	Pativilca	Yanapampa	700	8	728	387	313	0.96	14	82	0	4
12	Huaura	Sayan	654	3	444	348	307	1.47	9	91	0	0
13	Ch. Huaral	Santo Domingo	579	1	341	286	303	1.70	9	91	0	0
14	Chillon	Larancocha	555	2	370	390	165	1.50	23	77	0	0
15	Rimac	Chosica	646	3	436	224	422	1.48	19	81	0	0
16	Cañete	Socsi	556	1	339	261	294	1.64	20	74	0	6
17	San Juan	Conta	393	4	496	274	119	0.79	32	63	0	5
18	Ica	La Achirana	432	5	554	325	107	0.78	38	58	0	4
19	Acari	Bella Union	486	8	715	394	92	0.68	23	51	0	26
20	Yauca	Puente Jaqui	422	11	873	348	74	0.48	50	25	0	25
21	Majes	Huatiapa	537	3	430	336	201	1.25	35	59	0	6
22	Camana	Pte. Camana	441	6	593	303	137	0.74	28	47	1	24
23	Chili	Pte del diablo	370	5	556	320	50	0.67	73	3	0	22
24	Tambo	Chucarapi	418	6	566	336	82	0.74	50	12	0	38
25	Moquegua	Chivaya	369	3	437	305	64	0.84	57	0	0	43
26	Caplina	Aguas Calientes	343	2	416	294	49	0.83	60	0	0	40

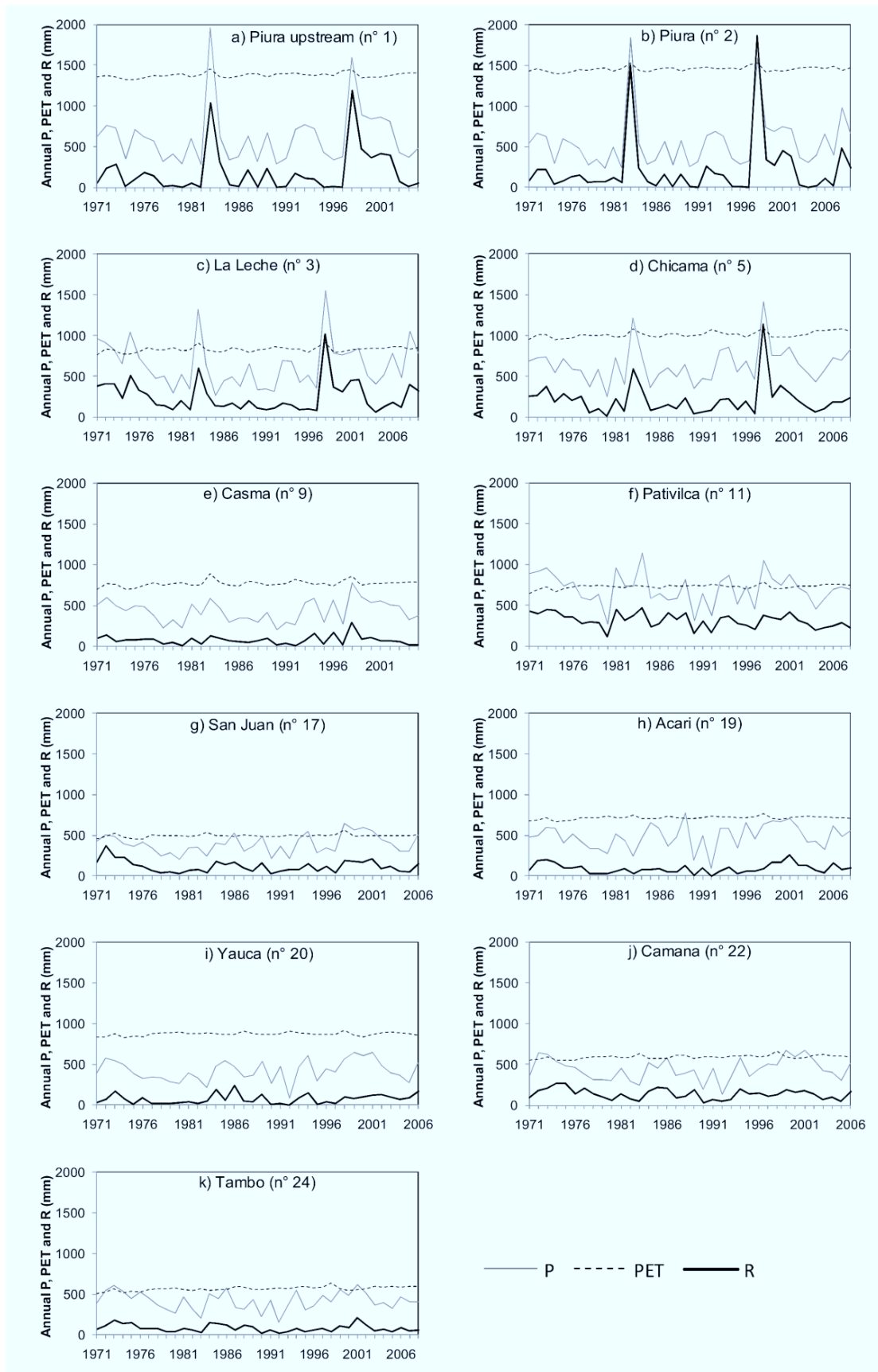


Figure 4.1. Long term variations of annual mean time series of precipitation (P), potential evapotranspiration (PET) and runoff (R) for eleven selected catchments over the 1970–2008 period.

These results corroborate the dryland conditions of the Pd, accentuating towards southern latitudes. This can be explained by the range of the aridity index (P/PET) proposed by Hassan and Dregne (1997) and contrasted with the annual precipitation module, a method recommended by the United Nations Environment Program (UNEP). Table 4.1 provides the values of the aridity index in most of the catchments below “1” and precipitation below 1000 mm in all catchments. Southern catchments present an annual precipitation around below 400 mm and are defined as arid areas. Catchments located in major rainy areas (Santa up ($n^{\circ}7$), Santa ($n^{\circ}8$), Huarmey ($n^{\circ}10$), Huaura ($n^{\circ}12$), Chancay Huaral ($n^{\circ}13$), Chillón ($n^{\circ}14$), Rimac ($n^{\circ}15$), Cañete ($n^{\circ}16$) and Majes ($n^{\circ}21$)) are found in the limits between semi-arid and dry sub-humid areas. The rest of catchments are defined as semi-arid areas.

4.3.2. Catchment water balance disparity

Based on the hydroclimatic time series calculated over the 26 catchments, series of dryness index (PET/P) and evaporative index (AET/P) are generated. Figures 4.2a and 4.2c show the dispersion of these two indices for two catchments (Piura upstream ($n^{\circ}1$) and Rimac ($n^{\circ}15$) respectively). Piura upstream shows the behaviour of a northern catchment with strong climate variability as a result of ENSO influence and Rimac shows the behaviour of a very anthropized catchment as a result of large hydraulic infrastructure to provide water to the city of Lima in lowlands. Both catchments represent the two main types of associations found in the study area, which were differentiated following the methodology explained in section 4.2.1 in terms of “ w ” and “%RSE” (i.e. see Figure 4.2a and Figure 4.2c) and “ r ” (i.e. see Figure 4.2b and Figure 4.2d).

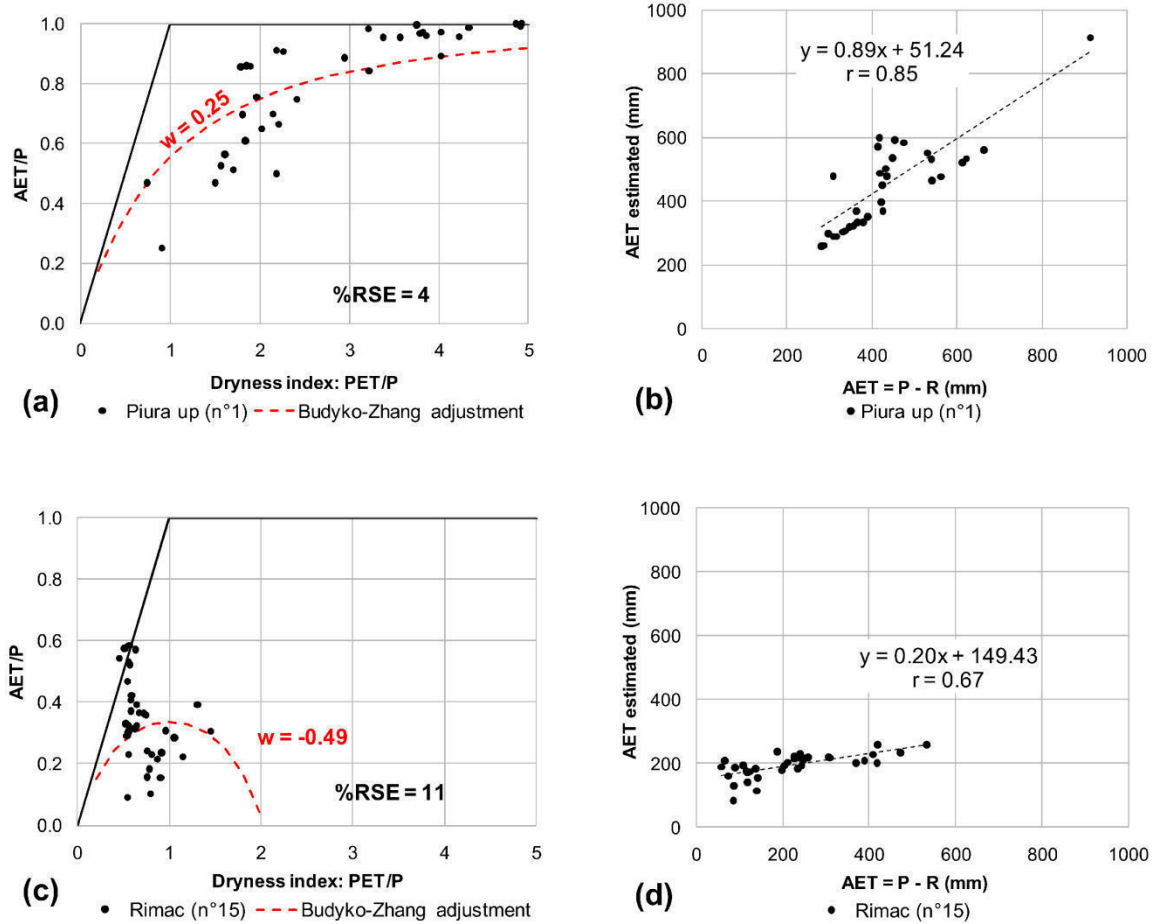


Figure 4.2. Comparison of two catchments with low (Piura up n°1) and high (Rimac n°15) water balance disparity according to the Budyko-Zhang framework. (a) and (c) black lines represent the energy limit (diagonal) and the water limit (horizontal). (b) and (d) scatter plot for correlation of annual AET obtained from water balance equation 4.1 and AET estimated by using equation 4.2.

Figure 4.3 shows the dispersion of indices for all the 26 catchments, highlighting the two types of association (the low and high water balance disparity). The “ w ” coefficients theoretically takes values between 0.1 and 2 (Zhang et al. 2001) which are associated with the predominance of bare soils and forest respectively (shown in Figure 4.3 as constraints), even though if some negative values on arid catchments were obtained by Chen et al. (2013). The “ w ” coefficient fall in the range of -0.58 to 4.30 and the best correlation coefficients “ r ” and acceptable %RSE are found with “ w ” positive values in the range of 0.02 to 1.78. That meant that only 11 catchments (shaded in gray in Table 4.2) follow a “quasi natural” shape of the Budyko-Zhang curve, presenting a low disparity in water balance which can be related to low climatic and anthropogenic influence. The average of “ w ” values is around 0.7, indicating mean values for the plant-available water coefficient related to predominance of grasslands over the semi-arid conditions of the Pd.

The fifteen remaining catchments are represented by grey points in Figure 4.3. Their AET/P values are located very near from the energy limit line (sometimes above the line) and far from the water limit line, which implies a complex combination of water losing systems (e.g. presence of open water surfaces, water lost to ground water system) with a non-natural behaviour of $P - R$ (see equation 4.1) affecting the AET calculation. Precipitation (P) time series follows a natural behaviour in all those catchments without strong trends or change-points, suggesting that runoff (R) has been altered. Also, those catchments are located mostly in an energy limited environment ($PET/P < 1$) where changes in P and PET are likely more evident in R (van der Velde et al. 2013), highlighting the strong climatic influence over R in this type of environments as well as the anthropogenic influence due to the points outside the Budyko-Zhang curve.

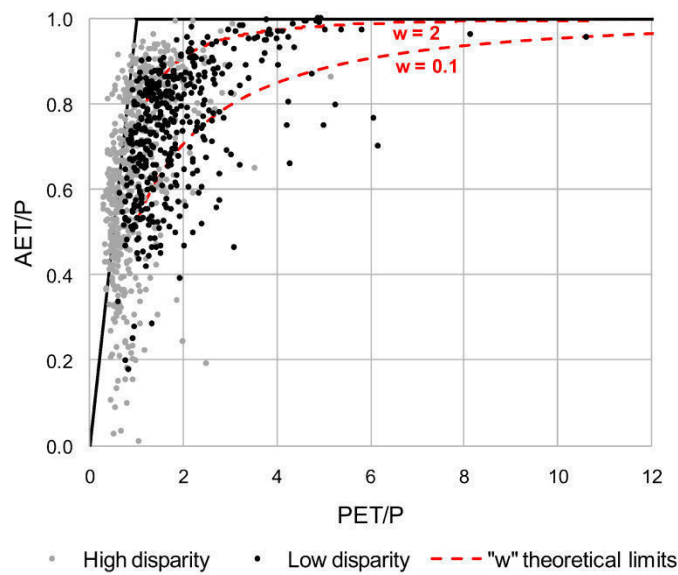


Figure 4.3. Budyko space over the 1970–2008 period over the 26 studied catchments. The black lines represent the energy limit (horizontal) and the water limit (diagonal). Black (Grey) points represent the association of yearly values from catchments showing a low (high) water balance disparity via the Budyko-Zhang framework. Red dashed curves represent the theoretical adjustment range for “ w ” parameter (“ $w_{min} = 0.1$ ”; “ $w_{max} = 2$ ”).

Table 4.2. Budyko-Zhang curve adjustment values. w : Budyko-Zhang coefficient; r : correlation coefficient between AET estimated by Budyko-Zhang and water balance; RSE: relative standard error from the curve adjustment. Catchments with low disparity in water balance are shaded in grey rows.

n°	Catchment	w	r	RSE %
1	Piura up	0.25	0.85	4
2	Piura	0.03	0.79	2
3	La Leche	0.18	0.88	5
4	Zaña	0.00	0.67	7
5	Chicama	0.32	0.83	5
6	Moche	2.59	0.85	28
7	Santa up	3.61	0.84	135
8	Santa	-0.58	0.56	33
9	Casma	1.16	0.95	8
10	Huarmey	3.12	0.85	40
11	Pativilca	0.02	0.91	6
12	Huaura	0.78	0.71	32
13	Ch. Huaral	0.65	0.64	48
14	Chillon	4.08	0.81	101
15	Rimac	-0.49	0.67	11
16	Cañete	0.27	0.66	35
17	San Juan	0.73	0.77	12
18	Ica	1.20	0.92	15
19	Acari	1.61	0.93	14
20	Yauca	0.78	0.89	9
21	Majes	1.16	0.90	39
22	Camana	0.47	0.88	9
23	Chili	2.79	0.96	29
24	Tambo	1.78	0.95	14
25	Moquegua	3.55	0.98	46
26	Caplina	4.30	0.97	53

The hypothesis about the anthropogenic effect as the main source of differentiation between catchments with high and low water balance disparity could not be easily validated due to the difficult access or/and the scarcity of water use data. A complementary analysis of the evolution of the land cover in the study area was performed using the LBA 1984, LBA 1992/1993, MODIS 2001 and MODIS 2008 datasets (see Figure 4.4). Even if improvements in resolution and data quality could impact estimates of spatial and temporal trends (from 10 to 1 km), the temporal evolution of the classes suggests that catchments with high water balance disparity presented great changes over land cover conditions of cropland from 28% to 1% (from 1984 to

1992/1993) and grassland from 39% to 63% (from 1992/1993 to 2001) as shown in Figure 4.4a. These changes were not observed in catchments with low water balance disparity (excepting croplands from 39% to 7% from 1984 to 1992/1993). In addition, Figure 4.4b shows the evolution of land cover over catchments grouped by latitudinal gradient and revealed that central catchments have a large change mainly in grassland cover from 40% to 75% (from 1992/1993 to 2001). It brings more confidence in northern and southern catchments, which presents certain homogeneity in the last decades.

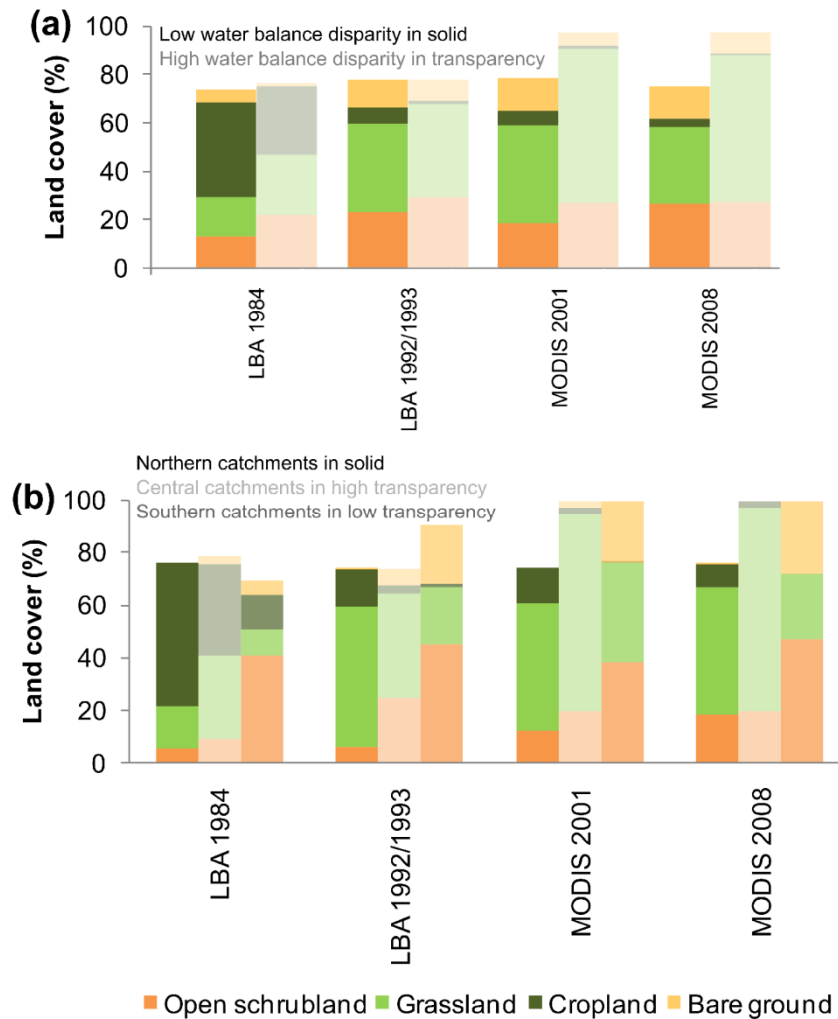


Figure 4.4. Evolution of land cover (%) with LBA and MODIS products over catchments grouped by (a) Low and high water balance disparity. (b) Latitudinal gradient: northern catchments (n°1 to n°6), central catchments (n°7 to n°18) and southern catchments (n°19 to n°26).

Location of large hydraulic systems is shown in Figure 2.5 in chapter 2. It is obvious that some catchments with high disparity were influenced by those systems which transfer water from the Atlantic drainage (i.e. Rimac (n°15) and Ica (n°18)) and by those which present large intakes and regulations for water supply in lower lands (Santa (n°8), Majes

(n°21) and Chili (n°23)). Also, there are some catchments with low water balance disparity that would still keep anthropogenic effects according to Figure 2.5 and Figure 2.6 (see Piura (n°2) and Camana (n°22)), however those effects were not noticeable in terms of the annual water balance disparity. Finally, the methodology made possible the separation of catchments with low and high water balance disparity related to low and high climatic and anthropogenic influence respectively. Further research is needed to separate these two types of influences in the region.

4.4. Conclusions

This chapter analyzes the hydroclimatic balance over 26 catchments of the Peruvian Pacific drainage region for the 1970–2008 period. We applied the Budyko-Zhang methodology to analyse the water balance disparity.

The study area experienced greater precipitation and runoff changes over the northern latitudes in relation with the ENSO influence. PET has been also studied for the first time in the region as an approach to relate it with temperature (and its relationship with the altitudinal gradient) using the Oudin method. This method is suitable for regions with non-dense climatic database as well as under arid and semi-arid conditions. Annual values of PET decrease southward with a slight increase over most arid catchment located in the south due to a predominance of bare ground and open shrubland areas.

Following the general hydroclimatic description of the region, the Budyko-Zhang conceptual framework was applied to identify plausible annual change disparity of water balance in catchments along the study area. This region is characterized mostly by semi-arid conditions and presents strong climate variability mainly in the northern regions. We identified 11 out of 26 catchments with low disparity according to the Budyko-Zhang framework related to a low climatic and anthropogenic influence; and suitable for an in-depth analysis with Budyko trajectories. The “*w*” parameter related to plant-available water in the Budyko-Zhang framework reaches an average value of 0.7, indicating the predominance of grasslands over the semi-arid conditions. Besides of climatic influence, large hydraulic systems and irrigation have been identified as one of the main factors of the human activity causing significant changes of runoff in most catchments. Catchments with high water balance disparity had a significant change in land cover mainly with a decrease in cropland and an increase in grassland over the studied period.

Finally, depending on the observational period of the analysis, limitations are mostly related to limited hydro-climatic data availability and related to the steady-state hypothesis of the Budyko framework. However, despite these limitations, the results provide a first assessment of the catchments with less climate and anthropogenic influence on water which has implication for regional water resources assessment and management.

Chapter 5

Runoff regime

This chapter presents the results obtained in the paper entitled: “Assessing freshwater runoff over Peruvian Pacific drainage catchments during the 1970–2010 period” submitted to *Hydrological Processes* in April 17, 2017 and currently it is under revision (see Annex A.3).

The chapter was organized as follows: It starts by a theoretical background in section 5.1, a methodology part in section 5.2, results and discussion in section 5.3 and conclusions in section 5.4.

Chapter highlights:

- Documentation of the interannual hydrological regimen of seven catchments with unimpaired conditions.
 - Methodology for freshwater runoff estimates in poorly gauged and ungauged conditions over the Peruvian Pacific drainage catchments.
 - Validation of a regional runoff model for unimpaired conditions, standing out its robustness through two conceptual lumped hydrological models.
 - Increasing regional unimpaired discharge from arid Peruvian Pacific coast to the Pacific Ocean over the last four decades.
-

5.1. Theoretical background

Under poorly gauged and ungauged conditions, regional runoff assessment through hydrological modelling represents the most common challenge in regional hydrology. Applying a regional hydrological model implies its repeated use everywhere within a region, using a global set of parameters generally transferred from gauged catchments (Engeland and Gottschalk, 2002; Seibert and Beven, 2009).

5.1.1. Hydrological lumped conceptual modelling

Hydrological models consist in abstractions of real systems and none of them can be anticipated as more accuracy for specific catchments and hydrologic conditions (Seiller et al., 2012). Conceptual lumped models are being increasingly used to evaluate their performance over regional water availability (Wale et al., 2009; Castiglioni et al., 2010; Ibrahim et al., 2015) and potential impacts of climate change on hydrological systems (Coron et al., 2012; Ruelland et al., 2012, 2015; Seiller et al., 2012, 2015; Wang et al., 2015; Fowler et al., 2016; Fabre et al., 2015, 2016).

Runoff estimates take into account historical observations of streamflow, which reflect the changes in environmental conditions such as climate and land use. Under changing climatic conditions, conceptual models would show more capability than previously thought (Fowler et al., 2016). However, conceptual modelling is regularly criticized for oversimplifying the physics of catchments and leading to unreliable simulations when conditions shift beyond the range of prior experience (Hublart et al., 2015). The usual sources of uncertainty in hydrological modelling under stationary conditions (concerning the climate and the physical characteristics of the catchment) are linked to the structure of the model, the calibration procedures and erroneous data used for calibration and validation (e.g. Liu and Gupta, 2007; Brigode et al., 2013). Under non-stationary conditions, such as climate variability or change, an additional source of uncertainty arises from parameters instability due to possible changes in the physical characteristics of the catchment and in the main processes at play (e.g. Coron et al., 2012; Thompson et al., 2013; Dakhlaoui et al., 2017). For this reason, it appears necessary to evaluate the modelling robustness and notably the transferability of the calibrated parameters to contrasted climate and/or anthropogenic conditions. Thirel et al. (2015) suggested a calibration and evaluation protocol for dealing with changing catchments, highlighting the advantages of the Differential Split-Sample Test (DSST; Klemes, 1986).

5.1.2. Regional runoff

One of the major obstacles in estimating regional and continental freshwater runoff is the lack of gauging records. Some methods have been applied to account for the contribution from poorly gauged regions in estimating long-term mean discharge as a simple sum of available streamflow records. However, those methods likely would contain discontinuities, which are a major issue in long term climate data analyses (Milliman and Farnsworth, 2011). Unimpaired runoff could be considered as a valuable source for identifying long term climate variability and change impacts, its application also includes legal and water management frameworks (Null and Viers, 2013). In this chapter, it is proposed the use of unimpaired runoff, which is defined as data from unregulated rivers or where regulation changes the natural monthly streamflow volumes by less than five percent (Boughton, 1999).

A few in-depth hydrological studies were developed in the Peruvian Pacific drainage: de Reparaz (2013) documented and analysed earlier hydrological and physical conditions along the entire study area (i.e. 54 catchments) from the 1920s until the 1960s. ANA (2012) analysed the water supply and demand in the main catchments with water management purposes, achieving to estimating the total annual volume of freshwater availability along the Pd from the 1970s to 2010 based on gauged catchments. Lavado et al. (2012) analysed streamflow mean conditions and its variability over 29 catchments from 1969 to 2004. In general, those studies made a weak approach about regional runoff behaviour and such a study has never been conducted in the Pd region, which would allow identifying some key elements of water resources management as the long term mean rate of runoff, its yearly and seasonal variability. In chapter 4, we identified 11 from 26 catchments associated with low water balance disparity or with quasi-natural conditions (hereafter unimpaired conditions) at interannual scale, explaining the annual runoff behaviour in each catchment from 1970 to 2008.

This chapter also describes the ability of two conceptual lumped hydrological models, GR1A (Mouelhi et al., 2006b) and GR2M (Mouelhi et al., 2006a) to simulate regional interannual unimpaired runoff over a multi-decadal period (i.e. the last four decades) characterized by a significant hydro-climatic variability.

5.2. Methods

5.2.1. Runoff simulation based on conceptual lumped models

Interannual runoff over each catchment was simulated with the GR1A lumped hydrological model (Mouelhi et al., 2006b) considering the hydrological year from September to August. The GR1A model was established as a revisit of the Manabe bucket model (Manabe, 1969) that belongs to the first generation of land surface models. The GR1A has a semi-empirical and lumped structure showing the usefulness of the antecedent annual precipitation and the less representativeness of a reservoir at the annual time step. It means a reduced model with only one-parameter as follows:

$$Q_k = P_k \left\{ 1 - \frac{1}{\left[1 + \left(\frac{0.7P_k + 0.3P_{k-1}}{X \cdot PET_k} \right)^2 \right]^{0.5}} \right\} \quad (5.1)$$

Q_k is the simulated streamflow of the year k , P_k is the annual precipitation of the year k , P_{k-1} is the annual precipitation of the year $k-1$, PET_k is the potential evapotranspiration of the year k , X is the one-parameter of the model to be optimized. The advantage of this one-parameter model is its high parsimony being a benchmark model for comparing the simulated long-term average streamflow with other models.

Seasonal runoff was simulated with the GR2M lumped monthly model (Mouelhi et al., 2006a). This model is based on two reservoirs and two calibration parameters. According to Figure 5.1, the soil quadratic reservoir (S') defines the production function with a maximal capacity $X1$; the gravity reservoir (R') defines the transfer function with the parameter $X2$, determining the runoff at the outlet and the exchange of water between the surface and the underground processes (Ibrahim et al., 2015). GR2M is a very used hydrological model due to its high parsimony. Its semi-empirical approach has been demonstrated to perform well when compared to similar monthly models and sensitivity analyses have determined that GR2M is sensitive to white noise errors on precipitation, but comparatively robust to random errors on potential evapotranspiration (Huard and Mailhot, 2008).

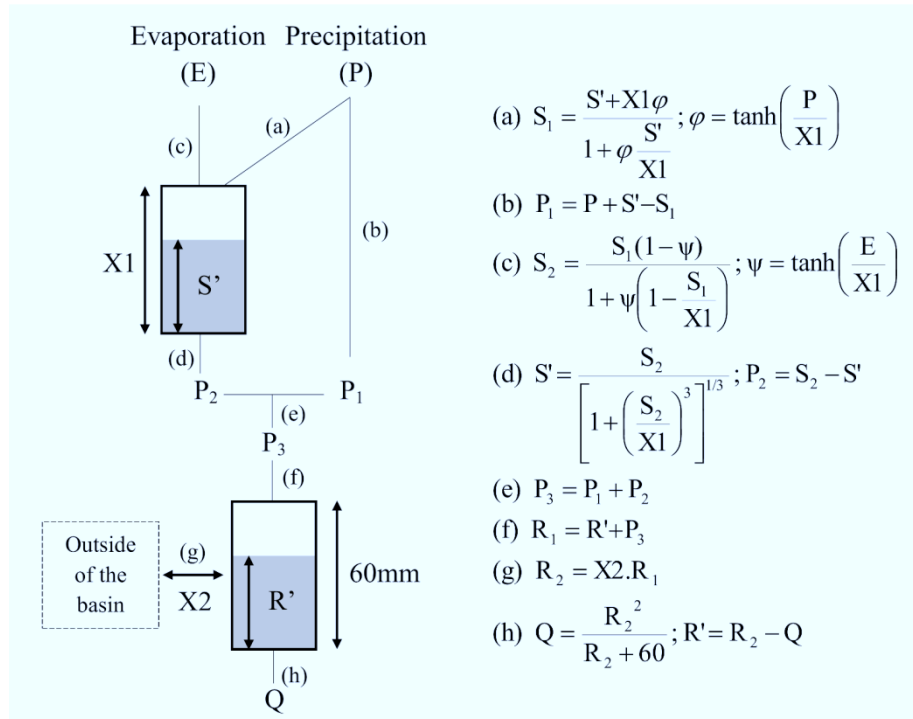


Figure 5.1. Scheme of the GR2M model with the parameters $X1$ and $X2$ (modified from Mouelhi et al., 2006a).

5.2.2. Performance and efficiency of conceptual lumped models

The performances of the models (i.e. GR1A and GR2M) were evaluated by an efficiency criterion consisting of two primary statistical scores considered as the basis for a careful hydrological evaluation (Thirel et al., 2015): the Nash-Sutcliffe Efficiency criterion (NSE; Nash and Sutcliffe, 1970) and the associated bias. NSE is related to the capacity of the model to simulate the general shape of the hydrograph, while giving more weight to high flows (simulated runoff and observed runoff expressed as Q_{sim} and Q_{obs} respectively). Bias is defined as the balance between the accumulated simulated volume (V_{sim}) and accumulated observed volume (V_{obs}) over an evaluation of n -months. The two criteria are shown in equations 5.2 and 5.3 as follows:

$$NSE = 1 - \frac{\sum_{t=1}^n (Q_{obs(t)} - Q_{sim(t)})^2}{\sum_{t=1}^n (Q_{obs(t)} - \mu_{Q_{obs}})^2} \quad (5.2)$$

$$Bias = \frac{\sum_{t=1}^n (V_{sim(t)} - V_{obs(t)})}{\sum_{t=1}^n V_{obs(t)}} \quad (5.3)$$

Perfect agreement between the observed and simulated values yields a NSE efficiency of 1, while a negative efficiency represents a lack of agreement worse than if the simulated values were replaced with the observed mean values. Following Moriasi et al. (2007), a model simulation is judged satisfactory here if NSE is above 0.5. Also the associated bias expressed in percentage should be around 0% within the range of -40% to 40% and this criterion was evaluated separately as a regard of the quality of the model performance via the NSE. The optimization of the parameters was done by the Generalized Reduced Gradient (GRG2) method (Lasdon and Smith, 1992) considering a warm-up period of two years in both models.

The model efficiency was evaluated following a Differential Split-Sample Test scheme (DSST; Klemeš, 1986) seeking to test the model over contrasted climatic periods in terms of precipitation as the dry years (DY) and wet years (WY) over the 40-year simulation period (1970–2010). Thus, it was defined two subperiods of equal length (20 DY and 20 WY) according to median annual precipitation over the period. The scheme follows two pairs of calibration and validation (Calibration↔Validation) as follows: DY→WY and WY→DY, making possible to test if the hydrological model calibrated on a given period is able to simulate streamflow with a similar efficiency on another period when it differs dramatically. It means to find a potential set of parameters calibrated and validated over the two pairs according to NSE and associated bias, which are keeping for the regionalization and also for representing the modelling uncertainty over contrasted conditions. The DSST methodology represents the most frequently used method for the diagnosis of model stability and the described evaluation of cross-calibration and validation over contrasted periods represents an approach of the temporal transposability of the model parameters over climate-contrasted periods (Thirel et al., 2015).

5.2.3. Regional runoff model (RRM) and freshwater estimates

In order to obtain regional unimpaired runoff signatures along the study area (i.e. 49 catchments), the 7 unimpaired gauged catchments were used to link information to the other 42 catchments. This information mainly related to precipitation-runoff relationship can be represented through a hydrological model (e.g. GR2M) and can be linked through a statistical regression method for predicting annual runoff in ungauged basins (Blöschl et al., 2013).

Multiple linear regressions methods search the relationship between runoff (including hydrological models parameters) and physical catchment characteristics (PCC) (Peel et

al., 2000; Wale et al., 2009; Castiglioni et al., 2010; Ibrahim et al., 2015). According to literature, PCC can be divided in five groups: climate, geography and physiography, geology, soil and land cover conditions (Wale et al., 2009), however the final selection is always restricted to the available information. It is established the following equations:

$$X_j = \sum_{i=1}^n a_i PCC_i + b \quad (5.4)$$

$$X_j = \sum_{i=1}^n a_i \ln PCC_i + b \quad (5.5)$$

$$\ln X_j = \sum_{i=1}^n a_i \ln PCC_i + b \quad (5.6)$$

where, X_j represents the parameters set with order j of the hydrological model (e.g. $X1$ and $X2$ for the GR2M obtained via a DSST scheme); a_i the regression coefficient of the PCC number i ; b is a constant or intercept of the regression line; n is the number of donor catchments (7 in this study). Equations 5.4, 5.5 and 5.6 represent regional runoff models (hereafter RRM) and its validation and final selection was made by the highest multiple correlation coefficient. A disadvantage of regression methods is that they may capture relationships that are evident in the data, but for which no theoretical explanation is available, for example due to the co-evolution of vegetation, landscape and hydrological response (Blöschl et al., 2013). However considering the expected goals of estimates of unimpaired freshwater at regional scale, its application can be judge as acceptable as long as the hydrological model shows good transferability under the DSST scheme. Also, the selected RRM was calibrated and validated following the same DSST scheme with DY↔WY pairs over the donor catchments as if they were ungauged catchments.

The RRM is then used to estimate the monthly and annual runoff time series along the 49 catchments belonging to the study area. As it is shown in Figure 2.3b in chapter 2, the 7 selected catchments present their gauge stations located mainly in the lower and middle altitude of the basin (i.e. not in the catchment outlet to the ocean). This is why the extension to the ocean through the RRM, represents the best way to generate a reference point for studying the unimpaired runoff over the Pd.

5.3. Results and discussion

5.3.1. Efficiency of the GR1A and GR2M models

The GR1A model was applied at annual time step following the DSST scheme defined in section 5.2.2. In general, the DY→WY pairs match with satisfactory values of NSE around 0.7 and associated bias reaching values around 0% in northern catchments as Piura (n°1) and Casma (n°2) but without showing a satisfactory performance over the rest

of central and southern catchments. The WY→DY pair shows a good agreement only for Casma (n°2) and for the rest of catchments show a very low efficiency even with negative values of NSE and with bias values out of range of -40% to 40% as shown in Table 5.1. According to equation 5.1, X parameter represents a compensation of water balance errors due to differences between forcing and control data and according to Perrin et al. (2007), it could be interpreted as a fraction of the evapotranspiration related to the influence of an external basin outlet (e.g. not an atmospheric outlet but an exchange with deep groundwater or with adjacent basins in the case of a non-superposition of topographical and geological boundaries). Results explain the contrasted difference between dry and wet years in semi-arid conditions at interannual level and a regional behaviour about gaining water in northern catchments defined by the X parameter always less than 1 (see Table 5.1).

Table 5.1. GR1A performance and mean annual runoff values for dry (DY) and wet (WY) years following the DSST scheme DY↔WY. Observed runoff at gauging station (R_{obs}); Simulated runoff (R_{sim}). Satisfactory results are shaded in grey rows.

		DY→WY						WY→DY					
R _{obs} mm/yr			X	NSE (Bias%)		R _{sim} mm/yr		X	NSE (Bias%)		R _{sim} mm/yr		
n°	DY	WY		Calibration	Validation	DY	WY		Calibration	Validation	DY	WY	
				DY	WY				WY	DY			
1	26	345	0.66	0.51 (20)	0.69 (-29)	31	247	0.46	0.86 (2)	-0.10 (12)	58	357	
2	102	321	0.63	0.70 (2)	0.71 (-4)	101	303	0.57	0.73 (4)	0.58 (16)	114	330	
3	40	109	0.74	0.50 (~0)	0.10 (40)	38	153	0.94	0.54 (3)	0.12 (-33)	26	112	
4	65	173	0.81	0.20 (-3)	0.09 (4)	60	175	0.87	-0.20 (-3)	0.06 (-13)	54	163	
5	57	127	0.84	0.61 (1)	0.10 (49)	58	179	1.15	0.22 (-1)	0.14 (-39)	5	21	
6	99	175	0.58	0.46 (-2)	0.12 (45)	96	254	0.87	-0.19 (-3)	-0.30 (-44)	55	171	
7	51	113	0.94	0.30 (-5)	0.21 (27)	48	142	1.13	0.60 (~0)	-0.19 (-30)	35	112	

Figure 5.2 resumes the efficiency of transposability of the GR2M parameters set from dry (DY) to wet (WY) years (colours shaded obtained via a kriging interpolation) and Table 5.2 shows the efficiency values for the DSST scheme DY↔WY. In general the DY→WY pairs match with values of NSE reaching high values around 0.80 (see Figures 5.2a, 5.2c and Table 5.2) and with associated biases within the range of -40% to 40% (see Figures 5.2b and 5.2d) for the 7 selected catchments. However calibration over dry years (DY) shows a low value of NSE of 0.4 for the southernmost catchment of Tambo (n°7) and presents an underestimation of observed runoff in all cases (see negative biases in Figure 5.2b).

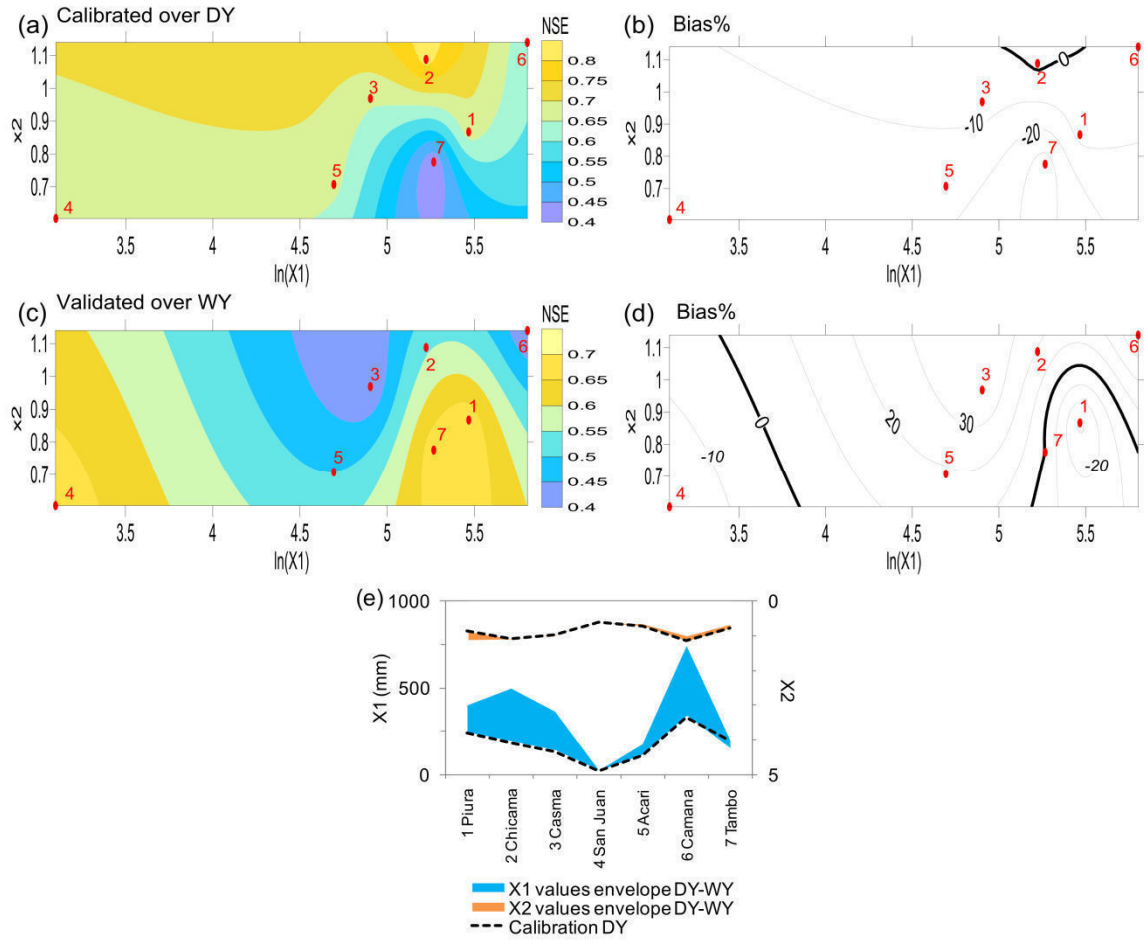


Figure 5.2. Evaluation of the performance of GR2M model (catchments in numbers) via parameter transposability (DSST). (a) NSE for the calibration over dry (DY) years. (b) Idem for the bias. (c) NSE for the validation over wet (WY) years. (d) Idem for the bias. (e) GR2M parameters values ($X1$ and $X2$) within the calibration envelope over DY and WY.

Validation over wet years (WY) also shows low values of NSE of 0.40 for Casma (n°3) and Camana (n°6). Additionally, the WY→DY pairs show a low efficiency with NSE values below 0.40 and biases are out of range of -40% to 40% for the validation over dry years (results of this transposition are shown in figures later). GR2M parameters set are shown in Figure 5.2e for the extreme case of calibration over DY and WY, which also envelope the parameters set for other scenarios as considering the total or the half total period for calibration. The envelope shows a large variability for $X1$ values except for catchments n°4, n°5 and n°6, however these values are particularly low, corresponding with semi-arid characteristics over the 7 catchments. $X2$ shows a relatively stable behaviour around 1, knowing its theoretical range between around 0.2 and 1.3 (Perrin et al., 2007).

Table 5.2. GR2M parameters set and efficiencies over dry (DY) and wet (WY) years following the DSST scheme DY↔WY. Satisfactory results are shaded in grey rows.

n°	DY→WY				WY→DY			
	X1 (mm)	X2	NSE (Bias%)		X1 (mm)	X2	NSE (Bias%)	
			Calibration DY	Validation WY			Calibration WY	Validation DY
1	237	0.87	0.68 (-7)	0.68 (-33)	397	1.11	0.72 (-14)	0.60 (78)
2	185	1.09	0.82 (2)	0.54 (19)	494	1.08	0.73 (-7)	0.58 (-28)
3	135	0.97	0.66 (-6)	0.41 (40)	361	0.95	0.73 (-1)	0.33 (-51)
4	22	0.60	0.67 (-16)	0.68 (-19)	16	0.62	0.70 (-7)	0.63 (6)
5	109	0.71	0.67 (-16)	0.49 (18)	175	0.64	0.64 (-16)	0.53 (-50)
6	331	1.14	0.61 (-4)	0.40 (39)	739	0.99	0.71 (-1)	0.32 (-46)
7	194	0.78	0.41 (-36)	0.68 (~0)	143	0.66	0.73 (-19)	0.36 (-48)

Table 5.3 shows the mean monthly values of the S' soil reservoir and the R' exchange water reservoir for the DY↔WY scheme. S' presents highest values in southern catchments (n°6 and n°7) and very low values for central catchments (n°3, n°4 and n°5) for a calibration over DY and validation over WY. This is related to the geological conditions of the study area. While southern catchments offers less impervious conditions than northern catchments for water storage, over central catchments is clearly the influence of the impervious batholith with mean values around ~0 mm/month for San Juan (n°4) and 24 and 19 mm/month for Casma (n°3) and Acari (n°5) catchments respectively over WY. R' keeps values nearly constant and in general is less than S'.

Table 5.3. Mean monthly values of S' and R' reservoirs for dry (DY) and wet (WY) years following the DSST scheme DY↔WY. Valid results are shaded in grey rows according to Table 5.2.

n°	Catchment	DY→WY				WY→DY			
		S'		R'		S'		R'	
		(mm/month)		(mm/month)		(mm/month)		(mm/month)	
		DY	WY	DY	WY	DY	WY	DY	WY
1	Piura	20	39	7	16	44	86	12	20
2	Chicama	28	40	16	22	106	153	15	22
3	Casma	16	24	11	17	64	102	8	16
4	San Juan	~0	~0	9	13	~0	~0	11	14
5	Acari	13	19	8	13	30	42	6	11
6	Camana	81	114	16	22	199	274	13	21
7	Tambo	41	57	8	13	26	36	7	11

Runoff associated with the last results is shown at seasonal scale in Figure 5.5. DY↔WY pairs are represented as runoff uncertainties in blue colour, corroborating the efficiency and GR2M model performance in comparison with observed runoff in gauged stations.

5.3.2. Regional runoff model evaluation

The seven studied catchments present a regional behaviour related to the parameter set transposability from dry to wet years in all catchments and also related to the interannual behaviour of gaining water in northern catchments. According to the results, it offered a great overview about the monthly hydrological response along the study area, as well as the selection of a valid PCC set. The PCC is related mainly to physical (non-climate or non-atmospheric) characteristics and mainly to those which can describe the exchange with soil and adjacent basins. After applying equations 5.4 to 5.6, the best set of PCCs found was: Area (A), Main channel longitude (L) and Perimeter (p). Figure 5.3 reveals the significant linear associations between $X1$, $X2$ and A, L and p.

Equation 5.6 generated the best RRM with a linear multiple correlation coefficient of 0.82 for $X1$ (a significant relationship) and 0.43 for $X2$ (a weak relationship). Equation 5.7 shows their potential representations as follows:

$$X1 = \frac{A^{0.393}L^{-4.107}p^{4.291}}{64.5}$$
$$X2 = 0.883A^{0.369}L^{-0.229}p^{-0.168} \quad (5.7)$$

It is worth to mention that $X1$ related to a soil reservoir can be considered as a buffer reservoir modulating the concentration time and easily explained by the geomorphology index of compactness (i.e. Gravelius's shape index) based on A and p. L is considered as a reference of the place where those exchanges become important according to the geological characteristics (see section 2.1.2b). $X2$ related to the water exchange with neighbouring catchments could not be easily explained with A, L and p. This parameter is judged for its ambiguity (between its natural and statistical meaning) as a correction factor (Mouelhi et al., 2006a). If $X2$ is less than 1, there is a water loss from the outside of the catchment; otherwise there is a gain. However $X2$ values did not reach a large range (i.e. from 0.6 to 1.1 in Table 5.2) and by theory $X2$ does not control the GR2M response to precipitation event, even does not control simulated runoff variability to a certain extent as does $X1$ (Huard and Mailhot, 2008). It is suggested that equations could be considered only as initial parameters set for its use at sub-basin scale, knowing also that the parameter $X1$ reflects the modelled storage dynamics, being necessary its comparison with field observations of groundwater table variations as done by Andermann et al. (2012) through a modified GR2M model. Also, there is a documented effect over other semi-arid areas in the world, where there is an increase of effective evapotranspiration losses over wet months (i.e. caused by the development of vegetation cover over poorly vegetated regions leading to increase of infiltration) and causing consequently a relative reduction in the runoff (Hughes, 2008). Those considerations are not studied here because of lack of observations and are out of scope of this work that is focused on a regional scale.

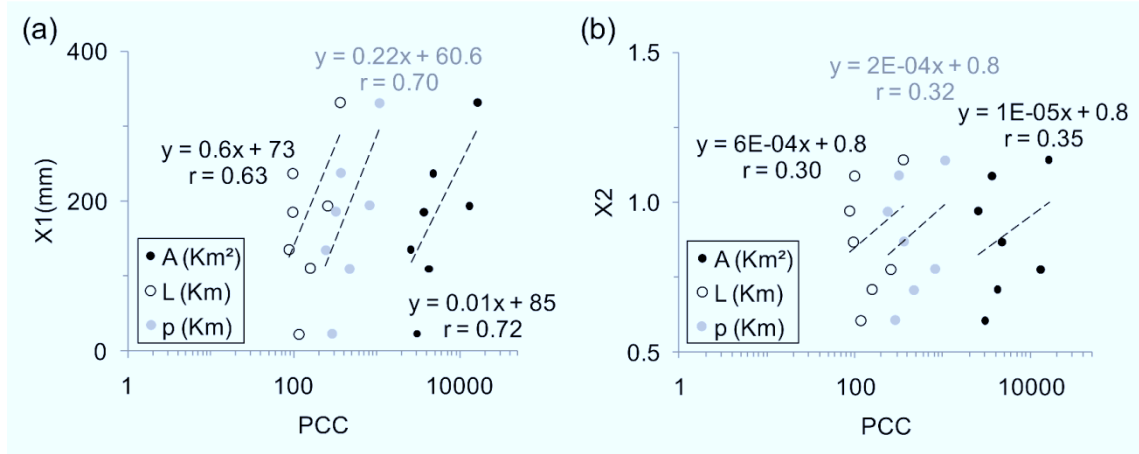


Figure 5.3. Linear associations between physical catchments characteristics (A: Area, L: Main channel length, p: Perimeter) using a natural bi-logarithmic scale (a) for the $X1$ parameter; (b) for the $X2$ parameter.

Then, the RRM from equation 5.7 was evaluated over each of the 7 gauged catchments as ungauged systems. This evaluation also considers the efficiency criteria with respect to the observed runoff. Figure 5.4 shows the values of NSE and the associated bias with the regional DSST scheme based on the calibration over dry years and validation over wet years. NSE presents high values around 0.70 and bias values within the range of -40% to 30% and also keeping low efficiency in the southernmost catchment of Tambo (n°7) with a NSE of 0.4 for the calibration over DY (see Figures 5.4a and 5.4b) and also a low efficiency NSE value of 0.30 for Casma (n°3) for the validation over WY (see Figure 5.4c). $X1$ keeps its low values as expected for the semi-arid conditions. $X2$ is reduced to values below 1, mainly over catchments n°3, n°4 and n°5 with values below 0.9 which could indicate that these catchments located inside the Andean batholith (see Figure 2.3b) are characterized by a marked water loss than the rest of catchments, this behaviour was also observed in the GR2M evaluation (see Figure 5.2) for catchments n°4 and n°5.

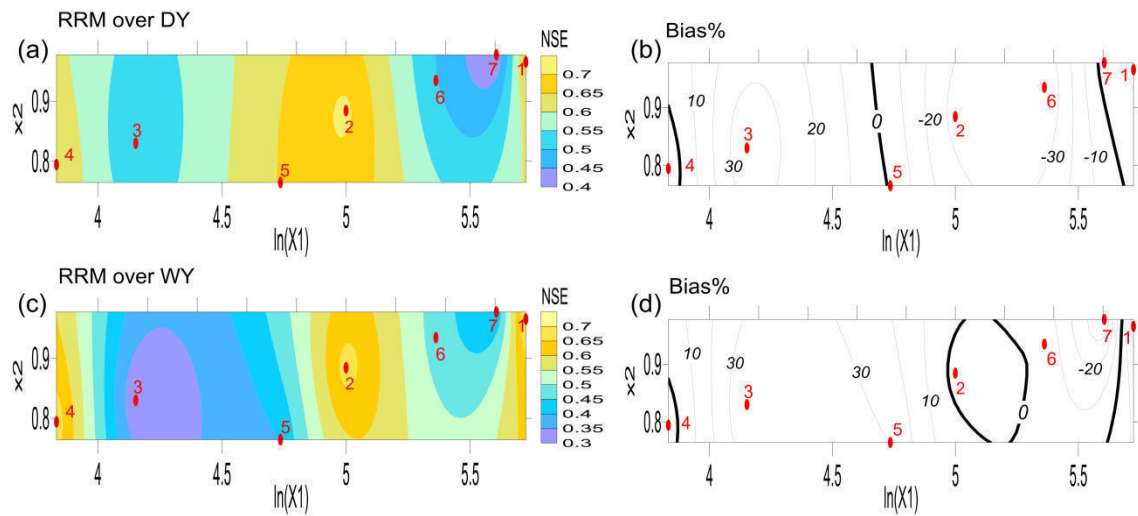


Figure 5.4. Performance of the Regional Runoff Model (catchments in numbers) via parameter transposability (DSST). (a) NSE for the calibration over dry years (DY). (b) Idem for the bias. (c) NSE for the validation over wet years (WY). (d) Idem for the bias.

Figure 5.5 shows the synthesis of calculations with the DSST scheme. The contrasted hydrological behaviour over dry (seasonal precipitation in orange) and wet years (seasonal precipitation in green) and the observed hydrological response (in black lines) are reflected in the difference of simulated runoff, projected in light blue colour as an uncertainty due to the contrasted evaluation via the DSST (DY↔WY), mainly in wet months from January to April. It is explained by the low model efficiency mainly for Casma (n°3) and Camana (n°6) catchments with a NSE around 0.40 and bias around 40% (see Table 5.2 and Figure 5.2). It also highlights that dry months from June to November does not present great uncertainty.

Simulated runoff by the RRM (in red dashed lines) follows the seasonality of observed precipitation and runoff. Simulated DSST contrasted runoff (in light blue colour) shows a lag of +1 month (a peak on March instead of February) with respect to the observed runoff in Camana catchment (n°6). Also over northern catchments the recession limb of the seasonal hydrograph is not well represented. This is explained by the effect of the hysteresis loop described in Section 2.1.3a mainly in those catchments where there are conditions for the transient storage during the wet months and its release over dry months (see catchments in Table 5.3 with high values of S' reservoir). However, even with the differences shown in Figure 5.5 and Figure 5.6 (reconstruction of dry and wet years over the studied period); simulated runoff corresponds to acceptable model efficiencies, according to the NSE and associated bias (Figure 5.4) and considering the meaningfulness of the extreme contrasted climatic evaluation of the DSST. A noteworthy case of very well simulated runoff in any condition at mean seasonal level is San Juan catchment (n°4), which presents a low uncertainty over wet months and RRM performance and could be related to its homogenous hydroclimatic conditions. RRM overestimates runoff over most wet month peaks, corresponding to the low model efficiency mainly in catchments n°3, 6 and 7 (see Figure 5.4 and 5.6).

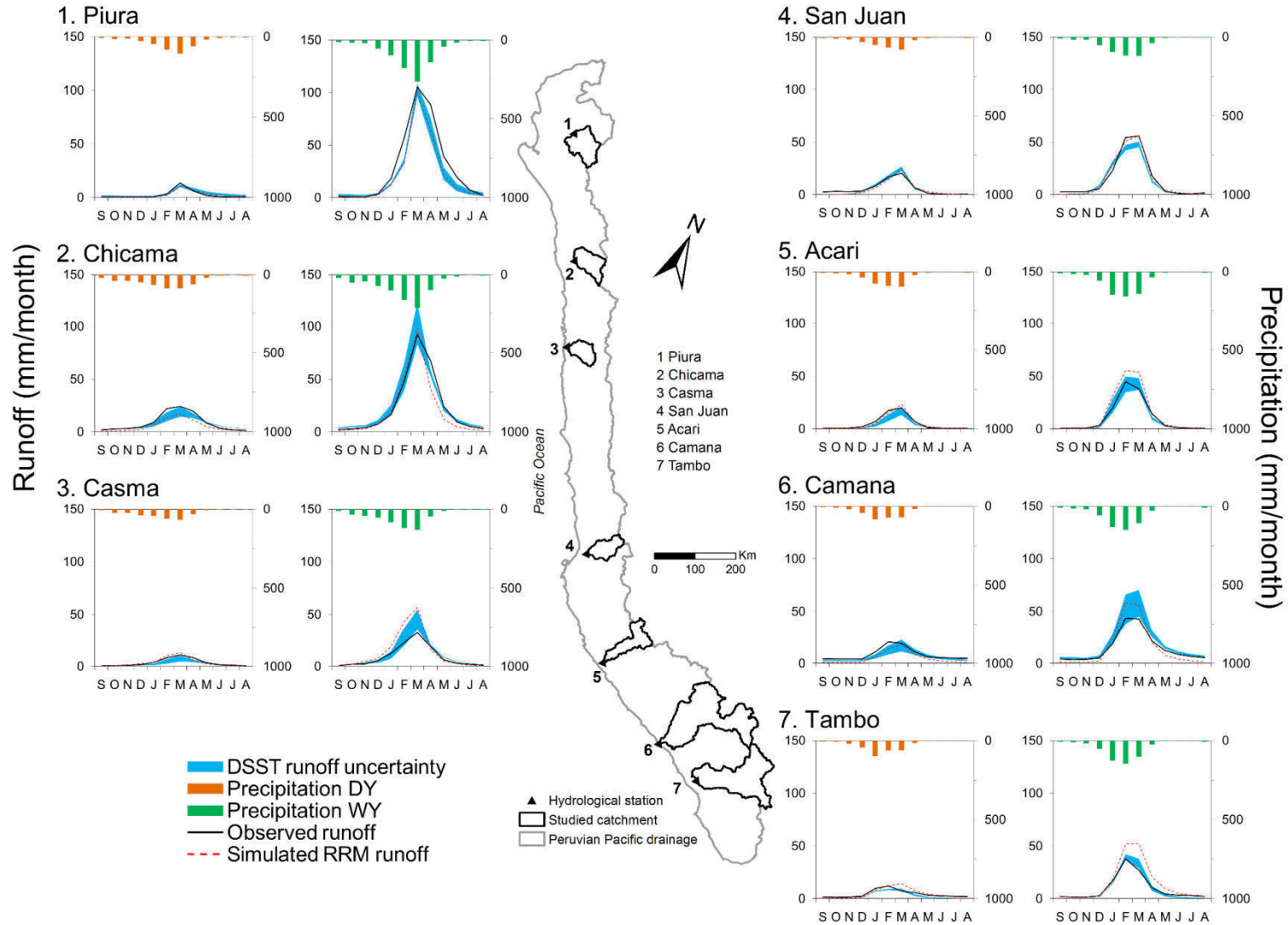


Figure 5.5. Mean seasonal runoff (observed, uncertainty by DSST, simulated by the regional runoff model) and precipitation over dry (DY) and wet (WY) years for each catchment. Calibration over DY and validation over WY considering a hydrological year (September to August).

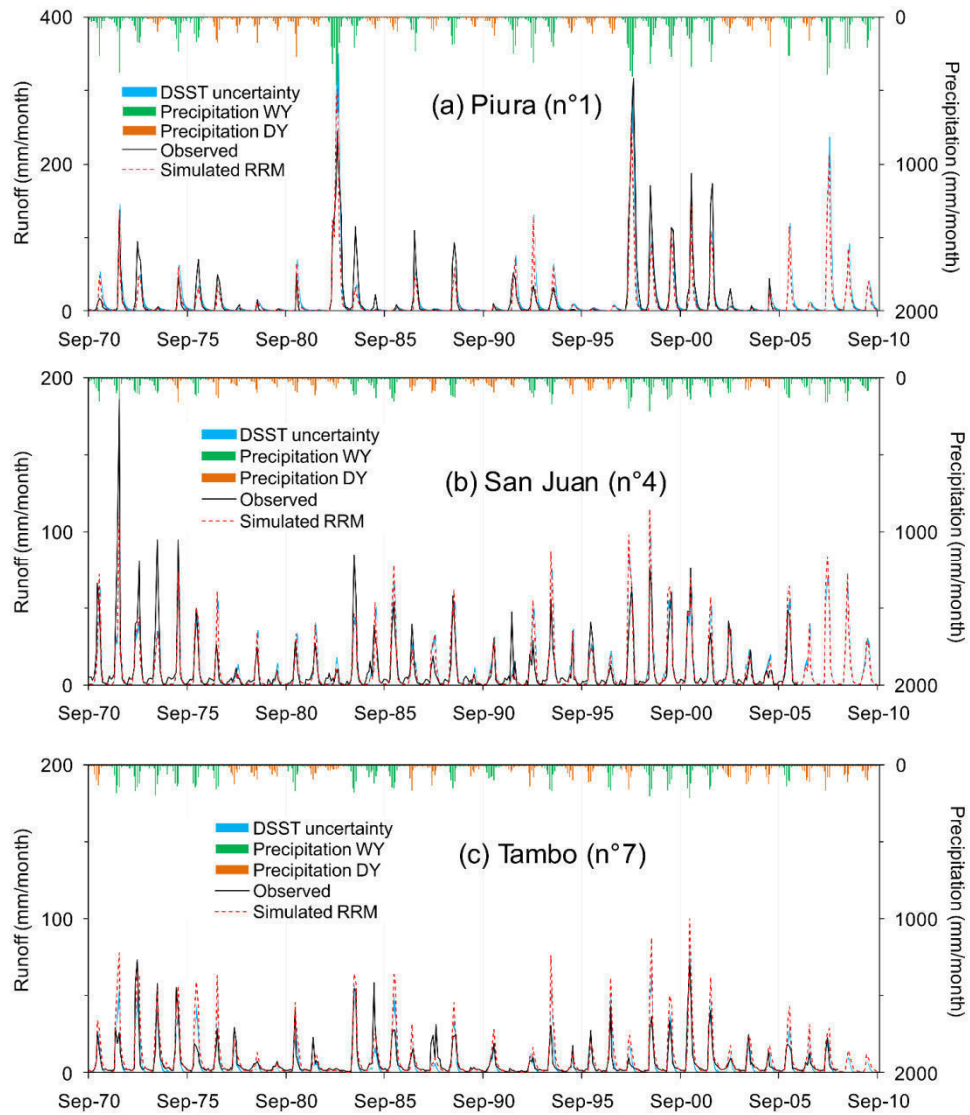


Figure 5.6. Runoff simulations along dry (DY) and wet (WY) years. Observed and simulated monthly runoff by GR2M and the regional runoff model. Runoff uncertainty via DSST.

5.3.3. Freshwater runoff estimation

Figure 5.7 shows RRM outputs expressed in terms of mean annual specific runoff and annual runoff time series along the 49 catchments for unimpaired conditions for the 1970–2010 period. It corroborates and quantifies the water scarcity in the region until the outlet points to the Pacific ocean, with a water yield range from 0.1 to 8 l/s/km² along the region, with a maximum value of 13 l/s/km² for Santa catchment (catchment n°13 in Figure 5.7a) with a persistence of very low values (catchments in red colour) towards southern latitudes. Figures 5.7b to 5.7f show the annual runoff for all catchments as a grey shaded area. For showing purposes, catchments were grouped following the general geographical classification proposed by de Reparaz (2013) in terms of river regime and

geomorphology (i.e. pluvial, nivo-glacial-pluvial, torrents and brooks) in the study area. Figure 5.7b groups the northern rivers with a pluvial regime; Figure 5.7c groups northern central rivers and torrents with a snow-pluvial and glacial-pluvial regime with the presence of natural lakes, as the catchment called Santa (n°13 in Figure 8a) whose upper part is located along a glacial mountain chain; Figure 5.7d groups central rivers with pluvial regime with moderated glacial regime with the presence of natural lakes; Figure 5.7e groups torrents and brooks with pluvial regime and high aridity conditions as the complex catchment called Grande (n°35 in Figure 5.7a) whose lower part belongs to an extensive desert plain, Figure 5.7f groups southern rivers and abrupt torrents with volcanic origin. Average annual runoff (black dotted line) in each group also follows a regional hydroclimatic pattern with the predominance of peaks during the ENSO years as the extreme events of 1982/1983 and 1997/1998 over northern catchments and the predominance of low values on the event of 1982/1983 over southern catchments.

Unimpaired freshwater runoff estimates is the first approach in the study area and it was expressed in terms of annual discharge as an estimation of the total water regional flux obtained by the sum of all time series. It reaches an annual mean of 747 m³/s for the 1970–2010 period and 709 m³/s without considering the ENSO extremes events of 1982/1983 and 1997/1998 (see Table 5.4 and Figure 5.7g). It was consistent with others estimations done in the region obtained only by observed records at gauge stations as listed in ANA (2012) as follows: ELECTROPERU in 1975 with 1025 m³/s, ONERN in 1980 with 855 m³/s, CEDEX in 1992 with 924 m³/s and ANA in 2012 with 802 m³/s, which could evidence a decrease but not concluding because of the discontinuity of the observed records. However for unimpaired conditions, the associated time series present a significant positive trend of 43 m³/s/decade based on a Mann Kendall test at 95% of confidence level with a 5-yr mean running for the scenario without ENSO extreme events as shown in Figure 5.7g. The regional trend is driven mainly by northern and central catchments (no trend was obtained for southern catchments plotted in Figure 5.7f). This can be explained by the effect of the significant increasing precipitation mainly in northern region (Rau et al., 2017a); as well as the potential snow and glacier melting due to increasing mean temperature around 0.2 °C per decade over the study area in the last four decades (see Annex A.2) and which is discussed in chapter 6. The differences between mean annual modules of unimpaired estimation, lower than the observed is due to the effects of water increase by the large hydraulic systems along the study area since seventies as explained in chapter 4.

A resulting regional discharge of 709 m³/s was estimated and also compared with some earlier references from 1980 (Milliman and Farnsworth, 2011) which estimates a discharge of 665 m³/s from gauge stations. From a continental hydrological perspective, considering a total discharge around 26,540 m³/s from western coast of South America (Milliman and Farnsworth, 2011), the results corroborate that rivers along the arid Peruvian coast contribute essentially no fresh water to the ocean. Nevertheless, the advantage of having unimpaired time series through a regional runoff model stays in the fact of its usefulness in identifying long-term relationships with climate variability and

climate change impacts and its application for water management purposes. Even if the RRM presented a weak relationship for X_2 in equation 5.7, this parameter only plays a correcting role for runoff time series generation (see section 5.3.2), which would not be decisive if runoff is expressed as anomalies (i.e. normalized indices) of monthly and annual variability (e.g. using a standard score), as a very well used tool for climate studies.

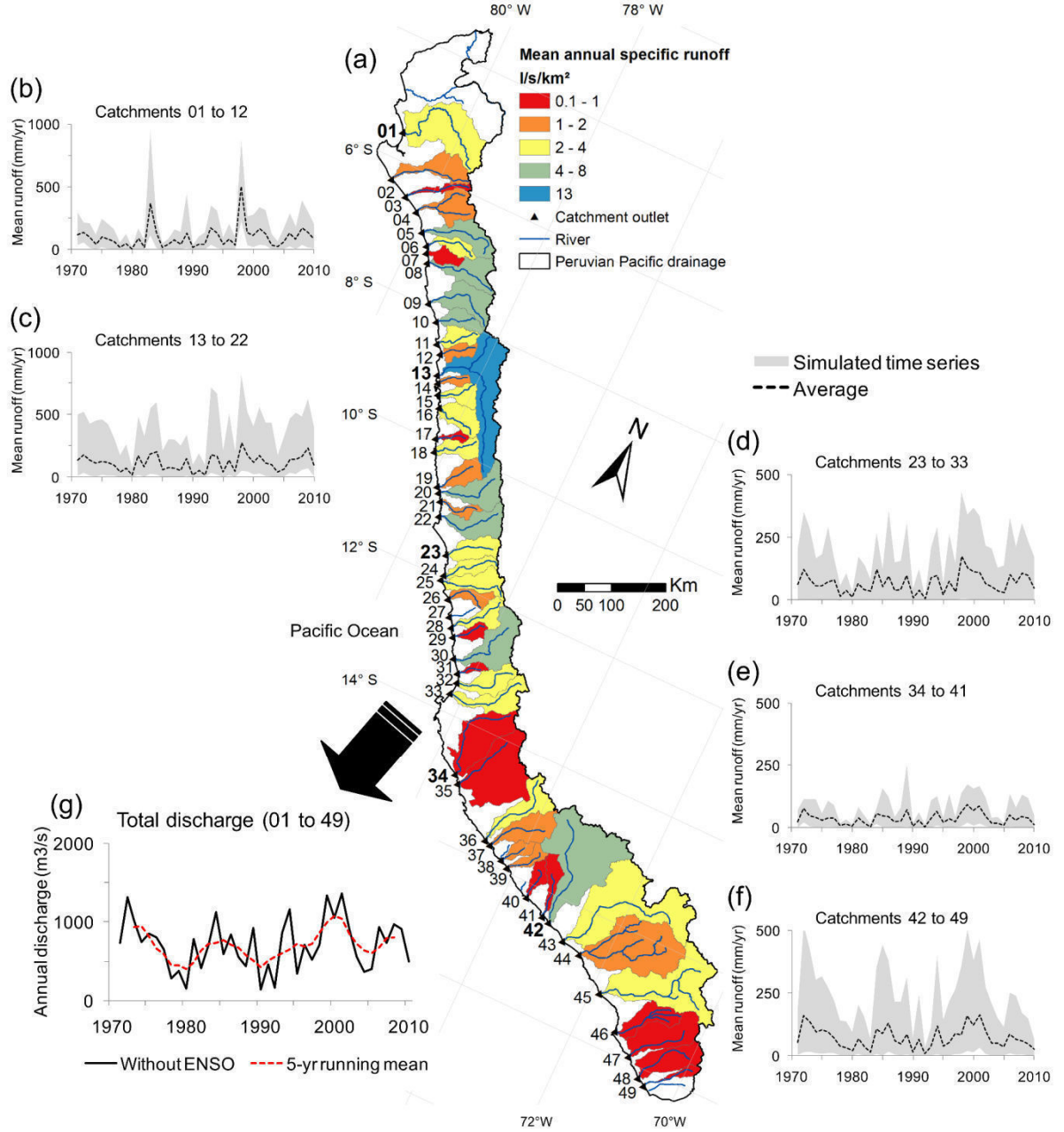


Figure 5.7. Spatial distribution of ungauged freshwater runoff (1970–2010) estimated by the RRM over 49 main catchments of the Pd: (a) Mean annual specific runoff by catchment. (b) to (f) Annual time series grouped in function of the regime characteristics. (g) Total annual discharge reaching 709 m³/s.

Table 5.4. Mean values of regional discharge (SD: Standard deviation)

Regional discharge	Including ENSO extreme years	Excluding ENSO extreme years
Mean (m ³ /s)	747	709
Minimal (m ³ /s)	136	136
Maximal (m ³ /s)	1876	1358
SD (m ³ /s)	375	322
Trend (m ³ /s/decade)	+58	+43

5.4. Conclusions

This chapter proposed a methodology for estimating unimpaired freshwater runoff from Peruvian Pacific drainage catchments based on hydrological modelling via two conceptual lumped models (GR1A and GR2M). They were evaluated via a Differential Split-Sample Test (DSST) to cope with the temporal transposability of models parameter sets and modelling robustness over contrasted climate conditions as dry and wet years according to the arid and semi-arid conditions of the study area. This methodology achieved to establish a regional runoff model (RRM) via the GR2M model at the monthly time step over 7 selected catchments.

It is concluded that GR2M shows more robustness than GR1A model over contrasted climatic conditions (i.e. in terms of acceptable NSE and bias criteria). The seven unimpaired selected catchments presented a remarkable hydrological regional monthly behaviour related to the transposing of their parameters set from dry to wet years, as well as their behaviour of gaining water at annual time step over northern catchments. GR2M parameters set (i.e. $X1$ and $X2$) were linked with physical catchment characteristics (as the area, main channel length and perimeter) which are geomorphological indices with a good relationship with the soil reservoir as interpreted by the $X1$ parameter. An acceptable multiple linear regression was established between them and the associated RRM was satisfactorily validated considering the seven selected catchments as ungauged systems. The RRM was applied over 49 catchments along the study area to simulate runoff for unimpaired conditions at outlet points to the Pacific Ocean.

In general, RRM and GR2M outputs revealed some deficiencies over northern catchments where the recession limb from mean seasonal hydrograph was not well reproduced. This can be explained by the effect of the hysteresis loop between precipitation and runoff found in all catchments, which after some discarded hypothesis, could be mainly related to a transient storage in river beds during the wet months and its release over dry months. Also, it was corroborated the influence of geological impervious conditions (i.e. Andean batholith) over the soil model reservoir.

Finally, unimpaired freshwater runoff was assessed for the first time through the study area. A total mean discharge of 709 m³/s was estimated for the whole 1970–2010 period. This discharge presented a trend of +43 m³/s/decade (significant at the 95% of confidence level based on a Mann Kendall test) over the whole period without considering the ENSO extreme events of 1982/1983 and 1997/1998. Output runoff time series via the RRM were objectively reproducible, because their bias was minimized by the multiple linear regressions method, and uncertainty associated with them can be quantified under the clear assumptions about geomorphologic parameters. A limitation of the methodology is related to the application of the RRM in other spatial scales. The proposed equations are mainly restricted to the size of evaluated catchments and for its use at regional scale. RRM outputs expressed in terms of runoff anomalies would offer a great tool based on the good relationship found for the *XI* parameter which controls the runoff variability in the GR2M model. The regional hydrological knowledge of the study area acquired via conceptual parsimonious lumped models represents a first step to expand the use and development of hydrological models at basin and regional scale over the Peruvian Pacific drainage.

Future work will be dedicated to further investigating the runoff sensitivity to climate change and the ENSO/runoff relationship based on the unimpaired time series as valuable indices that are not significantly disturbed by direct human activities on a long-term hydrological record. This includes improvements to the regional runoff model for other spatial scales.

Chapter 6

Impacts of climate variability and hydroclimatic change on precipitation and runoff

This chapter is divided into two parts. The first one is devoted to analyse the impacts of climate variability (ENSO mainly) on precipitation and runoff and it is based on extended results over the entire Peruvian Pacific drainage (from north to south) following the published paper entitled: “Low-frequency modulation and trend of the relationship between precipitation and ENSO along the northern to centre Peruvian Pacific coast” submitted to *Hydrological Processes* in June 12, 2013, accepted in May 15, 2014 (<http://dx.doi.org/10.1002/hyp.10247>) and published in an issue in March 2, 2015 (Bourrel et al., 2015, see Annex A.4).

It is also complemented with the results obtained in the second part of the published paper presented in chapter 3, entitled: “Regionalization of rainfall over the Peruvian Pacific slope and coast” (Rau et al., 2017a, see Annex A.1). This sub-chapter is organized as follows: It starts by a theoretical background in section 6.1.1, a methodology part in section 6.1.2, results and discussion in section 6.1.3 and conclusions in section 6.1.4.

The second part is devoted to analyse the impacts of hydroclimatic change on precipitation and runoff over the Peruvian Pacific drainage and it is based on the results obtained in the second part of the paper presented in chapter 4 entitled: “Hydroclimatic change disparity of Peruvian Pacific drainage catchments” (see Annex A.2). This sub-chapter is organized as follows: It starts by a theoretical background in section 6.2.1, a methodology part in section 6.2.2, results and discussion in section 6.2.3 and conclusions in section 6.2.4.

Chapter highlights:

- Revisiting of ENSO/precipitation relationship over the Peruvian Pacific slope and coast. Quasi-decadal modulation of interannual precipitation regime associated with ENSO over nine representative precipitation regions.
 - Influence of Eastern and Central El Niño over interannual precipitation with an increasing precipitation over northern mid-lowland regions and a decreasing precipitation over highland regions respectively.
 - Preliminary results of ENSO/runoff relationship along 49 catchments for unimpaired conditions. ENSO/runoff is shown stronger than ENSO/precipitation relationship.
 - Significant warming of 0.2°C per decade over Peruvian Pacific drainage catchments and sensitivity estimation of unimpaired catchments to hydroclimatic change.
-

6.1. Precipitation and runoff variability associated with ENSO

6.1.1. Theoretical background

ENSO consists in a non-stationary phenomenon (Boucharel *et al.*, 2009) presenting a significant modulation of its characteristics (amplitude, frequency, asymmetry) at decadal timescales (Torrence and Compo, 1998; Guilderson and Schrag, 1998). For instance, there has been a climate shift in the 1970s from when EP El Niño events became stronger (Miller *et al.*, 1994). The 1980s and 1990s are in fact the decades over which the relationship between ENSO and hydrology (precipitations and discharges) in Peru (Lagos *et al.*, 2008; Lavado *et al.*, 2013), in Chile (Montecinos and Aceituno, 2003) and in Ecuador (Bourrel *et al.*, 2010; 2011) is the most significant due to the strong signature on the regional circulation of the two extremes events of 1982/83 and 1997/98. Over the last two decades, the CP El Niño has however become more frequent relatively to the EP El Niño (Yeh *et al.*, 2009; Lee and McPhaden, 2010; Takahashi *et al.*, 2011). Such change in the ENSO characteristics has been shown to modify features of the equatorial oceanic and atmospheric circulation in the Pacific, that is the oceanic equatorial Kelvin waves (Dewitte *et al.*, 2012) and the intraseasonal atmospheric variability (Gushchina and Dewitte, 2012) including the Madden and Julian Oscillation (MJO) (Madden and Julian, 1972).

All these aspects of the change in ENSO properties have been somewhat overlooked in studies addressing the impact of ENSO on precipitation along the Peruvian Pacific slope

and coast, although they can provide guidance for refining current forecasting strategies aimed at improving resource management (agriculture, water resources).

In this chapter, relationship between ENSO and precipitations along the Pd is revisited taking into account different aspects of ENSO manifestations on SST and in the atmosphere in the tropical Pacific. As well as its low-frequency property changes, in particular the increased occurrence of CP El Niño in recent decades (Lee and McPhaden, 2010; Takahashi *et al.*, 2011). In that sense this subchapter extends the ones by Lagos *et al.* (2008) and Lavado *et al.* (2013). Due to the interplay between large scale and regional oceanic conditions, such relationship is thought to result from the non-linear interaction between local and remote influences, which a study based on a diversity of indices, may help to disentangle. For instance, precipitation events in the Piura region (5°S) are associated with SST warm episodes along the coast that are not necessary related to EP El Niño events (Woodman, 1985). Simply, former studies focused on extreme El Niño events that caused large economic losses for Peru but little has been said on moderate events. In a context of climate change, there is also a clear need to better understand the natural low-frequency of the teleconnection pattern. Here it is taken in advantage of a long-term data record and a revisited interpretation of the ENSO variability over the last 5 decades, where ENSO is viewed as two distinct and independent regimes, one associated with extreme events, that is the case of the 1982/83 and 1997/98 strong El Niño events, and the other one associated with moderate warm event and La Niña events (Takahashi *et al.*, 2011).

Also, based on the regionalized precipitation product, our aim is to estimate to which extent the decomposition of a large complex narrow area into a reduced number of homogeneous regions can grasp the salient features of the ENSO influence onto precipitation over the Pacific slope and coast of Peru (Horel and Cornejo-Garrido, 1986; Goldberg *et al.*, 1987; Tapley and Waylen, 1990; Takahashi, 2004; Nickl, 2007; Lagos *et al.*, 2008; Lavado *et al.*, 2012; Lavado and Espinoza, 2014; Bourrel *et al.*, 2015). The identified regions are also aimed at being used for ecological and water resources management and easing the interpretation of the manifestation of the main climatic modes in the region as described in Muñoz-Díaz and Rodrigo (2004), Sönmez and Kömüştü (2011) and Parracho *et al.* (2015).

6.1.2. Methods

a. Principal Component Analysis (PCA)

The selection of ENSO indices that best explain precipitation indices was performed using the PCA, a factorial method of data analysis, which explores the connections between variables to be studied as a whole, to highlight possible correlations (Lagarde, 1983; von Storch and Zwiers, 2003).

b. The wavelets and coherence analysis

To study the periodicity of the series (ENSO indices and precipitation), wavelet analysis are introduced. For a more extensive review of wavelet theory and applications, the reader is referred to Labat *et al.* (2000) or Labat (2005).

The basic aim of wavelet analyses is both to determine the frequency (or scale) content of a signal and to assess and determine the temporal variation of this frequency content (Heil and Walnut, 1989). Therefore the wavelet transform is the tool of choice when signals are characterised by localised high frequency events or when signals are characterised by a large numbers of scale-variable processes. Because of its localisation properties in both time and scale, the wavelet transform allows for tracking the time evolution of processes at different scales in the signal. This time-scale wavelet transformation $C_{\psi}^x(a, \tau)$ is defined in the case of a continuous time signal as:

$$C_{\psi}^x(a, \tau) = \frac{1}{\sqrt{a}} \int_{-\infty}^{+\infty} x(t) \cdot \psi^* \left(\frac{t - \tau}{a} \right) dt \quad (6.1)$$

where * corresponds to the complex conjugate. The function $\psi(t)$, which can be real or complex, plays the role of a convolution-kernel and is called a wavelet.

The parameters a and τ are used to adjust the shape and location of the wavelets respectively in scale and time domains. Changing t for example allows for moving the center of the wavelet. Then, the wavelet transform is a sort of microscope with magnification $1/a$ and location given by the parameter τ .

Then, another concept is also used; the wavelet coherence. Classically, the notion of coherence in signal processing consists of a measure of the correlation between two signals or between two representations of these signals.

Here it is used the wavelet coherence of two signals defined by Torrence and Webster (1999). They propose to determine wavelet coherence between two signals $X(t)$ and $Y(t)$ using a smooth estimate of the wavelet spectrum and to define a smooth wavelet spectrum and cross spectrum, respectively noted $SW_{XX}(a, \tau)$ and $SW_{XY}(a, \tau)$.

$$SW_{XX}(a, \tau) = \int_{t-\delta/2}^{t+\delta/2} W_{XX}^*(a, \tau) W_{XX}(a, \tau) da d\tau \quad (6.2)$$

$$SW_{XY}(a, \tau) = \int_{t-\delta/2}^{t+\delta/2} W_{XX}^*(a, \tau) W_{YY}(a, \tau) da d\tau \quad (6.3)$$

The scalar δ represents the size of the two dimensional filter, used for time and scale averaging as a necessary step for coherence calculation. The wavelet coherence WC can then be defined by analogy with Fourier coherence as:

$$WC(a, \tau) = \frac{|SW_{XY}(a, \tau)|}{\sqrt{|SW_{XX}(a, \tau)| \cdot |SW_{YY}(a, \tau)|}} \quad (6.4)$$

A temporal mean of the wavelet coherence can also be relevant in order help to identify ENSO indices that have a major influence on precipitation variability from a global point of view.

c. Correlation analysis

The correlation analysis is used to estimate the ENSO/precipitation relationship. The significance of the correlation coefficients was estimated using a t-test.

Correlation analysis was first performed for the monthly-averaged anomalies relative to the mean seasonal cycle over the whole record. Since the rainy season for the coastal regions is concomitant with the periods when precipitation anomalies are the strongest, the results are similar if the correlation analysis is performed for the yearly-averaged data, which corresponds to the annual hydrological cycle spanning from September to August. ENSO indices were averaged over September to February, which corresponds to the ENSO extended peak phase. The results of the correlation analysis presented in this paper correspond to the yearly-averaged data, respectively from September to August for precipitation and from September to February for the ENSO indices.

d. Covariance analysis

In order to investigate the relationship between precipitation and ENSO, a covariance analysis (i.e. singular value decomposition - SVD) is used, which consists in deriving the eigenvectors and eigenvalues of the covariance matrix between precipitation anomalies (Dec-Jan-Feb-Mar-Apr mean) over the Peruvian Pacific slope and coast and the SST anomalies over the Pacific and Atlantic basins (Dec-Jan-Feb mean) that maximizes the fraction of the cumulative squared covariance (Yang and Lau, 2004). Data were previously detrended in the period 1964 to 2011. More details and comments about this technique can be found in Bretherton *et al.* (1992) and Cherry (1997). In order to provide an estimate of the statistical significance of the SVD modes, a Monte Carlo test is performed that consists in creating a surrogate data, a randomized data set of precipitation and sea surface temperature by scrambling 40 yearly maps among the 48 years in the time domain. The SVD is then performed on the scrambled data set. The same procedure of scrambling the data set and performing the analysis is repeated 500 times, each time keeping the value of the explained covariance of the first two dominant modes and comparing the SVD modes of the original data set and the ones of the scrambled data set. The method is described in Björnsson and Venegas (1997). The 90% confidence level of the mode patterns is defined so as to the 10% and 90% percentiles of the ensemble correspond to a value that differs from the estimated mode by less than 0.5 times the standard deviation among the ensemble.

6.1.3. Results and discussion

a. PCA analysis of ENSO indices

In order to select the ENSO indices that best explain the precipitation, it was performed the Principal Component Analysis method. In Figure 6.1, most indices have a large projection on SST3 (i.e. the angle between the indices and SST3 is less than 45°) which indicates that they are all highly correlated. Only the SST1+2 index that accounts for extreme and/or coastal El Niño has a weak projection on the SST4 index (i.e. the two indices are almost orthogonal). As it was explained in Chapter 2, in a recent study (Takahashi *et al.*, 2011), two new indices were proposed, the so-called E and C indices that can describe two regimes of variability accounting for extreme warm events (or EP El Niño) and moderate events (La Niña and CP El Niño). These indices are by construction independent (orthogonal). They are comparable to the SST1+2 and SST4 indices respectively (see Figure 6.1). By construction the C index is orthogonal to the E index, the correlation analysis using this index will emphasize the relationship between precipitation variability and moderate El Niño and La Niña events. Note that the E and C indices were calculated from monthly mean values and it is considered the mean over SONDJF for the principal component analysis (see Figure 6.1), so that they do not appear strictly orthogonal.

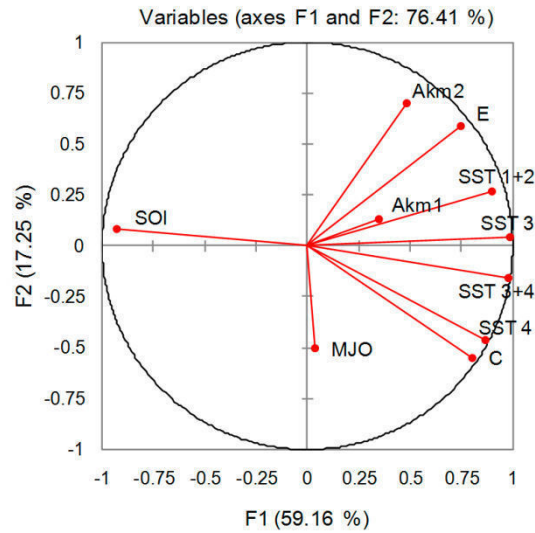


Figure 6.1. Projection of ENSO indices into a Principal Component Analysis (PCA). Note that the E and C indices are by construction orthogonal based on the monthly averaged data. For the PCA, averaged data from September to February were used.

b. Coherence between ENSO indices and precipitation series

Wavelet analysis for precipitation series (i.e. Region 1 (R1) and Region 2 (R2), see location map in Figure 3.4 in chapter 3) through the scale band between 2 to 16 years, has allowed identifying clearly the strong events over the period 1964–2011, that are the 1982/1983 and 1997/1998 El Niño events (see Figure 6.2a for R1). Without considering these strong events, it was identified events of lower intensity and higher frequency (see Figure 6.2b for R1). It is also noted that the influence of these strong events is not clear from Region 3 (R3) to Region 9 (R9) (see Figure 6.2c for Region 8

(R8)). For all nine regions, the major peaks are located in the period bands of 2–4, 4–8 and 8–16 years. It is implemented the classical statistical significance estimation based on comparison with red noise (Torrence and Webster, 1999). It is chosen here an 80% statistical significance based on the relative shortness of the data. For example, similar statistical significances were used by Labat (2006). The 80% threshold was chosen here in order to get statistical significance on all the three peaks mentioned (2–4, 4–8 and 8–16 years).

In the same way, the ten ENSO indices for the period 1964–2011 show that ENSO events are also associated with periods in the range of 2–4, 4–8 and 8–16 years. These results are consistent with those of other authors (Diaz and Markgraf, 2000) which showed the ENSO periodicity has three dominant modes of frequency variation: quasi-biennial, quasi-quadrennial and quasi-decadal (see Figure 6.2d for E index). That also confirms that the quasi-biennial and quasi-quadrennial modes are dominant in the Intertropical Convergence Zone (Lagos and Buizer, 1992).

The wavelet analyses suffer here from the classical “cone influence issue”, i.e. the region of the wavelet spectrum in which edge effects become important and make questionable the possible interpretation of the wavelet analysis. Then, the wavelet analysis gives only unquestionable results on the 1977–2000 interval for scales larger than 16 years. Therefore, even though if the validity of the presence of the 16-years oscillation may be questionable, the absence of discontinuity in the 16-years spectral band on the time intervals corresponding to the cone of influence suggest that this oscillation is present over all the 1964–2011 time interval.

The wavelet coherence analysis between ENSO indices and precipitation series allowed us to quantify the relation between an ENSO index and precipitation over a region. The vectors in black on Figure 6.2e indicate the values of the phase-shift between two time series. Thus, a vector pointing to the right shows a direct relation while a vector pointing left indicates an inverse relation (negative correlation). Figure 6.2e displays the wavelet coherence of R1 precipitation and E index, which shows a strong coherence (red coloration); the average maximum coherences are above 0.8 for periods of 4 to 16 years (Figure 6.2f), for quasi-decadal and quasi-quadrennial periods with a change of phase (change of direction of the arrows) in periods of 8–16 years.

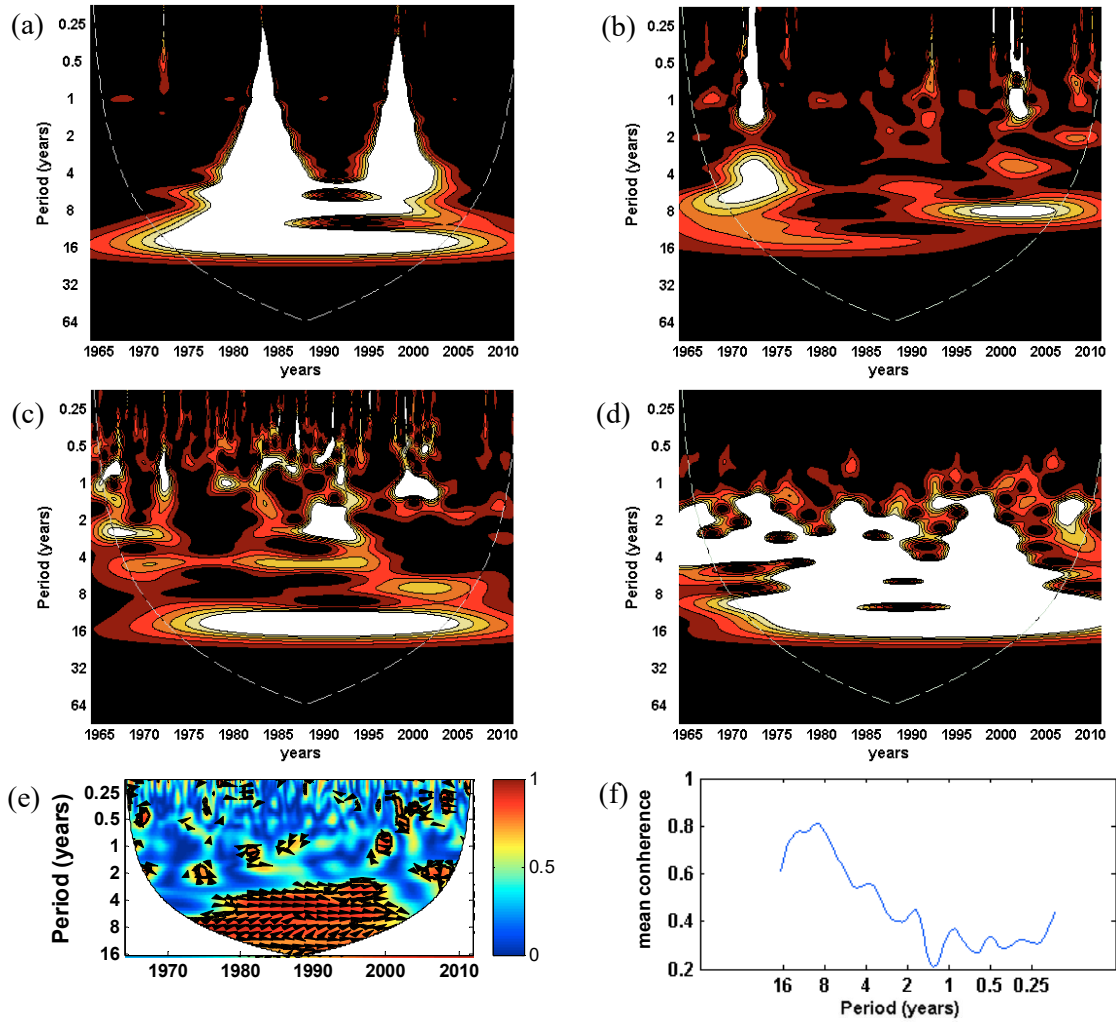


Figure 6.2. (a) Wavelet of R1 precipitation; (b) Wavelet of R1 precipitation not considering strong El Niño events; (c) Wavelet of R6 precipitation; (d) Wavelet of E index; (e) Wavelet coherence between E index and R1 precipitation; (f) Mean coherence peaks for wavelet coherence between E index and R1.

Table 6.1 provided the values of maximal coherence for all regions. Interestingly all maximal coherences are found at the decadal frequency which indicate that the low-frequency ENSO modulation is the most influential on precipitation along the coast of Peru. This justifies the selection of sub-periods for the correlation analysis (see below). The results also indicate that some indices are more relevant for the Northern part of Peru (SST 1+2, SST 3) whereas others are more relevant for regions of central and south Peru (SST4, SST 3.4). Not surprisingly, the E index exhibits a large coherence in the North (R1 and R2) because it accounts for extreme warm events. For MJO, the values of highest coherence are located on the upstream basins (R2, R4, R5 and R6, values between 0.62 to 0.79) consistent with the expectation that MJO is influential at relatively high altitudes. For oceanic indices, the Akm1 index is more influential in the North and in the basins downstream of R1 and R3, whereas the AKm2 index has the largest coherence with R1 and R2. Coherence values for the

region R9 are not significant for any index: they are lower than 0.50 and the highest is that of the MJO (0.49).

Table 6.1. Summary of maximal coherences for each region (in all cases, coherences correspond to quasi-decadal frequency).

Latitudinal range °Sur	Region	Wavelet coherence ENSO indices with maximal coherences (c)
4.2-7.3	R1	SST 1+2 (c=0.8), SST 3 (c=0.6), SST 4 (c=0.6), SST 3.4 (c=0.6), MJO (c=0.5), E (c=0.8), C (c=0.6), AKm1 (c=0.7), AKm2 (c=0.6)
3.4-7.3	R2	SST 1+2 (c=0.8), SST 3 (c=0.6), SST 4 (c=0.7), SST 3.4 (c=0.6), MJO (c=0.6), E (c=0.9), C (c=0.8), AKm1 (c=0.6), AKm2 (c=0.6)
3.6-8.3	R3	SST 1+2 (c=0.6), SST 3 (c=0.75), SST 4 (c=0.85), SST 3.4 (c=0.8), MJO (c=0.75), E (c=0.8), C (c=0.65), AKm1 (c=0.6), AKm2 (c=0.6)
7.3-15.5	R4	SST 1+2 (c=0.6), SST 3 (c=0.6), SST 4 (c=0.7), SST 3.4 (c=0.7), MJO (c=0.8), E (c=0.7), C (c=0.9), AKm1 (c=0.65), AKm2 (c=0.6)
7-11	R5	SST 1+2 (c=0.5), SST 4 (c=0.5), SST 3.4 (c=0.5), MJO (c=0.6), E (c=0.5), C (c=0.5), AKm2 (c=0.5)
11-15	R6	SST 4 (c=0.6), E (c=0.65), C (c=0.5),
15.5-18.4	R7	SST 1+2 (c=0.5), SST 3 (c=0.5), MJO (c=0.5), E (0.6), AKm1 (c=0.6), AKm2 (c=0.55)
14.6-17.8	R8	SST 3 (c=0.5), E (c=0.5), C (c=0.55), AKm1 (c=0.6), AKm2 (c=0.55)
14.4-17.7	R9	SST 1+2 (c=0.5), C (c=0.5), AKm1 (c=0.5)

c. Low frequency modulation of ENSO and precipitation regime

The two main climate shifts in the tropical Pacific over the last five decades include the 1976/77 climate shift (Miller *et al.*, 1994; others) and more recently documented, the 2000 shift when the mean state became cooler (Tsonis *et al.*, 2007; McPhaden, 2012; Luo *et al.*, 2012; Xiang *et al.*, 2012, Hong *et al.*, 2013). Change in mean SST is influential on the teleconnection pattern and may impact precipitation at the regional scale. Here as a first step, it is considered three periods corresponding to these two transitions: P1 (1964–1976), P2 (1978–1999) and P3 (2000–2011). Instantaneous correlation analyses are carried out between the five indices (indices shown in Table 6.1) and the nine regions (R_i; i=1,2,...,9). It is retained results for the E, C, AKm1, AKm2 and MJO indices considering that the E and C indices grasp the behavior of other indices based on SST through linear combination (Takahashi *et al.*, 2011) and that the other ones account for specific oceanographic and atmospheric processes (see section 2). Figure 6.3 displays the results for the regions grouped as follows: northern regions (R1, R2 and R3), coastal regions or lowlands (R4 and R7), highlands and southern regions (R5, R6, R8 and R9). For the 1964–1976 first period, it is provided

statistics with and without extreme events, which indicates that the known relationship between precipitation and ENSO over Northern Peru (Lagos *et al.*, 2008) is mostly the result of the influence of the two El Niño events of 1982/83 and 1997/98. For instance the correlation over the regions R1 and R2 is above 0.7 for the E index and the AKm2 index when these events are considered (Fig. 6.3a). These correlation remain hardly significant when the events are not considered (white circles). Interestingly the MJO index is almost unsensitive to the consideration of extreme events with correlation value above the significance level for all Ri except R3 and R5, whereas the C index exhibits a relatively large correlation (significant) in some regions when the influence of extreme events is removed.

Another interesting feature arising from the results of Figure 6.3 is the significant change in correlation according to the period under consideration for some indices. In particular, the C index and AKm1 index become more influential on precipitation during 2000–2011 and 2000–2005 respectively on average over the regions. The C index exhibits a large correlation with precipitation over the regions R6, R8 and R9 during 2000–2011. On the other hand the MJO index exhibits a reduced correlation with precipitation over 2000–2011 compared to 1976–1999 period. Besides the low-frequency modulation of the correlation, a large latitudinal variability is also observed, which is difficult to interpret.

Regarding the oceanic Kelvin waves, first of all, from Figure 6.1, Akm1 and Akm2 indices have a comparable behaviour than the SST 1+2 and E indices, verifying their influence on coastal conditions changes. In particular, when we considered the strong El Niño events of 1982/1983 and 1997/1998 (Figure 6.3d, 6.3e), the Akm2 index has a comparable relationship with precipitation than the E index, i.e. large correlation in the Northern part of Peru that decreases southward. The AKm2 index captures well the peak of strong El Niño (Dewitte *et al.*, 2012) where the AKm1 index is more relevant for intraseasonal Kelvin activity prior to the development of strong El Niño (Gushchina and Dewitte, 2012), which may explain its low correlation with precipitation over the period 1977–99 dominated by strong El Niño activity. On the other hand, the influence of the first mode Kelvin wave (AKm1) on precipitation increases over the 2000–2011 period (Figure 6.3d) characterized by both occurrences of Central Pacific El Niño and La Niña events. Its influence on precipitation is the largest for the southernmost regions (R6 to R9) and is comparable to the C index that grasps the central Pacific variability.

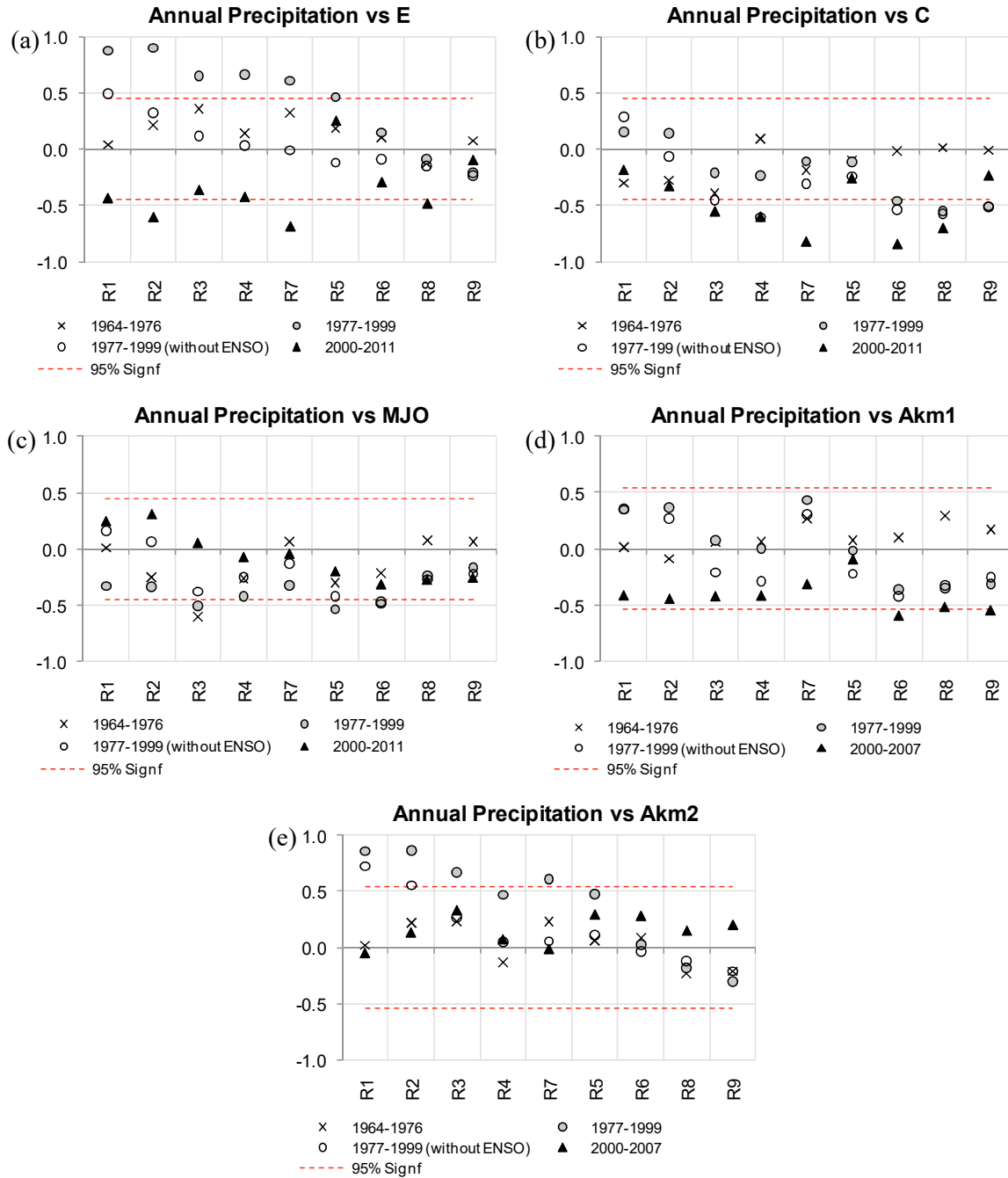


Figure 6.3. Correlation coefficients between precipitation and ENSO indices for 4 periods: 1964–1976, 1977–1999, 1977–1999 without ENSO (not considering strong El Niño events of 1982/1983 and 1997/1998) and 2000–2011. For Akm1 and Akm2 the last period correspond to 2000–2007 (a) For E index; (b) For C index; (c) For MJO index; (d) For Akm1 index and (e) For Akm2 index. Maximal significance of 95% obtained for the shorter periods 2000–2011 and 2000–2007.

Considering the significant decadal variability in the relationship between ENSO and precipitation evidenced above, it was investigated if a long-term trend in this relationship can be observed in some regions. It is considered here the E and C

indices. The 11-year running correlation between these two indices and precipitations is presented in Figures 6.4abc (this leads to a loss of 5 years in the beginning and at the end of the period). Here again we consider the analysis without the 1982/83 and 1997/98 extreme events in order to highlight the change in teleconnection pattern associated with moderate warm events. This results in computing the correlation from 9 points instead of 11 points over the periods that encompasses the 1982/83 and 1997/98 El Niño events. Figure 6.4a indicates that no clear trend can be detected in most regions with a large meridional and temporal variability of the correlation. The E index accounts for SST variability in the far eastern Pacific that can be associated with intraseasonal Kelvin activity and the development of extreme El Niño events like the 1982/83 and 1997/98 El Niño events. Since they are not taken into account in the calculation of Figure 6.4a, the variable correlation traduces local effects of the either intraseasonal Kelvin waves on SST or local atmospheric perturbations that modify SST along the coast. In order to illustrate the impact of the two extremes El Niño events, the similar figure than Figure 6.4a is presented to take them into account (Figure 6.4b). It clearly shows that statistics are completely changed when these events are considered, with a very high correlation between the E index and precipitation all over the coast over the period encompassing these events. The Central Pacific El Niño, accounted by the C index, is also characterized by a warming in the eastern Pacific but at a different time in the year (in Austral winter rather than in Austral Summer) and with a much less amplitude characterized by a warming in the central Pacific (Dewitte *et al.*, 2011). This warming in the eastern Pacific usually disappears after a few months and cooling conditions develops (Dewitte *et al.*, 2012). The Figure 6.4c displays the 11-year mean correlation between the C index and precipitation. It indicates a more constrained behavior compared to the E index, with in particular a more clearer decadal modulation of the ENSO/precipitation relationship. In addition, the correlation is mostly negative indicating that Central Pacific El Niño activity is associated with drier conditions along the coast of Peru. This situation is emphasized from the 90s in particular for the regions R3, R6, R8 and R9, with a marked negative trend of the running correlation. The strongest negative correlations and trends are found for the Northern region R3 during the 2000s which corresponds to the period of occurrence of only CP El Niño events.

The above interpretation of the low-frequency changes in the relationship between the E and C indices and precipitation relies on the assumption that precipitation along the coast of Peru can be influenced by some aspects of the intraseasonal tropical variability both in the ocean and the atmosphere. As a consistency check, it is provided a comparable analysis than Figure 6.4 but for the Akml and MJO indices (Figure 6.5). The results indicate that there is also a low-frequency modulation of correlation between the indices and precipitation. The negative trend is obvious for the Akml index due to the decrease in correlation from the 90s in the central and southern regions. This is consistent with the interpretation that intraseasonal downwelling Kelvin wave activity during Central Pacific El Niño (Gushchina and Dewitte, 2012) is enhanced while the SST along the coast is reduced from the 90s. Here is not possible

to conclude if it is the La Niña-like mean conditions (leading to cool conditions off Peru) from the 90s or the coastal cooling associated with Central Pacific El Niño that produce the decreased precipitation during interannual events. Interestingly the relationship between precipitation and the MJO index has an opposite trend (i.e. positive), which suggests that the MJO activity leads to increased precipitation in recent years, in particular in the northern regions.

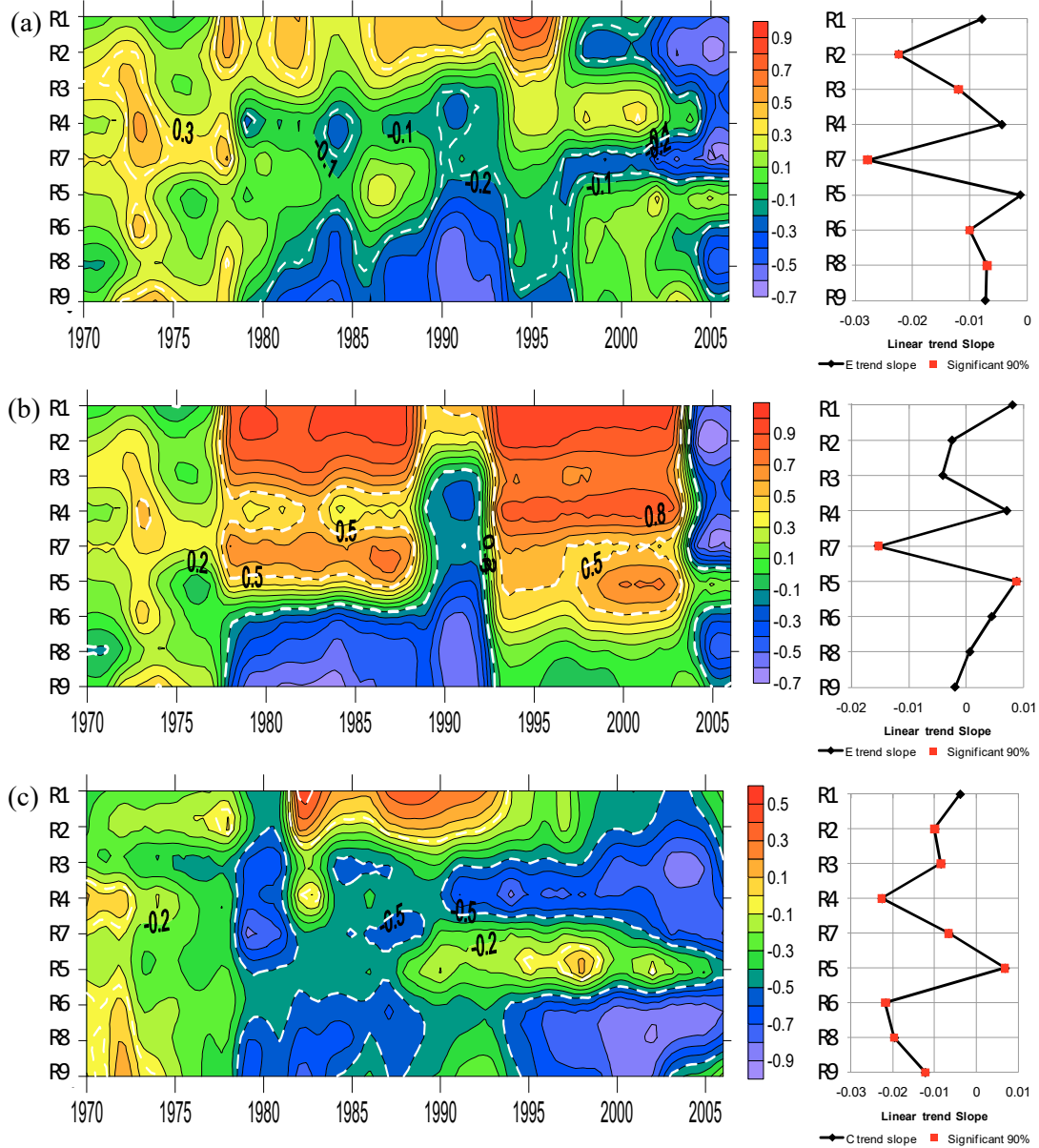


Figure 6.4. 11-year running correlation coefficients between precipitation and (a) the E index and within each region (R1 to R9) not considering the ENSO strong events of 1982/1983 and 1997/1998. The plot on the right hand side displays the slope of the linear trend of the running correlation (red dots indicates that the trend is significant at the 90% level using a t-student test). The white dashed lines indicate the significance level of the correlation at the 90% level; (b) *Idem* for E index but considering the ENSO strong events of 1982/1983 and 1997/1998; (c) *Idem* for C index not considering the ENSO strong events of 1982/1983 and 1997/1998.

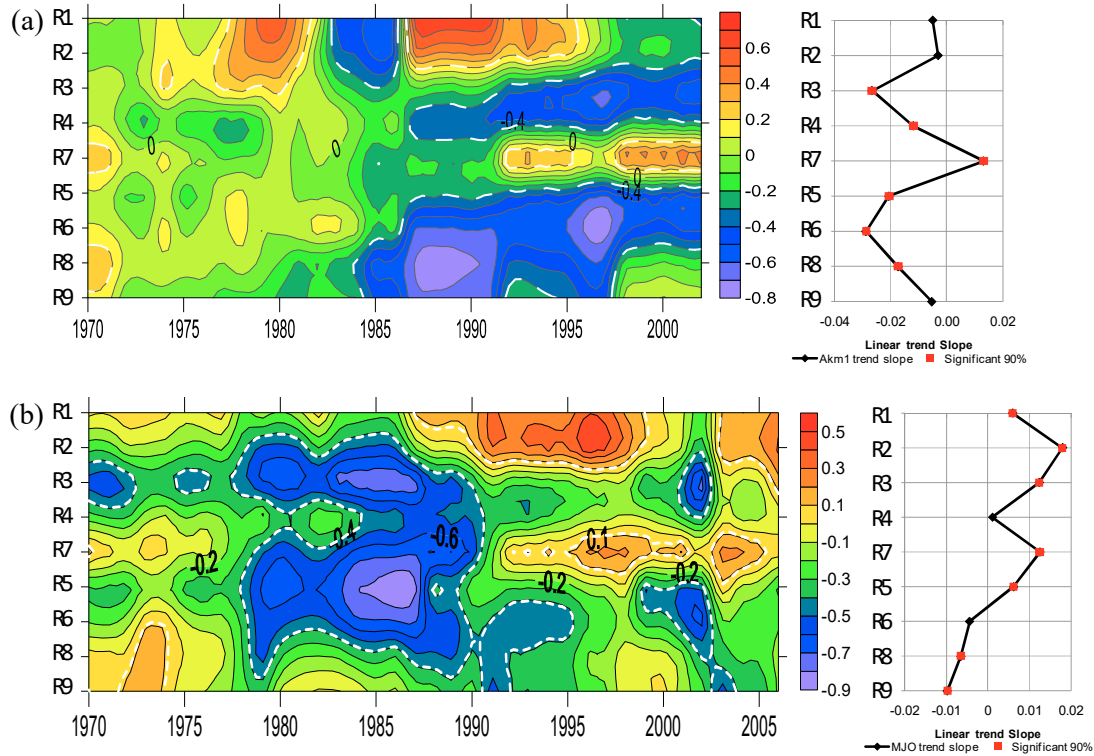


Figure 6.5. 11-year running correlation coefficients between precipitation and (a) Akml index within each region (R1 to R9) not considering the ENSO strong events of 1982/1983 and 1997/1998. The plot on the right hand side displays the slope of the linear trend of the running correlation (red dots indicates that the trend is significant at the 90% level using a t-student test). The white dashed lines indicate the significance level of the correlation at the 90% level. (b) *Idem* for MJO index.

d. Precipitation variability and sea surface temperature anomalies

In order to estimate the value of the regionalization for interpreting the impact of climatic variability over precipitation along the Pacific slope and coast of Peru, a covariance analysis is performed between the precipitation time series of the nine regions found in Chapter 3 and the SST anomalies over the Tropical Pacific and Atlantic Oceans. For clarity, the SST anomalies are considered for the peak ENSO season (i.e. December-January-February mean, hereafter DJF) whereas the precipitation fluctuations are considered for the approximate rainy season (i.e. December-January-February-March-April season, hereafter DJFMA). The results of the covariance analysis (see section 6.1.2d for details) are presented in Figures 6.6. and 6.7, showing the patterns and time series of the first (Figure 6.6) and second (Figure 6.7) SVD modes between SST in the tropical Pacific and Atlantic over DJF and precipitation over the regions over DJFMA. Values of the mode patterns, significant at the 90% level, are indicated by the colour shading (Figures 6.6b and 6.7b) and the red colour (Figures 6.6a and 6.7a, see method in section 6.1.2d). The results indicate a significant relationship between both fields since the percentage of

covariance is 66% and 23% for the first and second modes respectively, and the associated time series of the mode patterns are significantly correlated (r value reaches 0.59 (0.54) for mode 1 (2) in Figure 6.6c (Figure 6.7c) respectively). The first mode for SST accounts for the strong eastern Pacific El Niño variability as suggested by the large positive skewness of the principal component time series associated with the two strong El Niño events of 1997/98 and 1982/83. The correlation between the time series associated with the SST mode pattern and the E index reaches 0.80. The second mode is reminiscent of the central Pacific El Niño variability since it has a strong positive loading near the deadline. Its associated principal component time series is strongly correlated to the C index reaching a correlation of 0.96, significant at the 95% level. Interestingly the time series associated with the first mode for SST is also highly correlated with the C index ($r=0.73$), which indicates that extreme precipitation events are related to both the E and C modes. It explains in particular why the SST mode pattern has a significant loading in the central Pacific which is not the case for the E mode pattern which is more confined towards the coast of Ecuador (see Takahashi *et al.*, 2011).

The analysis of the mode patterns for precipitation clearly indicates that the first mode accounts for extreme precipitation events in the northern part of Peru (regions 1 and 2) whereas the second mode pattern has a larger loading (negative value) for the upstream regions (region 3, 6, 8 and 9), clearly indicative that during central Pacific El Niño events, the Pacific slope of Peru experiences a deficit in precipitation that increases with altitude. Note that this analysis is consistent with results from previous works (Lavado and Espinoza, 2014; Bourrel *et al.*, 2015), which analyzed the relationship between E and C indices and stations over the Peruvian territory and over the North to Centre of the Peruvian Pacific coast and slope respectively. It is here provided a more quantitative estimate of this relationship through the covariance analysis, which indicates its potential for climate impact studies. In particular, the SVD modes would allow building a linear statistical model of precipitation over the Peruvian Pacific coast using SST as a predictor. The regionalization procedure prior to conducting the SVD analysis is also valuable in easing the interpretation of the ENSO impact on precipitation, in particular, by avoiding likely spurious effects associated with outliers or multiple atmospheric influences. Another important result arising from this analysis is that the extreme precipitation events over the Peruvian Pacific coast are not solely influenced by extreme El Niño events (accounted for by the E mode) but are also influenced by SST in the central equatorial Pacific, as evidenced by the strong correlation between the principal component of the first SVD mode for SST and the C index. This suggests that the magnitude and location along the equator of the SST anomalies in the central Pacific are important parameters to determine the ENSO impact of precipitation over the Peruvian Pacific coast.

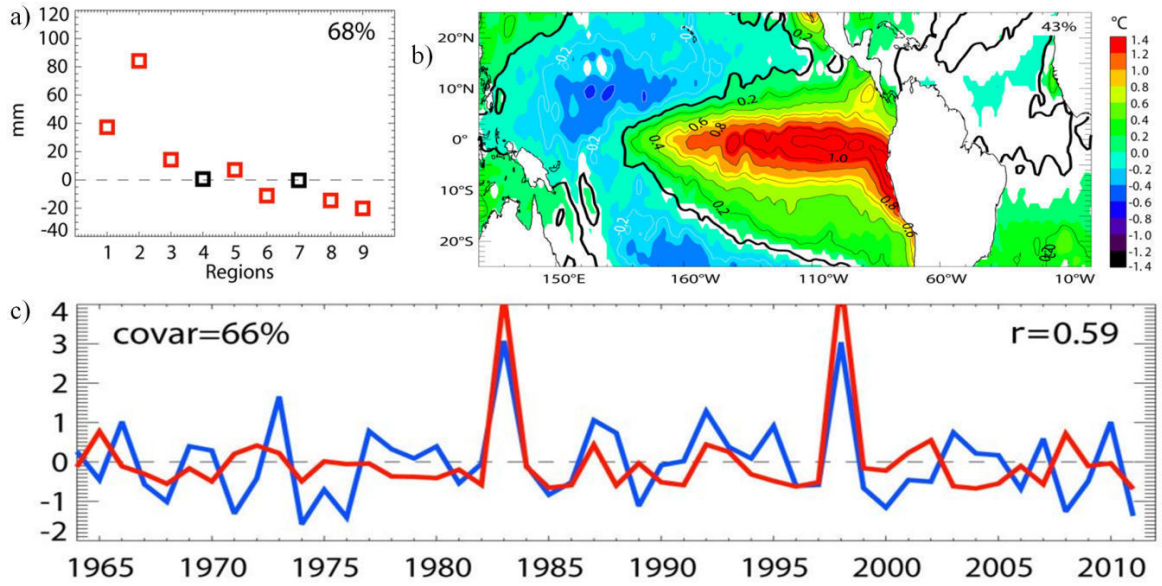


Figure 6.6. Dominant SVD mode between precipitation in DJFMA over the 9 regions and SST anomalies in DJF over the tropical Pacific and Atlantic: **a)** Mode pattern for precipitation; **b)** Mode pattern for SST (contour interval is every 0.2°C); **c)** Associated SVD time series for precipitation (red colour) and SST (blue colour). The percentage of variance of the modes is indicated in panels a) and b), whereas the percentage of covariance (covar) is indicated in panel c). The correlation (r) between the SVD time series is also indicated in panel c). The contour in thick black line in panel b) indicates the zero-contour. The shading (red) colour in panel b) (a) respectively, indicates where the mode pattern is statistically significant at the 90% level.

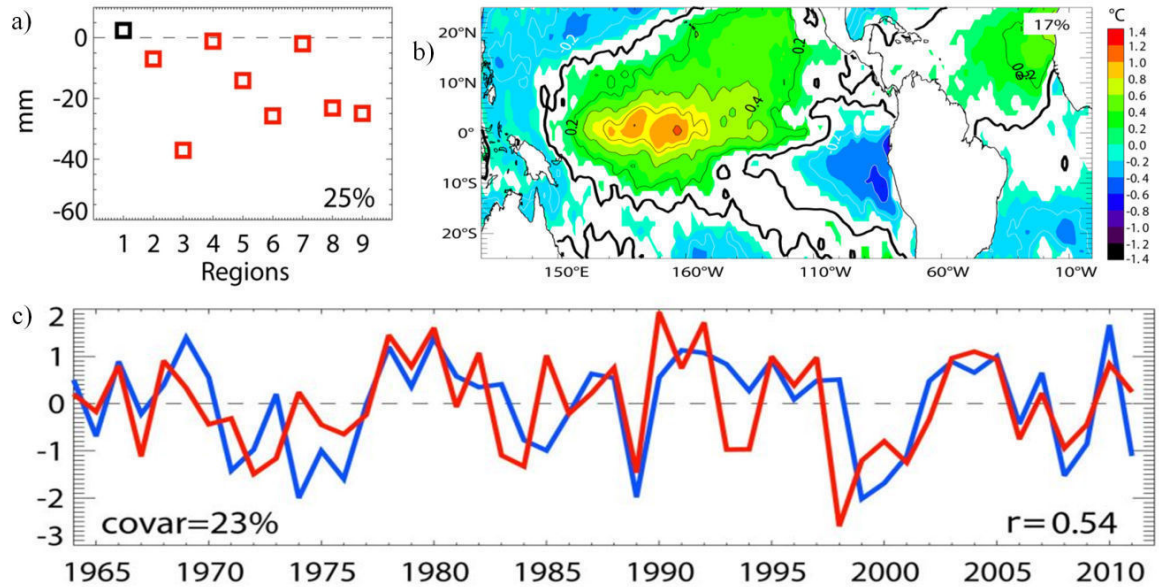


Figure 6.7. Same as Figure 6.6, but for the second SVD mode.

e. Low frequency modulation of ENSO and runoff regime

Extreme precipitation is often used as an early indicator of flooding during extreme ENSO events. However, the nonlinearity between precipitation and streamflow means that it is important to assess the impact of ENSO not just on precipitation, but on runoff (Stephen et al., 2015; Emerton et al., 2017). Some encouraging results are shown here as a perspective work about relationship of ENSO indices and runoff for unimpaired conditions along the Pd considering the methodology of running correlation applied in Section 6.1.3c for precipitation. Figure 6.8 shows the direct influence (in red shades) of Eastern El Niño through the E index over northern catchments and its inverse influence (in blue shades) over southern catchments. See numbering from 1 to 49 following north-south latitudinal direction in Figure 5.7 in Chapter 5. The strong event of 1982/1983 is predominant with significant opposite effects in northern and southern latitudes and the strong event of 1997/1998 is predominant with significant direct influence over northern until central catchments. Correlation values surpass those obtained for the relationship between precipitation and E index in Figure 6.4b. Over the study period, there is positive trend of correlations mostly over central catchments.

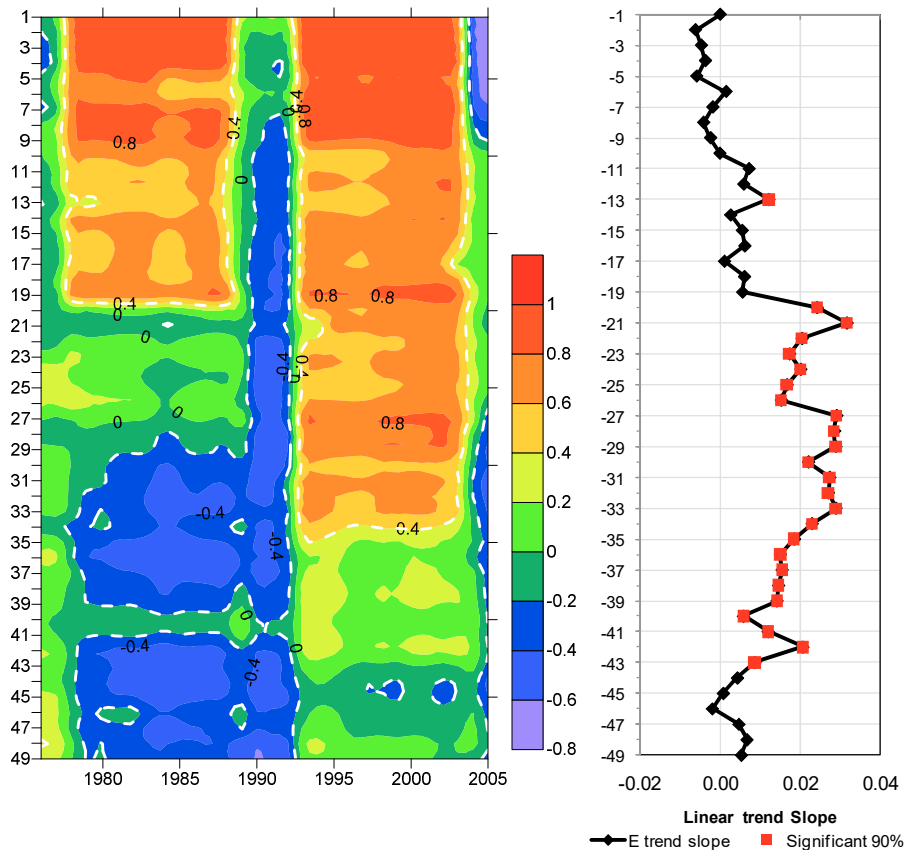


Figure 6.8. 11-year running correlation coefficients between unimpaired runoff and E index within each catchment (1 to 49) considering the ENSO strong events of 1982/1983 and 1997/1998. The plot on the right hand side displays the slope of the linear trend of the running correlation (red dots indicates that the trend is significant at the 90% level using a t-student test). The white dashed lines indicate the significance level of the correlation at the 90% level.

Without considering these two strong events, the E index explains the inverse relationship (blue shades) in only some southern catchments between 1980 and 1995 (see Figure 6.9). Over the study period, there is a negative trend of correlations mostly over northern catchments.

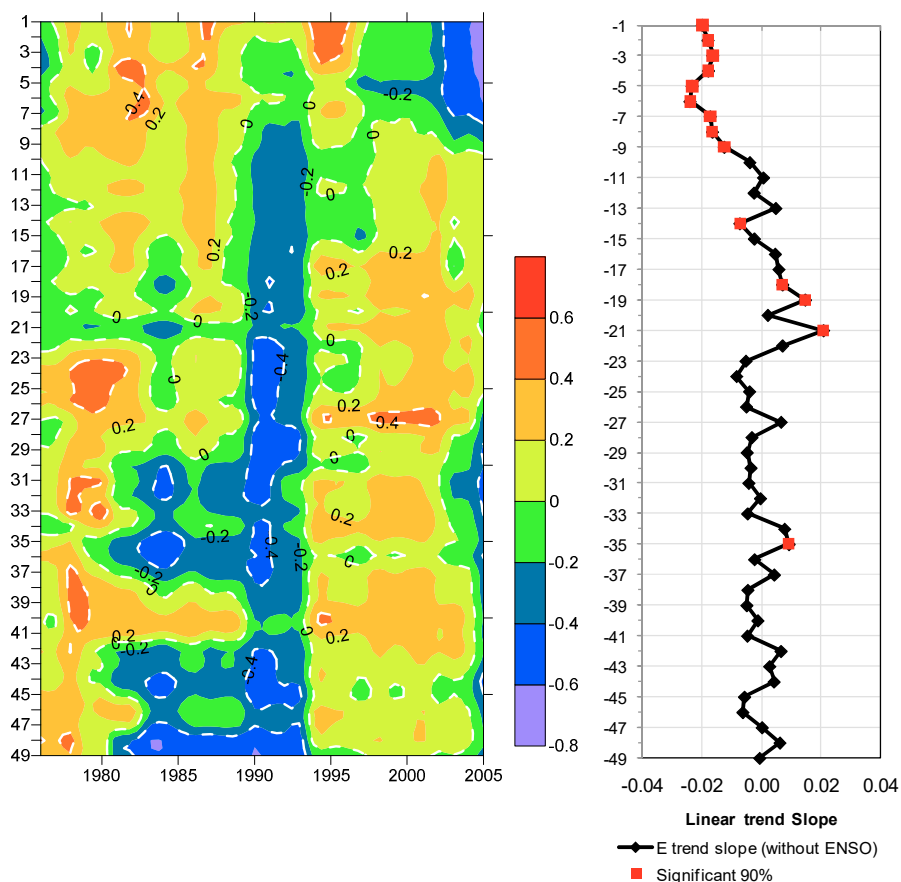


Figure 6.9. Idem as previous Figure 6.8 but not considering the ENSO strong events of 1982/1983 and 1997/1998.

Figure 6.10 shows the significant inverse influence (in blue shades) of Central El Niño through the C index over central and southern catchments without considering the two strong events of 1982/1983 and 1997/1998. It is notorious the strong inverse relationship (in purple shades) after 2000s. Correlation values surpass those obtained for the relationship between precipitation and C index in Figure 6.4c. Over the study period, there is negative trend of correlations along most catchments of the Pd. The strongest negative correlations and trends are found for central and southern catchments during the 2000s which corresponds to the period of occurrence of only CP El Niño events.

These preliminary results could be corroborating the statement from Chiew and McMahon (2002). They proposed that ENSO/streamflow relationship is likely stronger than the ENSO/precipitation relationship because the variability in precipitation is enhanced in runoff and because streamflow integrates information spatially.

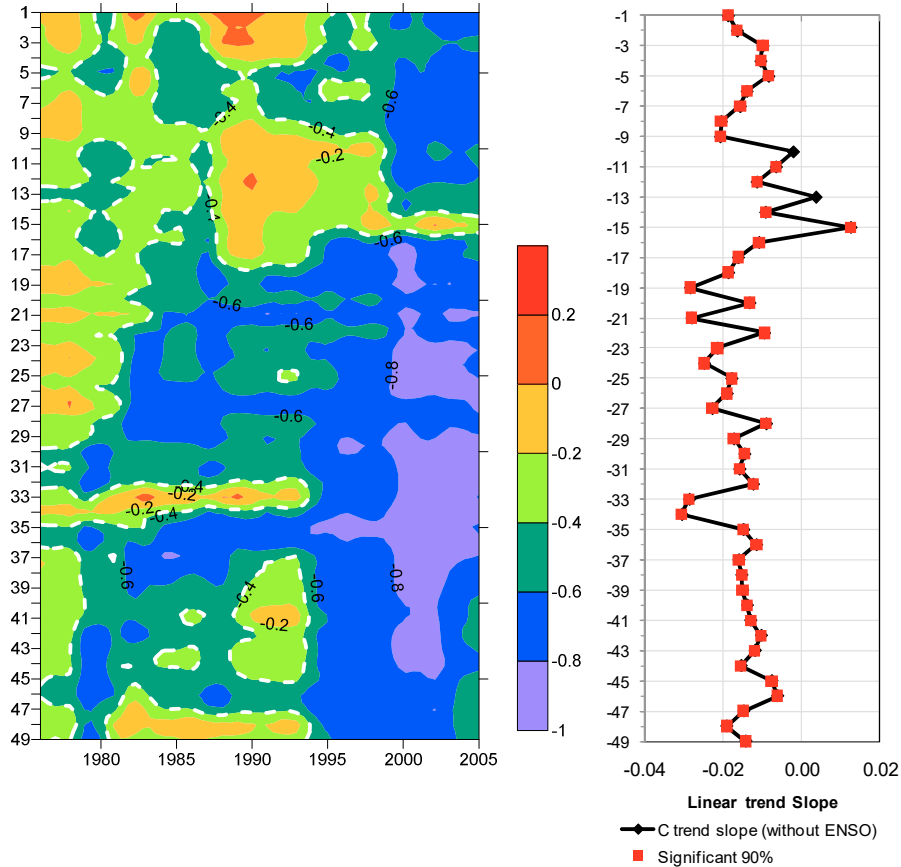


Figure 6.10. Idem as previous Figure 6.8 but for C index and not considering the ENSO strong events of 1982/1983 and 1997/1998.

6.1.4. Conclusions

In this subchapter, we used the regionalized precipitation product presented in Chapter 3. We here show that the strong positive relationship between precipitation and ENSO over the entire records results mostly from the influence of the strong events of 1982/83 and 1997/98. Without considering these extremes events, the relationship between ENSO and precipitation exhibits a significant decadal modulation with the larger ENSO impact over the 1990s and afterwards. In particular in the 2000s, the relationship between ENSO variability and precipitation reverses compared to the previous decade, i.e. El Niño occurrence is associated with reduce precipitation. This period is also associated with the occurrence of only CP El Niño events that are associated with neutral to cool SST anomalies along the coast of Peru.

A variety of ENSO indices, including the C and E indices recently defined by Takahashi *et al.* (2011) are used to estimate trends in the ENSO/precipitation relationship. We also used indices derived from equatorial oceanic Kelvin wave estimates in order to take into account oceanic influences not directly related to the interannual variability over the entire tropical Pacific. Oceanic Kelvin wave at intraseasonal timescales can in particular impact SST along the coast and modify the mixing in the marine boundary layer along the coast leading to either increased convection (mostly in the northern part of Peru) or

increased stability under upwelling events (all along the coast). The analysis indicated that in the recent decades, the ENSO influence on precipitation along the coast is characterized by an inverse relationship, which results from both the increased occurrence of CP El Niño events that lead to cooler SST conditions off Peru (Dewitte *et al.*, 2012) and from the influence of La Niña events and upwelling events. The mean SST off Peru has cooled in the recent decades (Dewitte *et al.*, 2012; Gutierrez *et al.*, 2011). A shift towards cooler conditions in the 1990s is also observed in the mean state of the tropical Pacific (Hong *et al.*, 2013) that is suggested to be concomitant to the increased occurrence of CP El Niño (Chung and Li, 2013). So both changes in mean upwelling and in upwelling variability may contribute to strengthen the inverse relationship between ENSO and precipitation along the coast of Peru over the recent decades.

Overall results suggest a significant change in the ENSO/precipitation relationship along the coast of Peru due to the predominance of CP El Niño-type in recent decades. It calls for better understanding the oceanic influence on the marine boundary layer considering cooler SST along the coast tends to stabilize the marine boundary layer and lead to drier conditions near-shore. On the other hand, most of the regions considered here are located at a 2000 m elevation which is above the marine boundary layer, so that precipitation changes may be influenced by non-local processes. A better understanding of the regional atmospheric circulation in this region is required, which will help in better identifying key indices that can be related to precipitation variability at different altitude along the coast. This can be addressed from the experimentation with a regional high-resolution atmospheric model, which is planned for future work.

In the same way, the use of the ten ENSO indices associated with different facets of ENSO (ENSO canonical vs. ENSO Modoki) improve the understanding of the complex relationship between precipitation and ENSO in Peru (from Northern to Center of Pacific coast). It is planned to extend this type of studies at regional scale to help improve climate and hydrological forecasts for the most affected countries of the Pacific coast of South America (Peru and Ecuador).

Finally, the nine identified regions are shown to grasp the salient features of the influence of ENSO onto precipitation along the Pacific slope and coast of Peru (Horel and Cornejo-Garrido, 1986; Goldberg *et al.*, 1987; Tapley and Waylen, 1990; Takahashi, 2004; Nickl, 2007; Lagos *et al.*, 2008; Lavado *et al.*, 2012; Lavado and Espinoza, 2014; Bourrel *et al.*, 2015), which illustrate its potential for climate impact studies. The dominant co-variability mode between SST in the tropical Atlantic and Pacific Oceans and the reduced set of time series associated with the nine regions has a strong positive loading over the northern part of Peru (regions 1 and 2) for precipitation and over the eastern tropical Pacific for SST, thus accounting for extreme El Niño events. On the other hand, the second mode pattern has a larger loading (negative value) for the upstream regions along the Pacific slope (region 3, 6, 8 and 9), clearly indicative that during central Pacific warming, this region experiences a deficit in precipitation that tends to increase with altitude (more negative in the north than in the south). This is consistent with the results

from Lavado and Espinoza (2014) who analyzed the relationship between the two types of ENSO and stations over the Peruvian territory, while providing a more synthetic picture of the ENSO influence. In addition, the first co-variability mode between precipitation and SST indicates that extreme precipitation events take place in the North (regions 1 and 2) and are influenced by SST anomalies in the central Pacific (i.e. SST anomalies that project on the C mode), which was not identified in previous works. We attribute this discrepancy between our result and the one by Lavado and Espinoza (2014) to the regionalization procedure that we perform prior to the statistical analysis with ENSO indices. In particular, our regionalization product accounts exclusively for precipitation variability over the Peruvian Pacific continental slope and coast, and is not influenced by stations located at high altitude regions that might be influenced by inland circulation patterns. The regionalisation procedure has also the advantage of reducing the influence of outliers in the covariance analysis.

About ENSO/streamflow relationship, the preliminary results suggest that correlation become stronger for ENSO/streamflow relationship than ENSO/precipitation relationship. It is due to the variability in precipitation is enhanced in runoff and because streamflow integrates information spatially according to Chiew and McMahon (2002).

6.2. Trends and hydroclimatic change disparity over catchments

6.2.1. Theoretical background

As mentioned in Chapter 4, in order to interpret climate variability and anthropogenic influence on water balance, the study was based on the Budyko theory (Budyko 1958, 1974). Thereby, all interactions through the hydrological cycle between vegetation, soil and atmosphere create an empirical equilibrium represented by the Budyko curve (van der Velde et al. 2013).

This study aims at explaining the hydroclimatic behaviour of the Pd catchments as a benchmark for understanding the sensitivity of catchments to changes in water balance along this region having a large latitudinal extent with a steep topography in the longitudinal direction. Firstly, a hydroclimatic complementary description of the Pd is achieved based on trend analysis of the available time series of precipitation, temperature, evapotranspiration and streamflow. Then, the use of Budyko space is considered for assessing the level of adaptation and sensitivity to climate variability and land use change over quasi-natural catchments identified in Chapter 4.

6.2.2. Methods

a. Characterization of hydroclimatic time series

After compiling all datasets by catchment, complementary analyses were performed for detecting plausible trends and changes using the non-parametric Mann-Kendall trend test, the double mass curve method and the Pettitt test.

The rank-based Mann–Kendall test (Mann 1945; Kendall 1975) was used to detect trends in the hydroclimatic series. The method is recommended by the World Meteorological Organization (WMO) and widely used for assessing the significance of monotonic trends in hydrological series. This method does not infer any distributional function for the data and has already proved its efficiency (e.g., Lavado et al. 2012; Chen et al. 2013; Wang et al. 2013). The double mass curve consists in the plot of the accumulated values of one variable versus the accumulated values of another related variable for a same period (Searcy and Hardison 1960). The plot is a straight line if the two variables are proportional, and the slope of this line represents the ratio between the two variables. A change in the gradient of the curve indicates that the original relationship between variables was modified. It can be used to check the consistency of hydrological records and has recently become an effective tool for detecting the changes of hydrological regime due to anthropogenic disturbances (e.g. Zhang and Lu 2009; Wang et al. 2013). In this study, a double mass curve between precipitation and runoff was employed as an auxiliary confirmation of the change-points when catchment changes mainly induced by human activities exert influences on the river.

The Pettitt test (Pettitt 1979) is a non-parametric approach to determine the occurrence of a change-point. This approach is a rank-based and distribution-free test for detecting a significant change in the mean of a time series when the exact time of the change is unknown. Pettitt test has been widely used to detect changes in the hydroclimatic records (e.g. Lavado et al. 2012; Wang et al. 2013). It is used the Pettitt test to identify the change-point of the runoff series and compare with the change-points detected by double mass curve.

b. Hydroclimatic change disparity

Based on Jones et al. (2012), under stationary conditions or natural climatic oscillations, catchments should fall on the Budyko curve (theory explained in section 4.2 in chapter 4). Under non-stationary conditions or anthropogenic climate change, catchments are likely to deviate from the Budyko curve in a predictable manner. Over these conditions and following van der Velde et al. (2013) and Jaramillo and Destouni (2014), the trajectories in Budyko space were defined, which are characterized by a direction (α) and magnitude (β) of change over the considered period. The direction of change is calculated from the equation:

$$\alpha = \arctan \left[\frac{\Delta AET.(P) - (AET).\Delta P}{\Delta PET.(P) - (PET).\Delta P} \right] \quad (6.5)$$

where AET (mm/yr) is the average AET over the period, and ΔAET (mm/yr²) is the change of AET over the period. Also, PET (mm/yr), ΔPET (mm/yr²), P (mm/yr) and ΔP (mm/yr²) are the average PET and change of PET over the period, the average P and change of P over the period, respectively. Here, α is calculated in degrees and counter clockwise from the negative y-axis. In the same way, the magnitude of change is expressed as the following equation and expressed in 1/yr.

$$\beta = \sqrt{\left(\frac{\Delta AET \cdot (P) - (AET) \cdot \Delta P}{(P)^2}\right)^2 + \left(\frac{\Delta PET \cdot (P) - (PET) \cdot \Delta P}{(P)^2}\right)^2} \quad (6.6)$$

Direction is related to change adaptations of ecosystems and magnitude related to ecosystems sensitivity to climate variability and land use change.

6.2.3. Results and discussion

a. Characterization of hydroclimatic time series

Mean annual values of hydroclimatic series are given in Table 4.1 in Chapter 4. Changes in hydroclimatic series are presented in Table 6.2. An increase or a decrease (i.e., positive or negative sign respectively) indicates the long term behaviour of the series. All slopes are significant at the 95% level using a Student t-test, however for highlighting the long term effect of these hydroclimatic series over catchments, the trends and their significance (at the 95% of confidence level) were estimated based on the Mann-Kendall test (significant trends are shown in bold in Table 6.2). Catchments with low disparity in water balance are shaded in grey rows according the methodology explained in Section 4.2 in Chapter 4.

On the one hand, changes in runoff and precipitation are greater in northern catchments (mainly positive changes) and decrease towards southern latitudes. On the other hand, changes in temperature (T) and PET are always positive (see Table 6.2). This can be explained by regional climate anomalous conditions along the Pd, in particular the well-known ENSO influence over precipitation and runoff in the northern areas (Lavado et al. 2012; Bourrel et al. 2015; Rau et al. 2016). Trend tests indicate that long-term increase in temperature time series are significant in all catchments with a mean value of $+0.02^\circ\text{C}/\text{yr}^2$ (\sim a mean warming of 0.2°C per decade). There is an area covering Moche (n°6) and Santa up (n°7) catchments with a mean warming above of $0.3^\circ\text{C}/\text{dec}$. This is consistent with previous climatological studies for the Andes such as the one by Vuille et al. (2015) that showed that most stations over the Pd had a significant positive trend in total temperature with a mean warming above of 0.2°C per decade. They suggested that at inland and higher elevations locations there is a clear evidence of warming and in coastal regions there is still a regional climate influence due to the variability of the Pacific Decadal

Oscillation (PDO) and of the intensity of the South Pacific anticyclone (SPA). Results support the interpretation of warming at basin scale (i.e. the influence of either global warming or climate variability at timescales longer than the PDO) where these changes in temperature are expected to have important consequences for western Andean glaciers.

Table 6.2. Mean annual change (Δ) in precipitation (P), temperature (T), potential evapotranspiration (PET), actual evapotranspiration (AET) and runoff (R). Values with significant trends at 95% of confidence level are shown in bold. Years of significant change-point at 95% of confidence level are indicated between parentheses. Catchments with low disparity in water balance are shaded in grey rows.

n°	Catchment	ΔP mm/yr ²	ΔT °C/yr ²	ΔPET mm/yr ²	ΔAET mm/yr ²	ΔR mm/yr ²
1	Piura up	2.84	0.02 (1986)	1.20 (1986)	-1.36	4.20
2	Piura	3.95 (1997)	0.02 (1986)	0.98 (1986)	1.11	3.28
3	La Leche	0.18	0.02	1.10	1.07	-0.90
4	Zaña	5.19 (1982)	0.01	0.73	4.00 (1983)	1.19
5	Chicama	3.31	0.03 (1982)	1.71 (1982)	3.15 (1992)	0.16
6	Moche	1.46	0.06	3.11	0.61	0.85
7	Santa up	3.80 (1992)	0.04 (1991)	2.12 (1996)	7.28 (1992)	-3.48
8	Santa	2.43	0.03	1.41	4.15 (1992)	-1.97
9	Casma	1.31	0.03 (1990)	1.53 (1982)	1.44 (1992)	-0.13
10	Huarmey	4.77	0.03 (1982)	1.75 (1982)	2.76	2.01
11	Pativilca	-2.90	0.02	1.08	0.33	-3.22 (1989)
12	Huaura	-2.70	0.02	1.19 (1996)	0.45	-3.15 (1987)
13	Ch. Huaral	-0.33	0.03 (1996)	1.13 (1996)	2.40	-2.78
14	Chillon	-0.43	0.03 (1996)	1.58 (1991)	-1.45	1.02
15	Rimac	-1.08	0.03 (1991)	1.48 (1991)	-2.71	1.63
16	Cañete	2.80	0.01	0.30	4.24 (1996)	-1.44
17	San Juan	2.38	0.01	0.55	3.77 (1992)	-1.39
18	Ica	2.43	0.02 (1979)	0.84 (1991)	1.17	1.26 (1993)
19	Acari	2.70	0.01 (1977)	0.75 (1977)	2.43	0.26
20	Yauca	2.29	0.01	0.69	0.98	1.31
21	Majes	1.53	0.03 (1986)	1.34 (1986)	2.72 (1995)	-1.19
22	Camana	1.23	0.02 (1986)	1.13 (1986)	2.75 (1995)	-1.52
23	Chili	0.76	0.03 (1986)	1.68 (1986)	0.23	0.53 (1996)
24	Tambo	-0.60	0.03 (1986)	1.57 (1986)	0.25	-0.85
25	Moquegua	-1.02 (1977)	0.03 (1982)	1.47 (1982)	-0.90	-0.12
26	Caplina	-0.75	0.02 (1982)	0.85 (1982)	-1.12	0.37 (1996)

No significant increase or decrease in P was observed over the study area (except only for Piura (n°2) catchment). The runoff (R) time series present a significant increase over Ica (n°18) which is related to water transfers from Atlantic basin (see Figure 2.5 in Chapter 5) and over Yauca (n°20) related to the no significant increase in PET. Runoff also presents a significant decrease over central catchments (Santa up n°7, Pativilca n°11 and Huaura n°12) whose upper basins benefit from the melting of the

Cordillera Blanca glacier and surroundings. At interannual time step, these decreases could be mainly related to the intensive water exploitation for agricultural activities. AET time series present a significant increase in Zaña (n°4), Chicama (n°5), Santa up (n°7), Cañete (n°16), San Juan (n°17) and Camana (n°22) and a significant decrease in Rimac (n°15) catchment.

Occurrence of change-points at 95% of confidence level detected by the Pettitt test and double mass curve methods is significant in some catchments and the year when the change-point occurred are indicated between parentheses in Table 3. Most catchments did not present change-points in P (except to Piura (n°2), Zaña (n°4), Santa up (n°7) and Moquegua (n°25)). Change-points for T time series were grouped by catchment proximity and regional localization along the Pd. For the northern catchments of Piura up (n°1) and Piura (n°2), the year of 1986 meant a change-point. Catchments in southern latitudes present significant change-points in the years 1977, 1982 and 1986. By the fact of presenting a warming on such a large scale, those change points could be related mainly by climatic influence (i.e. ENSO changes and climate shifts; see the work by Bourrel et al. 2015 for precipitation). Change-points in R are mainly related to the development of new phases into the large hydraulic infrastructure as the case of Ica (n°18), Chili (n°23) and Caplina (n°26) and also with the land cover change (which is discussed in next section) as the case of Pativilca (n°11) and Huaura (n°12).

b. Hydroclimatic change disparity

According to the Budyko space shown in Figure 4.3 in Chapter 4, most Pd catchments move closer to the theoretical water and energy limits. Following the premise that 11 catchments previously selected in Chapter 4 have a “quasi natural” behaviour with less anthropogenic and climatic influence, it is expected that these catchments move in all directions through Budyko space. The direction and magnitude of change is presented in Figure 6.11a and 6.11b respectively, where most of the years in all catchments are characterized by energy (i.e. $PET/P < 1$) and water limitations (i.e. $PET/P > 1$). Direction and magnitude values are provided in Table 6.3.

Figure 6.11a indicates two types of change adaptations represented mostly with green and red points in one group (i.e. towards more energy limited environments to the left) and yellow and orange points in the other (i.e. towards more water limited environments to the right). Red and green points tend to be an energy-limited environment ($PET/P < 1$) and those catchments are plotted in Figure 6.12a. According to Table 6.2, these catchments present a decrease in runoff, which can be explained by the increase of both T and PET and the non-alteration in precipitation, concluding that those catchments have already the tendency to become less energy limited. Yellow and orange points group present high values of PET/P representing the strong variability of runoff and precipitation, corresponding to catchments with strong climatic influence as the ENSO and semi-arid conditions.

Figure 6.11b shows two types of catchment sensitivity to climate variability (i.e. likely with high sensitivity to future climate) and land use changes, represented mostly with orange and yellow points in one group (i.e. towards more energy limited environments to the left) and red and purple points in the other (i.e. towards more water limited environments to the right). A large change in magnitude means that climate or human induced changes were particularly large in this region and that any direction from Figure 6.12a having a very small magnitude (see values in Table 6.3) can be considered as of little relevance (van der Velde et al. 2013). Orange and yellow points group has a low magnitude of change corresponding to catchments with low variability on precipitation and runoff. Red and purple points group coincides with catchments presenting significant variability in both precipitation and runoff. Figure 6.12b shows the magnitude of change of the 11 selected catchments and Table 6.3 highlights in grey the 6 catchments identified as with major sensitivity.

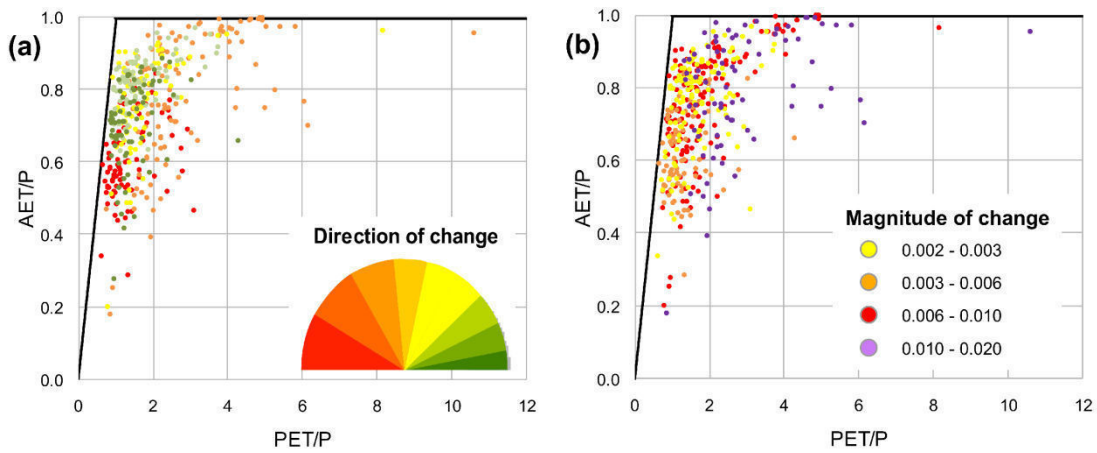


Figure 6.11. Grouping of Budyko trajectories defined by their direction (a) and the magnitude (b) of change for the 11 selected catchments in the Budyko space over the 1970–2008 period.

They can be described in the light of Table 6.2 as follows: purple points represent the catchments of Piura (n°2) and Yauca (n°20), which are located mostly in a water limited environment ($PET/P > 1$) and where increase in P is likely to increase the assessment of AET through the Budyko equation (increase in PET due to increase in T over the studied period has the opposite effect). As results indicate that there is an increase in the AET in both cases with a significant increase in P for Piura (n°2) and a significant increase in R for Yauca (n°20), it is concluded that increase in precipitation is more likely to drive these ecosystems changes than the increase in temperature (i.e. increase in PET). Red points represent the catchments of Piura up (n°1), Chicama (n°5), San Juan (n°17) and Acari (n°19) which are located mostly in a water limited environment. However, Piura up (n°1) presents a decreasing in AET, suggesting that both precipitation and temperature (i.e. increase in PET) drive these ecosystem changes. San Juan (n°17) presents a decrease in R and because of its location in both water and energy limited environment, it suggests that both precipitation and temperature (i.e. increase in PET) drive this ecosystem changes. The remaining

catchments: Chicama (n°5) and Acari (n°19) suggest that increase in precipitation is more likely to drive these ecosystems changes than the increase in temperature.

Table 6.3. Budyko trajectories defined by direction (α) and magnitude (β) values across the selected catchments. Catchments with major sensitivity to climate variability and land use changes are shaded in grey rows. Errors expressed in (%) were obtained via a 10-year moving window.

n°	Catchment	α °Deg	β 1/yr
1	Piura up	97 (2%)	0.009 (30%)
2	Piura	99 (1%)	0.017 (32%)
3	La Leche	138 (1%)	0.002 (15%)
5	Chicama	75 (6%)	0.006 (25%)
9	Casma	67 (13%)	0.002 (46%)
11	Pativilca	124 (3%)	0.003 (13%)
17	San Juan	49 (9%)	0.008 (22%)
19	Acari	86 (3%)	0.007 (25%)
20	Yauca	103 (2%)	0.010 (27%)
22	Camana	16 (32%)	0.004 (16%)
24	Tambo	73 (3%)	0.002 (2%)

Piura upstream (n°1) and Piura (n°2) catchments exhibit a large increase in precipitation and runoff changes, and Chicama (n°5) shows a large increase only in precipitation change, influenced by the ENSO climate conditions and as shown in their time series (see Figure 4.1 in Chapter 4), those peaks are somehow inconsistent with the mean dry conditions.

It is worth pointing out that the hydrologic cycle of the 11 quasi-natural catchments is still influenced by human activities but only marginally (e.g. see changes in land cover in Figure 4.4 in Chapter 4). From an ecosystemic point of view and according to the Budyko theory (see van der Velde et al. 2013), in those “quasi natural” environments, any changes in vegetation is due to a co-evolution with the landscape to optimize water and energy use for given climatic conditions. It maintains a steady-state. However, the anthropogenic influence prevents a natural adaptation of vegetation species, as expected under the co-evolution. Strong disturbance could modify this behaviour (as found with the 15 remaining catchments) in a long term, where it would be valid to reconsider the statement of a steady-state.

The direction and magnitude values in the Budyko relationship are presented in Table 6.3. Equations 6.5 and 6.6 were also validated over different periods through a 10-year moving window along the 1970-2008 period, which yields a range of values expressed in error rates (%).

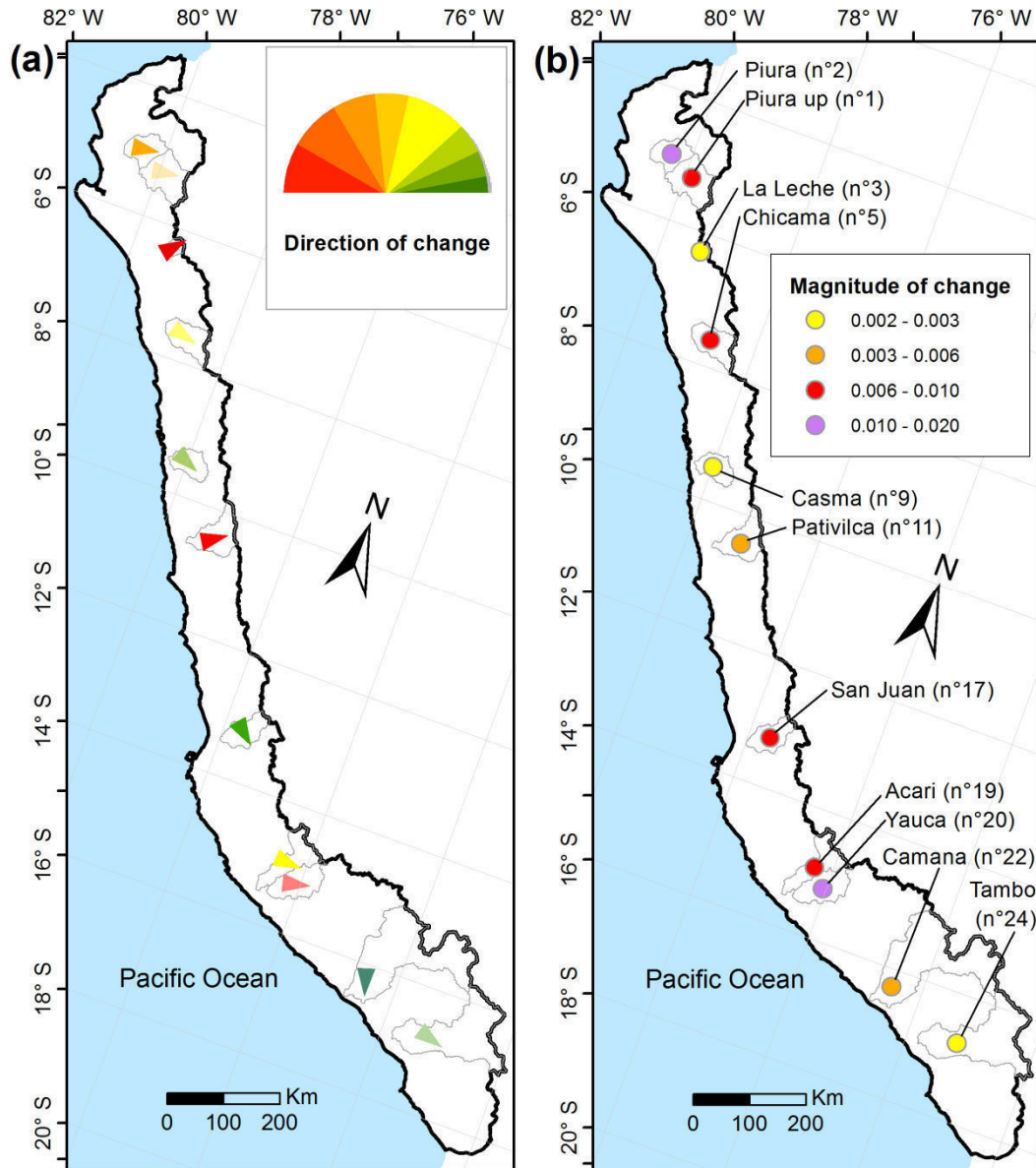


Figure 6.12. Budyko trajectories defined by their direction (a) and magnitude (b) plotted across catchments. Red/orange, yellow and green arrows in Figure 6.12a show the three regions grouped by their hydroclimatic change adaptation. Purple and red points in Figure 6.12b show the catchments with major sensitivity to climate variability and land use changes.

6.2.4. Conclusions

This chapter analyzed the hydroclimatic change over 26 catchments of the Peruvian Pacific drainage region for the 1970–2008 period.

According to significant upward trends in annual temperature found in all catchments and regional change-points found in most catchments, results showed a significant warming in the study area with a mean of 0.2°C per decade as already identified in studies for South American Andes as the one by Vuille et al. (2015). Precipitation data do not

exhibit significant trends and change-points in most catchments. The runoff time series presented a significant decrease over central catchments with a change-point in the years 1987 and 1989, which is mainly related to the intensive water exploitation for agricultural activities and land cover change.

Changes in trajectories in the Budyko space over those 11 selected catchments revealed two groups of catchments. Six catchments: Piura upstream (n°1), Piura (n°2), Chicama (n°5), San Juan (n°17), Acari (n°19) and Yauca (n°20) were shown to be sensitive to climate variability (i.e. likely with high sensitivity to future climate) and land use changes, where precipitation and temperature are the most likely drivers of these environments change. The five other catchments do not reveal any clear behaviour in terms of the sensitivity to climate variability.

Finally, depending on the observational period of the analysis, limitations are mostly related to limited hydro-climatic data availability and related to the steady-state hypothesis of the Budyko framework. However, despite these limitations, these results provide a first assessment of the catchments and their sensitivity to hydroclimatic change which has implication for regional water resources assessment and management.

(This page has been left blank intentionally)

Chapter 7

General conclusions and perspectives

7.1. General conclusions

This thesis answers the general scientific question: What is the role of hydroclimatic variability over the hydroclimatological regime in the Peruvian Pacific slope and coast? It is divided into two sub-questions: the first one related to the influence of climate variability and the second one related to the influence of hydroclimatic change over precipitation and runoff regimes. The study area represents the most important economical region of Peru and presents a high vulnerability to extreme climate events related to climate variability as well as a serious concern regarding freshwater resources availability because of its arid and semi-arid conditions.

A complete presentation of the study area and an in-depth analysis and treatment of in-situ hydroclimatic database is reported in Chapter 2. Hydroclimatic context was presented as a result of ocean-atmospheric conditions over physical landscape and hydrological characteristics. Mean climatic conditions and modes of variability as the El Niño phenomenon, decadal and intraseasonal variability were described. Physical landscape (i.e. topography, geology and vegetation) and the hydrological characteristics evidenced the arid conditions and anthropogenization degree. About database analysis, two approaches were considered. The first one was to assume the Peruvian Pacific slope and coast as a whole region. It was focused on the obtaining of high quality time series over each hydrometeorological station. Afterwards, Peruvian Pacific drainage was considered as a set of main catchments. It was focused on the obtaining of hydroclimatological time series over each catchment by a lumped way.

Specific scientific questions are answered throughout the thesis and are presented as follows: Chapter 3 answers the question: What is the spatio-temporal variability of interannual precipitation? This was focused on precipitation regionalization as a way to document and understand precipitation regime over the 1964–2011 period. Through a statistical analysis of a network of 145 precipitation stations, we proposed a methodology for regionalization of precipitation under non-stationary and/or non-Gaussian time-series condition based on a combined process consisting in k-means clustering and regional vector (RVM) methodologies. The k-means clustering analysis allows for a preliminary grouping of station data that is used as a first guess for the RVM and this step constrains to a large extend the regionalization procedure. As a result, nine regions were identified with a homogeneous precipitation regimes following a latitudinal and altitudinal gradient over the study area. It

highlights the distinction between northern, central and southern regions as well as the distinction between low, mid and high lands.

Precipitation variability is higher at the northern latitudes and it decreases to the south in high altitudes. The motivation for performing a classification using cluster analysis prior to the regionalisation by RVM stood in the complex of processes influencing precipitation variability over this region. In particular, previous studies (Lavado and Espinoza, 2014; Bourrel *et al.*, 2015) have shown that precipitation along the Peruvian Pacific slope and coast experiences the influence of both type of El Niño, and due to the strong positive skewness of strong El Niño events, the distribution of precipitation data is not Gaussian, limiting to some extents the linear analysis approach (i.e. RVM).

In Chapter 4 we addressed the issue of strong climate variability and anthropogenization and their susceptible interferences over hydroclimatic time series. The theoretical Budyko framework was used, which plot the relationship between dryness index and evaporative index. An empirical model called Budyko-Zhang was applied to identify plausible annual change disparity of water balance along 26 studied catchments of the study area over the 1970–2008 period. After corroborating semi-arid conditions at lumped catchment-scale with the vegetation Budyko-Zhang model parameter, 11 out of 26 catchments were identified as catchments following a Budyko-Zhang curve. This means 11 catchments with low water balance disparity related to both low climatic and anthropogenic influence. These catchments can be considered as hydrological systems with quasi-natural or unimpaired conditions at annual time scale. To validate this hypothesis derived from Budyko theory, spatial land cover and land use products as MODIS and LBA were analyzed. Catchments with high water balance disparity presented a significant change in land cover mainly with a decrease in cropland and an increase in grassland over the studied period.

Despite non-stationary limitations of the method, the results provided a first assessment of the catchments with less climate and anthropogenic influence on water which has implication for regional water resources assessment and management.

Chapter 5 answers the question: What is the spatio-temporal variability of interannual unimpaired runoff? We decided to analyse unimpaired catchments because of their high quality runoff time series with low anthropogenization influence. An initial documentation of runoff regime of seven catchments was done and some of them are reported in Chapter 2 mainly related to runoff in semi-arid conditions. Here, Chapter 5 was focused in a proposed methodology for estimating unimpaired freshwater runoff from Peruvian Pacific drainage catchments based on hydrological modelling via two conceptual lumped models at annual and monthly time scale (GR1A and GR2M respectively). A Differential Split-Sample Test (DSST) was used to cope with the temporal transposability of models parameter sets and modelling robustness over contrasted climate conditions as dry and wet years according to the semi-arid conditions of the study area. This methodology achieved to establish a regional runoff model (RRM) via the GR2M model at the monthly time step over seven selected catchments. From a hydrological modelling perspective, GR2M showed more robustness than GR1A model over contrasted climatic conditions (i.e. in terms of acceptable NSE and associated bias criteria). The seven unimpaired selected catchments presented a remarkable

hydrological regional monthly behaviour related to the transposing of their parameters set from dry to wet years. GR2M parameters set were linked with physical catchment characteristics (as the area, main channel length and perimeter) with a significant relationship with the soil reservoir parameter. The RRM was applied over 49 catchments along the study area to simulate runoff for unimpaired conditions at outlet points to the Peruvian Pacific Ocean. These results also showed an increasing regional unimpaired discharge from arid Peruvian Pacific coast to the Pacific Ocean over the last four decades (1970–2010 period). Limitations of methodology are related to its application in other spatial scales out of values used to obtain multiple regressions. However, RRM outputs expressed in terms of runoff anomalies would offer a great tool based on the good relationship found for the *XI* parameter which controls the runoff variability in the GR2M model

Finally, Chapter 6 discussed the scope of the thesis related to the impacts of climate variability and hydroclimatic change over precipitation and runoff regimes taking into consideration the three hydroclimatological products obtained in the previous chapters: the regionalized precipitation, the quasi-natural catchments set and the regional unimpaired runoff.

In the first part, ENSO/precipitation relationship was revisited by accounting for the regionalized precipitation product obtained in Chapter 3. A first approach about ENSO/runoff relationship was also proposed by accounting the unimpaired runoff time series obtained in Chapter 5. A variety of ENSO indices, including the C and E indices recently defined by Takahashi *et al.* (2011) were used to estimate trends in the ENSO/precipitation relationship. We also used indices derived from equatorial oceanic Kelvin wave estimates in order to take into account oceanic influences not directly related to the interannual variability over the entire tropical Pacific. Oceanic Kelvin wave at intraseasonal timescales can in particular impact SST along the coast and modify the mixing in the marine boundary layer along the coast leading to either increased convection (mostly in the northern part of Peru) or increased stability under upwelling events (all along the coast). The analysis indicated that in the recent decades, the ENSO influence on precipitation along the coast is characterized by an inverse relationship, which results from both the increased occurrence of CP El Niño events that lead to cooler SST conditions off Peru (Dewitte *et al.*, 2012) and from the influence of La Niña events and upwelling events. The mean SST off Peru has cooled in the recent decades (Dewitte *et al.*, 2012; Gutierrez *et al.*, 2011). A shift towards cooler conditions in the 1990s is also observed in the mean state of the tropical Pacific (Hong *et al.*, 2013) that is suggested to be concomitant to the increased occurrence of CP El Niño (Chung and Li, 2013). So both changes in mean upwelling and in upwelling variability may contribute to strengthen the inverse relationship between ENSO and precipitation along the coast of Peru over the recent decades.

We show that the strong positive relationship between precipitation and ENSO over the entire records results mostly from the influence of the strong events of 1982/83 and 1997/98. Without considering these extremes events, the relationship between ENSO and precipitation exhibits a significant decadal modulation with the larger ENSO impact over the 1990s and afterwards. In particular in the 2000s, the relationship between ENSO variability and precipitation reverses compared to the previous decade. Overall results suggest then a

significant change in the ENSO/precipitation relationship along the coast of Peru due to the predominance of CP El Niño-type in recent decades. Also, the nine identified regions are shown to grasp the salient features of the influence of ENSO onto precipitation along the Pacific slope and coast of Peru (Horel and Cornejo-Garrido, 1986; Goldberg *et al.*, 1987; Tapley and Waylen, 1990; Takahashi, 2004; Nickl, 2007; Lagos *et al.*, 2008; Lavado *et al.*, 2012; Lavado and Espinoza, 2014; Bourrel *et al.*, 2015), which illustrate its potential for climate impact studies. The dominant co-variability mode between SST in the tropical Atlantic and Pacific Oceans and the reduced set of time series associated with the nine regions has a strong positive loading over the northern part of Peru (regions 1 and 2) for precipitation and over the eastern tropical Pacific for SST, thus accounting for extreme El Niño events. On the other hand, the second mode pattern has a larger loading (negative value) for the upstream regions along the Pacific slope (region 3, 6, 8 and 9), clearly indicative that during central Pacific warming, this region experiences a deficit in precipitation that tends to increase with altitude (more negative in the north than in the south).

About ENSO/streamflow relationship, the preliminary results suggest that correlation become stronger for ENSO/streamflow relationship than ENSO/precipitation relationship. It is due to the variability in precipitation is enhanced in runoff and because streamflow integrates information spatially according to Chiew and McMahon (2002).

In the second part, hydroclimatic change study was provided through a trend analysis. This was done over hydroclimatic variables (precipitation, temperature, evapotranspiration and runoff) from 26 catchments studied in Chapter 4. According to significant upward trends in annual temperature found in all catchments and regional change-points found in most catchments, results showed a significant warming in the study area with a mean of 0.2°C per decade as already identified in studies for South American Andes as the one by Vuille *et al.* (2015). Precipitation data do not exhibit significant trends and change-points in most catchments. The runoff time series presented a significant decrease over central catchments with a change-point in the years 1987 and 1989, which is mainly related to the intensive water exploitation for agricultural activities and land cover change. However, according to Chapter 4 and 5, only 11 catchments could offer a quasi-natural runoff signal because of their unimpaired conditions at annual time step. Changes in trajectories in the Budyko space over those 11 selected catchments revealed two groups of catchments. Six catchments: Piura upstream (n°1), Piura (n°2), Chicama (n°5), San Juan (n°17), Acari (n°19) and Yauca (n°20) were shown to be sensitive to climate variability (i.e. likely with high sensitivity to future climate) and land use changes, where precipitation and temperature are the most likely drivers of these environments change. The five other catchments do not reveal any clear behaviour in terms of the sensitivity to climate variability. Catchments following the same change trajectory pointed a common water balance adaptation to regional climatic and/or anthropogenic forcings. The nearby catchment pairs of Piura (n°2) and Chicama (n°5); Acari (n°19) and Yauca (n°20) suggest that increase in precipitation is more likely to drive these ecosystems changes than the increase in temperature. Piura upstream (n°1) and San Juan (n°17) could be isolated from the rest but is likely that both precipitation and temperature drive these ecosystem changes.

7.2. Perspectives

Each chapter showed many results and conclusions, which open many perspectives for further research and they are organized in two sections as follows:

7.2.1. Impact of climate variability over seasonal hydrological regime as a forecasting tool

Impacts of climate variability over precipitation and runoff regimes were addressed at interannual time step offering a great perspective about the use of seasonal time scales. Current studies about ENSO in Peru are addressed in two ways as the study of the impact of ENSO over precipitation and its evolution in time and the study of the physics of the ENSO/precipitation relationship. A seasonal approach will allow merging these two approaches addressing the forecasting perspective as a valuable tool to anticipate and mitigate ENSO impacts. This work also could be done with the use of climate models, reanalysis and remote sensing products as it is worked in neighbour South American countries as in Ecuador in Recalde-Coronel et al. (2014), Pineda y Willems (2016), Vicente-Serrano et al. (2016), de Guenni et al. (2016).

The initial approach done about ENSO/runoff relationship opens an interesting discussion about the influence of ENSO over unimpaired and anthropogenized runoff. A few studies in Peru addressed this issue but they generally did not make any difference within the degree of catchment anthropogenization. Also, the regional runoff analysis did by hydrological modelling offers an interesting perspective about the influence of climate variability on the robustness of hydrological models. Calibration and validation methodologies generally did not consider low-frequency variability in hydroclimatic attributes in finding the most optimal parameter model set (see Wang et al., 2015).

Studying a variety of climatic, atmospheric and oceanic indices and their relationship with precipitation calls for a better understanding of the oceanic influence on the marine boundary layer. Considering cooler SST along the coast tends to stabilize the marine boundary layer and lead to drier conditions near-shore. On the other hand, most of the regions analyzed here are located over 2000 m elevation which is above the marine boundary layer, so that precipitation changes may be influenced by non-local processes. A better understanding of the regional atmospheric circulation in this region is required, which will help in better identifying key indices that can be related to precipitation variability at different altitude along the coast. This can be addressed from the experimentation with a regional high-resolution atmospheric model, which is planned for future work.

About the regionalized products of precipitation and the unimpaired runoff time series obtained in this thesis, they will provide valuable information with the aim of improving ecological and water resources management in the Peruvian Pacific drainage.

7.2.2. Impact of climate and catchment change over the hydrological regimes

In Chapter 4 we introduced the topic of the separation of climate and anthropogenization effects on water balance and runoff. Current international researches are still in development to address this issue (Zhou S et al., 2015; Greve et al., 2015); however they agree the need to evolve towards a non steady-state analysis. It means that depending on the observational period of the analysis, current limitations are mostly related to limited hydro-climatic data availability and related to the steady-state hypothesis of the Budyko framework (i.e. not considering water storage change).

Recent works as Zhou S et al. (2015) gave some hypothesis about the consideration of a “change” term in climate and catchment characteristics in the Budyko framework and Greve et al. (2015) showed a non-stationary Budyko framework when evapotranspiration exceeds precipitation at lower time scales than annual or when storage change in the land–water balance is not negligible. Also Zhou G et al. (2015) proposed a global pattern for the effect of climate and land cover on water yield.

However, despite the already mentioned limitations, the results obtained in this thesis provide the first assessment of the catchments and their sensitivity to hydroclimatic change which has implication for regional water resources assessment and management. These results also will be the base for future studies related to the impacts of climate change over hydrological regime, runoff and water availability. It is well-known the high uncertainty of climate models (i.e. Global Climate Models GCM) in precipitation over the Peruvian Pacific drainage (IPCC, 2014) offering a great perspective about uncertainty estimation in the arid and semi-arid hydrological context. DSST methodology used in Chapter 5 could offer another set of scenarios to validate properly any hydrological model. Regional runoff model could be improved towards the use of other conceptual hydrological models and finer time scale for the study of runoff sensitivity.

Conclusions générales et perspectives

(Version française)

7.1. Conclusions générales

Cette thèse s'est attachée à répondre à la question scientifique générale suivante : Quelle est l'influence de la variabilité climatique sur le régime hydroclimatique du Versant Pacifique péruvien ? Cette question est divisée en deux sous-questions : la première concerne l'influence de la variabilité climatique et la seconde concerne à l'influence du changement hydroclimatique sur les régimes des précipitations et des débits. La zone d'étude représente la région économique la plus importante du Pérou et présente une vulnérabilité élevée aux événements climatiques extrêmes (liés à la variabilité climatique dont principalement celle due au phénomène ENSO) ainsi qu'une grave préoccupation concernant la disponibilité des ressources en eau douce en raison de ses conditions arides et semi-arides.

Une présentation complète de la zone d'étude et une analyse et un traitement approfondi de la base de données hydroclimatiques in-situ sont décrites dans le Chapitre 2. Le contexte hydroclimatique est présenté en regard des conditions océaniques et atmosphériques, les conditions climatiques moyennes et les modes de variabilité comme le phénomène ENSO (El Niño – La Niña), la variabilité décennale et saisonnière. Nous présentons ensuite les caractéristiques physiques et hydrologiques de la zone d'étude. Le paysage physique (topographie, géologie et végétation) et les caractéristiques hydrologiques mettent en évidence les conditions semi-arides et arides et le degré d'anthropisation de notre zone d'étude. Concernant l'analyse de la base de données hydroclimatiques, deux approches ont été prises en considération. La première était d'étudier le Versant Pacifique péruvien dans sa dimension régionale. Notre démarche a donc dans un premier temps été axée sur l'obtention de séries chronologiques de haute qualité sur chaque station hydrométéorologique. Par la suite, le Versant Pacifique péruvien a été considéré comme un ensemble de bassins versants principaux pour lequel il était nécessaire d'obtenir des séries chronologiques hydroclimatiques à l'échelle de chaque bassin versant étudié, en agrégeant les données ponctuelles.

Des questions scientifiques spécifiques ont également été appréhendées dans cette thèse. Le Chapitre 3 répond à la question : Quelle est la variabilité spatio-temporelle des précipitations interannuelles ? Ce chapitre a été axé sur la régionalisation des précipitations comme moyen de documenter et de comprendre le régime des précipitations au cours de la période 1964 – 2011. Grâce à une analyse statistique d'un réseau de 145 stations

hydrométéorologiques, nous avons proposé une méthodologie pour la régionalisation des précipitations (compte tenu du fait que celles-ci sont des séries temporelles non stationnaires et/ou non gaussiennes) basée sur un processus combiné consistant à utiliser les méthodologies du clustering k-means (classification statistique) et du vecteur régional (RVM). L'analyse du clustering k-means permet un regroupement préliminaire de données des stations qui est utilisé comme une première estimation du RVM et cette étape réduit considérablement l'extension de la procédure de régionalisation. En conséquence, neuf régions ont été identifiées avec des régimes homogènes de précipitation en suivant un gradient latitudinal et altitudinal sur la zone d'étude. Il met en évidence la distinction entre les régions du nord, du centre et du sud, ainsi que la distinction entre les bassins avals, moyens et amonts.

La variabilité des précipitations est plus élevée aux latitudes du nord et elle diminue vers le sud en haute altitude. La motivation pour effectuer une classification utilisant l'analyse k-means avant la régionalisation par RVM réside dans la complexité des processus influençant la variabilité des précipitations sur cette région. En particulier, des études antérieures (Lavado et Espinoza, 2014, Bourrel et al., 2015) ont montré que les précipitations le long du versant Pacifique connaissent l'influence de deux types d'El Niño et en raison de l'asymétrie positive des événements El Niño extrêmes, la distribution des données des précipitations n'est pas gaussienne, ce qui limite les résultats obtenus par une approche via l'analyse linéaire (RVM).

Le Chapitre 4 a permis d'aborder la question de la forte variabilité climatique et de l'anthropisation et de leurs influences sur les séries chronologiques hydroclimatiques. Le cadre théorique de la méthode de Budyko a été utilisé, celui-ci a permis d'étudier la relation entre l'indice de sécheresse et l'indice d'évaporation. Le modèle empirique dérivé Budyko-Zhang a été appliqué pour identifier la disparité du bilan annuel hydrique existant entre les 26 bassins versants de la zone d'étude sur la période 1970 – 2008. Après avoir corroboré les conditions semi-arides à l'échelle du bassin versant avec le paramètre lié à la végétation du modèle Budyko-Zhang, 11 des 26 bassins versants ont été identifiés comme étant des bassins hydrographiques qui suivent la courbe de Budyko-Zhang. Ces 11 bassins versants sont caractérisés par une faible disparité du bilan hydrique liée à une faible influence climatique et anthropique. Ces bassins versants peuvent donc être considérés comme des systèmes hydrologiques présentant des conditions quasi naturelles ou naturelles à l'échelle annuelle. Pour valider cette hypothèse dérivée de la théorie de Budyko, les dynamiques d'occupation du sol observées par les produits MODIS et LBA ont été analysées. Les bassins ayant une disparité élevée dans le bilan hydrique ont présenté un changement significatif dans l'occupation du sol avec principalement une diminution de la superficie des terres cultivées et une augmentation des prairies au cours de la période étudiée.

En dépit des limitations non stationnaires de la méthode, les résultats ont fourni une première caractérisation des bassins hydrographiques ayant une influence climatique et anthropique mineure, ce qui donne des éléments objectifs pour l'évaluation et la gestion régionale des ressources en eau.

Le Chapitre 5 cherche à répondre à la question : Quelle est la variabilité spatio-temporelle de l'écoulement interannuel naturel ? Nous avons décidé d'analyser les bassins versants quasi naturels ou naturels décrits par des séries chronologiques de haute qualité du fait qu'ils présentent une faible influence anthropique. Une première documentation du régime d'écoulement de sept bassins versants a été effectuée et certains d'entre eux sont décrits dans le Chapitre 2 comme présentant principalement un type de fonctionnement de l'écoulement caractéristique de conditions semi-arides. Le Chapitre 5 a été axé sur une méthodologie proposée pour estimer les écoulements superficiels naturels des bassins hydrographiques du versant du Pacifique péruvien à partir de modèles hydrologiques conceptuels globaux fonctionnant au pas de temps annuel et mensuel (GR1A et GR2M respectivement). Un test d'échantillonnage différentiel (DSST) a été utilisé pour tester la transposition temporelle des ensembles de paramètres des modèles et à la robustesse de la modélisation par rapport aux conditions climatiques contrastées en période sèche et humide selon les conditions semi-arides de la zone d'étude. Cette méthodologie a permis d'établir un modèle d'écoulement régional (RRM) via le modèle GR2M à l'échelle de temps mensuelle sur les sept bassins sélectionnés. Du point de vue de la modélisation hydrologique, GR2M a montré plus de robustesse que le modèle GR1A par rapport aux conditions climatiques contrastées (c'est-à-dire en termes des critères du NSE et du biais associé acceptables). Les sept bassins « naturels » sélectionnés ont présenté un remarquable comportement mensuel régional hydrologique lié à la transposition de leurs paramètres entre les années sèches et humides. Le jeu de paramètres GR2M a été lié aux caractéristiques physiques du bassin versant (comme l'aire, la longueur du canal principal et le périmètre) avec une relation significative avec le paramètre du réservoir du sol. Le RRM a été appliqué sur 49 bassins versants le long de la zone d'étude pour simuler les écoulements pour des conditions naturelles aux exutoires des bassins vers l'océan Pacifique péruvien. Ces résultats ont également montré une augmentation régionale des débits naturels depuis la côte Pacifique péruvienne vers l'océan Pacifique au cours des quatre dernières décennies (période 1970 – 2010). Cependant, les résultats de RRM exprimés en termes d'anomalies de débits offriraient un excellent outil basé sur la bonne relation trouvée pour le paramètre X1 qui contrôle la variabilité des écoulements dans le modèle GR2M.

Enfin, le Chapitre 6 aborde la partie de la thèse concernant l'étude des impacts de la variabilité climatique et des changements hydroclimatiques sur les précipitations et écoulements utilisant les trois produits hydroclimatologiques obtenus dans les chapitres précédents i.e. les précipitations régionalisées, les écoulements pour les bassins versants quasi-naturels et l'écoulement régional naturel.

Dans la première partie, la relation ENSO/précipitations a été revisitée en tenant compte du produit de précipitations régionalisées obtenu dans le chapitre 3. Une première approche concernant la relation ENSO/débits a également été proposée en considérant les séries temporelles des écoulements naturels simulés dans le Chapitre 5. Une variété des indices ENSO, y compris les indices E et C récemment définis par Takahashi et al. (2011) ont été utilisés pour estimer les tendances dans la relation ENSO/précipitations. Nous avons également utilisé des indices dérivés des estimations des ondes océaniques équatoriales de

Kelvin afin de tenir compte des influences océaniques qui ne sont pas directement liées à la variabilité interannuelle sur l'ensemble du Pacifique tropical. L'onde océanique de Kelvin aux échelles de temps saisonnière peut en particulier influencer la SST le long de la côte et modifier le mélange dans la couche limite marine le long de la côte, ce qui entraîne une convection accrue (principalement dans le nord du Pérou) ou une stabilité accrue lors des événements d'upwelling (tout le long de la côte). L'analyse a indiqué que, au cours des dernières décennies, l'influence de l'ENSO sur les précipitations le long de la côte se caractérise par une relation inverse, résultant à la fois de l'apparition accrue d'événements CP El Niño qui conduisent à des conditions SST plus froides au large du Pérou (Dewitte et al. 2012) et de l'influence des événements La Niña et des événements d'upwelling. La SST moyenne du Pérou s'est refroidie au cours des dernières décennies (Dewitte et al., 2012 ; Gutierrez et al., 2011). Un changement vers des conditions plus froides dans les années 1990 est également observé dans l'état moyen du Pacifique tropical (Hong et al., 2013) qui est supposé être concomittant à l'apparition accrue du El Niño CP (Chung et Li, 2013). Ainsi, les deux changements dans l'upwelling moyen et la variabilité de l'upwelling peuvent contribuer à renforcer la relation inverse entre l'ENSO et les précipitations le long de la côte du Pérou au cours des dernières décennies.

Nous avons montré que la forte relation positive entre les précipitations et l'ENSO sur l'ensemble des enregistrements résultait principalement de l'influence des événements extrêmes de 1982/83 et 1997/98. Sans tenir compte de ces événements extrêmes, la relation entre l'ENSO et les précipitations présente une modulation décennale significative avec l'impact ENSO plus important au cours des années 1990 et après. En particulier dans les années 2000, la relation entre la variabilité ENSO et la précipitation est inversée par rapport à la décennie précédente. Les résultats généraux suggèrent alors un changement significatif dans la relation ENSO/précipitations le long de la côte du Pérou en raison de la prédominance d'El Niño CP au cours des dernières décennies. En outre, les neuf régions identifiées prennent en compte les caractéristiques dominantes de l'influence de l'ENSO sur les précipitations le long du versant Pacifique de la cordillère des Andes et de la côte du Pérou (Horel et Cornejo-Garrido, 1986 ; Goldberg et al., 1987 ; Tapley et Waylen, 1990 ; Takahashi, 2004 ; Nickl, 2007 ; Lagos et al., 2008 ; Lavado et al., 2012 ; Lavado et Espinoza, 2014 ; Bourrel et al., 2015), qui illustrent son potentiel pour les études d'impact climatique. Le mode de co-variabilité dominant entre la SST dans les océans Pacifique et Atlantique tropical et l'ensemble réduit des séries chronologiques associées aux neuf régions ont une forte charge positive sur la partie nord du Pérou (régions 1 et 2) pour les précipitations et vers l'est du Pacifique tropical pour la SST, ce qui explique les événements extrêmes d'El Niño. D'autre part, le deuxième mode a une charge plus importante (valeur négative) pour les régions amont du versant Pacifique de la cordillère des Andes (région 3, 6, 8 et 9), ce qui indique clairement que, lors du réchauffement central du Pacifique, cette région connaît un déficit des précipitation qui tend à augmenter avec l'altitude (plus négative dans le nord que dans le sud).

À propos de la relation ENSO/débits, les résultats préliminaires montrent que la corrélation est plus forte que celle de la relation ENSO/précipitations du fait que la variabilité des précipitations est renforcée via l'écoulement, le débit intégrant en effet l'information spatiale de pluie sur l'ensemble de la superficie des bassins versants selon Chiew et McMahon (2002).

Dans la deuxième partie, l'étude du changement hydroclimatique a été réalisée grâce à une analyse des tendances des variables hydroclimatiques (précipitations, température, évapotranspiration et écoulement) des 26 bassins versants identifiés dans le Chapitre 4. Selon les tendances ascendantes significatives de la température annuelle observée dans tous les bassins versants et les points de ruptures régionaux trouvés dans la plupart des bassins versants, les résultats ont montré un réchauffement important dans la zone d'étude avec une moyenne de 0,2°C par décennie déjà identifiée dans les études concernant la Cordillère des Andes sud-américaines comme celle de Vuille et al. (2015). Les données sur les précipitations ne présentent pas de tendance et de points de ruptures significatifs dans la plupart des bassins versants. Les séries chronologiques de débits révèlent une diminution significative des écoulements sur les bassins situés dans le centre de la zone d'étude avec un point de rupture dans les années 1987 et 1989. Cette diminution serait liée principalement à l'exploitation intensive de l'eau pour les activités agricoles et le changement d'occupation de sols. Toutefois, selon les Chapitres 4 et 5, seuls 11 bassins versants pourraient offrir un signal d'écoulement quasi naturel en raison de leurs conditions naturelles à l'échelle de temps annuelle. Les changements de trajectoires dans l'espace de Budyko sur ces 11 bassins versants sélectionnés ont révélé deux groupes de bassins versants. Six bassins versants : Piura en amont (n°1), Piura (n°2), Chicama (n°5), San Juan (n°17), Acari (n°19) et Yauca (n°20) ont été identifiés comme sensibles à la variabilité du climat (c'est-à-dire probablement de présenter une forte sensibilité au climat futur) et aux changements de l'utilisation des sols, où les précipitations et la température sont les facteurs les plus susceptibles de changer ces environnements. Les cinq autres bassins versants ne révèlent aucun comportement clair en termes de sensibilité à la variabilité climatique. Les bassins qui suivent la même trajectoire de changement montrent une adaptation commune du bilan hydrique aux forçages climatiques et/ou anthropiques régionaux. Les bassins adjacents de Piura (n°2) et Chicama (n°5) ; Acari (n°19) et Yauca (n°20) suggèrent que l'augmentation des précipitations est plus susceptible d'induire des changements dans ces écosystèmes que l'augmentation de la température. Piura en amont (n°1) et San Juan (n°17) s'individualisent par rapport aux autres groupes, mais il est probable que les précipitations ainsi que la température entraînent des changements dans ces écosystèmes.

7.2. Perspectives

Chaque chapitre a montré de nombreux résultats et conclusions, qui ouvrent de nombreuses perspectives pour de nouvelles recherches que l'on peut répartir dans les deux axes suivants :

7.2.1. Impact de la variabilité climatique sur le régime hydrologique saisonnier en tant qu'outil de prévision

Les impacts de la variabilité climatique sur le régime de précipitations et de débits ont été abordés à l'échelle de temps interannuelle offrant une excellente perspective sur l'utilisation des échelles de temps saisonnières. Les études actuelles sur l'ENSO au Pérou sont

abordées de deux façons comme l'étude de l'impact de l'ENSO sur les précipitations et son évolution dans le temps et l'étude de la physique de la relation ENSO/précipitations. Une approche intra-annuelle permettra de fusionner ces deux approches en vue de la perspective de prévision et de l'élaboration d'un outil précieux pour anticiper et atténuer les impacts de l'ENSO. Ce travail pourrait également se faire avec l'utilisation de modèles climatiques, de réanalyses et de produits de télédétection, tel qu'il est abordé dans les pays voisins d'Amérique du Sud, comme en Equateur dans Recalde-Coronel et al. (2014), Pineda y Willems (2016), Vicente-Serrano et al. (2016), de Guenni et al. (2016).

L'approche initiale de la relation ENSO/débits ouvre une discussion intéressante sur l'influence de l'ENSO sur les écoulements naturels et anthropisés. Quelques études au Pérou ont abordé cette question, mais elles n'ont généralement pas tenu en compte du degré d'anthropisation des bassins versants. En outre, l'analyse régionale du débit réalisée via la modélisation hydrologique offre une perspective intéressante sur la prise en compte de l'influence de la variabilité climatique et la robustesse des modèles hydrologiques correspondante. Les méthodologies de calage et de validation ne considéraient généralement pas la variabilité de basse fréquence dans les attributs hydroclimatiques pour identifier le jeu de paramètres du modèle le plus optimal (voir Wang et al., 2015).

Étudier une variété d'indices climatiques, atmosphériques et océaniques et leurs relations avec les précipitations appelle à une meilleure compréhension de l'influence océanique sur la couche limite marine. La SST plus froide le long de la côte tend à stabiliser la couche limite marine et à conduire à des conditions plus sèches à proximité de la côte. D'autre part, la plupart des régions analysées ici sont situées à plus de 1000 m d'altitude soit au-delà de l'influence de la couche limite marine, de sorte que les changements de précipitations peuvent être influencés par des processus non locaux. Une meilleure compréhension de la circulation atmosphérique régionale dans cette région est nécessaire, ce qui aidera à mieux identifier les indices clés qui peuvent être liés à la variabilité des précipitations à différentes altitudes le long du versant Pacifique. Cela peut être abordé à partir de l'expérimentation avec un modèle atmosphérique régional haute résolution, qui peut être prévue pour les travaux futurs.

Concernant les produits régionalisés des précipitations et des séries temporelles d'écoulements naturels obtenus dans cette thèse, ils fourniront des informations précieuses dans le but d'améliorer la gestion des ressources hydriques et écologiques tout le long du versant Pacifique péruvien.

7.2.2. Impact des changements du climat et du bassin versant sur les régimes hydrologiques

Dans le Chapitre 4, nous avons introduit le thème de la séparation des effets climatiques et anthropiques sur le bilan hydrique et l'écoulement. Les recherches sont encore en cours de développement pour résoudre ce problème (e.g. Zhou S et al., 2015 ; Greve et al., 2015 ; Fabre et al., 2015 ; Hublart et al., 2016) mais ils s'accordent sur la nécessité d'évoluer vers une analyse non-stationnaire. Cela signifie que, en fonction de la période d'observation de l'analyse, les limitations actuelles sont principalement liées à la disponibilité limitée des

données hydro-climatiques et liées à l'hypothèse de l'équilibre du cadre de Budyko (c'est-à-dire de ne pas considérer la variation du stock d'eau).

Des travaux récents comme Zhou S et al. (2015) ont formulé une hypothèse sur la prise en compte d'un terme de «changement» dans le climat et les caractéristiques du bassin versant dans le cadre de Budyko, et Greve et al. (2015) ont montré un cadre Budyko non stationnaire lorsque l'évapotranspiration dépasse les précipitations à des échelles de temps inférieures à l'échelle annuelle ou lorsque le changement de stockage dans le bilan sol-eau n'est pas négligeable. Aussi Zhou G et al. (2015) ont proposé un schéma global en montrant l'effet du climat et de l'occupation de sols sur le rendement en eau.

Enfin, malgré les limites déjà mentionnées du versant Pacifique péruvien, les résultats obtenus dans cette thèse fournissent la première caractérisation des bassins versants et leur sensibilité aux changements hydroclimatiques qui permettront une évaluation et une gestion régionale des ressources en eau. Ces résultats seront également la base d'études futures liées aux impacts du changement climatique sur le régime hydrologique, l'écoulement et la disponibilité en eau. La forte incertitude des modèles climatiques (c'est-à-dire Global Climate Models GCM) actuelle pour reconstituer les précipitations sur le versant Pacifique péruvien (IPCC, 2014) pourra être améliorée dans ce contexte hydrologique aride et semi-aride. La méthodologie DSST utilisée au chapitre 5 pourrait ainsi offrir un autre ensemble de scénarios pour valider correctement tout modèle hydrologique. Le modèle d'écoulement régional pourrait être amélioré en fonction de l'utilisation d'autres modèles hydrologiques conceptuels et à une échelle de temps plus fine pour l'étude de la sensibilité de l'écoulement.

(This page has been left blank intentionally)

References

- An S.I, Jin F.F. 2004. Nonlinearity and asymmetry of ENSO. *Journal of Climate* 17: 2399–2412.
- ANA. 2012. Recursos Hídricos en el Perú. 2nd edn. Ministerio de Agricultura. Autoridad Nacional del Agua, Lima; pp 45-189.
- Andermann C, Longuevergne L, Bonnet S, Crave A, Davy P, Gloaguen R. 2012. Impact of transient groundwater storage on the discharge of Himalayan rivers. *Nature Geoscience* 5: 127–132.
- Ashok K, Behera S.K, Rao S.A, Weng H, Yamagata T. 2007. El Niño Modoki and its possible teleconnection. *Journal of Geophysical Research* 112: C11007.
- BCEOM. 1999. Estudio hidrológico-meteorológico en la vertiente del Pacífico del Perú con fines de evaluación y pronóstico del fenómeno El Niño para prevención y mitigación de desastres. Asociación BCEOM-Sofi Consult S.A - ORSTOM, Programa de apoyo a la emergencia Fenómeno del Niño. Contrato de préstamo n°4250-PE-BIRF, Presidencia de la Republica, Perú. Volumen I.
- Björnsson H, Venegas S.A. 1997. A manual for EOF and SVD analyses of climatic data. McGill University, CCGCR Report No. 97-1, Montréal, Québec.
- Blöschl G, Sivapalan M, Wagener T, Viglione A, Savenije H. 2013. Runoff prediction in ungauged basins. Synthesis across processes, places and scales. Cambridge University Press. Cambridge; pp 53–134.
- Bograd S.J, Schroeder I, Sarkar N, Qiu X, Sydeman W.J and Schwing F.B. 2009. The phenology of coastal upwelling in the California Current. *Geophysical Research Letters* 36: L01602.
- Boucharel J, Dewitte B, Garel B, du Penhoat Y. 2009. ENSO's non-stationary and non-Gaussian character: the role of climate shifts. *Nonlinear Processes in Geophysics* 16: 453-473.
- Boucharel J, Dewitte B, Du Penhoat Y et al. 2011. ENSO nonlinearity in a warming climate. *Climate Dynamics* 37: 9-10, 2045-2065.
- Boughton WC. 1999. A Century of Water Resources Development in Australia 1900–1999. Institution of Engineers. Australia; 256 pp.
- Bourrel L, Labat D, Vera A, Coutaud A, Ronchail J, Guyot J.L, Armijos E, Pombosa R. 2010. Correlation between the climatic indices of the ENSO phenomenon (El Niño - La Niña) and the rains and discharges indices on the Pacific coast of South America: Esmeraldas river basin, International Workshop on ENSO, Decadal Variability and CC in South America, October 12 - 14, 2010: Guayaquil, Ecuador.

-
- Bourrel L, Melo P, Vera A, Pombosa R, Guyot J.L. 2011. Study of the erosion risks of the Ecuadorian Pacific coast under the influence of ENSO phenomenon: case of the Esmeraldas and Guayas basins, World's Large Rivers Conference 2011, International Conference on the Status and Future of the World's Large Rivers. April 11 – 14, 2011: Vienna, Austria.
- Bourrel L, Rau P, Dewitte B, Labat D, Lavado W, Coutaud A, Vera A, Alvarado A, Ordoñez J. 2015. Low-frequency modulation and trend of the relationship between ENSO and precipitation along the northern to centre Peruvian Pacific coast. *Hydrological Processes* 29(6): 1252-1266.
- Bretherton C.S, Smith C, Wallace J.M. 1992. An intercomparison of methods for finding coupled patterns in climate data. *Journal of Climate* 5: 541–560.
- Brigode P, Oudin L, Perrin C. 2013. Hydrological model parameter instability: A source of additional uncertainty in estimating the hydrological impacts of climate change? *Journal of Hydrology* 476: 410–425.
- Brouwer C, Heibloem M. 1986. *Irrigation Water Measurement: Irrigation Water Needs*, vol. 3. United Nations Food and Agriculture Organization, Rome; 102 pp.
- Brown A.E, Zhang L, McMahon T.A, Western A.W, Vertessy R.A. 2005. A review of paired catchment studies for determining changes in water yield resulting from alterations in vegetation. *Journal of Hydrology* 310: 28–61.
- Brunet-Moret Y. 1979. Homogénéisation des précipitations. *Cahiers ORSTOM. Serie Hydrologie* 16: 3–4.
- Budyko M.I. 1958. *The Heat Balance of the Earth's Surface*. U.S. Department of Commerce, Washington; 259 pp.
- Budyko M.I. 1974. *Climate and Life*. International Geophysics Series, vol. 18. Academic, New York; 508 pp.
- Buytaert W, Celleri R, Willems P et al. 2006. Spatial and temporal rainfall variability in mountainous areas: A case study from the south Ecuadorian Andes. *Journal of Hydrology* 329: 413–421.
- Carranza L. 1892. Contra-corriente marítima en Paita y Pacasmayo. *Boletín Sociedad Geográfica de Lima* 1, 9, 344-345.
- Castiglioni S, Lombardi L, Toth E, Castellarin A, Montanari A. 2010. Calibration of rainfall-runoff models in ungauged basins: a regional maximum likelihood approach. *Advances in Water Resources* 33(10): 1235–1242.
- Changnon S, Kenneth K. 2006. Changes in Instruments and Sites Affecting Historical Weather Records: A Case Study. *Journal of Atmospheric and Oceanic Technology* 23: 825–828.
- Chen Z, Chen Y, Li B. 2013. Quantifying the effects of climate variability and human activities on runoff for Kaidu River basin in arid region of northwest China. *Theoretical and Applied Climatology* 111: 537-545.
- Cherry S. 1997. Some comments on singular value decomposition analysis. *Journal of Climate* 10: 1759–1761.
- Chiew F.H.S, McMahon T.A. 2002. Global ENSO-streamflow teleconnection, streamflow forecasting and interannual variability. *Hydrological Sciences Journal* 47, 505–522.

- Chung P-H, Li T. 2013. Interdecadal relationship between the state and El Niño types. *Journal of Climate* 26 (2): 361-379.
- Condom T, Escobar M, Purkey D, Pouget J.C, Suarez W, Ramos C, Apaestegui J, Tacsí A, Gomez J. 2012. Simulating the implications of glaciers' retreat for water management: a case study in the Rio Santa basin, Peru. *Water International* 37(4): 442-459.
- Coron L, Andréassian V, Perrin C, Lerat J, Vaze J, Bourqui M, Hendrickx F. 2012. Crash testing hydrological models in contrasted climate conditions: An experiment on 216 Australian catchments. *Water Resources Research* 48: W05552.
- Coron L, Andréassian V, Perrin C, Le Moine N. 2015. Graphical tools based on Turc-Budyko plots to detect changes in catchment behaviour. *Hydrological Sciences Journal* 60(7-8): 1394-1407.
- Dakhlaoui H, Ruelland D, Trambly Y, Bargaoui Z. 2017. Evaluating robustness of conceptual rainfall-runoff models under climate variability in Northern Tunisia. *Journal of Hydrology* 550: 201-217
- de Reparaz G. 2013. Los rios de la zona arida peruana. Universidad de Piura Eds, Piura. Institut Cartografic de Catalunya Eds. Barcelona; 352 pp.
- DeFries R, Hansen M, Townshend J.R.G, Sohlberg R. 1998. Global land cover classifications at 8 km spatial resolution: The use of training data derived from Landsat imagery in decision tree classifiers. *International Journal of Remote Sensing* 19(16): 3141-3168.
- Dewitte B, Purca S, Illig S.L, Renault L, Giese B. 2008. Low frequency modulation of the intraseasonal equatorial Kelvin wave activity in the Pacific Ocean from SODA: 1958-2008. *Journal of Climate* 21: 6060-6069.
- Dewitte B, Illig S, Renault L, Goubanova K, Takahashi K, Gushchina D, Mosquera K, Purca S. 2011. Modes of covariability between sea surface temperature and wind stress intraseasonal anomalies along the coast of Peru from satellite observations (2000-2008). *Journal of Geophysical Research* 116: C04028.
- Dewitte B, Choi S.-I, An J, Thual S. 2011: Vertical structure variability and equatorial waves during Central Pacific and Eastern Pacific El Niño in a coupled general circulation model. *Climate Dynamics*. DOI: 10.1007/s00382-011-1215-x.
- Dewitte B, Vazquez-Cuervo J, Goubanova K, Illig S, Takahashi K, Cambon G, Purca S, Correa D, Gutierrez D, Sifeddine A, Ortlieb L. 2012. Change in El Niño flavours over 1958-2008: Implications for the long-term trend of the upwelling off Peru. *Deep Sea Research II*. DOI: 10.1016/j.dsr2.2012.04.011.
- Dezfuli A.K. 2010. Spatio-temporal variability of seasonal rainfall in western equatorial Africa. *Theoretical and Applied Climatology* 104(1-2): 57-69.
- Diaz H, Markgraf V. 2000. El Niño and the Southern Oscillation: Multiscale variability and global and regional impacts. Cambridge University Press, Cambridge; 496.
- Diodato N. 2005. The influence of topographic co-variables on the spatial variability of precipitation over small regions of complex terrain. *International Journal of Climatology* 25: 351-363.
- Donohue R.J, Roderick M.L, McVicar T.R. 2007. On the importance of including vegetation dynamics in Budyko's hydrological model. *Hydrology and Earth System Sciences* 11: 983-995.

-
- Donohue R.J, Roderick M.L, McVicar T.R. 2011. Assessing the differences in sensitivities of runoff to changes in climatic conditions across a large basin. *Journal of Hydrology* 406: 234–244.
- Emerton R, Cloke H.L, Stephens E.M, Zsoter E, Woolnough S.J, Pappenberger F. 2017. Complex picture for likelihood of ENSO-driven flood hazard. *Nature Communications* 8: 14796. DOI: 10.1038/ncomms14796.
- Enfield D. 1981. Thermally driven wind variability in the planetary boundary layer above Lima, Peru. *Journal of Geophysical Research* 86: C3 2005-2016.
- Engeland K, Gottschalk L. 2002. Bayesian estimation of parameters in a regional hydrological model. *Hydrology and Earth System Sciences* 6(5): 883–898.
- Espinoza J.C, Ronchail J, Guyot J.L, Cochonneau G et al. 2009. Spatio-temporal rainfall variability in the Amazon basin countries (Brazil, Peru, Bolivia, Colombia and Ecuador). *International Journal of Climatology* 29: 1574–1594.
- Fabre J, Ruelland D, Dezetter A, Grouillet B. 2016. Sustainability of water uses in managed hydrosystems: human- and climate-induced changes for the mid-21st century. *Hydrology and Earth System Sciences* 20: 3129–3147.
- Fabre J, Ruelland D, Dezetter A, Grouillet B 2015. Simulating past changes in the balance between water demand and availability and assessing their main drivers at the river basin scale. *Hydrology and Earth System Sciences* 19: 1263–1265.
- Fowler K.J.A, Peel M.C, Western A.W, Zhang L, Peterson T.J. 2016. Simulating runoff under changing climatic conditions: Revisiting an apparent deficiency of conceptual rainfall-runoff models. *Water Resources Research* 52: 1820–1846.
- Garreaud R, Rutllant J, Fuenzalida H. 2002. Coastal lows along the Subtropical West Coast of South America: Mean Structure and Evolution. *Monthly Weather Review* 130: 75-88.
- Garreaud R.D, Vuille M, Compagnucci R, Marengo J. 2009. Present-day South American climate. *Palaeogeography, Palaeoclimatology, Palaeoecology* 281(3–4): 180–195.
- Gilboa Y. 1971. Replenishment Sources of the Alluvial Aquifers of the Peruvian Coast. *Groundwater* 9: 39–46. DOI: 10.1111/j.1745-6584.1971.tb03559.x
- Goldberg R.A, Tisnado G, Scofield R.A. 1987. Characteristics of extreme rainfall events in north-western Peru during the 1982– 1983 El Niño period, *Journal of Geophysical Research* 92: C14 225–241.
- Goovaerts P. 2000. Geostatistical approaches for incorporating elevation into the spatial interpolation of rainfall. *Journal of Hydrology* 228: 113–129.
- Gottschalk J, Higgins W. 2008. Madden Julian Oscillation Impacts. NOAA/NWS/NCEP Climate Prediction Center.
- Greve P, Gudmundsson L, Orłowsky B, Seneviratne S. 2015. Introducing a probabilistic Budyko framework. *Geophysical Research Letters* 42(7): 2261-2269.
- Greve P, Gudmundsson L, Orłowsky B, Seneviratne S.I. 2016. A two-parameter Budyko function to represent conditions under which evapotranspiration exceeds precipitation. *Hydrology and Earth System Sciences* 20(6): 2195–2205.
- Guilderson T.P, Schrag D.P. 1998. Abrupt shift in subsurface temperatures in the tropical Pacific associated with changes in El Niño. *Science* 281: 240–243.
- Gushchina D, Dewitte B. 2012. Intraseasonal tropical atmospheric variability associated to the two flavors of El Niño. *Monthly Weather Review* 140: N° 11. 3669-3681.

- Gutiérrez D, Bertrand A, Wosnitz-Mendo C, Dewitte B, Purca S, Peña C, Chaigneau A, Tam J, Graco M, Echevin V, Grados C, Fréon P, Guevara-Carrasco R. 2011. Sensibilidad del sistema de afloramiento costero del Perú al cambio climático e implicancias ecológicas. *RPGA SENAMHI* 3: 1-24.
- Hansen M, DeFries R, Townshend J.R.G, Sohlberg R. 2000. Global land cover classification at 1km resolution using a decision tree classifier. *International Journal of Remote Sensing* 21: 1331-1365.
- Hartigan J.A, Wong M.A. 1979. Algorithm AS 136: A K-means clustering algorithm. *Journal of the Royal Statistical Society, Series C* 28(1): 100-108.
- Hassan H, Dregne H.E. 1997. Natural habitats and ecosystems management in drylands: An overview. *Environment Department Paper N51*. World Bank, Washington. pp 1-53
- Hayashi Y, 1982. Space-time spectral analysis and its applications to atmospheric waves. *Journal of the Meteorological Society of Japan* 60: 156–171.
- Heil C, Walnut D. 1989. Continuous and discrete wavelet transforms. *SIAM Review* 31: 628-666.
- Hendon H.H, Wheeler M.C, Zhang C. 2007. Seasonal dependence of the MJO-ENSO relationship. *Journal of Climate* 20: 531-543.
- Hevesi J, Istok J, Flint A. 1992a. Precipitation estimation in mountainous terrain using multivariate geostatistics. Part I: structural analysis. *Journal of Applied Meteorology and Climatology* 31: 661-676.
- Hevesi J, Flint A, Istok J. 1992b. Precipitation estimation in mountainous terrain using multivariate geostatistics. Part II: Isohyetal maps. *Journal of Applied Meteorology and Climatology* 31: 677-688.
- Hong C.C, Wu Y.K, Li T, Chang C.C. 2013. The climate regime shift over the Pacific during 1996/1997. *Climate Dynamics*. DOI: 10.1007/s00382-013-1867-9.
- Horel J.D, Cornejo-Garrido A.G. 1986. Convection along the coast of northern Peru during 1983: Spatial and temporal variation of clouds and rainfall. *Monthly Weather Review* 114: 2091–2105.
- Huard D, Mailhot A. 2008. Calibration of hydrological model GR2M using Bayesian uncertainty analysis. *Water Resources Research* 44: W02424.
- Hublart P, Ruelland D, Dezetter A, Jourde H. 2015. Reducing structural uncertainty in conceptual hydrological modelling in the semi-arid Andes. *Hydrology and Earth System Sciences* 19: 2295-2314.
- Hublart P, Ruelland D, García de Cortázar-Atauri I, Gascoin S, Lhermitte S, Ibacache A. 2016. Reliability of lumped hydrological modeling in a semi-arid mountainous catchment facing water-use changes. *Hydrology and Earth System Sciences* 20: 3691-3717.
- Hughes D.A. 2008. Modeling semi-arid and arid hydrology and water resources: the southern African experience, in: Wheeler, H., Sorooshian, S., Sharma K.D. (Eds.), *Hydrological modelling in arid and semi-arid areas*. Cambridge University Press. Cambridge; pp 29–40.
- Ibrahim B, Wisser D, Barry B, Fowe T, Aduna A. 2015. Hydrological predictions for small ungauged watersheds in the Sudanian zone of the Volta basin in West Africa. *Journal of Hydrology Regional Studies* 4: 386–397.

-
- IPCC, 2014: Climate Change 2014: Synthesis Report. Contribution of Working Groups I, II and III to the Fifth Assessment Report of the Intergovernmental Panel on Climate Change. Core Writing Team, R.K. Pachauri and L.A. Meyer (eds.) IPCC, Geneva, Switzerland; 151 pp.
- Jackson I.J, Weinand H. 1995. Classification of tropical rainfall stations: A comparison of clustering techniques. *International Journal of Climatology* 15(9): 985–994.
- Jaramillo F, Destouni G. 2014. Developing water change spectra and distinguishing change drivers worldwide. *Geophysical Research Letters* 41: 8377–8386.
- Jones J, Creed I, Hatcher K, Warren R, Adams M, Benson M et al. 2012. Ecosystem processes and human influences regulate streamflow response to climate change at long-term ecological research sites. *BioScience* 62(4): 390-404.
- Kaufman L, Rousseeuw P. 1990. *Finding Groups in Data: An Introduction to Cluster Analysis*. John Wiley & Sons, Inc, Hoboken; 342 pp.
- Kendall M.G. 1975. *Rank correlation measures*. Charles Griffin, London; 202 pp.
- Kiem A, Franks S. 2001. On the identification of ENSO-induced rainfall and runoff variability: a comparison of methods and indices. *Hydrological Sciences Journal* 46(5): 715-727.
- Kim S.T, Yu J-Y. 2012. The Two Types of ENSO in CMIP5 Models. *Geophysical Research Letters* 39: L11704.
- Klemeš V. 1986. Operational testing of hydrological simulation- models. *Hydrological Sciences Journal* 31(1): 13–24.
- Kononenko I, Kukar M. 2007. *Machine learning and data mining: Introduction to principles and algorithms*. Horwood Publishing, Chichester; 480 pp.
- Kug J.S, Jin F.F, An S.I. 2009. Two types of El Niño events: cold tongue El Niño and warm pool El Niño. *Journal of Climate* 22: 1499–1515.
- Labat D, Ababou R, Mangin A. 2000. Rainfall–runoff relations for karstic springs. Part II: continuous wavelet and discrete orthogonal multiresolution analyses. *Journal of Hydrology* 238(3): 149-178.
- Labat D. 2005. Recent advances in wavelet analyses: Part 1. A review of concepts. *Journal of Hydrology* 314-1: 275-288.
- Labat D. 2006. Oscillations in land surface hydrological cycle. *Earth and Planetary Science Letters* 242 (1): 143-154.
- Lagarde J. 1983. *Initiation à l'analyse des données*, BORDAS (eds)., Paris, 157 pp.
- Lagos P, Buizer J. 1992. El Niño and Peru Interannual Climate Variability, Natural and Technological Disasters. Chapter 17. *The Pennsylvania Academy of Science*.
- Lagos P, Silva Y, Nickl E, Mosquera K. 2008. El Niño – related precipitation variability in Peru. *Advances in Geosciences* 14: 231–237.
- Lasdon L.S, Smith S. 1992. Solving sparse nonlinear programs using GRG, *ORSA Journal on Computing* 4(1): 2–15.
- Lavado W.S, Ronchail J, Labat D, Espinoza J.C, Guyot J.L. 2012. Basin-scale analysis of rainfall and runoff in Peru (1969–2004): Pacific, Titicaca and Amazonas drainages. *Hydrological Sciences Journal* 57(4): 1–18.

- Lavado W.S, Labat D, Ronchail J, Espinoza JC, Guyot JL. 2013. Trends in rainfall and temperature in the Peruvian Amazon-Andes basin over the last 40 years (1965–2007). *Hydrological Processes* 27: 2944-2957.
- Lavado W, Silvestre E, Felipe O, Bourrel L. 2013. ENSO impact on hydrology in Peru. *Advances in Geosciences* 11: 1–7, 2013.
- Lavado W, Espinoza J.C. 2014. Impactos de El Niño y La Niña en las lluvias del Peru. *Revista Brasileira de Meteorologia* 29: 171 – 182.
- Lee T, McPhaden M. 2010. Increasing intensity of El Nino in the central equatorial Pacific. *Geophysical Research Letters* 37: L14603.
- Liu Y, Gupta HV. 2007. Uncertainty in hydrologic modeling: Toward an integrated data assimilation framework. *Water Resources Research* 43: W07401.
- Luo J.J, Sasaki W, Masumoto Y. 2012. Indian Ocean warming modulates Pacific climate change, *Proceedings of the National Academy of Sciences of the United States of America*, Volume 109: 18701-18706.
- Madden R, Julian P. 1972. Description of global-scale circulation cells in the tropics with a 40–50 day period. *Journal of the Atmospheric Sciences* 29: 1109–1123.
- Madl P. 2000. The El-Niño (ENSO) phenomenon. *Environmental Physics/Lettner*, Vol 437-503. <http://biophysics.sbg.ac.at/atmo/elnino.htm>. Accessed 10 Apr 2017.
- Mair A, Fares A. 2011. Comparison of rainfall interpolation methods in a Mountainous Region of a Tropical Island. *Journal of Hydrological Engineering* 16(4): 371-383.
- Maliva R, Missimer T, 2012. *Arid Lands Water Evaluation and Management*, Environmental Science and Engineering. Springer-Verlag Berlin Heidelberg; pp 21-39
- Manabe S. 1969. Climate and the ocean circulation. 1. The atmospheric circulation and the hydrology of the Earth's surface. *Monthly Weather Review* 97(11): 739–774.
- Mann H.B. 1945. Non-parametric tests against trend. *Econometrica* 13: 245–259.
- McPhaden M.J, Zhang X, Hendon H.H, Wheeler M.C. 2006. Large Scale Dynamics and MJO Forcing of ENSO Variability. *Geophysical Research Letters* 33(16): L16702.
- McPhaden M.J. 2012. A 21st Century Shift in the Relationship between ENSO SST and Warm Water Volume Anomalies. *Geophysical Research Letters*. 39: L09706.
- Mehta V.M. 2017. *Natural Decadal Climate Variability: Societal Impacts*. CRC Press Taylor & Francis Group. 316 pp.
- Mernild S.H, Liston G.E, Hiemstra C, Beckerman A.P, Yde J.C, McPhee J. 2016. The Andes Cordillera. Part IV: spatio-temporal freshwater run-off distribution to adjacent seas (1979–2014). *International Journal of Climatology*. DOI: 10.1002/joc.4922
- Miller A, Cayan D, Barnett T, Graham N, Oberhuber J. 1994. The 1976–77 climate shift of the Pacific Ocean. *Oceanography* 7: 21–26.
- Milliman J.D, Farnsworth K.L. 2011. *River Discharge to the Coastal Ocean: A Global Synthesis*. Cambridge University Press. Cambridge; 384 pp.
- MINAM. 2016. *El Perú y el Cambio Climático. Tercera Comunicación Nacional del Perú a la Convención Marco de las Naciones Unidas sobre el Cambio Climático*. Ministerio del Ambiente, Lima; 326 pp.
- Montecinos, A., and P. Aceituno, 2003. Seasonality of the ENSO-related rainfall variability in central Chile and associated circulation anomalies. *Journal of Climate* 16: 281-296.

-
- Moriasi D.N, Arnold J.G, Van Liew M.W, Bingner R.L, Harmel R.D, Veith T.L. 2007. Model evaluation guidelines for systematic quantification of accuracy in watershed simulations. *Transactions of the ASABE* 50(3): 885–900.
- Mortimore M. 2009. Dryland opportunities. International Union for Conservation of Nature and Natural Resources. IUCN. IIED. UNDP, Gland-Switzerland; 86 pp.
- Mosquera K, Dewitte B, Illig S, Takahashi K, Garric G. 2013. The 2002/03 El Niño: Equatorial wave sequence and their impact on Sea Surface Temperature. *Journal of Geophysical Research: Oceans* 118: 1-12.
- Mouelhi S, Michel C, Perrin C, Andréassian C. 2006a. Stepwise development of a two-parameter monthly water balance model. *Journal of Hydrology* 318: 200–214.
- Mouelhi S, Michel C, Perrin C, Andréassian V. 2006b. Linking stream flow to rainfall at the annual time step: The Manabe bucket model revisited. *Journal of Hydrology* 328: 283–296.
- Muñoz R, Garreaud R. 2005. Dynamics of the Low-Level Jet off the West coast of Subtropical South America. *Monthly Weather Review* 133: 3661-3677.
- Muñoz-Díaz D, Rodrigo F. 2004. Spatio-temporal patterns of seasonal rainfall in Spain (1912-2000) using cluster and principal component analysis: comparison. *Annales Geophysicae* 22: 1435–1448.
- Nash J.E, Sutcliffe J.V. 1970. River flow forecasting through conceptual models, a discussion of principles. *Journal of Hydrology* 10: 282–290.
- Nicholson S. 2011. Dryland climatology. Cambridge University Press. Cambridge; 516 pp.
- Nickl E. 2007. Teleconnections and climate in the Peruvian Andes. MSc Thesis. Department of Geography. University of Delaware. US.
- Null S.E, Viers J.H. 2013. In bad waters: Water year classification in nonstationary climates. *Water Resources Research* 49: 1137–1148.
- Ochoa A, Pineda L, Crespo P, Willems P. 2014. Evaluation of TRMM 3B42 precipitation estimates and WRF retrospective precipitation simulation over the Pacific–Andean region of Ecuador and Peru. *Hydrology and Earth System Sciences* 18: 3179–3193.
- OPS. 2000. Perú: Fenómeno El Niño, 1997-1998. Organización Panamericana de la Salud. Fenómeno El Niño, 1997-1998, Washington DC; 294 pp.
- Oudin L, Hervieu F, Michel C, Perrin C, Andreassian V, Anctil F, Loumagne C. 2005. Which potential evapotranspiration input for a lumped rainfall-runoff model? Part 2-Towards a simple and efficient potential evapotranspiration model for rainfall-runoff modeling. *Journal of Hydrology* 303: 290–306.
- Parracho A, Melo-Gonçalves P, Rocha A. 2015. Regionalization of precipitation for the Iberian Peninsula and climate change. *Physics and Chemistry of the Earth*. DOI: 10.1016/j.pce.2015.07.004
- Peel M.C, Chiew F.H.S, Western A.W, McMahon T.A. 2000. Extension of unimpaired monthly streamflow data and regionalization of parameter values to estimate streamflow in ungauged catchments. In: Australian Natural Resources. Report prepared for the National Land and Water Resources Audit. Australia; 37 pp.
- Penman H.L. 1948. Natural evaporation from open water, bare soil and grass. *Proceedings of the Royal Society of London. Series A. Mathematical and Physical Sciences*. Vol 193. 1032: 120-145.

- Perrin C, Michel C, Andréassian V. 2007. Modèles hydrologiques du Génie Rural (GR). Cemagref UR Hydrosystèmes et Bioprocédés, Antony; 16 pp.
- Pettitt AN. 1979. A non-parametric approach to the change-point problem. *Applied Statistics* 28: 126-135.
- Pezet F. 1896. The counter-current El Niño, on the coast of Northern Peru. 6th International Geography Congress, 603-606. London. United Kingdom.
- Ramos M. 2001. Divisive and hierarchical clustering techniques to analyse variability of rainfall distribution patterns in a Mediterranean region. *Atmospheric Research* 57: 123-138.
- Rasmusson E, Carpenter T. 1992. Variations in tropical sea surface temperatures and wind fields Associated with the Southern Oscillation/El Nino. *Monthly Weather Review* 110: 354-384.
- Rau P, Bourrel L, Labat D, Melo P, Dewitte B, Frappart F, Lavado W, Felipe O. 2017a. Regionalization of rainfall over the Peruvian Pacific slope and coast. *International Journal of Climatology* 37(1): 143-158. DOI: 10.1002/joc.4693
- Rau P, Bourrel L, Labat D, Frappart F, Ruelland D, Lavado W, Dewitte B, Felipe O. 2017b. Hydroclimatic change disparity of Peruvian Pacific drainage catchments. *Theoretical and Applied Climatology*. (under review)
- Rau P, Bourrel L, Labat D, Ruelland D, Frappart F, Lavado W, Dewitte B, Felipe O. 2017c. Assessing freshwater runoff over Peruvian Pacific drainage catchments during the 1970-2010 period. *Hydrological Processes*. (under review)
- Rayner N.A, Parker D.E, Horton E.B, Folland C.K, Alexander L.V, Rowell D.P, Kent E.C, Kaplan A. 2003. Global analyses of sea surface temperature, sea ice, and night marine air temperature since the late nineteenth century. *Journal of Geophysical Research* 108: D14 4407.
- Raziei T, Bordi I, Pereira L.S. 2008. A precipitation-based regionalization for Western Iran and regional drought variability. *Hydrology and Earth System Sciences* 12: 1309-1321.
- Renner M, Bernhofer C. 2012. Applying simple water-energy balance frameworks to predict the climate sensitivity of streamflow over the continental United States. *Hydrology and Earth System Sciences* 16: 2531-2546.
- Roundy P.E, Kiladis G.N. 2006. Observed relationship between oceanic Kelvin waves and atmospheric forcing. *Journal of Climate* 19: 5253-5272.
- Rousseeuw P. 1987. Silhouettes: a graphical aid to the interpretation and validation of cluster analysis. *Journal of Computational and Applied Mathematics* 20: 53-65.
- Ruelland D, Ardoin-Bardin S, Collet L, Roucou P. 2012. Simulating future trends in hydrological regime of a large Sudano-Sahelian catchment under climate change. *Journal of Hydrology* 424-425: 207-216.
- Ruelland D, Dezetter A, Hublart P. 2014. Sensitivity analysis of hydrological modelling to climate forcing in a semi-arid mountainous catchment. In: *Hydrology in a changing world: environmental and human dimensions*. IAHS Publ 363: 145-150.
- Ruelland D, Hublart P, Tramblay Y. 2015. Assessing uncertainties in climate change impacts on runoff in Western Mediterranean basins. In: *Hydrologic non-stationarity and extrapolating models to predict the future*. IAHS Publ. 371: 75-81.

-
- Searcy J.K, Hardison C.H. 1960. Double-mass curves. US Geol. Survey Water-Supply Paper. 1541-B: 31-66.
- Segura H, Espinoza J.C, Junquas C, Takahashi K. 2016. Evidencing decadal and interdecadal hydroclimatic variability over the Central Andes. *Environmental Research Letters* 11, 9.
- Seibert J, Beven K.J. 2009. Gauging the ungauged basin: how many discharge measurements are needed? *Hydrology and Earth System Sciences* 13: 883–892.
- Seiler C, Hutjes R.W.A, Kabat P. 2013. Climate variability and trends in Bolivia. *Journal of Applied Meteorology and Climatology* 52: 130–146.
- Seiller G, Anctil F, Perrin C. 2012. Multimodel evaluation of twenty lumped hydrological models under contrasted climate conditions. *Hydrology and Earth System Sciences* 16: 1171–1189.
- Seiller G, Hajji I, Anctil F. 2015. Improving the temporal transposability of lumped hydrological models on twenty diversified U.S. watersheds. *Journal of Hydrology Regional Studies* 3: 379–399.
- Sivapalan M, Thompson SE, Harman CJ, Basu NB, Kumar P. 2011. Water cycle dynamics in a changing environment: improving predictability through synthesis. *Water Resources Research* 47(10): W00J01.
- Sneyers R, Vandiepenbeeck M, Vanlierde R. 1989. Principal component analysis of Belgian rainfall. *Theoretical and Applied Climatology* 204: 199–204.
- Sönmez İ, Kömüscü A.Ü. 2011. Reclassification of rainfall regions of Turkey by K-means methodology and their temporal variability in relation to North Atlantic Oscillation (NAO). *Theoretical and Applied Climatology* 106(3-4): 499–510.
- Stephens E, Day J.J, Pappenberger F, Cloke H. 2015. Precipitation and Floodiness. *Geophysical Research Letters* 43, 316–323.
- Stooksbury D, Michaels P. 1991. Cluster analysis of southeastern US climate stations. *Theoretical and Applied Climatology* 150: 143–150.
- Suarez W. 2007. Le bassin versant du fleuve Santa (Andes du Pérou): Dynamique des écoulements en contexte glacio-pluvio-nival. Dissertation, Université Montpellier II.
- Takahashi K. 2004. The atmospheric circulation associated with extreme rainfall events in Piura, Peru, during the 1997—1998 and 2002 El Niño events. *Annales Geophysicae* 22: 3917-3926.
- Takahashi K, Battisti D. 2007. Processes controlling the mean Tropical Pacific precipitation pattern. Part II: The SPCZ and the Southeast Pacific Dry Zone. *Journal of Climate* 20: 5696-5706.
- Takahashi K, Montecinos A, Goubanova K, Dewitte B. 2011. ENSO regimes: reinterpreting the canonical and Modoki Niño. *Geophysical Research Letters* 38: L10704.
- Takahashi K, Dewitte B. 2015. Strong and moderate nonlinear El Niño regimes. *Climate Dynamics* DOI: 10.1007/s00382-015-2665-3.
- Tapley T, Waylen P. 1990. Spatial variability of annual precipitation and ENSO events in western Peru. *Hydrological Sciences Journal* 35(4): 429-446.
- Thirel G, Andréassian V, Perrin C, Audouy JN, Berthet L, Edwards P, Folton N, Furusho C, Kuentz A, Lerat J, Lindström G, Martin E, Mathevet T, Merz R, Parajka J, Ruelland D, Vaze J. 2015. Hydrology under change: an evaluation protocol to investigate how

- hydrological models deal with changing catchments. *Hydrological Sciences Journal* 60(7–8): 1184–1199.
- Thompson S.E, Sivapalan M, Harman C.J, Srinivasan V, Hipsey M.R, Reed P, Montanari A, Blöschl G. 2013. Developing predictive insight into changing water systems: Use-inspired hydrologic science for the anthropocene. *Hydrology and Earth System Sciences* 17(12): 5013–5039.
- Torrence C, Compo G. 1998. A practical guide to wavelet analysis. *The Bulletin of the American Meteorological Society* 79: 61–78.
- Torrence C, Webster P.J. 1999. Interdecadal Changes in the ENSO–Monsoon System. *Journal of Climate* 12: 2679–2690.
- Tsonis A, Swanson K, Kravtsov S. 2007. A new dynamical mechanism for major climate shifts. *Geophysical Research Letters* 34: 113705.
- Türkeş M, Sümer U.M, Kılıç G. 2002. Persistence and periodicity in the precipitation series of Turkey and associations with 500 hPa geopotential heights. *Climate Research* 21: 59–81.
- Ünal Y, Kindap T, Karaca M. 2003. Redefining the climate zones of Turkey using cluster analysis. *International Journal of Climatology* 23: 1045–1055.
- Valéry A, Andréassian V, Perrin C. 2010. Regionalization of precipitation and air temperature over high-altitude catchments - learning from outliers. *Hydrological Sciences Journal* 55(6): 928–940.
- van der Velde Y, Vercauteren N, Jaramillo F, Dekker, S, Destouni G, Lyon S. 2013. Exploring hydroclimatic change disparity via the Budyko framework. *Hydrological Processes* 28: 4110–4118.
- Vauchel P. 2005. Hydraccess: Software for Management and processing of Hydro–meteorological data software, Version 2.1.4. Free download www.mpl.ird.fr/hybam/utills/hydraccess.html.
- Vecchi G.A, Harrison D.E. 2000. Tropical Pacific sea surface temperature anomalies, El Niño and equatorial westerly wind events. *Journal of Climate* 13(11): 1814–1830.
- Vega-Jácome F, Lavado-Casimiro W, Felipe-Obando O. 2017. Assessing hydrological changes in a regulated river system over the last 90 years in Rimac Basin (Peru). *Theoretical and Applied Climatology*. DOI: 10.1007/s00704-017-2084-y.
- Virji H. 1981. A preliminary study of summertime Tropospheric circulation patterns over South America estimated from cloud wind. *Monthly Weather Review* 109: 599–610.
- von Storch H. and Zwiers F. 2003. *Statistical Analysis in Climate Research*, Cambridge University Press, Cambridge; 495 pp.
- Vuille M, Bradley R.S, Keimig F. 2000. Interannual climate variability in the Central Andes and its relation to tropical Pacific and Atlantic forcing. *Journal of Geophysical Research* 105: 12447–12460.
- Vuille M, Franquist E, Garreaud R, Lavado W, Caceres B. 2015. Impact of the global warming hiatus on Andean temperature. *Journal of Geophysical Research: Atmospheres* 120: 3745–3757.

-
- Wagener T, Sivapalan M, Troch P.A, McGlynn B.L, Harman C.J, Gupta H.V, Kumar P, Rao P.S.C, Basu N.B, Wilson J.S. 2010. The future of hydrology: An evolving science for a changing world. *Water Resources Research* 46(5): W05301.
- Wale A, Rientjes THM, Gieske ASM, Getachew HA. 2009. Ungauged catchment contributions to Lake Tana's water balance. *Hydrological Processes* 23: 3682–3693.
- Waliser D.E, Lau K.M, Stern W, Jones C. 2003. Potential Predictability of the Madden-Julian Oscillation. *Bulletin of the American Meteorological Society* 84: 33-50.
- Waliser D.E. 2005. Predictability and Forecasting. Intraseasonal Variability of the Atmosphere-Ocean Climate System. W. K. M. Lau, and D. E. Waliser. Springer (eds), Heidelberg; pp 389-493.
- Wang D, Hejazi M. 2011. Quantifying the relative contribution of the climate and direct human impacts on mean annual streamflow in the contiguous United States. *Water Resources Research* 47(10): W00J12.
- Wang W, Shao Q, Yang T, Peng S, Xing W, Sun F, Luo Y. 2013. Quantitative assessment of the impact of climate variability and human activities on runoff changes: a case study in four catchments of the Haihe river basin, China. *Hydrological Processes* 27: 1158-1174.
- Wang H, Sankarasubramanian A, Ranjithan R.S. 2015. Understanding the low-frequency variability in hydroclimatic attributes over the southeastern US. *Journal of Hydrology* 521: 170–181.
- Waylen P, Poveda G. 2002. El Niño-Southern Oscillation and aspects for western South American hydro-climatology. *Hydrological Processes* 16: 1247-1260.
- Wheeler M, Kiladis G. 1999. Convectively Coupled Equatorial Waves. Analysis of Clouds and Temperature in the Wavenumber-Frequency Domain. *Journal of the Atmospheric Sciences* 56: 374-399.
- Wheeler M, Weickmann K.M. 2001. Real-time monitoring and prediction of modes of coherent synoptic to intraseasonal tropical variability. *Monthly Weather Review* 129: 2677-2694.
- White C. 2012. Understanding water scarcity: Definitions and measurements. GWF Discussion Paper 1217, Global Water Forum, Canberra, Australia. Available online at: <http://www.globalwaterforum.org/2012/05/07/understanding-water-scarcity-definitions-and-measurements/>
- Woodman R. 1985. Recurrencia del Fenómeno El Niño con intensidad comparable a la del Niño 1982-1983. Consejo Nacional de Ciencia y Tecnología (CONCYTEC). Lima; pp 301-332.
- Xiang B, Wang B, Li T. 2012. A new paradigm for the predominance of standing Central Pacific Warming after the late 1990s. *Climate Dynamics* DOI: 10.1007/s00382-012-1427-8.
- Yang F, Lau K-M. 2004. Trend and variability of China precipitation in spring and summer: Linkage to sea-surface temperature. *International Journal of Climatology* 24: 1625-1644.

-
- Yang D, Shao W, Yeh P, Yang H, Kanae S, Taikan O. 2009. Impact of vegetation coverage on regional water balance in the nonhumid regions of China. *Water Resources Research* 45: W00A14.
- Yeh S.W, Kug S.J, Dewitte B, Kwon M, Kirtman B, Jin F. 2009. El Niño in a changing climate. *Nature* 461: 511-514.
- Zhang L, Dawes WR, Walker G.R. 2001. The response of mean annual evapotranspiration to vegetation changes at catchment scale. *Water Resources Research* 37: 701–708.
- Zhang S, Lu X.X. 2009. Hydrological responses to precipitation variation and diverse human activities in a mountainous tributary of the lower Xijiang, China. *Catena* 77: 130-142.
- Zhao G, Mu X, Tian P, Wang F, Gao P. 2013. Climate changes and their impacts on water resources in semiarid regions: a case study of the Wei River basin, China. *Hydrological Processes* 27: 3852-3863.

(This page has been left blank intentionally)

Annex A

List of scientific articles made throughout the thesis

Scientific articles

Annex A.1

Rau P, Bourrel L, Labat D, Melo P, Dewitte B, Frappart F, Lavado W, Felipe O. 2017a. Regionalization of rainfall over the Peruvian Pacific slope and coast. *International Journal of Climatology* 37(1): 143–158. DOI: 10.1002/joc.4693

Annex A.2

Rau P, Bourrel L, Labat D, Frappart F, Ruelland D, Lavado W, Dewitte B, Felipe O. 2017b. Hydroclimatic change disparity of Peruvian Pacific drainage catchments. *Theoretical and Applied Climatology*. DOI: 10.1007/s00704-017-2263-x

Annex A.3

Rau P, Bourrel L, Labat D, Ruelland D, Frappart F, Lavado W, Dewitte B, Felipe O. 2017c. Assessing freshwater runoff over Peruvian Pacific drainage catchments during the 1970-2010 period. *Hydrological Processes*. (under review)

Annex A.4

Bourrel L, Rau P, Dewitte B, Labat D, Lavado W, Coutaud A, Vera A, Alvarado A, Ordoñez J. 2015. Low-frequency modulation and trend of the relationship between ENSO and precipitation along the northern to centre Peruvian Pacific coast. *Hydrological Processes* 29(6): 1252-1266. DOI: 10.1002/hyp.10247

Annex B

List of scientific collaborations, communications, and vulgarizations made throughout the thesis

Scientific collaboration

Sanabria J, Bourrel L, Dewitte B, Frappart F, Rau P, Solis O, Labat D. 2017. Rainfall along the coast of Peru during strong El Niño events. *International Journal of Climatology*. DOI: 10.1002/joc.5292

Communications in congresses

Rau P, Bourrel L, Dewitte B, Labat D, Lavado W, Coutaud A, Vera A, Alvarado A, Ordoñez J. 2014. Low-frequency modulation and trend of the relationship between precipitation and ENSO along the Northern to Center Peruvian Pacific coast. 2nd Hydrology, Ocean, Atmosphere Conference HOAC. ENGII. 13-15 June. Pekin, China.

Rau P, Bourrel L, Labat D, Melo P, Dewitte B, Frappart F, Lavado W, Felipe O. 2016. Regionalization of rainfall over the Peruvian Pacific slope and coast. I SINAPSIS Meeting. 11-13 July. Paris, France.

Rau P, Bourrel L, Dewitte B, Labat D, Frappart F, Lavado W. 2016 Variacion de baja frecuencia y tendencias en la relacion entre el Fenomeno El Nino y las precipitaciones en la Vertiente del Pacifico Peruano. XXVII Congreso Latinoamericano de Hidraulica LADHI IAHR. 26-30 September. Lima, Peru. (in Spanish)

Scientific vulgarizations

Dewitte B, Takahashi K, Goubanova K, Montecinos A, Mosquera K, Illig S, Montes I, Paulmier A, Purca S, Flores R, Bourrel L, Rau P, Labat D, Lavado W, Espinoza JC. 2014. Las diversas facetas de El Niño y sus efectos en la costa del Perú. El Perú frente al cambio climático. MINAM Ministerio del Ambiente, IRD. Lima; pp 125-140. (in Spanish)

Rau P, Bourrel L, Dewitte B, Labat D. 2017. La distribución de las lluvias en la vertiente del Pacifico peruano y su relación con El Niño. Boletín Técnico "Generación de información y monitoreo del Fenómeno El Niño". Instituto Geofísico del Perú. 4(1), 4-7. (in Spanish)

Annex A.1

Published article in International Journal of Climatology

Regionalization of rainfall over the Peruvian Pacific slope and coast.
Rau P, Bourrel L, Labat D, Melo P, Dewitte B, Frappart F, Lavado W, Felipe O.

Submitted in January 16, 2015
Accepted in January 21, 2016
Published in an issue in January 2, 2017

<http://dx.doi.org/10.1002/joc.4693>

Regionalization of rainfall over the Peruvian Pacific slope and coast

Pedro Rau,^{a*} Luc Bourrel,^a David Labat,^a Pablo Melo,^a Boris Dewitte,^b Frédéric Frappart,^{a,b} Waldo Lavado^c and Oscar Felipe^c

^a *Géosciences Environnement Toulouse, UMR 5563, Université de Toulouse, CNRS-IRD-OMP-CNES, France*

^b *LEGOS, UMR 5566, Université de Toulouse, CNRS-IRD-OMP-CNES, France*

^c *Dirección General de Hidrología y Recursos Hídricos, SENAMHI, Lima, Peru*

ABSTRACT: Documenting the heterogeneity of rainfall regimes is a prerequisite for water resources management, mitigation of risks associated to extremes weather events and for impact studies. In this paper, we present a method for regionalization of rainfall over the Peruvian Pacific slope and coast, which is the main economic zone of the country and concentrates almost 50% of the population. Our approach is based on a two-step process based on k-means clustering followed by the regional vector method (RVM) applied to a network of 145 rainfall stations covering the period 1964–2011. The advantage of combining cluster analysis and RVM is demonstrated compared with just applying each of these methods. Nine homogeneous regions are identified that depict the salient features of the rainfall variability over the study area. A detailed characterization of the rainfall regime in each of the identified regions is presented in response to climate variability at seasonal and interannual timescale. They are shown to grasp the main modes of influence of the El Niño Southern Oscillation (ENSO), that is, increased rainfall over downstream regions in northern Peru during extreme El Niño events and decreased rainfall over upstream regions along the Pacific slope during central Pacific El Niño events. Overall our study points to the value of our two-step regionalization procedure for climate impact studies.

KEY WORDS rainfall; regionalization; k-means; regional vector; Peruvian Pacific slope; Peruvian coast; ENSO

Received 16 January 2015; Revised 20 January 2016; Accepted 21 January 2016

1. Introduction

Rainfall along the Pacific slope and coast of South America is characterized by a complex pattern of spatial and seasonal variability related to its meridional extension and the prominent topography of the Andes Cordillera (Waylen and Poveda, 2002; Garreaud *et al.*, 2009). The Peruvian Pacific slope and coast is located at tropical latitudes and rainfall is mainly influenced by orographic conditions, ocean and atmosphere. The region is characterized by a steep topography that inhibits cross-shore atmospheric flow and disrupt a geotropically balanced zonal wind, inducing a northward sea level pressure gradient along the coast that accelerate the wind northward (Muñoz and Garreaud, 2005). Such a low-level northward mean circulation is associated to cool sea surface temperature (SST) through inducing upwelling and evaporation, which makes this region persistently free of convective rainfall year-around (Takahashi and Battisti, 2007). The Pacific coast of Peru is thus mostly a ‘dry zone’ that only episodically experiences rainfall events. At interannual timescales, those rainfall events are associated to the El Niño Southern Oscillation

(ENSO) phenomenon that is the main climatic influence over rainfall over the Peruvian Pacific coast (Lagos *et al.*, 2008). A rainy season can also be developed owed to a slight weakening of the southeast Pacific anticyclone and the southward displacement of the Pacific Inter-Tropical Convergence Zone (ITCZ) (Lavado *et al.*, 2012).

Although this region concentrates more than 50% of population of Peru, it remains poorly documented in terms of rainfall regionalization. Recent works (Suarez, 2007; Lavado *et al.*, 2012; Ochoa *et al.*, 2014; Bourrel *et al.*, 2015) mostly focused on principal stations or major watersheds. In 1999, a technical report (BCEOM, 1999) proposed a previous rainfall regionalization for the Peruvian Pacific slope and coast based on the Regional Vector Method (RVM) (Brunet-Moret, 1979), which consists in assuming that for the same climatic zone under the same rainfall regime, the annual rainfall is proportional in-between stations, with a little random variation due to rain distribution in the zone (Espinoza *et al.*, 2009). In that report, nine regions were delineated mainly located over the northern coastal region.

Multivariate analysis techniques have proved their efficiency to delineate homogeneous regions based on climatic features such as rainfall data. Many authors have used factor analysis, principal components, clustering techniques or a mixture of all these techniques, to define more precisely climatic zones or rainfall regions (e.g.

* Correspondence to: P. Rau, Géosciences Environnement Toulouse, UMR 5563, Université de Toulouse, CNRS-IRD-OMP-CNES, 14, avenue Édouard Belin, Toulouse 31400, France. E-mail: pedro.rau@get.obs-mip.fr

Ünal *et al.*, 2003; Raziei *et al.*, 2008), to classify rainfall stations (e.g. Stooksbury and Michaels, 1991; Jackson and Weinand, 1995) and to analyse rainfall variability or distribution patterns (Sneyers *et al.*, 1989; Ramos, 2001; Muñoz-Díaz and Rodrigo, 2004; Dezfúli, 2010). Recently Sönmez and Kömüscü (2011) proposed a rainfall reclassification for Turkey based on k-means methodology highlighting the benefit over prior techniques as regionalization based on topographic and climatic parameters, long-term seasonal rainfall patterns (Türkeş *et al.*, 2002) and hierarchical clustering (Ünal *et al.*, 2003). Sönmez and Kömüscü (2011) in particular indicate that their method is efficient in grasping shifts in time periods. The advantage of using a cluster analysis in the regionalization procedure stands in the fact that rainfall time series may be non-stationary and/or non-Gaussian due to the complex influence of climate phenomena (Takahashi and Dewitte, 2015). For instance, the ENSO has a strong positive asymmetry resulting from the fact that strong extreme events are warm events (An and Jin, 2004; Boucharel *et al.*, 2011), resulting in a non-Gaussian distribution of most historical indices (Boucharel *et al.*, 2009). Such non-linearity in the large-scale circulation over the tropical Pacific is likely to influence the rainfall over the Peruvian Pacific slope and coast, which calls for refining regionalization procedures just based on linear techniques (e.g. RVM). This is one of the main motivations of this work that proposes to estimate the improvement brought to rainfall regionalization by applying a hybrid procedure consisting of a combination of two widely used techniques: k-means clustering (Hartigan and Wong, 1979) to obtain a coarse regionalization that is used as first guess in the regionalization using the RVM. Our aim is also to estimate to which extent the decomposition of a large complex narrow area into a reduced number of homogeneous regions can grasp the salient features of the ENSO influence onto rainfall over the Pacific slope and coast of Peru (Horel and Cornejo-Garrido, 1986; Goldberg *et al.*, 1987; Tapley and Waylen, 1990; Takahashi, 2004; Nickl, 2007; Lagos *et al.*, 2008; Lavado *et al.*, 2012; Lavado and Espinoza, 2014; Bourrel *et al.*, 2015). The identified regions are also aimed at being used for ecological and water resources management and easing the interpretation of the manifestation of the main climatic modes in the region as described in Muñoz-Díaz and Rodrigo (2004), Sönmez and Kömüscü (2011) and Parracho *et al.* (2015).

2. Study area

The study area comprises the Peruvian Pacific slope and coast that covers an area of $\sim 280,500 \text{ km}^2$. This region borders with the Andes mountains by the east (69.8°W), whereas extending west to the Pacific Ocean (81.3°W). It borders with Ecuador in the north (3.4°N) and with Chile in the south (18.4°S). Its maximum width, perpendicular to the coastline reaches 230 km in the southern part and is only 100 km in the northern part. This area is characterized by a significant altitudinal gradient ranging

from 0 to $\sim 6500 \text{ m asl}$ and includes 54 main river watersheds that cover near 90% of this region. The rivers generally flows from east to west from the Andes towards the Pacific Ocean with bare and steep slopes that favour significant rising, flooding and erosion during highly rainy episodes (Lavado *et al.*, 2012). On the one hand, under normal conditions, this region is influenced by the Southern Pacific Anticyclone in combination with the Humboldt current (cold SSTs) which produces dry and stable conditions to the western central Andes, with moist air trapped below the inversion zone at about 900 hPa – 1000 m asl (Vuille *et al.*, 2000; Garreaud *et al.*, 2002), conditions that produce extreme aridity until about that altitude (Lavado *et al.*, 2012). Over this altitudinal limit, it is known that there is an influence of the southward displacement of the ITCZ and is supposed that other mechanisms influencing over the Peruvian Andes, also influence over the Peruvian Pacific slope (i.e. humidity transport from the Amazon, Bolivian High, etc.) (Nickl, 2007; Lagos *et al.*, 2008), nevertheless this has not been studied to date. On the other hand, this region exhibits greater seasonal and interannual rainfall variability than the two main others hydrological regions of Peru: the Amazon and the endorheic Titicaca drainage areas (Lavado *et al.*, 2012), mainly caused by the ENSO influence in the northern areas during the rainy season, with no clear evidence of the ENSO influence for central and southern areas (Lagos *et al.*, 2008; Lavado *et al.*, 2012; Lavado and Espinoza, 2014).

3. Data

3.1. Rainfall dataset

The database includes monthly rainfall records from 139 meteorological stations managed by the SENAMHI (National Meteorological and Hydrological Service of Peru) and 6 meteorological stations managed by the INAMHI (National Meteorological and Hydrological Institute of Ecuador). It was necessary to extend the area into the foothills of the northern Andes, which cover bi-national river watersheds between Peru and Ecuador. Monthly rainfall data are available over 1964–2011 period. Over the 145 stations, 124 stations are located in the Pacific slope and coastal region of Peru (see Figure 1) and 11 belong to the Peruvian Atlantic drainage and 4 to the Titicaca drainage. A careful quality check of this data was performed using the RVM. In this dataset containing 145 stations records, 76% of them present more than 45 years of continuous records, 20% of them between 20 and 45 years of continuous records and only 4% of them between 15 and 20 years of continuous records.

3.2. Sea surface temperature and ENSO indices

We used global values of *in situ* monthly SST obtained from the Hadley Centre Global Sea Ice and Sea Surface Temperature (HadISST) dataset (Rayner *et al.*, 2003) over 1964–2011 time interval at 150° – 0°E , 25°S – 25°N of the Pacific and Atlantic basins, which can be downloaded at: <http://www.metoffice.gov.uk/hadobs/hadisst/data/>

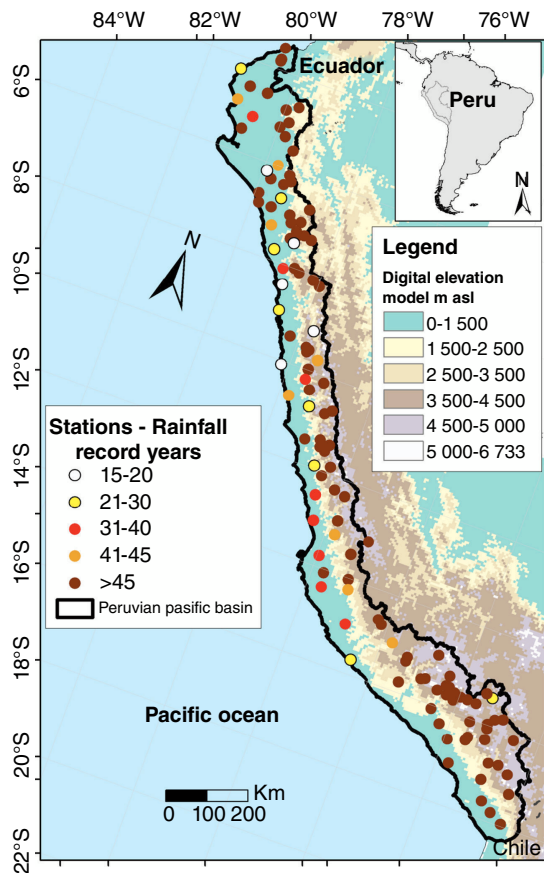


Figure 1. Geographical distribution of stations over the Peruvian Pacific slope and coast. The contour in black thick line delimits the region of interest. Rainfall record length of the stations is indicated by the colours of the dots (five stations are represented by white points and have between 15 and 20 years of data record, eight by yellow that have between 21 and 30 years, eight by red that have between 31 and 40 years, eight by orange that have between 41 and 45 years and 95 stations have more than 45 years of data records, represented by brown points). A Digital Elevation Model (SRTM – 90 m) shows the topographical characteristics and altitudes of the study area.

download.html available on a $1^\circ \times 1^\circ$ grid. The evaluation of the relationship between rainfall variability and Tropical Pacific SST was conducted by using two oceanic indices (the E and C indices) proposed in a recent study by Takahashi *et al.* (2011). These indices are by construction independent (orthogonal) and describe the two main modes of ENSO related to the variability of Eastern equatorial Pacific (E) and Central equatorial Pacific (C). These indices were also used in Lavado and Espinoza (2014) and Bourrel *et al.* (2015) for depicting the influence of the tropical Pacific SST onto rainfall over Peru.

4. Methods

The methodology is composed of three steps summarized in Figure 2: the first one corresponds to the reviewing of rainfall data, their homogenization by RVM and the filling of missing monthly rainfall data; the second one corresponds to the regionalization process including k-means clustering and RVM analysis using an iterative

process by trial and error with the goal of searching regions that present similar annual rainfall amount, and interannual variability; and the last one corresponds to a detailed characterization of the rainfall regime in each region in response to climate variability at seasonal and interannual timescales.

4.1. Data homogenization and validation

It was carried out in three steps:

- 1 The analysis period was chosen to be as long as possible for a significant number of stations over the Pacific slope and coast and complementary stations presented in data section. We also impose that the selected stations should have at least continuous records longer than 15 years.
- 2 To evaluate the homogeneity of datasets for identifying inconsistent information in terms of quality issues as: station microenvironment, instrumentation, variations in time and position (Changnon and Kenneth, 2006); we used here the RVM. It relies on the principle of annual rainfall proportionality between neighbouring stations represented as rainfall indexes which characterize the rainfall pattern of a predetermined area. The RVM is based on the calculation of an extended rainfall vector within the study period. This concept refers to the calculation of a weighted average of rainfall anomalies for each station, overcoming the effects of stations with extreme and low values of rainfall. Then, the regional annual pluviometric indices Z_i and the extended average rainfall P_j are found by using the least squares technique. This could be obtained by minimizing the sum of Equation (1).

$$\sum_{i=1}^N \sum_{j=1}^M \left(\frac{P_{ij}}{P_j} - Z_i \right) \quad (1)$$

where i is the year index, j the station index, N the number of years, and M the number of stations. P_{ij} stands for the annual rainfall in the station j , year i ; P_j is the extended average rainfall period of N years; and finally, Z_i is the regional pluviometric index of year i . The complete set of Z_i values over the entire period is known as ‘regional annual pluviometric indexes vector’. Being an iterative process, this method allows to calculate the vector of each of the predefined regions, then provides a stations – vector interannual variability comparison, for finally discards those that are not consistent with the regional vector (RV). This process is repeated as much as necessary. See more details of this method in Espinoza *et al.* (2009).

- 3 For the stations that were selected during the homogenization process and also had missing monthly data, once their spatial representation proved significant, were subjected to a process of information completion. In this case, this procedure was performed using the values of rainfall index calculated from the RV and the mean value of rainfall monthly data of the concerned station.

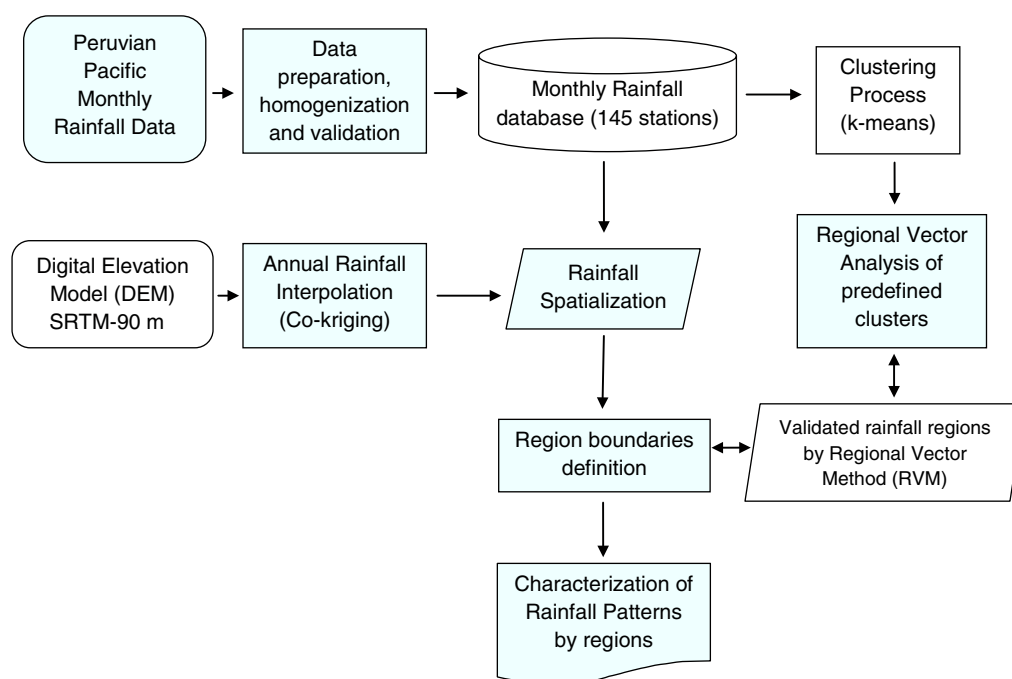


Figure 2. Schematic of the methodological steps for the regionalization of the rainfall time series.

A more detailed description can be found in Bourrel *et al.* (2015).

Through these three stages, 145 pluviometric stations were validated. The geographical location of the 124 Peruvian Pacific slope and coastal stations is depicted in Figure 1, which also mentions the rainfall record length for each station.

4.2. Classification and regionalization process

In this section, we described the regionalization process using the RVM approach, which required a first guess to initialize the process. In this study, this first guess is obtained performing a k-means clustering as a classification of rainfall data from the stations selected in 3.1.

4.2.1. k-Means clustering technique

k-Means clustering is a statistical technique designed to assign objects to a fixed number of groups (clusters) based on a set of specified variables. One of the principal advantages of k-means technique consists in its cluster's identifying performance which allows ranking the obtained clusters as a function of their representativeness. The process involves a partitioning schema into k different clusters previously defined. Objects that are within those k clusters must be as similar as possible to those that belongs to its own group and completely dissimilar to the objects that are in the other clusters. Similarity depends on correlation, average difference or another type of metrics. By definition each cluster is characterized by its own centroid with the cluster members located all around it. The algorithm used at annual rainfall timescale was the Hartigan–Wong

which adopts the squared Euclidean distance as a dissimilarity measurement. See more details of this method in Hartigan and Wong (1979).

A key part of the k-means application is to define an optimum number of clusters. In order to succeed in the definition of partitioning groups, an estimation of the silhouette number must be performed for each desired number of groups. The silhouette width is used to evaluate the statistical significance of each identified cluster (Rousseeuw, 1987). The silhouette value is obtained following Rousseeuw (1987) as:

$$S(i) = \frac{\min \{b(i, k)\} - a(i)}{\max \{a(i), \min \{b(i, k)\}\}} \quad (2)$$

where $a(i)$ corresponds to the average similarity between the i th object and the other objects of the same group and $b(i, k)$ is the average similarity between the i th object and the members of the k th clusters. The range of variation for this silhouette index is between -1 and $+1$, when the silhouette value is close to $+1$ means that there is a better member correspondence to its own cluster, whereas a negative value represents the object this is not well located in the appropriate cluster. Meanwhile the value of 0 means that objects could belong to any k cluster. We also compute an average silhouette width for the whole k clusters which represents the mean of $S(i)$, and it can be used to choose the best number of clusters, by taking the value of k for which $S(i)$ is maximal.

4.2.2. Regionalization analysis

There are classical ways to predefine regions; it can be based on stations proximity and homogeneity, physiographic patterns or topographical constraints related to isohyets (Espinoza *et al.*, 2009; Bourrel *et al.*, 2015). Here,

rainfall stations grouped by k-means clustering are set up as predefined regions. The criteria for using k-means clustering as first step of regionalization is based on the advantages in time solving and the preset number of groups at the beginning of the process whilst RVM requires defining the stations grouped into a predefined region, being a long and exhaustive methodology if it is not provided an accurate number of groups.

Regionalization was performed using the RVM, which is generally oriented to: (a) assess rainfall data quality based on the homogeneity within a predetermined region (Espinoza *et al.*, 2009) and (b) achieve rainfall regionalization processes (establishment of representative vectors of homogeneous rainfall zones) to gather the stations exhibiting the same interannual variability. The process for regionalization is similar to the process explained in Section 4.1 (item 2). It depends on the computation of a 'mean station' or 'vector' from all data involved in the study area that will be compared with each pluviometric station (Brunet-Moret, 1979). Prior to the use of the RVM, it is necessary to group stations into predefined regions.

Once calculated, the RV is compared iteratively with data station for discarding those stations whose data are not consistent with the RV and reprise the process. The rejection of a given station could mean that this station belongs to a neighbouring region that could present greater consistency. Therefore in many cases, stations or areas are re-grouped or divided in order to obtain regions that show homogeneous features. The main statistical criteria for regrouping stations into homogeneous regions is based on thresholds applied to the standard deviation of the differences between annual pluviometric indices of stations and the RV indices; and to the correlation coefficient between RV and annual pluviometric values of stations. These thresholds are fixed to the standard deviation lower than 0.4 and correlation coefficient greater than 0.7. Rainfall database management and RVM were carried out using the HYDRACCESS software (Vauchel, 2005).

4.2.3. Rainfall data interpolation

After regionalization based on punctual information (i.e. rainfall stations), it was done a rainfall spatialization by isohyets allowing to delimit polygonal regions. Annual rainfall was interpolated incorporating elevation data using the co-kriging classical geostatistical approach, which is widely used in the hydrometeorological field (Goovaerts, 2000; Diodato, 2005; Buytaert *et al.*, 2006). Co-kriging, which is a multivariate version of kriging technique, took into account the digital elevation model (DEM) provided by NASA-NGA, Shuttle Radar Topographic Mission (SRTM – 90 m) data (<http://srtm.csi.cgiar.org>) as correlated secondary information based on a spherical variogram (Goovaerts, 2000; Mair and Fares, 2011). This rainfall interpolation map was used as a background raster guide for delineating polygonal regions involving the station points grouped with regionalization analysis. These polygons follow the isohyets shape with geometrical approach (perpendicular and bisector criteria of boundaries of regions traversing isohyets and stations) and a

statistical approach (revalidation of new defined areas with the RVM with proper fit of stations inside each region).

Finally, representative monthly rainfall time series of each region were obtained with the co-kriging methodology because of better performance than other techniques (e.g. Thiessen Polygons, Inverse Distance Weighted and Kriging) over mountains areas (Hevesi *et al.*, 1992a, 1992b; Goovaerts, 2000; Diodato, 2005). Time series were assigned to centroids as representative points for obtain mean latitude, longitude and altitude of each region.

4.3. Rainfall variability and sea surface temperature anomalies

In order to investigate the relationship between rainfall and ENSO, a covariance analysis (i.e. singular value decomposition – SVD) is used, which consists in deriving the eigenvectors and eigenvalues of the covariance matrix between rainfall anomalies (December–January–February–March–April mean) over the Peruvian Pacific slope and coast and the SST anomalies over the Pacific and Atlantic basins (December–January–February mean) that maximizes the fraction of the cumulative squared covariance (Yang and Lau, 2004). Data were previously detrended in the period 1964 to 2011. More details and comments about this technique can be found in Bretherton *et al.* (1992) and Cherry (1997). In order to provide an estimate of the statistical significance of the SVD modes, a Monte–Carlo test is performed that consists in creating a surrogate data, a randomized dataset of rainfall and sea surface temperature by scrambling 40 yearly maps among the 48 years in the time domain. The SVD is then performed on the scrambled dataset. The same procedure of scrambling the dataset and performing the analysis is repeated 500 times, each time keeping the value of the explained covariance of the first two dominant modes and comparing the SVD modes of the original dataset and the ones of the scrambled dataset. The method is described in Björnsson and Venegas (1997). The 90% confidence level of the mode patterns is defined so as to the 10 and 90% percentiles of the ensemble correspond to a value that differs from the estimated mode by less than 0.5 times the standard deviation among the ensemble.

5. Results

5.1. Rainfall classification

A cluster analysis of the annual rainfall data was performed by applying k-means technique on the 124 rainfall stations previously selected. The optimal value for the cluster numbers was determined by an average silhouette value and a negative silhouette number for a number of cluster groups varying from 3 to 10 (see Table 1).

Maximum silhouette values are obtained for cluster 3 group (0.64), cluster 4 group (0.60) and cluster 6 group (0.55), considering as a reasonable structure a cluster having a silhouette value greater than 0.50 and as a weak structure a silhouette value less than 0.50 following Kononenko

Table 1. Results of the k-means analysis for number of cluster groups varying from 3 to 10.

Number of cluster groups	3	4	5	6	7	8	9	10
Average silhouette value	0.64	0.60	0.54	0.55	0.54	0.54	0.46	0.45
Negative silhouette number	6	4	9	6	8	6	11	9

Optimal values for selecting the number of cluster groups are shown in bold.

and Kukar (2007). The number of negative silhouette values is minimal for cluster 3 group (6), cluster 4 group (4) and cluster 6 group (6). After plotting the cluster groups into a map showing their spatial distribution, we select the cluster 3 and cluster 6 groups among them, as these two clusters show certain arrangement of rainfall stations according to topographical and latitudinal variation (Figure 3(a) and (b)). Cluster 4 group was an intermediate group that corresponds to one sub-region in the north.

The two cluster groups (clusters 3 and 6) exhibit a similar spatial distribution. Pluviometric stations from both groups present an altitudinal distribution along the Pacific slope and coast, defining three regions: the stations located in lowlands (green triangles), in middle altitude basin (white circles) and in highlands (black points). Cluster 6 group presents three additional regions, two of them closely related to northern rainfall features for the middle altitude basin (cluster 4 of cluster 6 group represented by red triangles) and highlands (cluster 6 of cluster 6 group represented by yellow circles). Two stations are considered as isolated (cluster 5 of cluster 6 group represented by blue circles).

Even if cluster 6 group is less representative than cluster 3 group in terms of silhouette value, cluster 6 group is considered acceptable for representing correctly the variability of northern rainfall, offering an initial classification of rainfall or initial approach of rainfall regionalization over the Peruvian Pacific slope and coast.

5.2. Regionalization

After cluster definition, the RVM was performed over these preliminary regions using an iterative process by trial and error, that adds and deletes stations from neighbouring regions considering the criteria described in Section 4.2.2. This process could be also verified by their interannual coefficient of variation (CV). In Figure 4, the stations located in the western area of the coast (lowlands) present greater values of CV (>1.8) than those located in middle altitude basin and in highlands. Northern region presents higher CV values in lowlands and in the middle altitude basin. Highlands present lower CV values (<0.8) along the Pacific slope independently of the latitude.

High CV values in the northern region correspond to strong interannual rainfall variability with anomalies greater than $1000 \text{ mm year}^{-1}$. High CV values are also observed along southern latitude which are mostly caused

by small values around the near zero annual average. These values are due to the large-scale mid-tropospheric subsidence over the southeastern subtropical Pacific Ocean, enhanced by the coastal upwelling of cold water (Enfield, 1981; Virji, 1981; Vuille *et al.*, 2000; Garreaud *et al.*, 2002; Lavado *et al.*, 2012).

Based on the iterative process of the RVM, we identify nine homogeneous rainfall patterns (see Figure 5). Comparing with the initial cluster groups derived from k-means, rainfall stations from clusters 1, 2 and 4 located in the coastal zone and northern Andes (see Figure 3(b)) exhibit higher coefficients of variation in coastal proximity (see Figure 4). Cluster 1 includes the regions 1, 4 and 7 along the coastal zone. Cluster 4 defines region 2: in this case, clustering process successfully assigned each station as well as RV reported them as separate from other regions. Cluster 5 and 6 are regrouped into region 3. Finally, cluster 3 defines regions 5, 6, 8 and 9: in this case, the low variability, their high altitude as the latitudinal extension, defines these four regions.

k-Means methodology and RVM did not provide a final regionalization by their own. For clustering method, some groups are not well defined because of isolated stations to be included in other groups, associated to low silhouette values (see cluster 2 from cluster 3 group in Figure 3(a) and clusters 2, 3 and 6 from cluster 6 group in Figure 3(b)). This can be explained by the characteristics of the annual rainfall database used, related to the presence of non-globular clusters with a chain-like shape or with not well defined centres (see regions 3, 8 and 9 in Figure 5), which are one of the principal disadvantages using this technique (Kaufman and Rousseeuw, 1990). For the RVM, it is possible to obtain grouped regions following only the statistical criteria with the thresholds presented in Section 4.2.2. However, there is the risk of increasing computing time and obtaining unrealistic groups because of using only a statistical criteria and not an initial arrangement inferred in this case from the k-means clustering. k-Means inferred three regions for lowlands, middle altitude basin and highlands (see Figure 3(b)) as a first guess to the final regionalization by the RVM in the north (see regions 1, 2 and 3 in Figure 5) and in the south (see regions 7, 8 and 9 in Figure 5), which it not was possible to identify using only the RVM (not shown). The two-step methodology (k-means and RVM) has also presented a slight improvement in the thresholds of Section 4.2.2. with respect to the thresholds obtained with RVM only, with about +6% for the standard deviation of the differences between annual pluviometric indices of stations and the RV indices (from 0.39 to 0.42); and about +0.5% for the correlation coefficient between RV and annual pluviometric values of stations (from 0.78 to 0.79).

Following the approach summarized in the flow chart presented in Figure 2 and applying the methodology described in Section 4.2.3.; the nine regions were well delineated taking into account the rainfall interpolation map as shown in Figure 5. Annual rainfall in each region exhibits a relationship with altitude and latitude, rainfall is higher at low latitudes and at southern latitudes in high altitudes as shown in Figures 5 and 6.

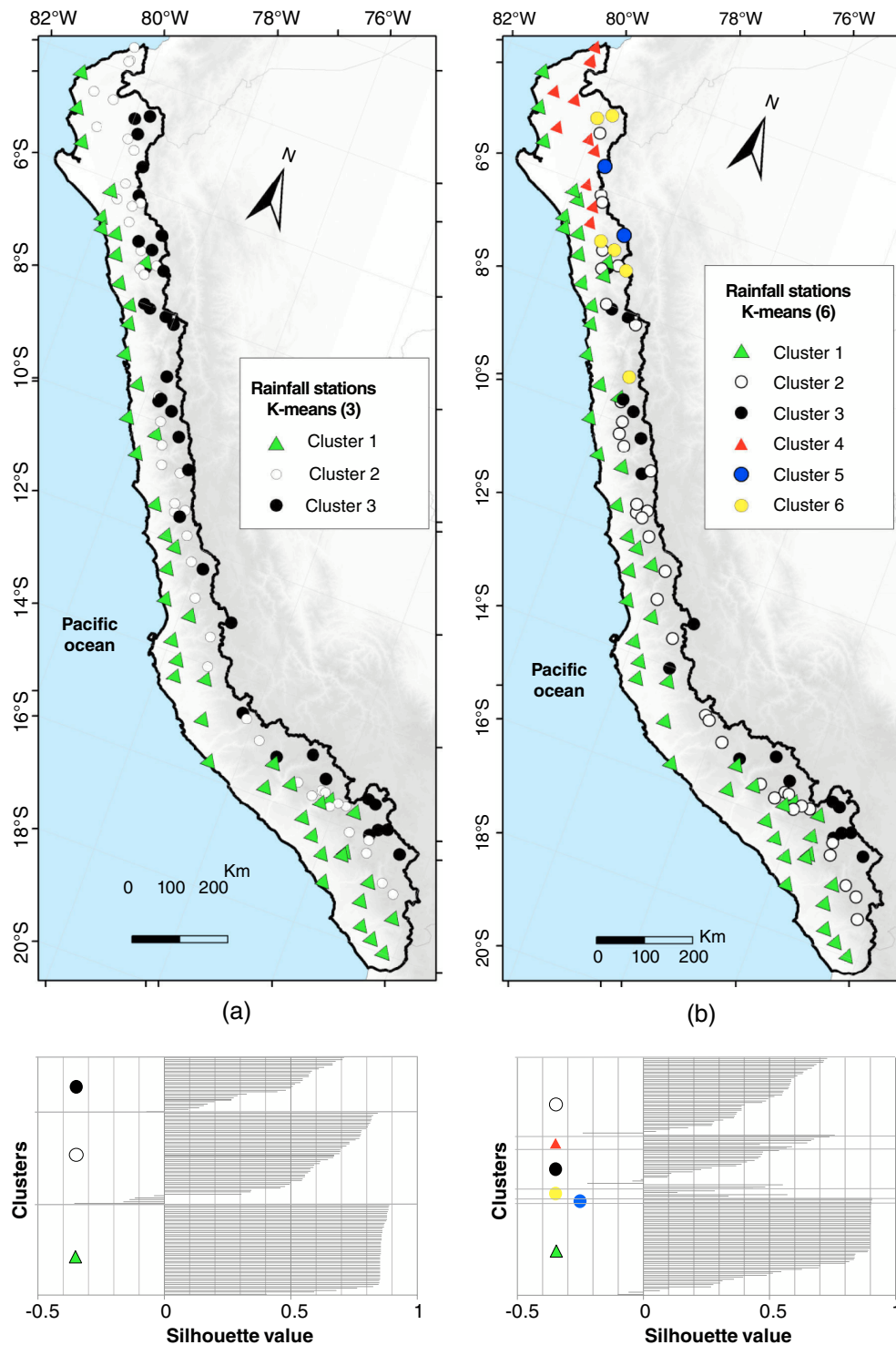


Figure 3. Spatial distribution of (a) cluster 3 group and (b) cluster 6 group obtained with the k-means process. Silhouette value for each cluster group is provided in the bottom panels.

Correlation coefficient between the stations and the regional vector of each region was calculated separately and the spatial distribution of these coefficients of correlation is shown in Figure 7. The purpose of this analysis is to emphasize the level of representation of the regional vector and identify locally the areas within a region where this vector is more representative. Considering regions 4 and 7, the coefficient of correlation is less than 0.7 and greater

than 0.5. These coefficients are considered as acceptable considering the dryer conditions with more than 90% of the rainfall records near zero throughout the year due to hydroclimatic features, where any value greater than zero causes a strong variability reducing the relationship with its RV. For the northern regions 1 and 2, the mean correlation is more than 0.9 being a very good representation of RV and the more representative areas are shown

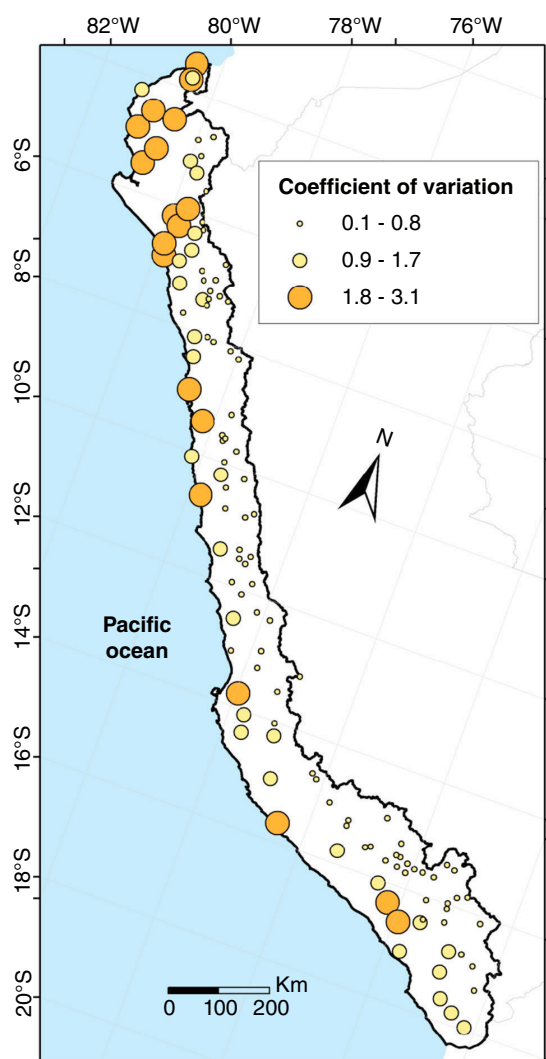


Figure 4. Spatial distribution and range of coefficient of variation (CV) for all of the pluviometric stations of the Peruvian Pacific slope and coast network.

in red coloration. The strong correlation values are due to extreme rainfall events related with ENSO strong events increasing the association level between stations and RV. Regions 3, 5, 6, 8 and 9 located in highlands, have correlations greater than 0.7 being a good representation of the RV with the more representatives areas in orange coloration.

5.3. Regions characterization

In this section, we document the rainfall seasonal distribution and interannual variability over the nine identified regions. Some of geographical features (area, latitudinal and altitudinal ranges) are presented in Table 2. All regions present a unimodal rainfall seasonal distribution (see Figure 8) and differ from their peak calendar month, intensity and duration of the rainy season.

Region 1 extends over northern lowlands including drier areas as the Sechura desert (79°–81°W and 5.5°–6.5°S) where the average interannual rainfall is about 90 mm year⁻¹. A maximum seasonal rainfall is observed in March (see Figure 8(a)1) with a rainy season

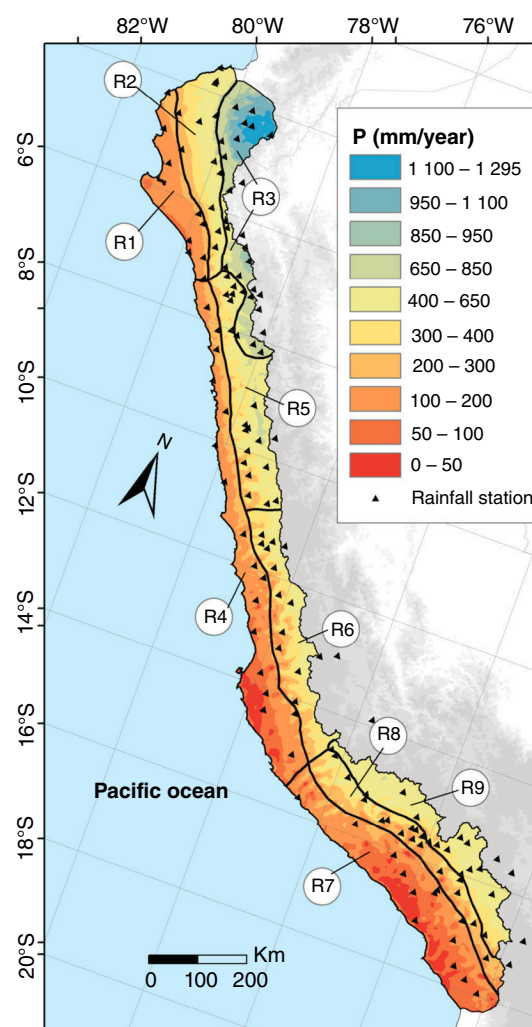


Figure 5. The nine homogeneous rainfall regions after the regionalization process of clustering and RVM. Interpolated surface of annual rainfall (isohyets obtained using co-kriging method) is also shown to demonstrate rainfall differences between regions.

from January to May (JFMAM) with values less than 50 mm month⁻¹ which represent near to 90% of the annual rainfall. The rest of the year is considered as dry due to values near or equal to zero, corroborating the irregularity in the seasonal rainfall pattern (see Figure 8(a)1) and in the interannual variability of monthly rainfall (see Figure 8(a)2) at the coast (Garreaud *et al.*, 2002; Lavado *et al.*, 2012).

Region 2 comprises a large part that belongs to the foothills of the northern Andes covering bi-national river watersheds of Peru and Ecuador. This zone exhibits an irregular seasonal rainfall pattern (see Figure 8(b)1) and an irregular interannual variability of monthly rainfall (see Figure 8(b)2). Average interannual rainfall value is around 370 mm year⁻¹. The wettest period occurs between January and April (JFMA) cumulating near to 90% of total rainfall.

Northern coastal regions as regions 1 and 2 are significantly affected by strong events represented by two peaks reaching 413 mm month⁻¹ in March 1983

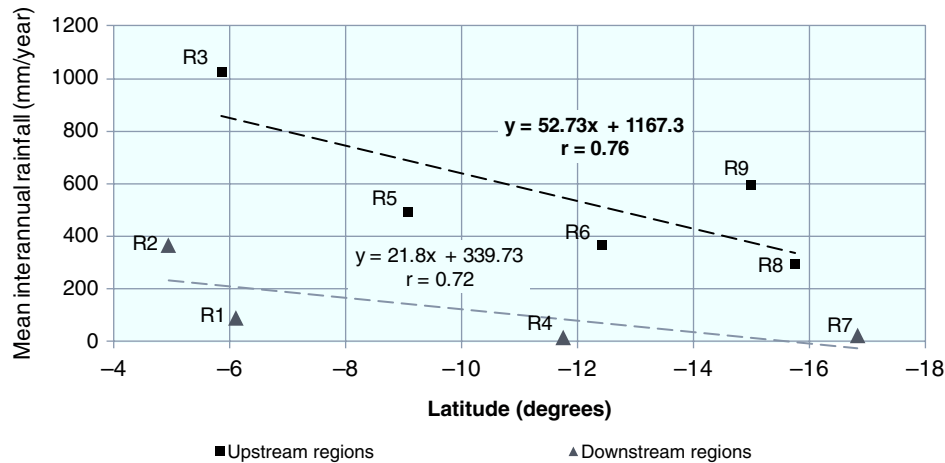


Figure 6. Relationship between mean interannual rainfall and latitude for the nine identified regions grouped in upstream and downstream regions. Representation for upstream regions is significant at the 90% level using a Student's *t*-test.

and 299 mm month⁻¹ in March 1998 for region 1 (see Figure 8(a)2); and 746 mm month⁻¹ in March 1983 and 708 mm month⁻¹ in March 1998 for region 2 (see Figure 8(b)2). A summary of rainfall statistics is given in Table 2 and a boxplot representation of monthly rainfall in Figure 9. Outliers from Figure 9, represented by small circles, correspond to values exceeding 1.5 times the interquartile range (IQR). All regions have observations that exceed $Q3 + 1.5(IQR)$, however, northern coastal regions 1 and 2 differs from the rest for having greater number of outliers values (14 and 17%, respectively) with the largest rainfall anomalies reaching 56 and 25 times of mean monthly rainfall for regions 1 and 2, respectively. Most of the interannual variability in rainfall, reflected as well in higher CV values (see Table 2), is directly due to the occurrence of the strong El Niño events indicating also a high intensity of interannual variability than other regions. This is particularly obvious for region 1 where three extreme rainfall events are observed corresponding to the year 1972, 1982 and 1997, known as strong El Niño years. Interestingly the more inland region 2 exhibits interannual variations of rainfall that does not necessarily corresponds to the strong El Niño years. These events may correspond to local convective events associated to coastal warm oceanic conditions related mainly to Kelvin waves and the Madden and Julian Oscillation (MJO) (Woodman, 1985; Bourrel *et al.*, 2015).

Region 3 covers bi-national river watersheds of Peru and Ecuador bordering with the Amazon Basin by the east. This is also the wettest region (see Figures 8(c)1, (c)2 and 9). On the other hand, rainfall amount decreases southward with rainfall regularity in the seasonal pattern (see Figure 8(c)1) and in the interannual variability of monthly rainfall (see Figure 8(c)2), with a rainy season from January to April (JFMA) that represents almost 70% of the annual rainfall. Mean interannual rainfall reaches 1024 mm year⁻¹, representing 11 times of the mean interannual rainfall of region 1 and 3 times of region 2 (see Table 2). The rainfall interannual variations are weakly associated to the extreme El Niño events (the correlation

between the *E* index and rainfall is 0.2) but is negatively correlated to the *C* index ($r = -0.4$) indicating that the R3 region is sensitive to cool enhanced coastal conditions during Central Pacific El Niño events (Bourrel *et al.*, 2015). The inter-events fluctuations are also noticeable which are related to local convective events not related to ENSO but mostly by the ITCZ and the large-scale atmospheric variability associated to the MJO (Tapley and Waylen, 1990; Takahashi, 2004; Bourrel *et al.*, 2015). Also noteworthy, there is an increase of rainfall peaks frequency over the last two decades (see Figure 8(c)2).

Region 4 is the longest region located between the coastal plain and the foothills of the western Andes and contains some of the major coastal cities as the capital Lima. This region corresponds to a zone influenced by the large-scale mid-tropospheric subsidence of the southeastern subtropical Pacific Ocean, enhanced by the coastal upwelling of cold water (Vuille *et al.*, 2000; Garreaud *et al.*, 2002; Lavado *et al.*, 2012) without presenting a relationship between strong rainfall peaks and strong ENSO events. Then, mean interannual rainfall reaches a value of 16 mm year⁻¹ defining the driest region in the country (see Table 2) with rainfall irregularity in the seasonal pattern (see Figure 8(d)1) and in the interannual variability of monthly rainfall (see Figure 8(d)2) very common in coastal regions (see Figure 9). The wet period from January to March (JFM) represents near to 75% of the annual rainfall. In the southern part, drier areas are found such as the Nazca desert (74.5°–75.5°W and 14.5°–15.5°S).

Region 5 comprises a border with region 3 and the Amazon Basin by the east. The mean interannual rainfall reaches 492 mm year⁻¹ and the wet period occurs between December and April (DJFMA) cumulating near to 80% of total rainfall. No rainfall peaks were identified during strong El Niño events (see Figure 8(e)2) as those in regions 1 and 2, suggesting that rainfall in regions 4 and 5 are probably to be affected by others processes, either local (e.g. coastal SST) or non-local (e.g. dry air transport from the southern region that reduce the rainfall), resulting in a heterogeneous interannual variability of monthly rainfall (see

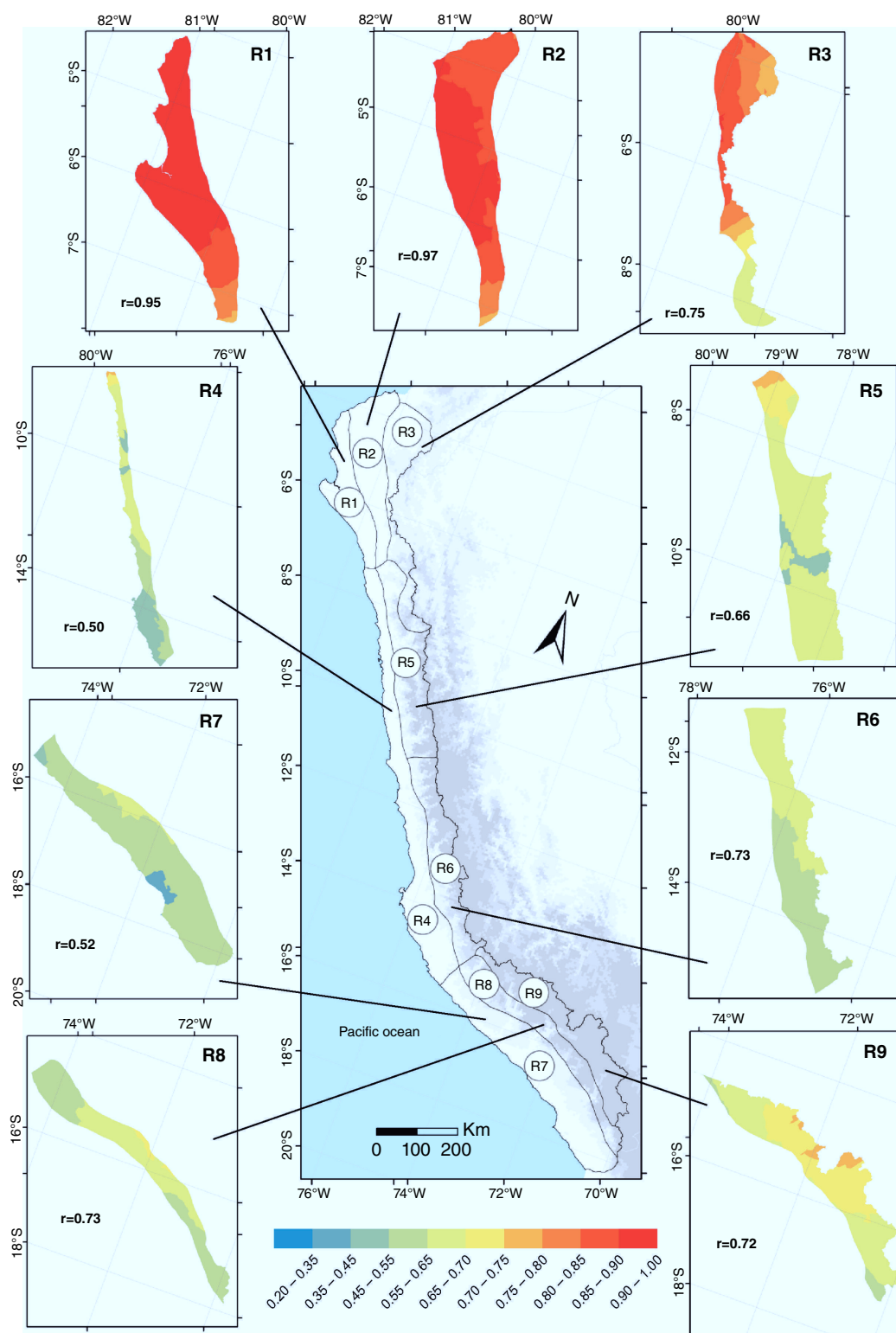


Figure 7. Coefficients of correlation of the stations and the final regional vector of each region identified after the regionalization process (k-means and RVM). A mean value of correlation is also provided by region in bold as well as the spatial distribution of correlation with the regional vector. Correlations are significant at the 90% level using a Student's *t*-test.

Figure 8(e)2) with a low value of coefficient of variation around 0.3 (see Table 2).

Region 6 borders with the Amazon Basin by the east and shows a heterogeneous rainfall pattern without distinguishing any peak corresponding to the strong El

Niño events (see Figure 8(f)2). Rainfall distribution is well defined with a rainy season from December to March (DJFM) that represents near to 85% of the annual rainfall (see Figure 8(f)1) and with a mean interannual rainfall reaching 366 mm year^{-1} .

Table 2. Geographical features and annual rainfall values for the nine identified regions.

Region	Area (km ²)	Altitudinal range (m asl)	Latitudinal range (°S)	Annual minimum rainfall (mm year ⁻¹)	Annual maximum rainfall (mm year ⁻¹)	Annual average rainfall (mm year ⁻¹)	CV	SD (mm year ⁻¹)
1	20 300	0–500	4.2–7.3	3.2	1345.2	89.7	2.6	233.3
2	27 600	0–1500	3.4–7.3	17.3	2772.2	366.5	1.5	534.2
3	27 200	1500–3500	3.6–8.3	533.0	1812.9	1023.7	0.3	294.4
4	48 600	0–1500	7.3–15.5	1.6	62.2	15.5	0.7	11.4
5	32 500	1000–5000	7–11	174.1	825.8	492.4	0.3	145.8
6	30 400	2000–5000	11–15	75.0	693.5	365.9	0.4	133.3
7	49 300	0–2500	15.5–18.4	5.1	54.9	23.2	0.6	13.5
8	25 400	2500–4000	14.6–17.8	23.2	528.8	296.1	0.4	111.8
9	30 100	3500–5500	14.4–17.7	220.5	833.2	594.0	0.2	143.2

Region 7 is characterized by lower rainfall regime with a rainy season from JFM accounting for 65% of the annual rainfall. Furthermore, this region is one of the driest areas in the country where the interannual rainfall (23 mm year⁻¹) presenting rainfall irregularity in the seasonal pattern (see Figure 8(g)1) and in the interannual variability of monthly rainfall (see Figure 8(g)2). This region could be considered as an extension of region 4, also influenced by the large-scale mid-tropospheric subsidence of the southeastern subtropical Pacific Ocean but differing in the increase of rainfall peaks frequency in the last decade unlike region 4 as can be seen in Figure 8(g)2.

Region 8 comprises an area thus belongs to the foothills of the southern Andes. This zone exhibits irregular rainfall in the seasonal pattern (see Figure 8(h)1) and in the interannual variability of monthly rainfall (see Figure 8(h)2). The mean interannual rainfall presents a higher value than region 7, reaching 296 mm year⁻¹. The wettest period occurs between December and March (DJFM) cumulating near to 90% of total rainfall (see Figure 8(h)1).

Finally, region 9 borders with the Titicaca Basin in the south and east and with the Amazon Basin by the east. The mean interannual rainfall reaches 594 mm year⁻¹ and the wet period occurs between December and March (DJFM) cumulating near to 80% of total rainfall. Similar to region 8, region 9 presents a deficit in rainfall during strong El Niño events (see Figure 8(h)2 and (i)2). However, unlike region 8, it presents rainfall regularity in the seasonal pattern (see Figure 8(i)1) and in the interannual variability of monthly rainfall (see Figure 8(i)2) associated with a low value of coefficient of variation around 0.2 (see Table 2) indicating also the lowest intensity of interannual variability. Up to this point, we propose a co-variability analysis between rainfall and tropical SST (see paragraphs below) to deepen the understanding of the relationship between regions and ENSO. Other climatological variables mentioned in Section 2 will need further research and are out of scope of this work.

In order to estimate the value of the regionalization for interpreting the impact of climatic variability over rainfall along the Pacific slope and coast of Peru, a covariance analysis is performed between the rainfall time series of the nine regions and the SST anomalies over the Tropical Pacific and Atlantic Oceans.

For clarity, the SST anomalies are considered for the peak ENSO season (i.e. December–January–February mean, hereafter DJF) whereas the rainfall fluctuations are considered for the approximate rainy season (i.e. December–January–February–March–April season, hereafter DJFMA). The results of the covariance analysis (see Section 4.3 for details) are presented in Figures 10 and 11, showing the patterns and time series of the first (Figure 10) and second (Figure 11) SVD modes between SST in the tropical Pacific and Atlantic over DJF and rainfall over the regions over DJFMA. Values of the mode patterns, significant at the 90% level, are indicated by the colour shading (Figures 10(b) and 11(b)) and the red colour (Figures 10(a) and 11(a), see method in Section 4.3). The results indicate a significant relationship between both fields because the percentage of covariance is 66% and 23% for the first and second modes, respectively, and the associated time series of the mode patterns are significantly correlated [r value reaches 0.59 (0.54) for mode 1 (2) in Figure 10(c) (Figure 11(c)), respectively]. The first mode for SST accounts for the strong eastern Pacific El Niño variability as suggested by the large positive skewness of the principal component time series associated to the two strong El Niño events of 1997/1998 and 1982/1983. The correlation between the time series associated to the SST mode pattern and the E index reaches 0.80. The second mode is reminiscent of the central Pacific El Niño variability because it has a strong positive loading near the deadline. Its associated principal component time series is strongly correlated to the C index reaching a correlation of 0.96, significant at the 95% level. Interestingly the time series associated to the first mode for SST is also highly correlated with the C index ($r = 0.73$), which indicates that extreme rainfall events are related to both the E and C modes. It explains in particular why the SST mode pattern has a significant loading in the central Pacific which is not the case for the E mode pattern with is more confined towards the coast of Ecuador (see Takahashi *et al.*, 2011).

The analysis of the mode patterns for rainfall clearly indicates that the first mode accounts for extreme rainfall events in the northern part of Peru (regions 1 and 2) whereas the second mode pattern has a larger loading (negative value) for the upstream regions (region 3, 6, 8 and

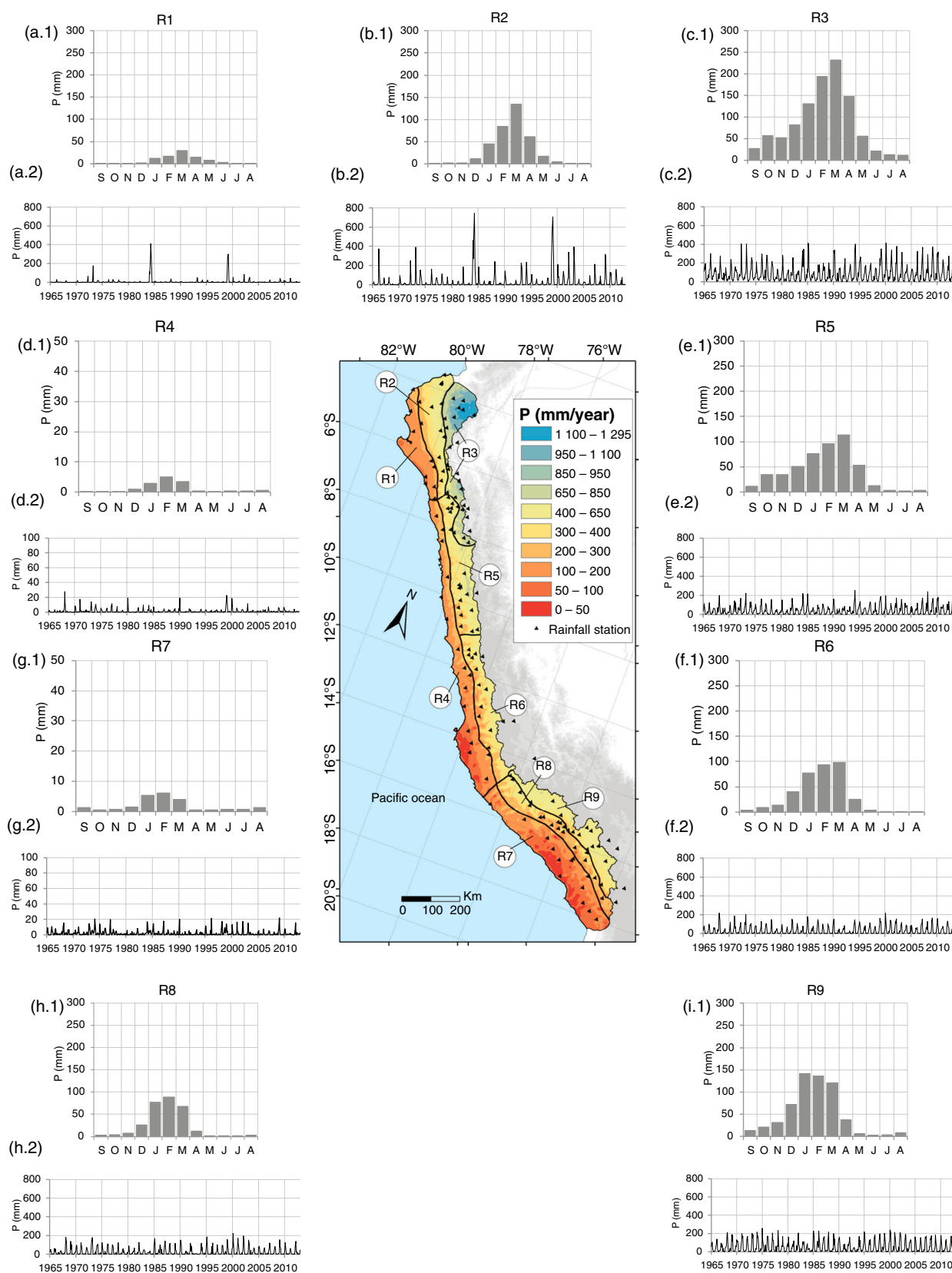


Figure 8. Monthly rainfall regime (1964–2011) for the nine identified regions. A rainfall time series is shown by region. Regions 4 and 7 are shown in a different rainfall scale.

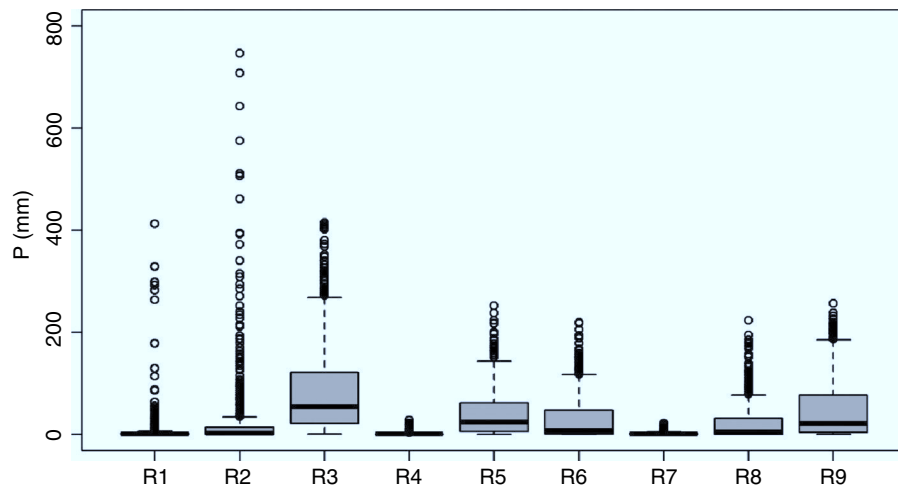


Figure 9. Boxplot of monthly rainfall for the nine identified regions.

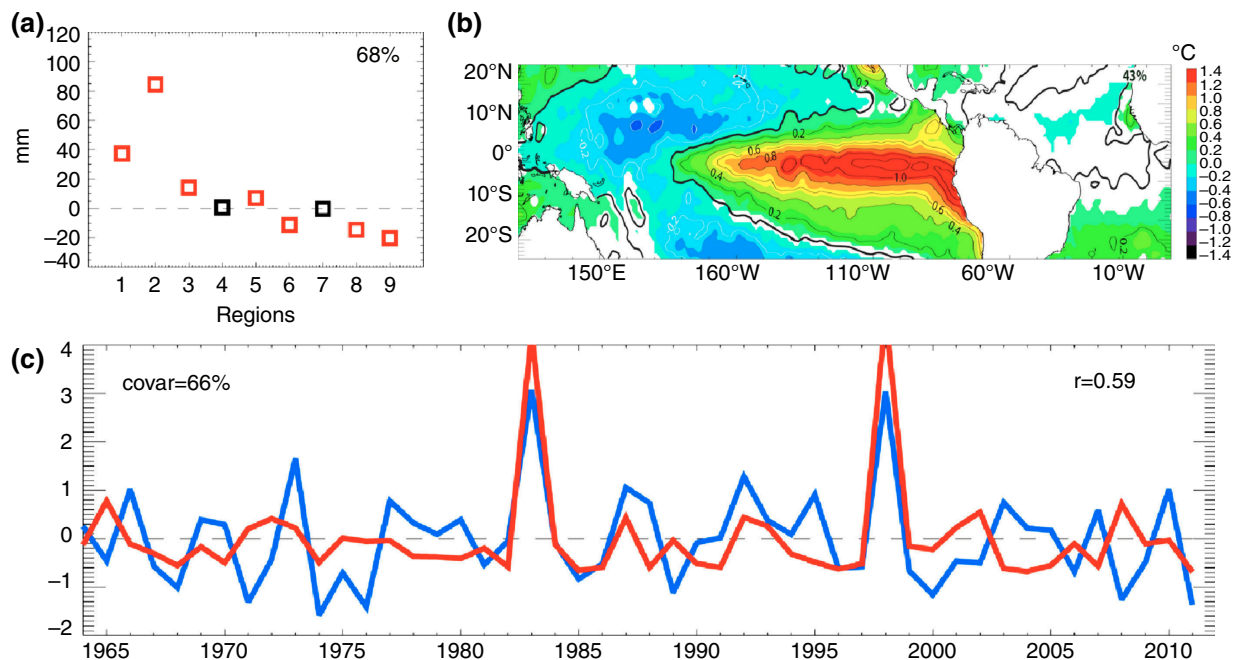


Figure 10. Dominant SVD mode between rainfall in DJFMA over the 9 regions and SST anomalies in DJF over the tropical Pacific and Atlantic. (a) Mode pattern for rainfall. (b) Mode pattern for SST (contour interval is every 0.2°C). (c) Associated SVD time series for rainfall (red colour) and SST (blue colour). The percentage of variance of the modes is indicated in panels a and b, whereas the percentage of covariance (covar) is indicated in panel c. The correlation (r) between the SVD time series is also indicated in panel c. The contour in thick black line in panel b indicates the zero-contour. The shading (red) colour in panel b (a) respectively, indicates where the mode pattern is statistically significant at the 90% level.

9), clearly indicative that during central Pacific El Niño events, the Pacific slope of Peru experiences a deficit in rainfall that increases with altitude. Note that this analysis is consistent with results from previous works (Lavado and Espinoza, 2014; Bourrel *et al.*, 2015), which analysed the relationship between E and C indices and stations over the Peruvian territory and over the North to Centre of the Peruvian Pacific coast and slope, respectively. We here provide a more quantitative estimate of this relationship through the covariance analysis, which indicates its potential for climate impact studies. In particular, the SVD modes would allow building a linear statistical model of rainfall over the Peruvian Pacific coast using SST as a

predictor. The regionalization procedure prior to conducting the SVD analysis is also valuable in easing the interpretation of the ENSO impact on rainfall, in particular, by avoiding probable spurious effects associated to outliers or multiple atmospheric influences. Another important result arising from this analysis is that the extreme rainfall events over the Peruvian Pacific coast are not solely influenced by extreme El Niño events (accounted for by the E mode) but are also influenced by SST in the central equatorial Pacific, as evidenced by the strong correlation between the principal component of the first SVD mode for SST and the C index. This suggests that the magnitude and location along the equator of the SST anomalies in the central Pacific are

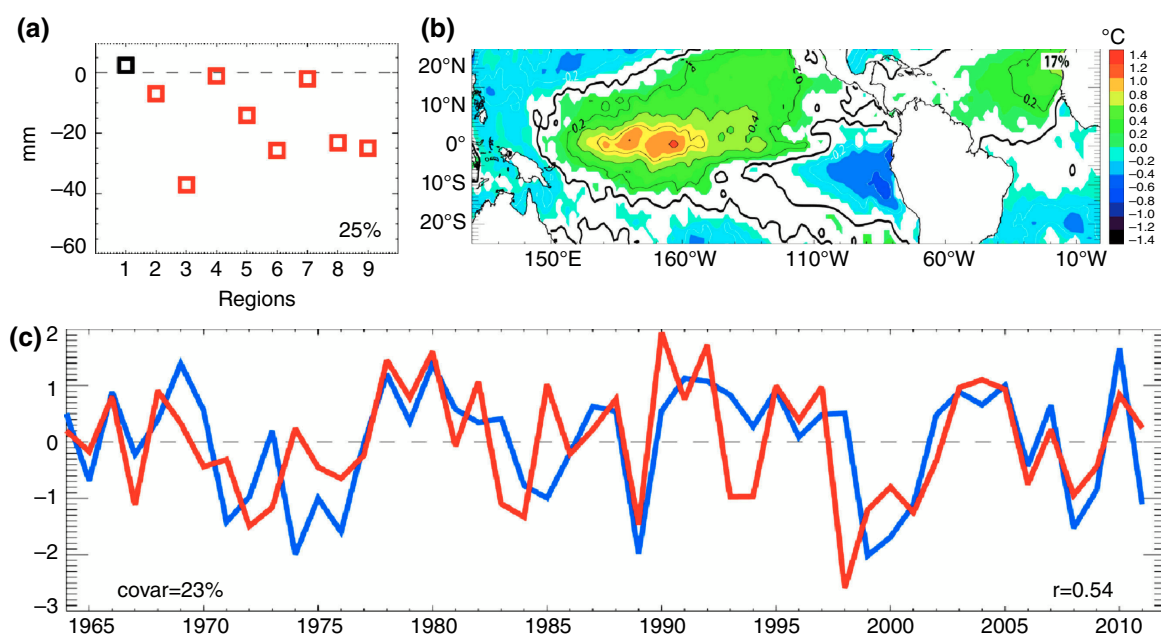


Figure 11. Same as Figure 10, but for the second SVD mode.

important parameters to determine the ENSO impact of rainfall over the Peruvian Pacific coast.

6. Conclusions

This study proposes a method for the regionalization of the rainfall in the Peruvian Pacific slope and coast that consists in a two-step procedure: a preliminary cluster analysis (k-means) followed by the RVM analysis. Using this procedure, nine regions are identified that depicts synthetically the relationship between rainfall variability and altitude and latitude. In particular, rainfall variability is higher at the northern latitudes and it decreases to the south in high altitudes. The motivation for performing a classification using cluster analysis prior to the regionalisation by RVM stands in the complex of processes influencing rainfall variability over this region. In particular, previous studies (Lavado and Espinoza, 2014; Bourrel *et al.*, 2015) have shown that rainfall along the Pacific slope and coast of Peru experiences the influence of both type of El Niño, and due to the strong positive skewness of strong El Niño events, the distribution of rainfall data is not Gaussian, limiting to some extents the linear analysis approach (i.e. RVM). It was in particular verified that our approach leads to a different definition of the regions than an approach based only on RVM. We inferred three regions for lowlands, middle altitude basin and highland in the northern and southern Pacific slope and coast, which was not possible to identify using the method based on the RVM only. The k-means clustering analysis allows for a preliminary grouping of station data that is used as a first guess for the RVM and this step constrains to a large extent the regionalization procedure. The proposed two-step methodology also leads to a slight improvement in the thresholds estimated with the RVM only.

The nine identified regions are shown to grasp the salient features of the influence of ENSO onto rainfall along the Pacific slope and coast of Peru (Horel and Cornejo-Garrido, 1986; Goldberg *et al.*, 1987; Tapley and Waylen, 1990; Takahashi, 2004; Nickl, 2007; Lagos *et al.*, 2008; Lavado *et al.*, 2012; Lavado and Espinoza, 2014; Bourrel *et al.*, 2015), which illustrate its potential for climate impact studies. The dominant co-variability mode between SST in the tropical Atlantic and Pacific Oceans and the reduced set of time series associated to the nine regions has a strong positive loading over the northern part of Peru (regions 1 and 2) for precipitation and over the eastern tropical Pacific for SST, thus accounting for extreme El Niño events. On the other hand, the second mode pattern has a larger loading (negative value) for the upstream regions along the Pacific slope (region 3, 6, 8 and 9), clearly indicative that during central Pacific warming, these regions experience a deficit in rainfall that tends to increase with altitude (more negative in the north than in the south). This is consistent with Lavado and Espinoza (2014) which analysed the relationship between the two types of ENSO and stations over the Peruvian territory, while providing a more synthetic picture of the ENSO influence. In addition, the first co-variability mode between rainfall and SST indicates that extreme rainfall events take place in the North (regions 1 and 2) and are influenced by SST anomalies in the central Pacific (i.e. SST anomalies that project on the C mode), which was not identified in previous works. We attribute this discrepancy between our result and the one by Lavado and Espinoza (2014) to the regionalization procedure that we perform prior to the statistical analysis with ENSO indices. In particular, our regionalization product accounts exclusively for rainfall variability over the Peruvian Pacific continental slope and coast, and is not influenced by stations located

at high-altitude regions that might be influenced by inland circulation patterns. The regionalisation procedure has also the advantage of reducing the influence of outliers in the covariance analysis.

Future work will be dedicated to further investigate the ENSO/rainfall relationship based on the nine identified regions, incorporating other atmospheric and oceanic key indices (cf. Bourrel *et al.*, 2015). Our product will also provide valuable information for hydrological sensitivity analysis over Peruvian Pacific watersheds (through hydrological modelling) for quantifying the effects of climate variability and human activities on runoff with the aim of improving ecological and water resources management.

Acknowledgments

This work was supported by Peruvian Ministry of Education (MINEDU-PRONABEC, scholarship). Authors would like to thank SENAMHI (Meteorological and Hydrological Service of Peru) for providing complete rainfall raw dataset. Boris Dewitte thanks the CNES for support through the TOSCA/CNES project Modokalt.

References

- An SI, Jin FF. 2004. Nonlinearity and asymmetry of ENSO. *J. Clim.* **17**: 2399–2412.
- BCEOM. 1999. Estudio hidrológico-meteorológico en la vertiente del Pacífico del Perú con fines de evaluación y pronóstico del fenómeno El Niño para prevención y mitigación de desastres. Asociación BCEOM-Sofi Consult S.A – ORSTOM, Programa de apoyo a la emergencia Fenómeno del Niño. Volumen I, Contrato de préstamo n°4250-PE-BIRF, Presidencia de la Republica, Perú, Lima.
- Björnsson H, Venegas SA. 1997. A manual for EOF and SVD analyses of climatic data. CCGCR Report No. 97-1, McGill University, Montréal, Québec.
- Boucharel J, Dewitte B, Garel B, du Penhoat Y. 2009. ENSO's non-stationary and non-Gaussian character: the role of climate shifts. *Nonlinear Process. Geophys.* **16**: 453–473.
- Boucharel J, Dewitte B, Du Penhoat Y *et al.* 2011. ENSO nonlinearity in a warming climate. *Clim. Dyn.* **37**(9–10): 2045–2065.
- Bourrel L, Rau P, Dewitte B, Labat D, Lavado W, Coutaud A, Vera A, Alvarado A, Ordoñez J. 2015. Low-frequency modulation and trend of the relationship between ENSO and precipitation along the northern to centre Peruvian Pacific coast. *Hydrol. Process.* **29**(6): 1252–1266.
- Bretherton CS, Smith C, Wallace JM. 1992. An intercomparison of methods for finding coupled patterns in climate data. *J. Clim.* **5**: 541–560.
- Brunet-Moret Y. 1979. Homogénéisation des précipitations. *Cahiers ORSTOM. Serie. Hydrol.* **16**: 3–4.
- Buytaert W, Cellier R, Willems P, De Bièvre B, Wyseure G. 2006. Spatial and temporal rainfall variability in mountainous areas: a case study from the south Ecuadorian Andes. *J. Hydrol.* **329**: 413–421.
- Changnon S, Kenneth K. 2006. Changes in instruments and sites affecting historical weather records: a case study. *J. Atmos. Ocean. Technol.* **23**: 825–828.
- Cherry S. 1997. Some comments on singular value decomposition analysis. *J. Clim.* **10**: 1759–1761.
- Dezfuli AK. 2010. Spatio-temporal variability of seasonal rainfall in western equatorial Africa. *Theor. Appl. Climatol.* **104**(1–2): 57–69.
- Diodato N. 2005. The influence of topographic co-variables on the spatial variability of precipitation over small regions of complex terrain. *Int. J. Climatol.* **25**: 351–363.
- Enfield D. 1981. Thermally driven wind variability in the planetary boundary layer above Lima, Peru. *J. Geophys. Res.* **86**(C3): 2005–2016.
- Espinoza JC, Ronchail J, Guyot JL, Cochonneau G, Naziano F, Lavado W, De Oliveira E, Pombosa R, Vauchel P. 2009. Spatio-temporal rainfall variability in the Amazon basin countries (Brazil, Peru, Bolivia, Colombia and Ecuador). *Int. J. Climatol.* **29**: 1574–1594.
- Garreaud R, Rutllant J, Fuenzalida H. 2002. Coastal lows along the Sub-tropical West Coast of South America: mean structure and evolution. *Mon. Weather Rev.* **130**: 75–88.
- Garreaud RD, Vuille M, Compagnucci R, Marengo J. 2009. Present-day South American climate. *Palaeogeogr. Palaeoclimatol. Palaeoecol.* **281**(3–4): 180–195.
- Goldberg RA, Tisnado G, Scofield RA. 1987. Characteristics of extreme rainfall events in north-western Peru during the 1982–1983 El Niño period. *J. Geophys. Res.* **92**(C14): 225–241.
- Goovaerts P. 2000. Geostatistical approaches for incorporating elevation into the spatial interpolation of rainfall. *J. Hydrol.* **228**: 113–129.
- Hartigan JA, Wong MA. 1979. Algorithm AS 136: a K-means clustering algorithm. *J. R. Stat. Soc. Ser. C* **28**(1): 100–108.
- Hevesi J, Istok J, Flint A. 1992a. Precipitation estimation in mountainous terrain using multivariate geostatistics. Part I: structural analysis. *J. Appl. Meteorol. Climatol.* **31**: 661–676.
- Hevesi J, Flint A, Istok J. 1992b. Precipitation estimation in mountainous terrain using multivariate geostatistics. Part II: isohyetal maps. *J. Appl. Meteorol. Climatol.* **31**: 677–688.
- Horel JD, Cornejo-Garrido AG. 1986. Convection along the coast of northern Peru during 1983: spatial and temporal variation of clouds and rainfall. *Mon. Weather Rev.* **114**: 2091–2105.
- Jackson JJ, Weinand H. 1995. Classification of tropical rainfall stations: a comparison of clustering techniques. *Int. J. Climatol.* **15**(9): 985–994.
- Kaufman L, Rousseeuw P. 1990. *Finding Groups in Data: An Introduction to Cluster Analysis*. John Wiley & Sons Inc: Hoboken, NJ.
- Kononenko I, Kukar M. 2007. *Machine Learning and Data Mining: Introduction to Principles and Algorithms*. Horwood Publishing: Chichester, UK.
- Lagos P, Silva Y, Nickl E, Mosquera K. 2008. El Niño – related precipitation variability in Peru. *Adv. Geosci.* **14**: 231–237.
- Lavado W, Espinoza JC. 2014. Impactos de El Niño y La Niña en las lluvias del Perú. *Rev. Bras. Med.* **29**: 171–182.
- Lavado WS, Ronchail J, Labat D, Espinoza JC, Guyot JL. 2012. Basin-scale analysis of rainfall and runoff in Peru (1969–2004): Pacific, Titicaca and Amazonas drainages. *Hydrol. Sci. J.* **57**(4): 1–18.
- Mair A, Fares A. 2011. Comparison of rainfall interpolation methods in a Mountainous Region of a Tropical Island. *J. Hydrol. Eng.* **16**(4): 371–383.
- Muñoz R, Garreaud R. 2005. Dynamics of the low-level Jet off the West coast of subtropical South America. *Mon. Weather Rev.* **133**: 3661–3677.
- Muñoz-Díaz D, Rodrigo F. 2004. Spatio-temporal patterns of seasonal rainfall in Spain (1912–2000) using cluster and principal component analysis: comparison. *Ann. Geophys.* **22**: 1435–1448.
- Nickl E. 2007. *Teleconnections and Climate in the Peruvian Andes*. MSc thesis, Department of Geography, University of Delaware: Newark, DE.
- Ochoa A, Pineda L, Crespo P, Willems P. 2014. Evaluation of TRMM 3B42 precipitation estimates and WRF retrospective precipitation simulation over the Pacific–Andean region of Ecuador and Peru. *Hydrol. Earth Syst. Sci.* **18**(3179–3193): 2014.
- Parracho A, Melo-Gonçalves P, Rocha A. 2015. Regionalization of precipitation for the Iberian Peninsula and climate change. *Phys. Chem. Earth*, doi: 10.1016/j.pce.2015.07.004.
- Ramos M. 2001. Divisive and hierarchical clustering techniques to analyse variability of rainfall distribution patterns in a Mediterranean region. *Atmos. Res.* **57**: 123–138.
- Rayner NA, Parker DE, Horton EB, Folland CK, Alexander LV, Rowell DP, Kent EC, Kaplan A. 2003. Global analyses of sea surface temperature, sea ice, and night marine air temperature since the late nineteenth century. *J. Geophys. Res.* **108**(D14): 4407.
- Raziei T, Bordi I, Pereira LS. 2008. A precipitation-based regionalization for Western Iran and regional drought variability. *Hydrol. Earth Syst. Sci.* **12**: 1309–1321.
- Rousseeuw P. 1987. Silhouettes: a graphical aid to the interpretation and validation of cluster analysis. *J. Comput. Appl. Math.* **20**: 53–65.
- Sneyers R, Vandiepenbeeck M, Vanlierde R. 1989. Principal component analysis of Belgian rainfall. *Theor. Appl. Climatol.* **204**: 199–204.
- Sönmez İ, Kömürcü AÜ. 2011. Reclassification of rainfall regions of Turkey by K-means methodology and their temporal variability in relation to North Atlantic Oscillation (NAO). *Theor. Appl. Climatol.* **106**(3–4): 499–510.
- Stooksbury D, Michaels P. 1991. Cluster analysis of southeastern US climate stations. *Theor. Appl. Climatol.* **150**: 143–150.

- Suarez W. 2007. *Le bassin versant du fleuve Santa (Andes du Pérou): Dynamique des écoulements en contexte glacio-pluvio-nival*. PhD thesis, Université Montpellier II, France.
- Takahashi K. 2004. The atmospheric circulation associated with extreme rainfall events in Piura, Peru, during the 1997–1998 and 2002 El Niño events. *Ann. Geophys.* **22**: 3917–3926.
- Takahashi K, Battisti D. 2007. Processes controlling the mean Tropical Pacific precipitation pattern. Part II: the SPCZ and the Southeast Pacific Dry Zone. *J. Clim.* **20**: 5696–5706.
- Takahashi K, Dewitte B. 2015. Strong and moderate nonlinear El Niño regimes. *Clim. Dyn.*, doi: 10.1007/s00382-015-2665-3.
- Takahashi K, Montecinos A, Goubanova K, Dewitte B. 2011. ENSO regimes: reinterpreting the canonical and Modoki Niño. *Geophys. Res. Lett.* **38**: L10704.
- Tapley T, Waylen P. 1990. Spatial variability of annual precipitation and ENSO events in western Peru. *Hydrol. Sci. J.* **35**(4): 429–446.
- Türkeş M, Sümer UM, Kılıç G. 2002. Persistence and periodicity in the precipitation series of Turkey and associations with 500 hPa geopotential heights. *Clim. Res.* **21**: 59–81.
- Ünal Y, Kindap T, Karaca M. 2003. Redefining the climate zones of Turkey using cluster analysis. *Int. J. Climatol.* **23**: 1045–1055.
- Vauchel P. 2005. *Hydraccess: Software for Management and Processing of Hydro-meteorological Data Software, Version 2.1.4. Free Download*. www.ore-hybam.org/index.php/eng/Logiciels/Hydraccess (accessed 1 September 2014).
- Virji H. 1981. A preliminary study of summertime Tropospheric circulation patterns over South America estimated from cloud wind. *Mon. Weather Rev.* **109**: 599–610.
- Vuille M, Bradley RS, Keimig F. 2000. Interannual climate variability in the Central Andes and its relation to tropical Pacific and Atlantic forcing. *J. Geophys. Res.* **105**: 12447–12460.
- Waylen P, Poveda G. 2002. El Niño–Southern Oscillation and aspects for western South American hydro-climatology. *Hydrol. Process.* **16**: 1247–1260.
- Woodman R. 1985. *Recurrencia del Fenómeno El Niño con intensidad comparable a la del Niño 1982–1983*. *Concejo Nacional de Ciencia y Tecnología (CONCYTEC)*: Lima, Peru, 301–332.
- Yang F, Lau K-M. 2004. Trend and variability of China precipitation in spring and summer: linkage to sea-surface temperature. *Int. J. Climatol.* **24**: 1625–1644.

Annex A.2

Published article in Theoretical and Applied Climatology

Hydroclimatic change disparity of Peruvian Pacific drainage catchments.
Rau P, Bourrel L, Labat D, Frappart F, Ruelland D, Lavado W, Dewitte B,
Felipe O.


Submitted in February 12, 2016

Accepted in August 23, 2017

Published online in September 5, 2017

<http://dx.doi.org/10.1007/s00704-017-2263-x>

Hydroclimatic change disparity of Peruvian Pacific drainage catchments

Pedro Rau¹  · Luc Bourrel¹ · David Labat¹ · Frédéric Frappart^{1,2} · Denis Ruelland³ · Waldo Lavado⁴ · Boris Dewitte^{2,5,6} · Oscar Felipe⁴

Received: 12 February 2016 / Accepted: 23 August 2017
© Springer-Verlag GmbH Austria 2017

Abstract Peruvian Pacific drainage catchments only benefit from 2% of the total national available freshwater while they concentrate almost 50% of the population of the country. This situation is likely to lead a severe water scarcity and also constitutes an obstacle to economic development. Catchment runoff fluctuations in response to climate variability and/or human activities can be reflected in extreme events, representing a serious concern (like floods, erosion, droughts) in the study area. To document this crucial issue for Peru, we present here an insightful analysis of the water quantity resource variability of this region, exploring the links between this variability and climate and/or anthropogenic pressure. We first present a detailed analysis of the hydroclimatologic variability at annual timescale and at basin scale over the 1970–2008 period. In addition to corroborating the influence of extreme El Niño events over precipitation and runoff in northern catchments, a mean warming of

0.2 °C per decade over all catchments was found. Also, higher values of temperature and potential and actual evapotranspiration were found over northern latitudes. We chose to apply the Budyko-Zhang framework that characterizes the water cycle as a function of climate only, allowing the identification of catchments with significant climatic and anthropogenic influence on water balance. The Budyko-Zhang methodology revealed that 11 out of 26 initial catchments are characterized by low water balance disparity related to minor climatic and anthropogenic influence. These 11 catchments were suitable for identifying catchments with contrasting change in their hydroclimatic behavior using the Budyko trajectories. Our analysis further reveals that six hydrological catchment responses can be characterized by high sensitivity to climate variability and land use changes.

1 Introduction

Changes in climatic conditions appear as more sensitive in dryland regions around the world. In these regions, the effects of climate variability and human activities on runoff are significantly more visible than in other climate regions (Mortimore 2009), resulting in a reduction or increase in water yield (Brown et al. 2005; Donohue et al. 2011; Chen et al. 2013).

Catchments in the Peruvian Pacific drainage region (hereafter Pd) are characterized by dryland conditions (e.g., arid and semiarid areas), implying water shortage problems for human consumption and economical activities in major cities located at lowlands. Besides, they are likely to be affected by the devastating effects of floods (ANA 2012). Previous studies such as Lavado et al. (2012) showed evidence of lack of uniform regional trend and changes mainly in minimum runoff, which they attributed to the anthropogenic influence over

✉ Pedro Rau
pedro.rau@get.obs-mip.fr

¹ UMR 5563 GET, Université de Toulouse - CNRS-IRD-OMP-CNES, 14 Avenue Edouard Belin, 31400 Toulouse, France

² UMR 5566 LEGOS, Université de Toulouse - CNRS-IRD-OMP-CNES, 14 Avenue Edouard Belin, 31400 Toulouse, France

³ CNRS, UMR 5569 HydroSciences Montpellier, 300 Avenue du Professeur Emile Jeanbrau, 34095 Montpellier, France

⁴ SENAMHI, Jirón Cahuide 785, 11 Lima, Peru

⁵ Facultad de Ciencias del Mar, Universidad Católica del Norte, Coquimbo, Chile

⁶ Centro de Estudios Avanzado en Zonas Áridas (CEAZA), Coquimbo, Chile

the 29 catchments that were analyzed. Earlier studies (ANA 2012) analyzed the water supply and demand in the main catchments as an approximation of water balance with water management purposes.

Quantifying and deciphering the effects of climate variability and human activities on hydrological regime represent a major challenge, especially at short scales of time and space (Donohue et al. 2007; Wagener et al. 2010). In order to decipher climate variability and anthropogenic influence on water balance, we based our study on the Budyko theory (Budyko 1958, 1974). This theory is widely used and is a well-established global empirical framework within the hydrological community (Donohue et al. 2011; Coron et al. 2015; Greve et al. 2015). This method relates the interannual evaporative index (ratio between actual evapotranspiration and precipitation) and the interannual dryness index (ratio between potential evapotranspiration and precipitation) in a global description called the “Budyko space.” Thereby, all interactions through the hydrological cycle between vegetation, soil, and atmosphere create an empirical equilibrium represented by the Budyko curve (van der Velde et al. 2013). To emphasize the impact of other factors on the water balance such as vegetation, an emerging general relationship proposed by Zhang et al. (2001) known as the Budyko-Zhang framework has been used. This empirical framework comes from an evaluation of 250 catchments worldwide including dryland regions (Zhang et al. 2001). It has been applied to single catchments and specific areas until nowadays, considering different approaches as the assessing of their sensitivity to climate change (Donohue et al. 2011; Renner and Bernhofer 2012; van der Velde et al. 2013). In order to answer properly the issues raised by the effects of climate change on water resources (Sivapalan et al. 2011), the Budyko curve is recognized “as a much valuable tool to back to the basics, it means, the physical basis of catchment water balance” (Coron et al. 2015).

The degree of anthropogenic influence can be determined using two types of influence on runoff change: human activity with direct influence (soil conservation, water control works, increasing water demand) and human activity with indirect influence (land use and land cover changes) (Wang et al. 2013). They constitute descriptive elements to understand the behavior of hydroclimatic data series at interannual scale and to identify the catchments presenting a low level of anthropogenization. This selection can be performed through an analysis of water balance disparity by catchment via the Budyko-Zhang framework, which assumes that catchments do not present changes in basin water storage over long-term averages (≥ 10 years) (Zhang et al. 2001). This steady-state assumption is related to a closed land water balance, which is expected to maintain over catchments with a low water balance disparity.

This study aims at explaining the hydroclimatic behavior of the Pd catchments as a benchmark for understanding the

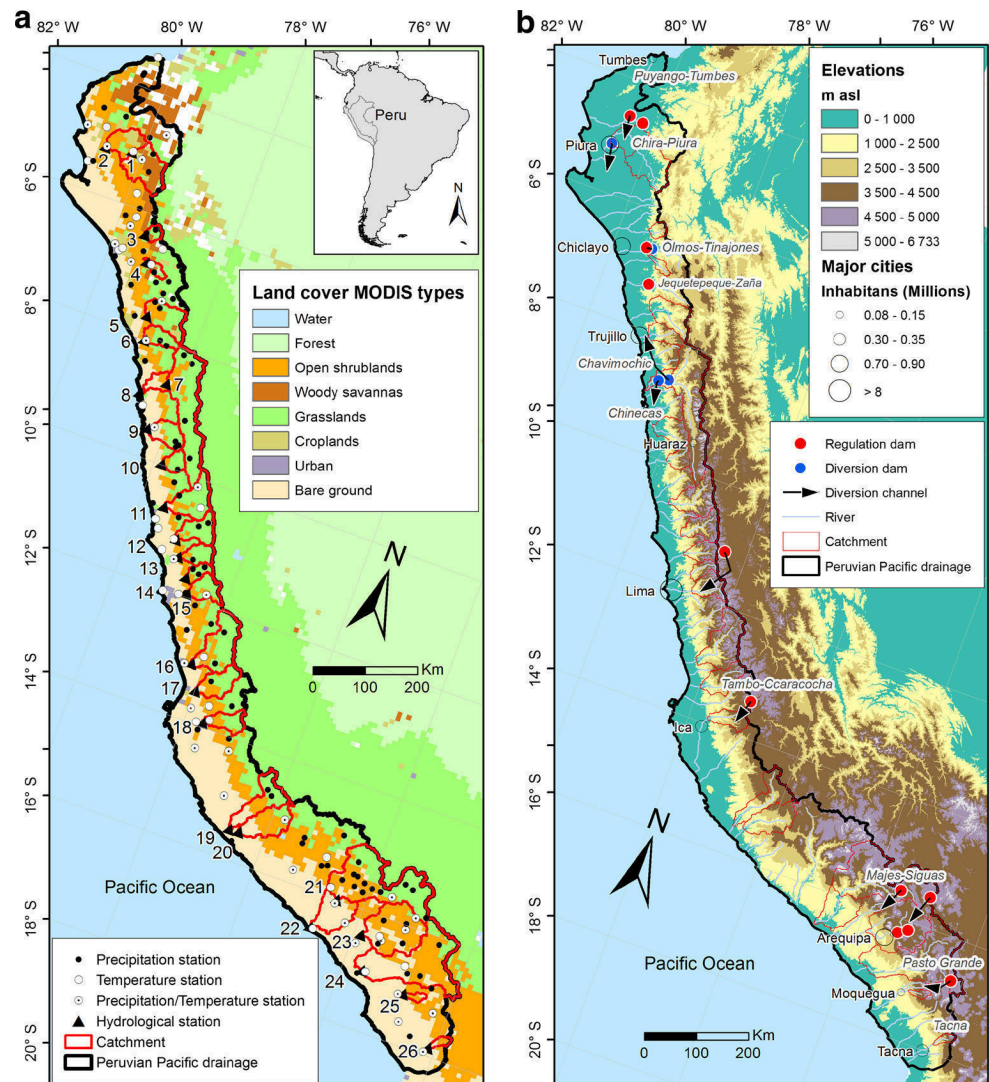
sensitivity of catchments to changes in water balance along this region having a large latitudinal extent with a steep topography in the longitudinal direction. Firstly, a hydroclimatic complete description of the Pd is achieved based on the available time series of precipitation, temperature, evapotranspiration, and streamflow. Then, the Budyko-Zhang framework was applied to this dataset in order to identify catchments with a low (high) water balance disparity, which are associated with environments with less (more) climatic and human activity influence. Lastly, the use of Budyko space is considered for assessing the level of adaptation and sensitivity to climate variability and land use change.

2 Study area

The study area comprises the Peruvian Pacific drainage region (Pd) that covers an area of $\sim 280,500$ km². This area is characterized by a significant altitudinal gradient ranging from 0 to ~ 6500 m asl and includes 54 main river catchments covering nearly 90% of this region. The rivers generally flow from east to west from the Andes toward the Pacific Ocean (see Fig. 1) with bare and steep slopes from 4 to 9% within small and medium catchment areas from 500 to 16,000 km² (see values in Table 1) that favor significant rising, flooding, and erosion during huge rainfall episodes. This region presents a large range of climate types from arid-tropical to tundra climate which results in altitudinal and latitudinal gradients in the climate conditions. While near the coast, dry climate conditions are heavily constrained by oceanic conditions that are characterized by a permanent upwelling south of $\sim 5^\circ$ S, the highlands experience more the influence from seasonal variations in the large-scale circulation patterns (i.e., Intertropical Convergence Zone, ITCZ) and the Southern Pacific Anticyclone (SPA). Also, at interannual timescale, anomalous rainfall events over the Pd are related to the El Niño Southern Oscillation (ENSO) (Rau et al. 2016).

The region under consideration concentrates more than 50% of the Peruvian population. Therefore, all catchments of Pd are characterized by recurrent conflicts about the water allocation between water uses located in arid lowlands ever since this region only benefits from 2% of the available freshwater in Peru. Water supply for human activities and consumption is about 80% of the national total and agriculture represents the greatest demand, which is based entirely on irrigation infrastructure systems because of little rainfall over arid lands (ANA 2012). This hydraulic infrastructure was built along main catchments since the beginning of the 1970s. This development implies the presence of ten large hydraulic systems with irrigation purposes (see their location and names in gray italic in Fig. 1b) and two systems mainly used for population

Fig. 1 Location of the 26 studied catchments over the Peruvian Pacific drainage region: **a** location of hydrometeorological stations considered and land cover derived from MODIS data in 2008; **b** location of major cities and main large hydraulic infrastructures (names of hydraulic systems in italic gray) built between 1970 and 2008, and topography from SRTM digital elevation model



supply and hydroelectricity purposes for the major cities of Lima and Arequipa. Figure 1b shows the large hydraulic infrastructure predominant in the studied period, where one system can present only lake intakes and diversions (not shown for a reason of scale) as in the case of “Tacna” located around latitude 17.5° S, present diversion channels only as in the case of “Chavimochic” and “Chinecas” located around latitude 9° S, present two mega-reservoirs of 1000 and 250 Hm³ capacity as in the case of “Chira-Piura” located around latitude 5° S, and present only one mega-reservoir as the general case of around 300 Hm³ capacity. These mega-reservoirs are located in highlands and midlands, and diversion channels are responsible in many cases of huge water transfer from the Atlantic to the Pacific drainage basins (see Fig. 1b for the cities of Lima and Ica). However, in some cases, this infrastructure has an influence restricted to areas located downstream of the hydrological stations and does not have relevant impacts over the water balance upstream of these stations.

3 Data

3.1 Hydroclimatic dataset and validation

The database covers the 1970–2008 period and includes monthly precipitation, temperature, and streamflow observations. Precipitation series were obtained from 139 pluviometric stations, temperature series from 59 meteorological stations, and monthly streamflow from 35 hydrological stations (see Fig. 1a) managed by the SENAMHI (National Meteorological and Hydrological Service of Peru).

A careful quality check of these data was performed as follows: monthly precipitation data were previously homogenized and validated in this region (see Bourrel et al. 2015 and Rau et al. 2016 for details about the processing). Mean monthly temperature data were homogenized and validated following Lavado et al. (2013). Missing values were filled by monthly average and by a multiple correlation method based on nearby geographical station data. Monthly streamflow data were

Table 1 General characteristics of the 26 studied catchments at their outlets gauging stations for the 1970–2008 period

No.	Catchment	Gauging station	Lat °S	Long °W	A (km ²)	Min alt (m asl)	Max alt (m asl)	S (%)	Q (m ³ /s)	Qsp (l/s/km ²)
1	Piura up	Pte. Ñacara	5.11	80.17	4762	119	3526	5.7	27.4	5.7
2	Piura	Pte. Sanchez Cerro	5.18	80.62	7622	23	3547	3.6	51.3	6.7
3	La Leche	Puchaca	6.38	79.47	771	355	3982	9.3	6.1	7.9
4	Zaña	Batan	6.8	79.29	664	260	3799	7.9	7.7	11.6
5	Chicama	Salinar	7.67	78.97	3684	350	4217	8.5	24.7	6.7
6	Moche	Quirihuac	8.08	78.87	1883	200	4238	9.2	8.1	4.3
7	Santa up	Condorcerro	8.65	78.25	1041	450	6567	8.1	142.2	13.7
8	Santa	Pte. Carretera	8.97	78.63	1166	18	6567	7.7	200.1	17.2
9	Casma	Sector Tutuma	9.48	78.3	2567	71	4769	9.1	6.1	2.4
10	Huarmey	Puente Huamba	9.97	77.87	1329	555	4742	8.3	5.4	4.0
11	Pativilca	Yanapampa	10.67	77.58	4196	800	5941	8.4	41.6	9.9
12	Huaura	Sayan	11.12	77.18	2893	650	5348	7.0	28.1	9.7
13	Ch. Huaral	Santo Domingo	11.38	77.05	1856	697	5122	7.7	17.8	9.6
14	Chillon	Larancocha	11.68	76.8	1207	1200	5099	8.6	6.3	5.2
15	Rimac	Chosica	11.93	76.69	2352	906	5370	7.2	31.5	13.4
16	Cañete	Socsi	13.03	76.2	5845	330	5632	6.7	54.5	9.3
17	San Juan	Conta	13.45	75.98	3057	350	5049	6.9	11.5	3.8
18	Ica	La Achirana	13.97	75.68	2119	500	4591	5.7	7.2	3.4
19	Acari	Bella Union	15.48	74.63	4242	70	4620	6.1	12.4	2.9
20	Yauca	Puente Jaqui	15.48	74.45	4140	214	4923	6.8	9.7	2.3
21	Majes	Huatiapa	16.0	72.47	13,414	699	6300	5.4	85.5	6.4
22	Camana	Pte. Camana	16.6	72.73	16,238	122	6300	5.4	70.7	4.4
23	Chili	Puente del diablo	16.42	71.87	8393	2360	5954	4.3	13.3	1.6
24	Tambo	Chucarapi	16.99	71.64	13,063	281	5554	5.0	33.9	2.6
25	Moquegua	Chivaya	17.13	70.83	469	2000	5279	5.8	1.0	2.0
26	Caplina	Aguas Calientes	17.85	70.12	548	130	5522	7.7	0.8	1.5

Lat: latitude; *Long*: longitude; *A*: drainage area; *Min alt*: minimum altitude; *Max alt*: maximum altitude; *S*: mean slope; mean annual values of *Q*: streamflow; *Qsp*: specific runoff

homogenized and validated considering the approaches of regionalization between neighboring catchments (Lavado et al. 2012). Missing values (less than 5% of total) were filled by monthly average.

Precipitation and temperature data were interpolated to a 5×5 -km grid using the inverse distance weighting technique. Orographic effects on precipitation and temperature were accounted for using the SRTM digital elevation model in a similar way as described in Ruelland et al. (2014). These effects on precipitation were considered using the approach proposed by Valéry et al. (2010) with a correction factor of $4 \times 10^{-4} \text{ m}^{-1}$ (estimated from the observed data), which corresponds to a 20% increase in local precipitation with an elevation of 500 m. Temperature was interpolated by accounting for a constant lapse rate of $-6.5 \text{ }^{\circ}\text{C/km}$ (estimated from the observed

data). Finally, since the only data available for calculating potential evapotranspiration (PET) were temperature data, a formula relying on clear monthly sky solar radiation and mean monthly air temperature was selected (Oudin et al. 2005):

$$\text{PET} = \frac{R_e}{\lambda \rho} \frac{T + K_2}{K_1} \text{ if } T + K_2 > 0$$

$$\text{PET} = 0, \text{ otherwise}$$
(1)

where PET is the rate of potential evapotranspiration (mm/day), R_e is the extraterrestrial radiation ($\text{MJ/m}^2/\text{day}$), λ is the latent heat flux (2.45 MJ/kg), ρ is the density of water (kg/m^3), T is the mean daily air temperature ($^{\circ}\text{C}$), and K_1 and K_2 are fitted parameters (for a general case: $K_1 \sim 100$ and $K_2 \sim 5$).

Equation 1 was applied at monthly time step. The Oudin formula is a temperature-based evapotranspiration model, which is adapted to arid and semiarid regions limited by scarcity of in situ climate data (see, e.g., Hublart et al. 2015, 2016). Indeed, Oudin et al. (2005) showed that from an operational point of view, this model is as efficient as more complex models such as the Penman model and its variants.

Finally, we restricted our analysis to 26 catchments (see Fig. 1a) characterized by a valuable and confident complete dataset of monthly precipitation, temperature, and streamflow series over 1970–2008.

3.2 Land cover data and digital elevation model

Four land cover maps based on remotely sensed images acquired between 1984 and 2008 were used in this study. They are based on multispectral images from different sensors with a spatial resolution increasing against time. The LBA (Large Scale Biosphere-Atmosphere Experiment in Amazonia) Regional Land Cover products for 1984 (DeFries et al. 1998; 8×8 km grid) and 1992/1993 (Hansen et al. 2000; 1×1 km grid) were derived from acquisitions from the Advanced Very High Resolution Radiometer (AVHRR) for comparative purposes. The land covers of 2001 and 2008 were derived from acquisitions from the Moderate Resolution Imaging Spectroradiometer (MODIS). These products, made available by the Global Land Cover Facility (GLCF, <http://glcf.umd.edu/data/lc>) on 10×10 km grid, have a spatial resolution of $5'$. The land cover map used in Fig. 1a is the MODIS land cover type for 2008. They show that the Pd region is characterized mainly by four types of land cover: bare ground, open shrublands, grasslands, and croplands. These different types of vegetation are directly related to the different climates observed in the Pd region.

The digital elevation model shown in Fig. 1b was obtained from the 90×90 -m grid SRTM data (Shuttle Radar Topography Mission, NASA-NGA, USA available from <http://srtm.csi.cgiar.org>). It allowed the orographic corrections to be applied for the climate forcing interpolation (see Section 3.1) and the 26 main river catchments located in the Pd to be delineated (catchment numbering and parameters are shown in Table 1).

4 Methods

The methodology consists of three steps:

- (a) Evaluation of hydroclimatic time series
- (b) Evaluation of the catchment water balance disparity via the Budyko-Zhang framework. Selection of catchments with low disparity

- (c) Analysis of the hydroclimatic change disparity of selected catchments using trajectories in Budyko space

4.1 Evaluation of hydroclimatic time series

After compiling all datasets by catchment, complementary analyses were performed for detecting plausible trends and changes using the nonparametric Mann-Kendall trend test, the double mass curve method, and the Pettitt test.

The rank-based Mann-Kendall test (Mann 1945; Kendall 1975) was used to detect trends in the hydroclimatic series. The method is recommended by the World Meteorological Organization (WMO) and widely used for assessing the significance of monotonic trends in hydrological series. This method does not infer any distributional function for the data and has already proven its efficiency (e.g., Lavado et al. 2012; Chen et al. 2013; Wang et al. 2013). The double mass curve consists of the plot of the accumulated values of one variable versus the accumulated values of another related variable for the same period (Searcy and Hardison 1960). The plot is a straight line if the two variables are proportional, and the slope of this line represents the ratio between the two variables. A change in the gradient of the curve indicates that the original relationship between variables was modified. It can be used to check the consistency of hydrological records and has recently become an effective tool for detecting the changes of hydrological regime due to anthropogenic disturbances (e.g., Zhang and Lu 2009; Wang et al. 2013). In this study, a double mass curve between precipitation and runoff was employed as an auxiliary confirmation of the change points when catchment changes mainly induced by human activities exert influences on the river.

The Pettitt test (Pettitt 1979) is a nonparametric approach to determine the occurrence of a change point. This approach is a rank-based and distribution-free test for detecting a significant change in the mean of a time series when the exact time of the change is unknown. Pettitt test has been widely used to detect changes in the hydroclimatic records (e.g., Lavado et al. 2012; Wang et al. 2013). We used the Pettitt test to identify the change point of the runoff series and compare with the change points detected by double mass curve.

4.2 Catchment water balance disparity

The water balance for a catchment can be basically described in a general form at annual scale as:

$$P = \text{AET} + R + \Delta S \quad (2)$$

where P is precipitation (mm/year), AET is the actual evapotranspiration (mm/year), R is runoff (mm/year), and ΔS is the change in basin water storage (mm/year). At the annual scale,

ΔS can be neglected especially for long periods (≥ 10 years) (Zhang et al. 2001).

Based on the Budyko theory (Budyko 1974) which considers that the available energy and water are the primary factors for determining the rate of actual evapotranspiration, we used here the approach developed by Zhang et al. (2001). It was called the Budyko-Zhang curve, which estimates the AET based on a simple model (see Eq. 3) that is written as follows:

$$\frac{\text{AET}}{P} = \frac{1 + w \left(\frac{\text{PET}}{P} \right)}{1 + w \left(\frac{\text{PET}}{P} \right) + \frac{P}{\text{PET}}} \quad (3)$$

where PET (mm/year) is the potential evapotranspiration and w (nondimensional) is the plant-available water coefficient related to vegetation type. The details of the relationship can be found in Zhang et al. (2001). The very sensitive parameter w is calibrated over the long-term interannual AET from Eq. 3. The use of the Budyko-Zhang curve over the Pd appears as a valuable method for the interpretation of the water balance considering the importance of vegetation (Donohue et al. 2007) over arid and semiarid areas. It has been used previously in comparable studies such as Yang et al. (2009), Zhao et al. (2013), and Chen et al. (2013).

Low disparity of a water balance was evaluated in terms of three criteria: (a) the shape of the association of points between dryness index (PET/P) and evaporative index (AET/P), which must follow a Budyko-Zhang curve with a positive value of w ; (b) the correlation coefficient r between the AET estimated using the Budyko-Zhang framework and estimated using the water balance ($P-R$) which must be higher than 0.7; and (c) the relative standard error (%RSE) from the curve adjustment which should be less than 15%. Any catchment outside these three criteria falls off the Budyko curve and is considered as a catchment with a high water balance disparity. According to Wang and Hejazi (2011), Jones et al. (2012), and Coron et al. (2015), such a catchment is interpreted as being strongly influenced by anthropogenization, a catchment under strong climatic variability conditions especially droughts, a catchment with other missing components of water balance (such as water demands, groundwater flow alteration), or in the worst case, a catchment where there were inadequate measures of the hydroclimatic variables.

4.3 Hydroclimatic change disparity

Based on Jones et al. (2012), under stationary conditions or natural climatic oscillations, catchments should fall on the Budyko curve. Under nonstationary conditions or anthropogenic climate change, catchments are likely to deviate from

the Budyko curve in a predictable manner. Over these conditions and following van der Velde et al. (2013) and Jaramillo and Destouni (2014), the trajectories in Budyko space were defined, which are characterized by a direction (α) and magnitude (β) of change over the considered period. The direction of change is calculated from the equation:

$$\alpha = \arctan \left[\frac{\Delta \text{AET} \cdot (P) - (\text{AET}) \cdot \Delta P}{\Delta \text{PET} \cdot (P) - (\text{PET}) \cdot \Delta P} \right] \quad (4)$$

where AET (mm/year) is the average AET over the period, and ΔAET (mm/year²) is the change of AET over the period. Also, PET (mm/year), ΔPET (mm/year²), P (mm/year), and ΔP (mm/year²) are the average PET and change of PET over the period, the average P , and change of P over the period, respectively. Here, α is calculated in degrees and counter-clockwise from the negative y -axis. In the same way, the magnitude of change is expressed as the following equation and expressed in 1/year.

$$\beta = \sqrt{\left(\frac{\Delta \text{AET} \cdot (P) - (\text{AET}) \cdot \Delta P}{(P)^2} \right)^2 + \left(\frac{\Delta \text{PET} \cdot (P) - (\text{PET}) \cdot \Delta P}{(P)^2} \right)^2} \quad (5)$$

Direction is related to change adaptations of ecosystems and magnitude related to ecosystem sensitivity to climate variability and land use change.

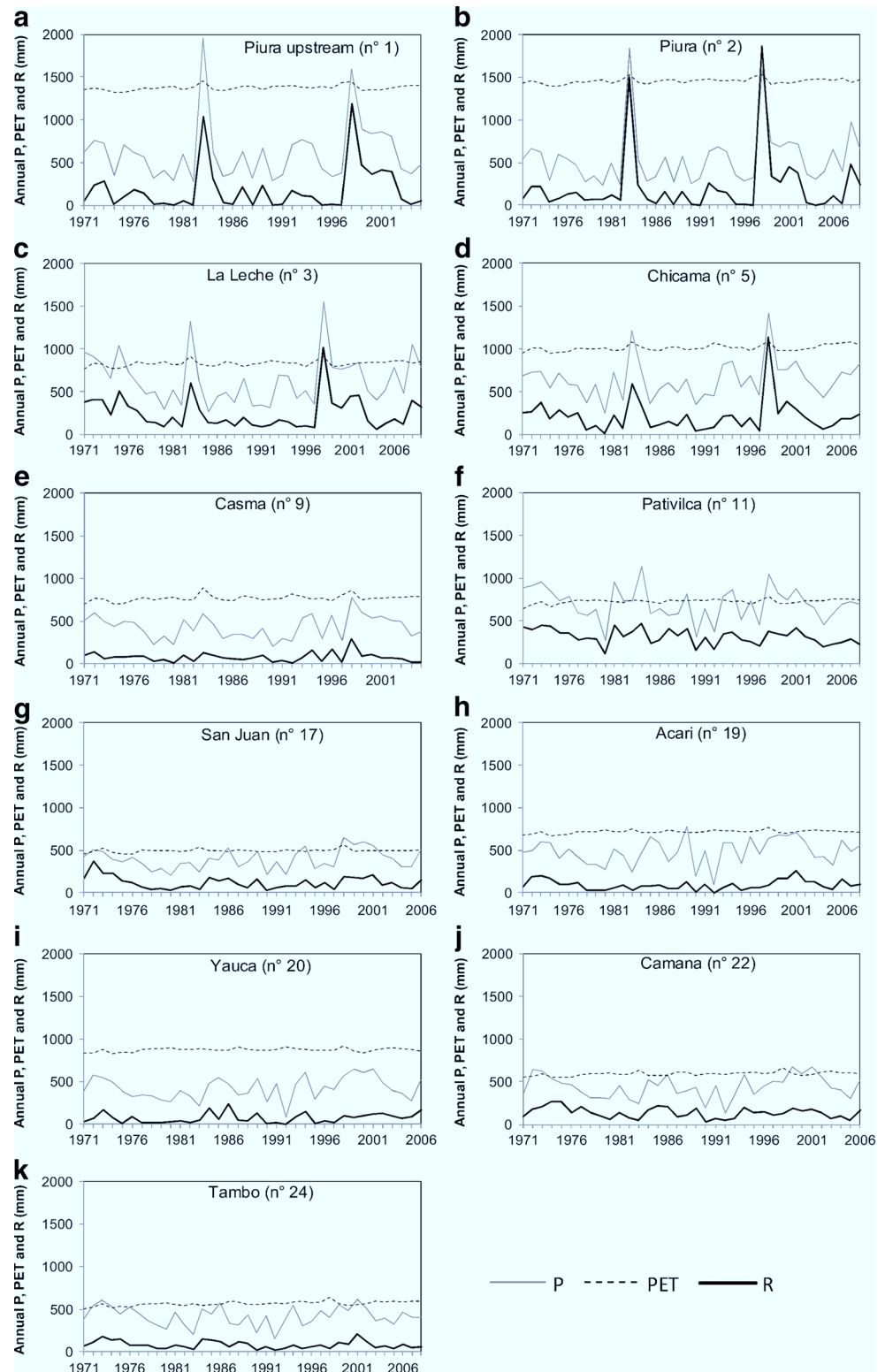
5 Results and discussion

5.1 Hydroclimatic time series

Based on the processing of the original monthly time step database, a complete monthly hydroclimatic dataset of precipitation (P), temperature (T), potential evapotranspiration (PET), and streamflow (Q), over the 1970–2008 period, was computed, for each of the 26 catchments in a lumped way. The series of annual PET, annual runoff (R) by the ratio between Q and catchment area, and annual actual evapotranspiration (AET) by water balance ($P-R$) following the hydrological year (September–August) were determined. Observed annual P , estimated PET, and R series from 11 catchments (mostly covering the 1970–2008 period) are presented for displaying purposes in Fig. 2 (the choice of these 11 catchments among the whole of our 26 studied catchments is discussed in Section 5.2).

Mean annual values of hydroclimatic series are given in Table 2. For mean annual precipitation, catchments located in northern areas generally present higher values above 600 mm/year than southern areas with values under around 400 mm/year. This is because of the influence of the ENSO phenomenon over northern catchments that clearly appears in

Fig. 2 a–k Long-term variations of annual mean time series of precipitation (P), potential evapotranspiration (PET), and runoff (R) for 11 selected catchments over the 1970–2008 period



peaks during 1982/1983 and 1997/1998 events known as years of extreme El Niño events (see Fig. 2a–d). This influence is also present in the runoff variability, decreasing toward southern latitudes in general, but showing high values above

400 mm/year in catchments located at central areas such as Santa upstream (no. 7), Santa (no. 8), and Rimac (no. 15), associated with the relationship of water availability and catchment size. For mean annual temperature, PET, and

Table 2 Hydroclimatic conditions over the 1970–2008 period and 2008 land cover types in the 26 studied catchments. Mean annual values of precipitation (P), temperature (T), potential evapotranspiration (PET), actual evapotranspiration (AET), runoff (R), and aridity index (P/PET). Land cover percentage from MODIS (2008) of open shrubland (OS), grasslands (GL), croplands (CL), and bare ground (BG)

No.	Catchment	Gauging station	P (mm/year)	T (°C/year)	PET (mm/year)	AET (mm/year)	R (mm/year)	P/PET	OS (%)	GL (%)	CL (%)	BG (%)
1	Piura up	Pte. Ñacara	613	20	1376	432	181	0.45	27	11	13	0
2	Piura	Pte. Sanchez Cerro	551	22	1456	355	212	0.38	34	12	20	0
3	La Leche	Puchaca	640	10	831	391	249	0.77	0	75	0	0
4	Zaña	Batan	817	12	933	450	367	0.88	0	50	12	0
5	Chicama	Salinar	643	14	1013	432	211	0.63	23	69	4	2
6	Moche	Quirihuac	645	8	703	509	136	0.92	26	74	0	0
7	Santa up	Condorcerro	936	2	400	505	431	2.34	13	86	0	1
8	Santa	Pte. Carretera	854	3	473	381	541	1.80	17	76	0	7
9	Casma	Sector Tutuma	430	9	769	354	75	0.56	10	63	0	27
10	Huarmey	Puente Huamba	580	6	576	453	127	1.01	14	86	0	0
11	Pativilca	Yanapampa	700	8	728	387	313	0.96	14	82	0	4
12	Huaura	Sayan	654	3	444	348	307	1.47	9	91	0	0
13	Ch. Huaral	Santo Domingo	579	1	341	286	303	1.70	9	91	0	0
14	Chillon	Larancocha	555	2	370	390	165	1.50	23	77	0	0
15	Rimac	Chosica	646	3	436	224	422	1.48	19	81	0	0
16	Cañete	Socsi	556	1	339	261	294	1.64	20	74	0	6
17	San Juan	Conta	393	4	496	274	119	0.79	32	63	0	5
18	Ica	La Achirana	432	5	554	325	107	0.78	38	58	0	4
19	Acari	Bella Union	486	8	715	394	92	0.68	23	51	0	26
20	Yauca	Puente Jaqui	422	11	873	348	74	0.48	50	25	0	25
21	Majes	Huatiapa	537	3	430	336	201	1.25	35	59	0	6
22	Camana	Pte. Camana	441	6	593	303	137	0.74	28	47	1	24
23	Chili	Pte. del diablo	370	5	556	320	50	0.67	73	3	0	22
24	Tambo	Chucarapi	418	6	566	336	82	0.74	50	12	0	38
25	Moquegua	Chivaya	369	3	437	305	64	0.84	57	0	0	43
26	Caplina	Aguas Calientes	343	2	416	294	49	0.83	60	0	0	40

AET, they decrease in general toward southern latitudes. Mean annual PET variability follows the same behavior of the mean annual temperature variability along the Pd because of the empirical nature of the Oudin method. However, there is a slight increase over arid catchment located in the south where there is a predominance of bare ground and open shrubland areas.

It is worth to mention that dryland regions encompass hyperarid, arid, semiarid, and dry subhumid areas (Brouwer and Heibloem 1986; Mortimore 2009), and these results corroborate the dryland conditions of the Pd, accentuating toward southern latitudes. This can be explained by the range of the aridity index (P/PET) proposed by Hassan and Dregne (1997) and contrasted with the annual precipitation module, a method recommended by the United Nations Environment Program (UNEP). Table 2 provides the values of the aridity index in most of the catchments below “1” and precipitation below 1000 mm in all catchments. Southern catchments present

an annual precipitation around below 400 mm and are defined as arid areas. Catchments located in major rainy areas (Santa up (no. 7), Santa (no. 8), Huarmey (no. 10), Huaura (no. 12), Chancay Huaral (no. 13), Chillon (no. 14), Rimac (no. 15), Cañete (no. 16), and Majes (no. 21)) are found in the limits between semiarid and dry subhumid areas. The rest of the catchments are defined as semi-arid areas.

Changes in hydroclimatic series are presented in Table 3. An increase or a decrease (i.e., positive or negative sign, respectively) indicates the long-term behavior of the series. All slopes are significant at the 95% level using Student’s t test; however, for highlighting the long-term effect of these hydroclimatic series over catchments, the trends and their significance (at the 95% of confidence level) were estimated based on the Mann-Kendall test (significant trends are shown in bold in Table 3).

On the one hand, changes in runoff and precipitation are greater in northern catchments (mainly positive changes) and

decrease toward southern latitudes. On the other hand, changes in T and PET are always positive (see Table 3). This can be explained by regional climate anomalous conditions along the Pd, in particular the well-known ENSO influence over precipitation and runoff in the northern areas (Lavado et al. 2012; Bourrel et al. 2015; Rau et al. 2016). Trend tests indicate that a long-term increase in temperature time series is significant in all catchments with a mean value of $+0.02\text{ }^{\circ}\text{C}/\text{year}^2$ (~a mean warming of $0.2\text{ }^{\circ}\text{C}$ per decade). There is an area covering Moche (no. 6) and Santa up (no. 7) catchments with a mean warming above of $0.3\text{ }^{\circ}\text{C}$ per decade. This is consistent with previous climatological studies for the Andes such as the one by Vuille et al. (2015) that showed that most stations over the Pd had a significant positive trend in total temperature with a mean warming above of $0.2\text{ }^{\circ}\text{C}$ per decade. They suggested that at inland and higher elevation locations, there is a clear evidence of warming, and in coastal regions, there is still a

regional climate influence due to the variability of the Pacific Decadal Oscillation (PDO) and of the intensity of the South Pacific Anticyclone (SPA). Our results support the interpretation of warming at basin scale (i.e., the influence of either global warming or climate variability at timescales longer than the PDO) where these changes in temperature are expected to have important consequences for western Andean glaciers.

No significant increase or decrease in P was observed over the study area (except only for Piura (no. 2) catchment). The R time series present a significant increase over Ica (no. 18) which is related to water transfers from the Atlantic basin (see Fig. 1b) and over Yauca (no. 20) related with the no significant increase in PET. Runoff also presents a significant decrease over central catchments (Santa up no. 7, Pativilca no. 11, and Huaura no. 12) whose upper basins benefit from the melting of the Cordillera Blanca glacier and surroundings. At

Table 3 Mean annual change (Δ) in precipitation (P), temperature (T), potential evapotranspiration (PET), actual evapotranspiration (AET), and runoff (R). Values with significant trends at 95% of confidence level are shown in bold. Years of significant change point at 95% of confidence level are indicated between parentheses

No.	Catchment	ΔP (mm/year ²)	ΔT (°C/year ²)	ΔPET (mm/year ²)	ΔAET (mm/year ²)	ΔR (mm/year ²)	w	r	RSE (%)
1	Piura up	2.84	0.02 (1986)	1.20 (1986)	−1.36	4.20	0.25	0.85	4
2	Piura	3.95 (1997)	0.02 (1986)	0.98 (1986)	1.11	3.28	0.03	0.79	2
3	La Leche	0.18	0.02	1.10	1.07	−0.90	0.18	0.88	5
4	Zaña	5.19 (1982)	0.01	0.73	4.00 (1983)	1.19	0.00	0.67	7
5	Chicama	3.31	0.03 (1982)	1.71 (1982)	3.15 (1992)	0.16	0.32	0.83	5
6	Moche	1.46	0.06	3.11	0.61	0.85	2.59	0.85	28
7	Santa up	3.80 (1992)	0.04 (1991)	2.12 (1996)	7.28 (1992)	− 3.48	3.61	0.84	135
8	Santa	2.43	0.03	1.41	4.15 (1992)	−1.97	−0.58	0.56	33
9	Casma	1.31	0.03 (1990)	1.53 (1982)	1.44 (1992)	−0.13	1.16	0.95	8
10	Huarmey	4.77	0.03 (1982)	1.75 (1982)	2.76	2.01	3.12	0.85	40
11	Pativilca	−2.90	0.02	1.08	0.33	− 3.22 (1989)	0.02	0.91	6
12	Huaura	−2.70	0.02	1.19 (1996)	0.45	− 3.15 (1987)	0.78	0.71	32
13	Ch. Huaral	−0.33	0.03 (1996)	1.13 (1996)	2.40	−2.78	0.65	0.64	48
14	Chillon	−0.43	0.03 (1996)	1.58 (1991)	−1.45	1.02	4.08	0.81	101
15	Rimac	−1.08	0.03 (1991)	1.48 (1991)	− 2.71	1.63	−0.49	0.67	11
16	Cañete	2.80	0.01	0.30	4.24 (1996)	−1.44	0.27	0.66	35
17	San Juan	2.38	0.01	0.55	3.77 (1992)	−1.39	0.73	0.77	12
18	Ica	2.43	0.02 (1979)	0.84 (1991)	1.17	1.26 (1993)	1.20	0.92	15
19	Acari	2.70	0.01 (1977)	0.75 (1977)	2.43	0.26	1.61	0.93	14
20	Yauca	2.29	0.01	0.69	0.98	1.31	0.78	0.89	9
21	Majes	1.53	0.03 (1986)	1.34 (1986)	2.72 (1995)	−1.19	1.16	0.90	39
22	Camana	1.23	0.02 (1986)	1.13 (1986)	2.75 (1995)	−1.52	0.47	0.88	9
23	Chili	0.76	0.03 (1986)	1.68 (1986)	0.23	0.53 (1996)	2.79	0.96	29
24	Tambo	−0.60	0.03 (1986)	1.57 (1986)	0.25	−0.85	1.78	0.95	14
25	Moquegua	−1.02 (1977)	0.03 (1982)	1.47 (1982)	−0.90	−0.12	3.55	0.98	46
26	Caplina	−0.75	0.02 (1982)	0.85 (1982)	−1.12	0.37 (1996)	4.30	0.97	53

Catchments with low disparity in water balance are italicized

w : Budyko-Zhang coefficient; r : correlation coefficient between AET estimated by Budyko-Zhang and water balance; RSE : relative standard error from the curve adjustment

interannual time step, these decreases could be mainly related to the intensive water exploitation for agricultural activities. AET time series present a significant increase in Zaña (no. 4), Chicama (no. 5), Santa up (no. 7), Cañete (no. 16), San Juan (no. 17), and Camana (no. 22) and a significant decrease in Rimac (no. 15) catchment.

Occurrence of change points at 95% of confidence level detected by the Pettitt test and double mass curve methods is significant in some catchments and the year when the change point occurred is indicated between parentheses in Table 3. Most catchments did not present change points in P (except Piura (no. 2), Zaña (no. 4), Santa up (no. 7), and Moquegua (no. 25)). Change points for T time series were grouped by catchment proximity and regional localization along the Pd. For the northern catchments of Piura up (no. 1) and Piura (no. 2), the year of 1986 meant a change point. Catchments in southern latitudes present significant change points in the years 1977, 1982, and 1986. By the fact of presenting a warming on such a large scale, those change points could be related mainly by climatic influence (i.e., ENSO changes and climate shifts; see the work by Bourrel et al. 2015 for precipitation). Change points in R are mainly related to the development of new phases into the large hydraulic infrastructure as in the case of Ica (no. 18), Chili (no. 23), and Caplina (no. 26) and also with the land cover change (which is discussed in the next section) as in the case of Pativilca (no. 11) and Huaura (no. 12).

5.2 Catchment water balance disparity

Based on the hydroclimatic time series calculated over the 26 catchments, we produced and analyzed series of dryness index (PET/P) and evaporative index (AET/P). Figure 3a, c shows the dispersion of these two indices for two catchments (Piura upstream (no. 1) and Rimac (no. 15), respectively). Piura upstream shows the behavior of a northern catchment with strong climate variability as a result of ENSO influence, and Rimac shows the behavior of a very anthropized catchment as a result of large hydraulic infrastructure to provide water to the city of Lima (the capital of Peru) in the lowlands. Both catchments represent the two main types of associations found in the study area, which were differentiated following the methodology explained in Section 4.2 in terms of w and “%RSE” (i.e., see Fig. 3a, c) and r (i.e., see Fig. 3b, d).

Figure 4 shows the dispersion of indices for all the 26 catchments, highlighting the two types of association (the low and high water balance disparity). The w coefficients theoretically take values between 0.1 and 2 (Zhang et al. 2001) which are associated with the predominance of bare soils and forest, respectively (shown in Fig. 4 as constraints), even though some negative values on arid catchments were obtained by Chen et al. (2013). Our w coefficient falls in the range of -0.58 to 4.30 and the best

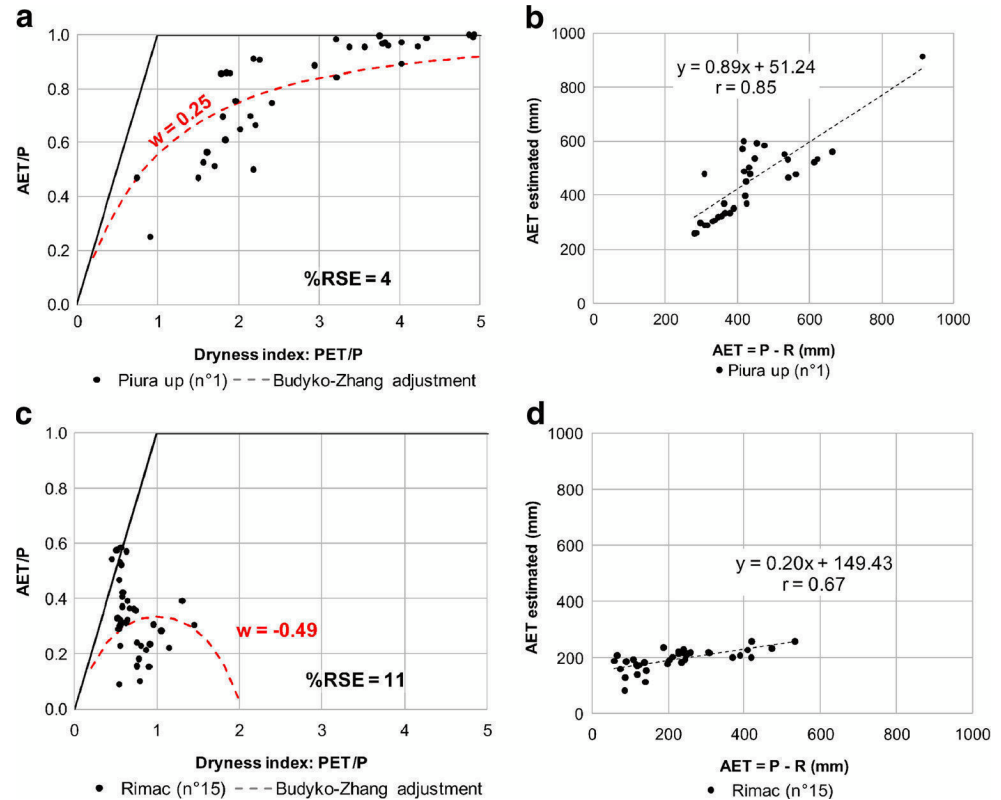
correlation coefficients r and acceptable %RSE are found with w positive values in the range of 0.02 to 1.78. That meant that only 11 catchments (italicized in Table 3) follow a “quasinatural” shape of the Budyko-Zhang curve, presenting a low disparity in water balance which can be related with low climatic and anthropogenic influence. The average of w values is around 0.7, indicating mean values for the plant-available water coefficient related to predominance of grasslands over the semiarid conditions of the Pd.

The 15 remaining catchments are represented by gray points in Fig. 4. Their AET/P values are located very near from the energy limit line (sometimes above the line) and far from the water limit line, which implies a complex combination of water losing systems (e.g., presence of open water surfaces, water lost to ground water system) with a nonnatural behavior of $P-R$ (see Eq. 2) affecting the AET calculation. Precipitation (P) time series follows a natural behavior in all those catchments without strong trends or change points, suggesting that runoff (R) has been altered. Also, those catchments are located mostly in an energy-limited environment ($PET/P < 1$) where changes in P and PET are likely more evident in R (van der Velde et al. 2013), highlighting the strong climatic influence over R in this type of environments as well as the anthropogenic influence due to the points outside the Budyko-Zhang curve.

The hypothesis about the anthropogenic effect as the main source of differentiation between catchments with high and low water balance disparity could not be easy to validate due to the difficult access or/and the scarcity of water use data. A complementary analysis of the evolution of the land cover in the study area was performed using the LBA 1984, LBA 1992/1993, MODIS 2001, and MODIS 2008 datasets (see Fig. 5). Even if improvements in resolution and data quality could impact estimates of spatial and temporal trends (from 10 to 1 km), the temporal evolution of the classes suggests that catchments with high water balance disparity presented great changes over land cover conditions of cropland from 28 to 1% (from 1984 to 1992/1993) and grassland from 39 to 63% (from 1992/1993 to 2001) as shown in Fig. 5a. These changes were not observed in catchments with low water balance disparity (excepting croplands from 39 to 7% from 1984 to 1992/1993). In addition, Fig. 5b shows the evolution of land cover over catchments grouped by latitudinal gradient and revealed that central catchments have a large change mainly in grassland cover from 40% to 75% (from 1992/1993 to 2001). It brings more confidence in northern and southern catchments, which presents certain homogeneity in the last decades.

About the influence of large hydraulic systems (see Fig. 1b), it is evident that some catchments with high disparity were influenced by those systems which transfer water from the Atlantic drainage (i.e., Rimac (no. 15) and Ica (no. 18))

Fig. 3 Comparison of two catchments with low (Piura up no. 1) and high (Rimac no. 15) water balance disparity according to the Budyko-Zhang framework. **a, c** Black lines represent the energy limit (diagonal) and the water limit (horizontal). **b, d** Scatter plot for correlation of annual AET obtained from water balance Eq. 2 and AET estimated by using Eq. 3



and by those which present large intakes and regulations for water supply in lower lands (Santa (no. 8), Majes (no. 21), and Chili (no. 23)). Also, there are some catchments with low water balance disparity that would still keep anthropogenic

effects according to Fig. 1b (see Piura (no. 2) and Camana (no. 22)); however, those effects were not noticeable in terms of the annual water balance disparity. Finally, the methodology made possible the separation of catchments with low and high water balance disparity related to low and high climatic and anthropogenic influence, respectively. Further research is needed to separate these two types of influences in the region.

5.3 Hydroclimatic change disparity

According to Fig. 4, most catchments move closer to the theoretical water and energy limits. Following the premise that 11 selected catchments have a “quasinatural” behavior with less anthropogenic and climatic influence, it is expected that these catchments move in all directions through Budyko space. The direction and magnitude of change is presented in Fig. 6a, b, respectively, where most of the years in all catchments are characterized by energy (i.e., $PET/P < 1$) and water limitations (i.e., $PET/P > 1$). Direction and magnitude values are provided in Table 4.

Figure 6a indicates two types of change adaptations represented mostly with green and red points in one group (i.e., toward more energy-limited environments to the left) and yellow and orange points in the other (i.e., toward more water-limited environments to the right). Red and green points tend to be an energy-limited environment ($PET/P < 1$) and those catchments are plotted in Fig. 7a. According to Table 3, these

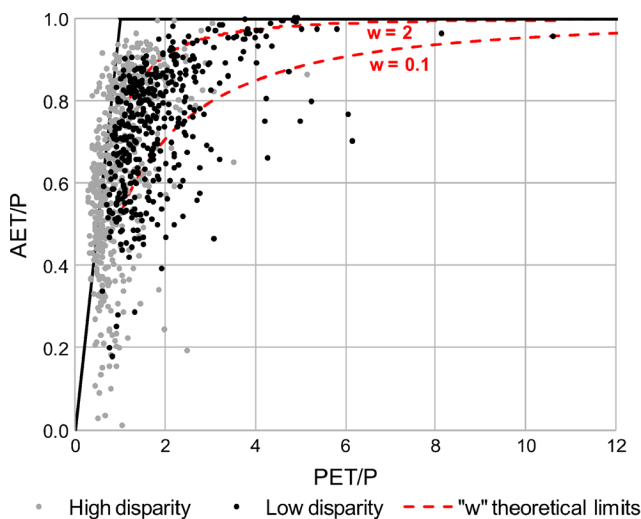


Fig. 4 Budyko space over the 1970–2008 period over the 26 studied catchments. The black lines represent the energy limit (horizontal) and the water limit (diagonal). Black (gray) points represent the association of yearly values from catchments showing a low (high) water balance disparity via the Budyko-Zhang framework. Red dashed curves represent the theoretical adjustment range for w parameter ($w_{min} = 0.1$; $w_{max} = 2$)

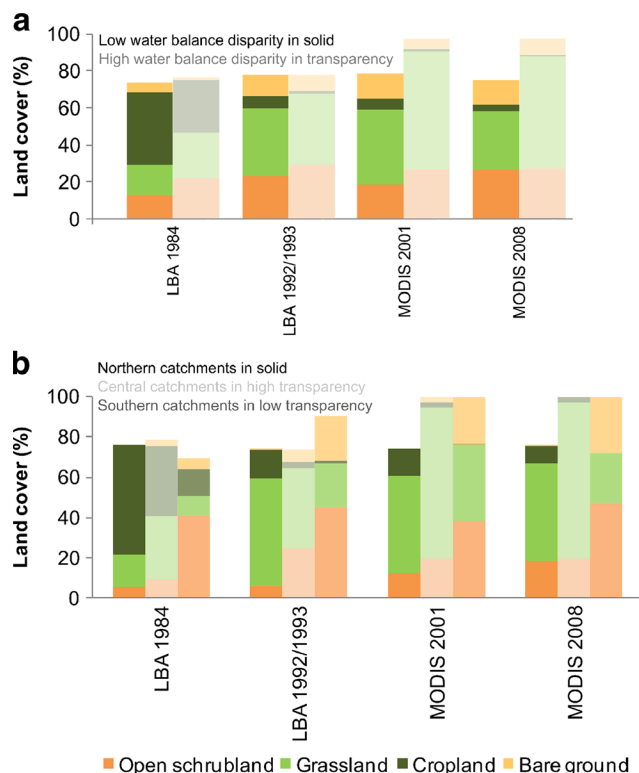


Fig. 5 Evolution of land cover (%) with LBA and MODIS products over catchments grouped by **a** low and high water balance disparity. **b** Latitudinal gradient: northern catchments (no. 1 to no. 6), central catchments (no. 7 to no. 18), and southern catchments (no. 19 to no. 26)

catchments present a decrease in runoff, which can be explained by the increase of both T and PET and the nonalteration in precipitation, concluding that those catchments have already the tendency to become less energy limited. The yellow and orange point groups present high values of PET/ P representing strong variability of runoff and precipitation, corresponding to catchments with strong climatic influence such as the ENSO and semiarid conditions.

Figure 6b shows two types of catchment sensitivity to climate variability (i.e., likely with high sensitivity to future

climate) and land use changes, represented mostly with orange and yellow points in one group (i.e., toward more energy-limited environments to the left) and red and purple points in the other (i.e., toward more water-limited environments to the right). A large change in magnitude means that climate- or human-induced changes were particularly large in this region and that any direction from Fig. 7a having a very small magnitude (see values in Table 4) can be considered as of little relevance (van der Velde et al. 2013). The orange and yellow point group has a low magnitude of change corresponding to catchments with low variability on precipitation and runoff. The red and purple point group coincides with catchments presenting significant variability in both precipitation and runoff. Figure 7b shows the magnitude of change of the 11 selected catchments, and Table 4 shows (italicized) the six catchments identified as having major sensitivity.

They can be described in the light of Table 3 as follows: purple points represent the catchments of Piura (no. 2) and Yauca (no. 20), which are located mostly in a water-limited environment ($PET/P > 1$) and where an increase in P is likely to increase the assessment of AET through the Budyko equation (increase in PET due to increase in T over the studied period has the opposite effect). As our results indicate that there is an increase in the AET in both cases with a significant increase in P for Piura (no. 2) and a significant increase in R for Yauca (no. 20), we conclude that an increase in precipitation is more likely to drive these ecosystem changes than the increase in temperature (i.e., increase in PET). Red points represent the catchments of Piura up (no. 1), Chicama (no. 5), San Juan (no. 17), and Acari (no. 19) which are located mostly in a water-limited environment. However, Piura up (no. 1) presents a decrease in AET, suggesting that both precipitation and temperature (i.e., increase in PET) drive these ecosystem changes. San Juan (no. 17) presents a decrease in R , and because of its location in both water- and energy-limited environment, it suggests that both precipitation and temperature (i.e., increase in PET) drive these ecosystem changes. The remaining catchments, Chicama (no. 5) and

Fig. 6 Grouping of Budyko trajectories defined by their direction (**a**) and the magnitude (**b**) of change for the 11 selected catchments in the Budyko space over the 1970–2008 period

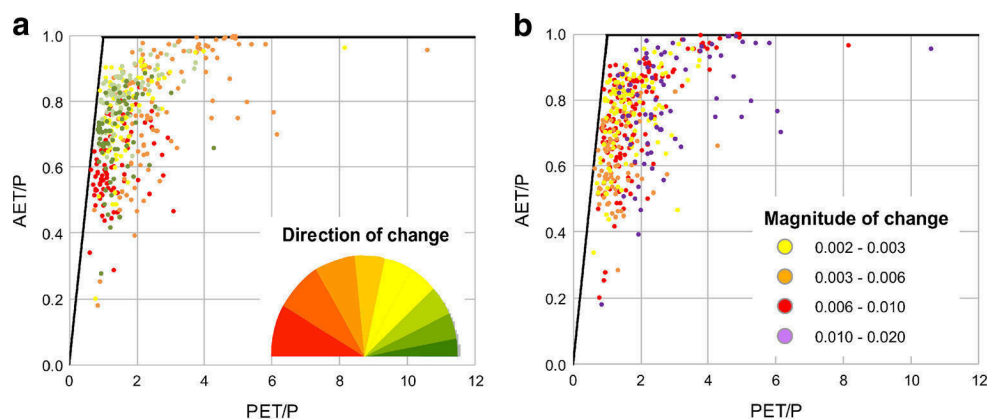


Fig. 7 Budyko trajectories defined by their direction (**a**) and magnitude (**b**) plotted across catchments. Red/orange, yellow, and green arrows in **a** show the three regions grouped by their hydroclimatic change adaptation. Purple and red points in **b** show the catchments with major sensitivity to climate variability and land use changes

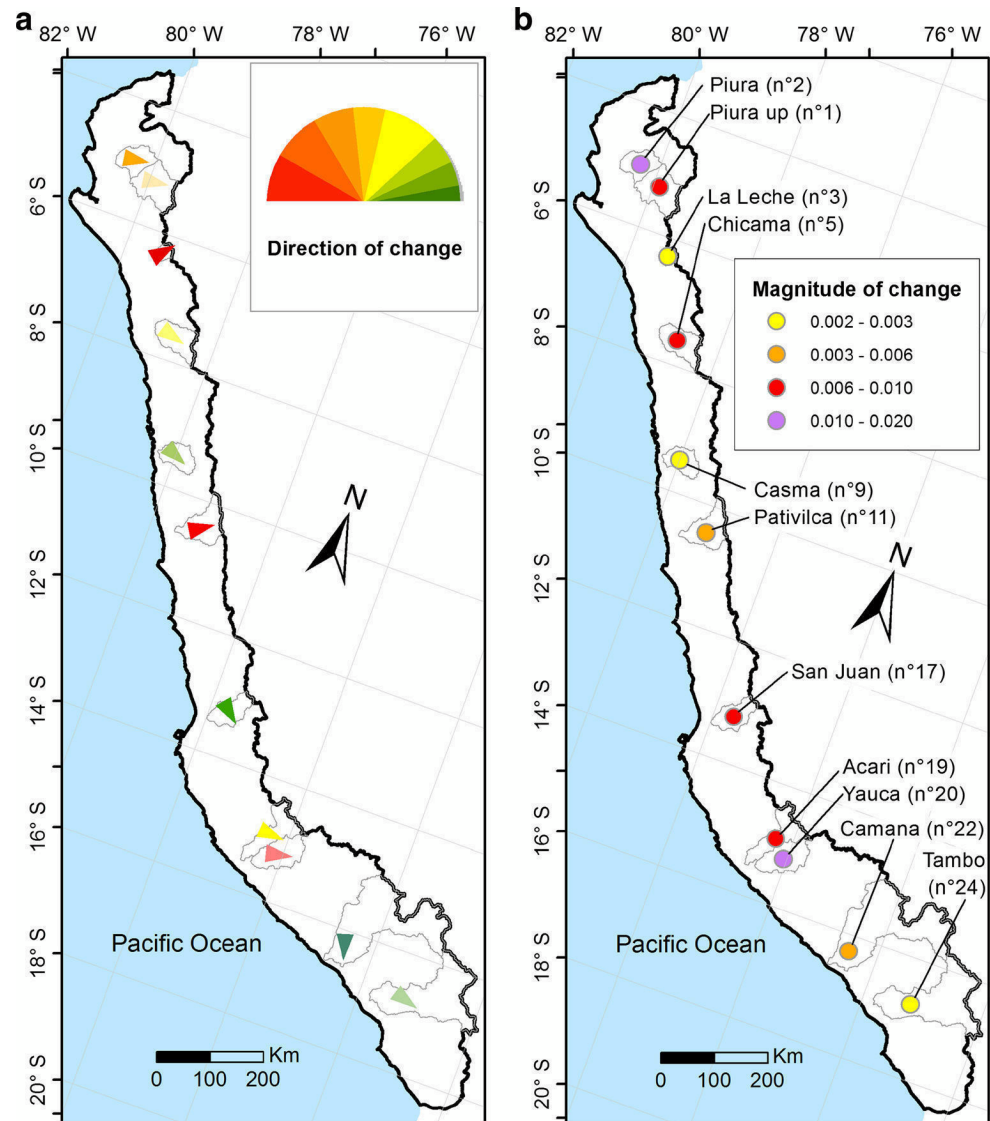


Table 4 Budyko trajectories defined by direction (α) and magnitude (β) values across the selected catchments. Catchments with major sensitivity to climate variability and land use changes are italicized. Errors expressed in (%) were obtained via a 10-year moving window

No.	Catchment	α (deg)	β (1/year)
1	<i>Piura up</i>	97 (2%)	0.009 (30%)
2	<i>Piura</i>	99 (1%)	0.017 (32%)
3	La Leche	138 (1%)	0.002 (15%)
5	<i>Chicama</i>	75 (6%)	0.006 (25%)
9	Casma	67 (13%)	0.002 (46%)
11	Pativilca	124 (3%)	0.003 (13%)
17	<i>San Juan</i>	49 (9%)	0.008 (22%)
19	<i>Acari</i>	86 (3%)	0.007 (25%)
20	<i>Yauca</i>	103 (2%)	0.010 (27%)
22	Camana	16 (32%)	0.004 (16%)
24	Tambo	73 (3%)	0.002 (2%)

Acari (no. 19), suggest that an increase in precipitation is more likely to drive these ecosystem changes than the increase in temperature.

Piura upstream (no. 1) and Piura (no. 2) catchments exhibit a large increase in precipitation and runoff changes, and Chicama (no. 5) shows a large increase only in precipitation change, influenced by the ENSO climate conditions, and as shown in Fig. 2, those peaks are somehow inconsistent with the mean dry conditions.

It is worth pointing out that the hydrologic cycle of the 11 selected catchments is still influenced by human activities but only marginally (e.g., see changes in land cover in Fig. 5a). From an ecosystemic point of view and according to the Budyko theory (see van der Velde et al. 2013), in those “quasinatural” environments, any changes in vegetation are due to a co-evolution with the landscape to optimize water and energy use for given climatic

conditions. It maintains a steady state. However, the anthropogenic influence prevents a natural adaptation of vegetation species, as expected under the co-evolution. Strong disturbance could modify this behavior (as found with the 15 remaining catchments) in a long term, where it would be valid to reconsider the statement of a steady state.

The direction and magnitude values in the Budyko relationship are presented in Table 4. Equations 4 and 5 were also validated over different periods through a 10-year moving window along the 1970–2008 period, which yields a range of values expressed in error rates (%).

6 Conclusions

This study analyzes the hydroclimatic variability over 26 catchments of the Peruvian Pacific drainage region for the 1970–2008 period. We applied the Budyko-Zhang methodology to analyze the water balance trends over the period and determine if climate variability or human activities may have influenced these trends.

The study area experienced greater precipitation and runoff changes over the northern latitudes in relation with the ENSO influence. PET has been also studied for the first time in the region as an approach to relate it with temperature (and its relationship with the altitudinal gradient) using the Oudin method. This method is suitable for regions with nondense climatic database as well as under arid and semiarid conditions. Annual values of PET decrease southward with a slight increase over most arid catchment located in the south due to a predominance of bare ground and open shrubland areas. According to significant upward trends in annual temperature found in all catchments and regional change points found in most catchments, our results showed a significant warming in the study area with a mean of 0.2 °C per decade as already identified in studies for South American Andes such as the one by Vuille et al. (2015). Precipitation data do not exhibit significant trends and change points in most catchments. The runoff time series presented a significant decrease over central catchments with a change point in the years 1987 and 1989, which is mainly related to the intensive water exploitation for agricultural activities and land cover change.

Following the hydroclimatic description of the region, we applied the Budyko-Zhang conceptual framework to identify plausible annual change disparity of water balance in catchments along the study area. This region is characterized mostly by semiarid conditions and presents strong climate variability mainly in the northern regions. We identified 11 out of 26 catchments with low disparity according to the Budyko-Zhang framework related to a low climatic and anthropogenic influence and suitable for an in-depth analysis with Budyko trajectories. The w parameter related to plant-available water

in the Budyko-Zhang framework reaches an average value of 0.7, indicating the predominance of grasslands over the semi-arid conditions. Besides having a climatic influence, large hydraulic systems and irrigation have been identified as one of the main factors of human activity causing significant changes in runoff in most catchments. Catchments with high water balance disparity presented a significant change in land cover mainly with a decrease in cropland and an increase in grassland over the studied period.

Changes in trajectories in the Budyko space over those 11 selected catchments revealed two groups of catchments. Six catchments—Piura upstream (no. 1), Piura (no. 2), Chicama (no. 5), San Juan (no. 17), Acari (no. 19), and Yauca (no. 20)—were shown to be sensitive to climate variability (i.e., likely with high sensitivity to future climate) and land use changes, where precipitation and temperature are the most likely drivers of these environments change. The five other catchments do not reveal any clear behavior in terms of sensitivity to climate variability.

Finally, depending on the observational period of the analysis, limitations are mostly related to limited hydroclimatic data availability and related to the steady-state hypothesis of the Budyko framework. However, despite these limitations, our results provide a first assessment of the catchments with less climate and anthropogenic influence on water balance and its sensibility to climate variability and land use change which has implication for regional water resources assessment and management.

Acknowledgements The authors would like to thank SENAMHI (Meteorological and Hydrological Service of Peru) for providing complete hydrometeorological raw dataset. We thank the anonymous reviewer for his constructive comments that helped improve the original manuscript. B. Dewitte acknowledges supports from FONDECYT (projects 1171861 and 1151185).

Funding information This work was supported by Peruvian Ministry of Education (MINEDU-PRONABEC scholarship).

References

- ANA (2012) Recursos Hídricos en el Peru, 2nd edn. Ministerio de Agricultura. Autoridad Nacional del Agua, Lima, pp 45–189
- Bourel L, Rau P, Dewitte B, Labat D, Lavado W, Coutaud A, Vera A, Alvarado A, Ordoñez J (2015) Low-frequency modulation and trend of the relationship between ENSO and precipitation along the northern to centre Peruvian Pacific coast. *Hydrol Process* 29(6):1252–1266
- Brouwer C, Heibloem M (1986) Irrigation water measurement: irrigation water needs, vol 3. United Nations Food and Agriculture Organization, Rome, p 102
- Brown AE, Zhang L, McMahon TA, Western AW, Vertessy RA (2005) A review of paired catchment studies for determining changes in water yield resulting from alterations in vegetation. *J Hydrol* 310:28–61

- Budyko MI (1958) The heat balance of the Earth's surface. U.S. Department of Commerce, Washington, p 259
- Budyko MI (1974) Climate and life. International geophysics series, vol 18. Academic, New York, p 508
- Chen Z, Chen Y, Li B (2013) Quantifying the effects of climate variability and human activities on runoff for Kaidu River basin in arid region of northwest China. *Theor Appl Climatol* 111:537–545
- Coron L, Andréassian V, Perrin C, Le Moine N (2015) Graphical tools based on Turc-Budyko plots to detect changes in catchment behaviour. *Hydrol Sci J* 60(7–8):1394–1407
- DeFries R, Hansen M, Townshend JRG, Sohlberg R (1998) Global land cover classifications at 8 km spatial resolution: the use of training data derived from Landsat imagery in decision tree classifiers. *Int J Remote Sens* 19(16):3141–3168
- Donohue RJ, Roderick ML, McVicar TR (2007) On the importance of including vegetation dynamics in Budyko's hydrological model. *Hydrol Earth Syst Sci* 11:983–995
- Donohue RJ, Roderick ML, McVicar TR (2011) Assessing the differences in sensitivities of runoff to changes in climatic conditions across a large basin. *J Hydrol* 406:234–244
- Greve P, Gudmundsson L, Orlowsky B, Seneviratne S (2015) Introducing a probabilistic Budyko framework. *Geophys Res Lett* 42(7):2261–2269
- Hansen M, DeFries R, Townshend JRG, Sohlberg R (2000) Global land cover classification at 1 km resolution using a decision tree classifier. *Int J Remote Sens* 21:1331–1365
- Hassan H, Dregne HE (1997) Natural habitats and ecosystems management in drylands: an overview. Environment department paper N51. World Bank, Washington, pp 1–53
- Hublart P, Ruelland D, Dezetter A, Jourde H (2015) Reducing structural uncertainty in conceptual hydrological modelling in the semi-arid Andes. *Hydrol Earth Syst Sci* 19:2295–2314
- Hublart P, Ruelland D, García de Cortázar-Atauri I, Gascoin S, Lhermitte S, Ibacache A (2016) Reliability of lumped hydrological modeling in a semi-arid mountainous catchment facing water-use changes. *Hydrol Earth Syst Sci* 20:3691–3717
- Jaramillo F, Destouni G (2014) Developing water change spectra and distinguishing change drivers worldwide. *Geophys Res Lett* 41: 8377–8386
- Jones J, Creed I, Hatcher K, Warren R, Adams M, Benson M et al (2012) Ecosystem processes and human influences regulate streamflow response to climate change at long-term ecological research sites. *Bioscience* 62(4):390–404
- Kendall MG (1975) Rank correlation measures. Charles Griffin, London, p 202
- Lavado WS, Ronchail J, Labat D, Espinoza JC, Guyot JL (2012) Basin-scale analysis of rainfall and runoff in Peru (1969–2004): Pacific, Titicaca and Amazonas drainages. *Hydrol Sci J* 57(4):625–642
- Lavado WS, Labat D, Ronchail J, Espinoza JC, Guyot JL (2013) Trends in rainfall and temperature in the Peruvian Amazon-Andes basin over the last 40 years (1965–2007). *Hydrol Process* 27:2944–2957
- Mann HB (1945) Non-parametric tests against trend. *Econometrica* 13: 245–259
- Mortimore M (2009) Dryland opportunities. International Union for Conservation of Nature and Natural Resources. IUCN. IIED. UNDP, Gland-Switzerland, p 86
- Oudin L, Hervieu F, Michel C, Perrin C, Andreassian V, Anctil F, Loumagne C (2005) Which potential evapotranspiration input for a lumped rainfall-runoff model? Part 2—towards a simple and efficient potential evapotranspiration model for rainfall-runoff modeling. *J Hydrol* 303:290–306
- Pettitt AN (1979) A non-parametric approach to the change-point problem. *Appl Stat* 28:126–135
- Rau P, Bourrel L, Labat D, Melo P, Dewitte B, Frappart F, Lavado W, Felipe O (2016) Regionalization of rainfall over the Peruvian Pacific slope and coast. *Int J Climatol*. <https://doi.org/10.1002/joc.4693>
- Renner M, Bernhofer C (2012) Applying simple water-energy balance frameworks to predict the climate sensitivity of streamflow over the continental United States. *Hydrol Earth Syst Sci* 16:2531–2546
- Ruelland D, Dezetter A, Hublart P (2014) Sensitivity analysis of hydrological modelling to climate forcing in a semi-arid mountainous catchment. In: *Hydrology in a changing world: environmental and human dimensions* (Proc. 7th FRIEND-Water Int. Conf., Montpellier, France, 7–10 Oct. 2014). IAHS Publ 363:145–150
- Searcy JK, Hardison CH (1960) Double-mass curves. US Geol Survey Water-Supply Paper 1541-B:31–66
- Sivapalan M, Thompson SE, Harman CJ, Basu NB, Kumar P (2011) Water cycle dynamics in a changing environment: improving predictability through synthesis. *Water Resour Res* 47(10):W00J01
- Valéry A, Andréassian V, Perrin C (2010) Regionalization of precipitation and air temperature over high-altitude catchments—learning from outliers. *Hydrol Sci J* 55(6):928–940
- van der Velde Y, Vercauteren N, Jaramillo F, Dekker S, Destouni G, Lyon S (2013) Exploring hydroclimatic change disparity via the Budyko framework. *Hydrol Process* 28:4110–4118
- Vuille M, Franquist E, Garreaud R, Lavado W, Caceres B (2015) Impact of the global warming hiatus on Andean temperature. *J Geophys Res Atmos* 120:3745–3757
- Wagener T, Sivapalan M, Troch PA, McGlynn BL, Harman CJ, Gupta HV, Kumar P, Rao PSC, Basu NB, Wilson JS (2010) The future of hydrology: an evolving science for a changing world. *Water Resour Res* 46(5):W05301
- Wang D, Hejazi M (2011) Quantifying the relative contribution of the climate and direct human impacts on mean annual streamflow in the contiguous United States. *Water Resour Res* 47(10):W00J12
- Wang W, Shao Q, Yang T, Peng S, Xing W, Sun F, Luo Y (2013) Quantitative assessment of the impact of climate variability and human activities on runoff changes: a case study in four catchments of the Haihe river basin, China. *Hydrol Process* 27:1158–1174
- Yang D, Shao W, Yeh P, Yang H, Kanae S, Taikan O (2009) Impact of vegetation coverage on regional water balance in the nonhumid regions of China. *Water Resour Res* 45:W00A14
- Zhang L, Dawes WR, Walker GR (2001) The response of mean annual evapotranspiration to vegetation changes at catchment scale. *Water Resour Res* 37:701–708
- Zhang S, Lu XX (2009) Hydrological responses to precipitation variation and diverse human activities in a mountainous tributary of the lower Xijiang, China. *Catena* 77:130–142
- Zhao G, Mu X, Tian P, Wang F, Gao P (2013) Climate changes and their impacts on water resources in semiarid regions: a case study of the Wei River basin, China. *Hydrol Process* 27:3852–3863

Annex A.3

Article under review in Hydrological Processes

Assessing freshwater runoff over Peruvian Pacific drainage catchments during
the 1970-2010 period.

Rau P, Bourrel L, Labat D, Ruelland D, Frappart F, Lavado W, Dewitte B,
Felipe O.

Submitted in April 17, 2017
Currently under revision

Assessing freshwater runoff of Peruvian Pacific drainage catchments over the 1970–2010 period

Journal:	<i>Hydrological Processes</i>
Manuscript ID	Draft
Wiley - Manuscript type:	Research Article
Date Submitted by the Author:	n/a
Complete List of Authors:	Rau, Pedro; Université Toulouse III Paul Sabatier, Geosciences Environnement Toulouse GET Bourrel, Luc; IRD, GET Labat, David; Université de Toulouse III (UPS), GET Ruelland, Denis; CNRS, HSM Frappart, Frédéric; GET, LEGOS Lavado, Waldo; SENAMHI, Direccion de Hidrologia y Recursos Hidricos Dewitte, Boris; IRD, LEGOS Felipe-Obando, Oscar; SENAMHI, Direccion de Hidrologia y Recursos Hidricos
Keywords:	hydrological modelling, GR1A, GR2M, regional runoff, poorly gauged basins, Peruvian Pacific drainage

SCHOLARONE™
Manuscripts

**Assessing freshwater runoff of Peruvian Pacific drainage catchments over the
1970–2010 period**

Pedro Rau¹, Luc Bourrel¹, David Labat¹, Denis Ruelland², Frédéric Frappart^{1,3}, Waldo
Lavado⁴, Boris Dewitte^{3,5,6}, Oscar Felipe⁴

¹ UMR 5563 GET, Université de Toulouse – CNRS – IRD – OMP - CNES, 14 Avenue
Edouard Belin, 31400 Toulouse, France.

² CNRS, UMR 5569 HydroSciences Montpellier, 300 Avenue du Professeur Emile
Jeanbrau, 34095 Montpellier, France.

³ UMR 5566 LEGOS, Université de Toulouse - CNRS - IRD - OMP - CNES, 14
Avenue Edouard Belin, 31400 Toulouse, France.

⁴ SENAMHI, Jirón Cahuide 785, Lima 11, Peru.

⁵ Universidad Católica del Norte, Facultad de Ciencias del Mar, Coquimbo, Chile

⁶ Centro de Estudios Avanzado en Zonas Áridas (CEAZA), Coquimbo, Chile

Submitted 17/04/2017

Corresponding author: Pedro Rau (pedro.rau@get.omp.eu)

Abstract

To represent the multi-decadal behaviour of freshwater runoff along Peruvian Pacific drainage catchments, a regional runoff analysis is proposed based on hydrological modelling at annual and monthly time step for unimpaired conditions over the 1970–2010 period. Differential Split-Sample Tests were used to assess the hydrological modelling robustness of the GR1A and GR2M conceptual lumped models, showing a satisfactory transposability from dry to wet years inside the thresholds efficiencies defined by Nash-Sutcliffe and bias criteria. This allowed relating physical catchment characteristics with calibrated and validated model parameters, thus offering a regional perspective about dryland conditions in the study area as the anticlockwise hysteresis loop found for seasonal precipitation-runoff relationship, as well as the effects of climate variability and catchment characteristics.

In a context of water scarcity in the region as a crucial issue for Peru added to poorly gauged and ungauged catchments, our methodology offers new perspectives for freshwater availability as a base reference for unimpaired conditions. Under those considerations it was estimated a regional discharge of 709 m³/s to the Pacific Ocean with a significant increasing regional trend around 43 m³/s/decade for the whole 1970–2010 period.

Key words: hydrological modelling, GR1A, GR2M, regional runoff, poorly gauged basins, Peruvian Pacific drainage

1. Introduction

Peruvian Pacific drainage catchments are characterized by dryland conditions and recurrent conflicts about the water allocation between water uses ever since this region only benefits from 2% of the available freshwater of Peru (ANA, 2012). This region concentrates more than 50% of Peruvian population and previous studies such as Lavado *et al.* (2012) and Rau *et al.* (2017b) showed evidence of poorly gauged and ungauged catchments conditions with strong anthropogenic influence over water balance and runoff in the last four decades.

Under these conditions, regional runoff assessment through hydrological modelling represents the most common challenge in regional hydrology. Applying a regional hydrological model implies its repeated use everywhere within a region, using a global set of parameters generally transferred from gauged catchments (Engeland and Gottschalk, 2002; Seibert and Beven, 2009). Hydrological models are abstractions of real systems and none of them can be anticipated as more accuracy for specific catchments and hydrologic conditions (Seiller *et al.*, 2012). Conceptual lumped models are being increasingly used to evaluate their performance over regional water availability (Wale *et al.*, 2009; Castiglioni *et al.*, 2010; Ibrahim *et al.*, 2015) and potential impacts of climate change on hydrological systems (Coron *et al.*, 2012; Ruelland *et al.*, 2012, 2015; Seiller *et al.*, 2012, 2015; Wang *et al.*, 2015; Fowler *et al.*, 2016; Fabre *et al.*, 2016).

Runoff estimates take into account historical observations of streamflow, which reflect the changes in environmental conditions such as climate and land use. Under changing climatic conditions, conceptual models would show more capability than previously

thought (Fowler *et al.*, 2016). However, conceptual modelling is regularly criticized for oversimplifying the physics of catchments and leading to unreliable simulations when conditions shift beyond the range of prior experience (Hublart *et al.*, 2015). The usual sources of uncertainty in hydrological modelling under stationary conditions (concerning the climate and the physical characteristics of the catchment) are linked to the structure of the model, the calibration procedures and erroneous data used for calibration and validation (e.g. Liu and Gupta, 2007; Brigode *et al.*, 2013). Under non-stationary conditions, such as climate variability or change, an additional source of uncertainty arises from parameters instability due to possible changes in the physical characteristics of the catchment and in the main processes at play (e.g. Coron *et al.*, 2012; Thompson *et al.*, 2013). For this reason, it appears necessary to evaluate the modelling robustness and notably the transferability of the calibrated parameters to contrasted climate and/or anthropogenic conditions. Thirel *et al.* (2015) suggested a calibration and evaluation protocol for dealing with changing catchments, highlighting the advantages of the Differential Split-Sample Test (DSST; Klemeš, 1986).

One of the major obstacles in estimating regional and continental freshwater runoff is the lack of gauging records. Some methods have been applied to account for the contribution from poorly gauged regions in estimating long-term mean discharge as a simple sum of available streamflow records. However, those methods likely would contain discontinuities, which are a major issue in long term climate data analyses (Milliman and Farnsworth, 2011). Unimpaired runoff could be considered as a valuable source for identifying long term climate variability and change impacts, its application also includes legal and water management frameworks (Null and Viers, 2013). In our study, we propose the use of unimpaired runoff, which is defined as data from

unregulated rivers or where regulation changes the natural monthly streamflow volumes by less than five percent (Boughton, 1999).

A few in-depth hydrological studies were developed in the Peruvian Pacific drainage: de Reparaz (2013) documented and analysed earlier hydrological and physical conditions along the entire study area (i.e. 54 catchments) from the 1920s until the 1960s. ANA (2012) analysed the water supply and demand in the main catchments with water management purposes, achieving to estimating the total annual volume of freshwater availability along the Pd from the 1970s to 2010 based on gauged catchments. Lavado *et al.* (2012) analysed streamflow mean conditions and its variability over 29 catchments from 1969 to 2004. Rau *et al.* (2017b) identified 11 from 26 catchments associated with low water balance disparity or with quasi-natural conditions (hereafter unimpaired conditions) at interannual scale, explaining the annual runoff behaviour in each catchment from 1970 to 2008. In general, those studies made a weak approach about regional runoff behaviour and to our knowledge such a study has never been conducted in the Pd region, which would allow identifying some key elements of water resources management as the long term mean rate of runoff, its yearly and seasonal variability. This paper also aims at assessing the ability of two conceptual lumped hydrological models, GR1A (Mouelhi *et al.*, 2006b) and GR2M (Mouelhi *et al.*, 2006a) to simulate regional interannual unimpaired runoff over a multi-decadal period (i.e. the last four decades) characterized by a significant hydro-climatic variability.

2. Study area and data

2.1 General description

The study area comprises the Peruvian Pacific drainage region (hereafter Pd) that covers an area of about 280,500 km² (see Figure 1a). This area is characterized by a significant altitudinal gradient ranging from 0 to around 6,500 m asl and includes 54 main river catchments. The rivers generally flows from east to west from the Andes towards the Pacific Ocean with bare and steep slopes from 4 to 9% within small and medium catchment areas from 500 to 16,000 km² which favours significant rising, flooding and erosion during huge precipitation events (see Lavado *et al.*, 2012; Rau *et al.*, 2017b). The seven studied catchments are shown in Figure 1.

While near the coast, dry climate conditions are heavily constrained by oceanic conditions that are characterized by a permanent upwelling south of ~5°S, the highlands experience more the influence from seasonal variations in the large scale circulation patterns (i.e. ITCZ, Inter Tropical Convergence Zone) and the Southern Pacific Anticyclone (SPA). Also, anomalous precipitation events over the Pd are related to the El Niño Southern Oscillation (ENSO) at interannual timescale (Rau *et al.*, 2017a).

The western flank of the Andes is composed of igneous rock following the next distribution: Until ~8°S lithology is composed of Palaeozoic to Cretaceous formations. From 8°S to 16°S geological formations are dominated by the continuous Andean batholith while from 16°S they are made of young volcanic cover, vast Tertiary pampas and coastal range. These conditions do not favour underflow through the Andes in some regions, mainly because of the continuous batholith acting as a barrier upper 2,000 to 4,000 m asl (see Figure 1b), limiting the precipitation drainage through the canyons and main channels in catchments (Gilboa, 1971).

Catchments in the Pd are characterized mainly by arid and semi-arid areas, implying water shortage issues for human consumption in major cities located in arid lowlands and agriculture and industrial activities located throughout catchment. Water supply for economical activities (agriculture, mining, industrial and livestock) and domestic use is about 87% of the national total consumption and agriculture represents the greatest demand (86% of the Pd total consumption), which is based entirely on irrigation infrastructure systems because of little rainfall over arid lands (ANA, 2012). Besides, they are likely to be affected by the devastating effects of floods (ANA, 2012).

Monthly precipitation and runoff at basin scale for the seven selected catchments, highlight a considerable scatter within the 40-year datasets (see scatter plots in Figure 1) and a seasonal regional behaviour (see mean seasonal hydrographs in Figure 1). Nevertheless, the chronology of the data exhibits a well-defined annual cycle, showing an increase of runoff with increasing precipitation during wet months from November to May and a slight decrease during the dry months of July and August. The data consequently show an annual anticlockwise hysteresis loop in all studied catchments regardless of the geology, glaciers or snow cover. This implies that precipitation is temporarily stored within the basins and not transferred directly to the river during the wet period whereas the storage compartment is drained during the dry period.

The mechanisms explaining the hysteresis effect are not enough documented over the study area and we suggest here some relationships between hydrologic variables. Snow and ice melt runoff represents ~14% and less than 1% respectively of annual mean distributed runoff located mainly over central and southern latitudes of the upper Pd (Mernild *et al.*, 2016). Release of water by snowmelt generally reaches its peaks over wet months, which is not consistent with the anticlockwise nature of the hysteresis.

Release of water by ice melt peaks over dry months (Condom *et al.*, 2012; Mernild *et al.*, 2016) and is consistent with the hysteresis effect. However given the low representativeness of ice melt runoff, it can be considered as negligible. This suggests that snow and ice melt runoff could be discarded as the main mechanisms explaining hysteresis. We can also note that hysteresis occurs even over non-glacierized and non-snow covered catchments as Piura (n°1), and Chicama (n°2). In the same way, evapotranspiration reaches maximum values in the wet months from December to March and could qualitatively explain the hysteresis effect mainly in the catchments of Piura (n°1) and San Juan (n°4) identified by Rau *et al.* (2017b) as catchments with a water balance sensitive to both precipitation and evapotranspiration. Finally, the main mechanism explaining the hysteresis effect is probably associated to a transient storage of water in a groundwater unit during the wet months and its release during dry months. It makes sense in the light of the mean seasonal hydrological behaviour of catchments (see the mean seasonal hydrographs in Figure 1) and lithologic composition in Figure 1b. Catchments located outside of the quasi impervious batholith reasonably present the hysteresis effect (catchments n°1, n°2, n°6 and n°7) which is corroborated with the extension of their recession limbs above zero runoff. Catchments located mainly inside the batholith (n°3, n°4 and n°5) also present the hysteresis effect, bringing out the relevance of the transient storage, which at unimpaired conditions is the main source of recharge of alluvial coastal aquifers at lowlands by way of infiltration from river beds (Gilboa, 1971).

There is still a lack of studies and proper instrumentation for separating the runoff contribution from rainfall, ice and snow melt, evapotranspiration and groundwater over mid and low lands (i.e. at the studied gauge stations).

At annual time step, according to Lavado *et al.* (2012) and Rau *et al.* (2017b), catchments in the study area generally follow a northern-southern gradient with respect to precipitation and evapotranspiration (i.e. a decrease of mean annual precipitation and evapotranspiration towards the South) as shown in Table 1.

2.2 Hydrometeorological data set and validation

The database covers the 1970–2010 period and includes monthly precipitation, and temperature. Available data period for streamflow observations are indicated in Table 1. Precipitation series were obtained from 139 pluviometric stations, temperature series from 59 meteorological stations (see Figure 1) and monthly streamflow from 7 hydrological stations managed by the SENAMHI (National Meteorological and Hydrological Service of Peru).

A careful quality check of these data was previously performed. Monthly precipitation, temperature and streamflow data were homogenized and validated (see Bourrel *et al.*, 2015, Rau *et al.*, 2017a; 2017b for details about the processing). Precipitation and temperature data were interpolated to a 5 x 5 km grid using the inverse distance weighting technique and considering altitudinal gradients. Orographic effects on precipitation and temperature were accounted for using the SRTM digital elevation model in a similar way described in Ruelland *et al.* (2014). These effects on precipitation and temperature were considered using the approach proposed by Valéry *et al.* (2010) with a correction factor of $4 \times 10^{-4} \text{ m}^{-1}$ for precipitation which corresponds to a 20% increase in local precipitation with an elevation of 500 m; and by accounting for a constant lapse rate of $-6.5^\circ\text{C}/\text{km}$ for temperature (estimated from the observed data). Potential evapotranspiration (PET) was calculated through a formula relying on

clear monthly sky solar radiation and mean monthly air temperature (Oudin *et al.*, 2005) and which is adapted to arid and semi-arid regions limited by scarcity of in-situ climate data (Hublart *et al.*, 2015).

$$PET = \frac{R_e T + K_2}{\lambda \rho K_1} \text{ if } T + K_2 > 0$$

$$PET = 0, \text{ otherwise}$$
(1)

where PET is the rate of potential evapotranspiration (mm/d), R_e is the extraterrestrial radiation (MJ/m²/d), λ is the latent heat flux (2.45 MJ/kg), ρ is the density of water (kg/m³), T is the mean daily air temperature (°C) and K_1 and K_2 are fitted parameters (for a general case: $K_1 \sim 100$ and $K_2 \sim 5$).

Finally, we restricted our analysis to 7 catchments (see Table 1 and Figure 1) characterized by a valuable and confident complete dataset of monthly precipitation, temperature and streamflow series over 1970–2010.

3. Methods

3.1 Runoff simulation based on conceptual lumped models

Interannual runoff over each catchment was simulated with the GR1A lumped hydrological model (Mouelhi *et al.*, 2006b) considering the hydrological year from September to August. The GR1A model was established as a revisit of the Manabe bucket model (Manabe, 1969) that belongs to the first generation of land surface models. The GR1A has a semi-empirical and lumped structure showing the usefulness of the antecedent annual precipitation and the less representativeness of a reservoir at the annual time step. It means a reduced model with only one-parameter as follow:

$$Q_k = P_k \left\{ 1 - \frac{1}{\left[1 + \left(\frac{0.7P_k + 0.3P_{k-1}}{X \cdot PET_k} \right)^2 \right]^{0.5}} \right\} \quad (2)$$

Q_k is the simulated streamflow of the year k , P_k is the annual precipitation of the year k , P_{k-1} is the annual precipitation of the year $k-1$, PET_k is the potential evapotranspiration of the year k , X is the one-parameter of the model to be optimized. The advantage of this one-parameter model is its high parsimony being a benchmark model for comparing the simulated long-term average streamflow with other models.

Seasonal runoff was simulated with the GR2M lumped monthly model (Mouelhi *et al.*, 2006a). This model is based on two reservoirs and two calibration parameters. According to Figure 2, the soil quadratic reservoir (S') defines the production function with a maximal capacity $X1$; the gravity reservoir (R') defines the transfer function with the parameter $X2$, determining the runoff at the outlet and the exchange of water between the surface and the underground processes (Ibrahim *et al.*, 2015). GR2M is a very used hydrological model due to its high parsimony. Its semi-empirical approach has been demonstrated to perform well when compared to similar monthly models and sensitivity analyses have determined that GR2M is sensitive to white noise errors on precipitation, but comparatively robust to random errors on potential evapotranspiration (Huard and Mailhot, 2008).

3.2 Performance and efficiency of conceptual lumped models

The performances of the models (i.e. GR1A and GR2M) were evaluated by an efficiency criterion consisting of two primary statistical scores considered as the basis

for a careful hydrological evaluation (Thirel *et al.*, 2015): the Nash-Sutcliffe Efficiency criterion (NSE; Nash and Sutcliffe, 1970) and the associated bias. NSE is related to the capacity of the model to simulate the general shape of the hydrograph, while giving more weight to high flows (simulated runoff and observed runoff expressed as Q_{sim} and Q_{obs} respectively). Bias is defined as the balance between the accumulated simulated volume (V_{sim}) and accumulated observed volume (V_{obs}) over an evaluation of n -months. The two criteria are shown in equations 3 and 4 as follows:

$$NSE = 1 - \frac{\sum_{t=1}^n (Q_{obs(t)} - Q_{sim(t)})^2}{\sum_{t=1}^n (Q_{obs(t)} - \mu_{Q_{obs}})^2} \quad (3)$$

$$Bias = \frac{\sum_{t=1}^n (V_{sim(t)} - V_{obs(t)})}{\sum_{t=1}^n V_{obs(t)}} \quad (4)$$

Perfect agreement between the observed and simulated values yields a NSE efficiency of 1, while a negative efficiency represents a lack of agreement worse than if the simulated values were replaced with the observed mean values. Following Moriasi *et al.* (2007), a model simulation is judged satisfactory here if NSE is above 0.5. Also the associated bias expressed in percentage should be around 0% within the range of -40% to 40% and this criterion was evaluated separately as a regard of the quality of the model performance via the NSE. The optimization of the parameters was done by the Generalized Reduced Gradient (GRG2) method (Lasdon and Smith, 1992) considering a warm-up of two years in both models.

The model efficiency was evaluated following a Differential Split-Sample Test scheme (DSST; Klemes, 1986) seeking to test the model over contrasted climatic periods in terms of precipitation as the dry years (DY) and wet years (WY) over the 40-year

simulation period (1970–2010). Thus, it was defined two subperiods of equal length (20 DY and 20 WY) according to median annual precipitation over the period. The scheme follows two pairs of calibration and validation (Calibration↔Validation) as follows: DY→WY and WY→DY, making possible to test if the hydrological model calibrated on a given period is able to simulate streamflow with a similar efficiency on another period when it differs dramatically. It means to find a potential set of parameters calibrated and validated over the two pairs according to NSE and associated bias, which are keeping for the regionalization and also for representing the modelling uncertainty over contrasted conditions. The DSST methodology represents the most frequently used method for the diagnosis of model stability and the described evaluation of cross-calibration and validation over contrasted periods represents an approach of the temporal transposability of the model parameters over climate-contrasted periods (Thirel *et al.*, 2015).

3.3 Regional runoff model (RRM) and freshwater estimates

In order to obtain regional unimpaired runoff signatures along the study area (i.e. 49 catchments), the 7 unimpaired gauged catchments were used to link information to the other 42 catchments. This information mainly related to precipitation-runoff relationship can be represented through a hydrological model (e.g. GR2M) and can be linked through a statistical regression method for predicting annual runoff in ungauged basins (Blöschl *et al.*, 2013).

Multiple linear regressions methods search the relationship between runoff (including hydrological models parameters) and physical catchment characteristics (PCC) (Peel *et al.*, 2000; Wale *et al.*, 2009; Castiglioni *et al.*, 2010; Ibrahim *et al.*, 2015). According to

literature, PCC can be divided in five groups: climate, geography and physiography, geology, soil and land cover conditions (Wale *et al.*, 2009), however the final selection is always restricted to the available information. We established the following equations:

$$X_j = \sum_{i=1}^n a_i PCC_i + b \quad (5)$$

$$X_j = \sum_{i=1}^n a_i \ln PCC_i + b \quad (6)$$

$$\ln X_j = \sum_{i=1}^n a_i \ln PCC_i + b \quad (7)$$

where, X_j represents the parameters set with order j of the hydrological model (e.g. $X1$ and $X2$ for the GR2M obtained via a DSST scheme); a_i the regression coefficient of the PCC number i ; b is a constant or intercept of the regression line; n is the number of donor catchments (7 in this study). Equations 5, 6 and 7 represent regional runoff models (hereafter RRM) and its validation and final selection was made by the highest multiple correlation coefficient. A disadvantage of regression methods is that they may capture relationships that are evident in the data, but for which no theoretical explanation is available, for example due to the co-evolution of vegetation, landscape and hydrological response (Blöschl *et al.*, 2013). However considering our expected goals of estimates of unimpaired freshwater at regional scale, its application can be judge as acceptable as long as the hydrological model shows good transferability under the DSST scheme. Also, the selected RRM was calibrated and validated following the same DSST scheme with DY↔WY pairs over the donor catchments as if they were ungauged catchments.

The RRM is then used to estimate the monthly and annual runoff time series along the 49 catchments belonging to the study area. As it is shown in Figure 1, the 7 studied catchments present their gauge stations located mainly in the lower and middle altitude of the basin (i.e. not in the catchment outlet to the ocean). This is why the extension to the ocean through the RRM, represents the best way to generate a reference point for studying the unimpaired runoff over the Pd.

4. Results and discussion

4.1 Efficiency of the GR1A and GR2M models

The GR1A model was applied at annual time step following the DSST scheme defined in section 3.2. In general, the DY→WY pairs match with satisfactory values of NSE around 0.7 and associated bias reaching values around 0% in northern catchments as Piura (n°1) and Casma (n°2) but without showing a satisfactory performance over the rest of central and southern catchments. The WY→DY pair shows a good agreement only for Casma (n°2) and for the rest of catchments show a very low efficiency even with negative values of NSE and with bias values out of range of -40% to 40% as shown in Table 2. According to equation 2, X parameter represents a compensation of water balance errors due to differences between forcing and control data and according to Perrin *et al.* (2007), it could be interpreted as a fraction of the evapotranspiration related to the influence of an external basin outlet (e.g. not an atmospheric outlet but an exchange with deep groundwater or with adjacent basins in the case of a non-superposition of topographical and geological boundaries). Results explain the contrasted difference between dry and wet years in semi-arid conditions at interannual

level and a regional behaviour about gaining water in northern catchments defined by the X parameter always less than 1 (see Table 2).

Figure 3 resumes the efficiency of transposability of the GR2M parameters set from dry (DY) to wet (WY) years (colours shaded obtained via a kriging interpolation) and Table 3 shows the efficiency values for the DSST scheme $DY \leftrightarrow WY$. In general the $DY \rightarrow WY$ pairs match with values of NSE reaching high values around 0.80 (see Figures 3a, 3c and Table 3) and with associated biases within the range of -40% to 40% (see Figures 3b and 3d) for the 7 selected catchments. However calibration over dry years (DY) shows a low value of NSE of 0.4 for the southernmost catchment of Tambo (n°7) and presents an underestimation of observed runoff in all cases (see negative biases in Figure 3b). Validation over wet years (WY) also shows low values of NSE of 0.40 for Casma (n°3) and Camana (n°6). Additionally, the $WY \rightarrow DY$ pairs show a low efficiency with NSE values below 0.40 and biases are out of range of -40% to 40% for the validation over dry years (results of this transposition are shown in figures later). GR2M parameters set are shown in Figure 3e for the extreme case of calibration over DY and WY, which also envelope the parameters set for other scenarios as considering the total or the half total period for calibration. The envelope shows a large variability for XI values except for catchments n°4, n°5 and n°6, however these values are particularly low, corresponding with semi-arid characteristics over the 7 catchments. $X2$ shows a relatively stable behaviour around 1, knowing its theoretical range between around 0.2 and 1.3 (Perrin *et al.*, 2007).

Table 4 shows the mean monthly values of the S' soil reservoir and the R' exchange water reservoir for the $DY \leftrightarrow WY$ scheme. S' presents highest values in southern catchments (n°6 and n°7) and very low values for central catchments (n°3, n°4 and n°5)

for a calibration over DY and validation over WY. This is related to the geological conditions of the study area. While southern catchments offers less impervious conditions than northern catchments for water storage, over central catchments is clearly the influence of the impervious batholith with mean values around ~ 0 mm/month for San Juan ($n^{\circ}4$) and 24 and 19 mm/month for Casma ($n^{\circ}3$) and Acari ($n^{\circ}5$) catchments respectively over WY. R' keeps values nearly constant and in general is less than S' .

Runoff associated to the last results is shown at seasonal scale in Figure 6. DY \leftrightarrow WY pairs are represented as runoff uncertainties in blue colour, corroborating the efficiency and GR2M model performance in comparison with observed runoff in gauged stations.

4.2 Regional runoff model evaluation

The 7 studied catchments present a regional behaviour related to the parameter set transposability from dry to wet years in all catchments and also related to the interannual behaviour of gaining water in northern catchments. According to the results, it offered a great overview about the monthly hydrological response along the study area, as well as the selection of a valid PCC set. The PCC is related mainly to physical (non-climate or non-atmospheric) characteristics and mainly to those which can describe the exchange with soil and adjacent basins. After applying equations 5 to 7, the best set of PCCs found was: Area (A), Main channel longitude (L) and Perimeter (p). Figure 4 reveals the significant linear associations between $X1$, $X2$ and A, L and p.

Equation 7 generated the best RRM with a linear multiple correlation coefficient of 0.82 for $X1$ (a significant relationship) and 0.43 for $X2$ (a weak relationship). Equation 8 shows their potential representations as follows:

$$X1 = \frac{A^{0.393}L^{-4.107}p^{4.291}}{64.5}$$

$$X2 = 0.883A^{0.369}L^{-0.229}p^{-0.168} \quad (8)$$

It is worth to mention that $X1$ related to a soil reservoir can be considered as a buffer reservoir modulating the concentration time and easily explained by the geomorphology index of compactness (i.e. Gravelius's shape index) based on A and p . L is considered as a reference of the place where those exchanges become important according to the geological characteristics (see section 2.1). $X2$ related to the water exchange with neighbouring catchments could not be easily explained with A , L and p . This parameter is judged for its ambiguity (between its natural and statistical meaning) as a correction factor (Mouelhi *et al.*, 2006a). If $X2$ is less than 1, there is a water loss from the outside of the catchment; otherwise there is a gain. However $X2$ values did not reach a large range (i.e. from 0.6 to 1.1 in Table 3) and by theory $X2$ does not control the GR2M response to precipitation event, even does not control simulated runoff variability to a certain extent as does $X1$ (Huard and Mailhot, 2008). We suggest that our equations could be considered only as initial parameters set for its use at sub-basin scale, knowing also that the parameter $X1$ reflects the modelled storage dynamics, being necessary its comparison with field observations of groundwater table variations as done by Andermann *et al.* (2012) through a modified GR2M model. Also, there is a documented effect over other semi-arid areas in the world, where there is an increase of effective evapotranspiration losses over wet months (i.e. caused by the development of vegetation cover over poorly vegetated regions leading to increase of infiltration) and causing consequently a relative reduction in the runoff (Hughes, 2008). Those considerations are

not studied here because of lack of observations and are out of scope of this work that is focused on a regional scale.

Then, the RRM from equation 8 was evaluated over each of the 7 gauged catchments as ungauged systems. This evaluation also considers the efficiency criteria with respect to the observed runoff. Figure 5 shows the values of NSE and the associated bias with the regional DSST scheme based on the calibration over dry years and validation over wet years. NSE presents high values around 0.70 and bias values within the range of -40% to 30% and also keeping low efficiency in the southernmost catchment of Tambo (n°7) with a NSE of 0.4 for the calibration over DY (see Figures 5a and 5b) and also a low efficiency NSE value of 0.30 for Casma (n°3) for the validation over WY (see Figure 5c). $X1$ keeps its low values as expected for the semi-arid conditions. $X2$ is reduced to values below 1, mainly over catchments n°3, n°4 and n°5 with values below 0.9 which could indicate that these catchments located inside the Andean batholith (see Figure 1) are characterized by a marked water loss than the rest of catchments, this behaviour was also observed in the GR2M evaluation (see Figure 3) for catchments n°4 and n°5.

Figure 6 shows the synthesis of our calculations with the DSST scheme. The contrasted hydrological behaviour over dry (seasonal precipitation in orange) and wet years (seasonal precipitation in green) and the observed hydrological response (in black lines) are reflected in the difference of simulated runoff, projected in light blue colour as an uncertainty due to the contrasted evaluation via the DSST (DY↔WY), mainly in wet months from January to April. It is explained by the low model efficiency mainly for Casma (n°3) and Camana (n°6) catchments with a NSE around 0.40 and bias around

40% (see Table 3 and Figure 3). It also highlights that dry months from June to November does not present great uncertainty.

Simulated runoff by the RRM (in red dashed lines) follows the seasonality of observed precipitation and runoff. Simulated DSST contrasted runoff (in light blue colour) shows a lag of +1 month (a peak on March instead of February) with respect to the observed runoff in Camana catchment (n°6). Also over northern catchments the recession limb of the seasonal hydrograph is not well represented. This is explained by the effect of the hysteresis loop described in Section 2.1 mainly in those catchments where there are conditions for the transient storage during the wet months and its release over dry months (see catchments in Table 4 with high values of S' reservoir). However, even with the differences shown in Figure 6 and Figure 7 (reconstruction of dry and wet years over the studied period); simulated runoff corresponds to acceptable model efficiencies, according to the NSE and associated bias (Figure 5) and considering the meaningfulness of the extreme contrasted climatic evaluation of the DSST. A noteworthy case of very well simulated runoff in any condition at mean seasonal level is San Juan catchment (n°4), which presents a low uncertainty over wet months and RRM performance and could be related to its homogenous hydroclimatic conditions. RRM overestimates runoff over most wet month peaks, corresponding to the low model efficiency mainly in catchments n°3, 6 and 7 (see Figure 5 and 7).

4.3 Freshwater runoff estimation

Figure 8 shows RRM outputs expressed in terms of mean annual specific runoff and annual runoff time series along the 49 catchments for unimpaired conditions for the 1970–2010 period. It corroborates and quantify the water scarcity in the region until the

outlet points to the Pacific ocean, with a water yield range from 0.1 to 8 l/s/km² along the region, with a maximum value of 13 l/s/km² for Santa catchment (catchment n°13 in Figure 8a) with a persistence of very low values (catchments in red colour) towards southern latitudes. Figures 8b to 8f show the annual runoff for all catchments as a grey shaded area. For showing purposes, catchments were grouped following the general geographical classification proposed by de Reparaz (2013) in terms of river regime and geomorphology (i.e. pluvial, nivo-glacial-pluvial, torrents and brooks) in the study area. Figure 8b groups the northern rivers with a pluvial regime; Figure 8c groups northern central rivers and torrents with a snow-pluvial and glacial-pluvial regime with the presence of natural lakes, as the catchment called Santa (n°13 in Figure 8a) whose upper part is located along a glacial mountain chain; Figure 8d groups central rivers with pluvial regime with moderated glacial regime with the presence of natural lakes; Figure 8e groups torrents and brooks with pluvial regime and high aridity conditions as the complex catchment called Grande (n°35 in Figure 8a) whose lower part belongs to an extensive desert plain, Figure 8f groups southern rivers and abrupt torrents with volcanic origin. Average annual runoff (black dotted line) in each group also follows a regional hydroclimatic pattern with the predominance of peaks during the ENSO years as the extreme events of 1982/1983 and 1997/1998 over northern catchments and the predominance of low values on the event of 1982/1983 over southern catchments.

Our unimpaired freshwater runoff estimates is the first approach in the study area and it was expressed in terms of annual discharge as an estimation of the total water regional flux obtained by the sum of all time series. It reaches an annual mean of 747 m³/s for the 1970–2010 period and 709 m³/s without considering the ENSO extremes events of 1982/1983 and 1997/1998 (see Table 5 and Figure 8g). It was consistent with others

estimations done in the region obtained only by observed records at gauge stations as listed in ANA (2012) as follows: ELECTROPERU in 1975 with 1025 m³/s, ONERN in 1980 with 855 m³/s, CEDEX in 1992 with 924 m³/s and ANA in 2012 with 802 m³/s, which could evidence a decrease but not concluding because of the discontinuity of the observed records. However for unimpaired conditions, the associated time series present a significant positive trend of 43 m³/s/decade based on a Mann Kendall test at 95% of confidence level with a 5-yr mean running for the scenario without ENSO extreme events as shown in Figure 8g. The regional trend is driven mainly by northern and central catchments (no trend was obtained for southern catchments plotted in Figure 8f). This can be explained by the effect of the significant increasing precipitation mainly in northern region (Rau *et al.*, 2017a); as well as the potential snow and glacier melting due to increasing mean temperature around 0.2 °C per decade over the study area in the last four decades as found in Rau *et al.* (2017b). The differences between mean annual modules of our unimpaired estimation, lower than the observed is due to the effects of water increase by the large hydraulic systems along the study area since seventies (Rau *et al.*, 2017b).

A resulting regional discharge of 709 m³/s was estimated and also compared with some earlier references from 1980 (Milliman and Farnsworth, 2011) which estimates a discharge of 665 m³/s from gauge stations. From a continental hydrological perspective, considering a total discharge around 26,540 m³/s from western coast of South America (Milliman and Farnsworth, 2011), our results corroborate that rivers along the arid Peruvian coast contribute essentially no fresh water to the ocean. Nevertheless, the advantage of having unimpaired time series through a regional runoff model stays in the fact of its usefulness in identifying long-term relationships with climate variability and

climate change impacts and its application for water management purposes. Even if the RRM presented a weak relationship for X_2 in equation 8, this parameter only plays a correcting role for runoff time series generation (see section 4.2), which would not be decisive if we express the runoff as anomalies (i.e normalized indices) of monthly and annual variability (e.g. using a standard score), as a very well used tool for climate studies.

5. Conclusions

This study proposes a methodology for estimating unimpaired freshwater runoff from Peruvian Pacific drainage catchments based on hydrological modelling via two conceptual lumped models (GR1A and GR2M). They were evaluated via a Differential Split-Sample Test (DSST) to cope with the temporal transposability of models parameter sets and modelling robustness over contrasted climate conditions as dry and wet years according to the arid and semi-arid conditions of the study area. This methodology achieved to establish a regional runoff model (RRM) via the GR2M model at the monthly time step over 7 selected catchments.

It is concluded that GR2M shows more robustness than GR1A model over contrasted climatic conditions (i.e. in terms of acceptable NSE and bias criteria). The seven unimpaired selected catchments presented a remarkable hydrological regional monthly behaviour related to the transposing of their parameters set from dry to wet years, as well as their behaviour of gaining water at annual time step over northern catchments. GR2M parameters set (i.e. X_1 and X_2) were linked with physical catchment characteristics (as the area, main channel length and perimeter) which are geomorphological indices with a good relationship with the soil reservoir as interpreted

by the XI parameter. An acceptable multiple linear regression was established between them and the associated RRM was satisfactorily validated considering the 7 selected catchments as ungauged systems. The RRM was applied over 49 catchments along the study area to simulate runoff for unimpaired conditions at outlet points to the Pacific Ocean.

In general, RRM and GR2M outputs revealed some deficiencies over northern catchments where the recession limb from mean seasonal hydrograph was not well reproduced. This can be explained by the effect of the hysteresis loop between precipitation and runoff found in all catchments, which after some discarded hypothesis, could be mainly related to a transient storage in river beds during the wet months and its release over dry months. Also, it was corroborated the influence of geological impervious conditions (i.e. Andean batholith) over the soil model reservoir.

Finally, unimpaired freshwater runoff was assessed for the first time through the study area. A total mean discharge of $709 \text{ m}^3/\text{s}$ was estimated for the whole 1970–2010 period. This discharge presented a trend of $+43 \text{ m}^3/\text{s/decade}$ (significant at the 95% of confidence level based on a Mann Kendall test) over the whole period without considering the ENSO extreme events of 1982/1983 and 1997/1998. Output runoff time series via the RRM were objectively reproducible, because their bias was minimized by the multiple linear regressions method, and uncertainty associated with them can be quantified under the clear assumptions about geomorphologic parameters. A limitation of the methodology is related to the application of the RRM in other spatial scales. Our proposed equations are mainly restricted to the size of evaluated catchments and for its use at regional scale. RRM outputs expressed in terms of runoff anomalies would offer a great tool based on the good relationship found for the XI parameter which controls

the runoff variability in the GR2M model. The regional hydrological knowledge of the study area acquired via conceptual parsimonious lumped models represents a first step to expand the use and development of hydrological models at basin and regional scale over the Peruvian Pacific drainage.

Future work will be dedicated to further investigating the runoff sensitivity to climate change and the ENSO/runoff relationship based on our unimpaired time series as valuable indices that are not significantly disturbed by direct human activities on a long-term hydrological record. This includes improvements to the regional runoff model for other spatial scales.

6. Acknowledgments

This work was supported by Peruvian Ministry of Education (MINEDU-PRONABEC, scholarship). Authors would like to thank SENAMHI (National Meteorological and Hydrological Service of Peru) for providing complete hydrometeorological raw dataset.

References

- ANA. 2012. *Recursos Hídricos en el Peru*. 2nd ed. Ministerio de Agricultura. Autoridad Nacional del Agua. Lima; 45–189.
- Andermann C, Longuevergne L, Bonnet S, Crave A, Davy P, Gloaguen R. 2012. Impact of transient groundwater storage on the discharge of Himalayan rivers. *Nature Geoscience* **5**: 127–132. DOI: 10.1038/NGEO1356
- Blöschl G, Sivapalan M, Wagener T, Viglione A, Savenije H. 2013. *Runoff prediction in ungauged basins. Synthesis across processes, places and scales*. Cambridge University Press. Cambridge; 53–134.
- Boughton WC. 1999. *A Century of Water Resources Development in Australia 1900–1999*. Institution of Engineers. Australia; 256.
- Bourrel L, Rau P, Dewitte B, Labat D, Lavado W, Coutaud A, Vera A, Alvarado A, Ordoñez J. 2015. Low-frequency modulation and trend of the relationship between ENSO and precipitation along the northern to centre Peruvian Pacific coast. *Hydrological Processes* **29**(6): 1252–1266. DOI: 10.1002/hyp.10247
- Brigode P, Oudin L, Perrin C. 2013. Hydrological model parameter instability: A source of additional uncertainty in estimating the hydrological impacts of climate change? *Journal of Hydrology* **476**: 410–425. DOI: 10.1016/j.jhydrol.2012.11.012
- Castiglioni S, Lombardi L, Toth E, Castellarin A, Montanari A. 2010. Calibration of rainfall-runoff models in ungauged basins: a regional maximum likelihood approach.

Advances in Water Resources **33**(10): 1235–1242. DOI:
10.1016/j.advwatres.2010.04.009

Condom T, Escobar M, Purkey D, Pouget JC, Suarez W, Ramos C, Apaestegui J, Tasci A, Gomez J. 2012. Simulating the implications of glaciers' retreat for water management: a case study in the Rio Santa basin, Peru. *Water International* **37**(4): 442–459. DOI: 10.1080/02508060.2012.706773

Coron L, Andréassian V, Perrin C, Lerat J, Vaze J, Bourqui M, Hendrickx F. 2012. Crash testing hydrological models in contrasted climate conditions: An experiment on 216 Australian catchments. *Water Resources Research* **48**: W05552. DOI: 10.1029/2011WR011721

de Reparaz G. 2013. *Los rios de la zona arida peruana*. Universidad de Piura Eds, Piura. Institut Cartografic de Catalunya Eds. Barcelona; 352.

Engeland K, Gottschalk L. 2002. Bayesian estimation of parameters in a regional hydrological model. *Hydrology and Earth System Sciences* **6**(5): 883–898.

Fabre J, Ruelland D, Dezetter A, Grouillet B. 2016. Sustainability of water uses in managed hydrosystems: human- and climate-induced changes for the mid-21st century. *Hydrology and Earth System Sciences* **20**: 3129–3147. DOI: 10.5194/hess-20-3129-2016

Fowler KJA, Peel MC, Western AW, Zhang L, Peterson TJ. 2016. Simulating runoff under changing climatic conditions: Revisiting an apparent deficiency of conceptual rainfall-runoff models. *Water Resources Research* **52**: 1820–1846. DOI: 10.1002/2015WR018068

Gilboa Y. 1971. Replenishment Sources of the Alluvial Aquifers of the Peruvian Coast. *Groundwater* **9**: 39–46. DOI: 10.1111/j.1745-6584.1971.tb03559.x

Huard D, Mailhot A. 2008. Calibration of hydrological model GR2M using Bayesian uncertainty analysis. *Water Resources Research* **44**: W02424. DOI: 10.1029/2007WR005949

Hublart P, Ruelland D, Dezetter A, Jourde H, 2015. Reducing structural uncertainty in conceptual hydrological modelling in the semi-arid Andes. *Hydrology and Earth System Sciences* **19**: 2295–2314. DOI: 10.5194/hess-19-2295-2015

Hughes DA. 2008. Modeling semi-arid and arid hydrology and water resources: the southern African experience, in: Wheeler, H., Sorooshian, S., Sharma K.D. (Eds.), *Hydrological modelling in arid and semi-arid areas*. Cambridge University Press. Cambridge; 29–40.

Ibrahim B, Wisser D, Barry B, Fowe T, Aduna A. 2015. Hydrological predictions for small ungauged watersheds in the Sudanian zone of the Volta basin in West Africa. *Journal of Hydrology Regional Studies* **4**: 386–397. DOI: 10.1016/j.ejrh.2015.07.007

Klemeš V. 1986. Operational testing of hydrological simulation- models. *Hydrological Sciences Journal* **31**(1): 13–24. DOI: 10.1080/02626668609491024

Lasdon LS, Smith S. 1992. Solving sparse nonlinear programs using GRG, ORSA *Journal on Computing* **4**(1): 2–15.

Lavado WS, Ronchail J, Labat D, Espinoza JC, Guyot JL. 2012. Basin-scale analysis of rainfall and runoff in Peru (1969–2004): Pacific, Titicaca and Amazonas drainages. *Hydrological Sciences Journal* **57**(4): 1–18. DOI: 10.1080/02626667.2012.672985

- 1
 - 2
 - 3
 - 4 Liu Y, Gupta HV. 2007. Uncertainty in hydrologic modeling: Toward an integrated data
 - 5 assimilation framework. *Water Resources Research* **43**: W07401. DOI:
 - 6 10.1029/2006WR005756
 - 7
 - 8
 - 9
 - 10
 - 11 Manabe S. 1969. Climate and the ocean circulation. 1. The atmospheric circulation and
 - 12 the hydrology of the Earth's surface. *Monthly Weather Review* **97**(11): 739–774.
 - 13
 - 14
 - 15
 - 16 Mernild SH, Liston GE, Hiemstra C, Beckerman AP, Yde JC, McPhee J. 2016. The
 - 17 Andes Cordillera. Part IV: spatio-temporal freshwater run-off distribution to adjacent
 - 18 seas (1979–2014). *International Journal of Climatology* DOI: 10.1002/joc.4922
 - 19
 - 20
 - 21
 - 22
 - 23
 - 24 Milliman JD, Farnsworth KL. 2011. *River Discharge to the Coastal Ocean: A Global*
 - 25 *Synthesis*. Cambridge University Press. Cambridge; 384.
 - 26
 - 27
 - 28
 - 29
 - 30 Moriasi DN, Arnold JG, Van Liew MW, Bingner RL, Harmel RD, Veith TL. 2007.
 - 31 Model evaluation guidelines for systematic quantification of accuracy in watershed
 - 32 simulations. *Transactions of the ASABE* **50**(3): 885– 900.
 - 33
 - 34
 - 35
 - 36
 - 37 Mouelhi S, Michel C, Perrin C, Andréassian C. 2006a. Stepwise development of a two-
 - 38 parameter monthly water balance model. *Journal of Hydrology* **318**: 200–214. DOI:
 - 39 j.jhydrol.2005.06.014
 - 40
 - 41
 - 42
 - 43
 - 44
 - 45
 - 46
 - 47
 - 48
 - 49
 - 50
 - 51
 - 52
 - 53
 - 54
 - 55
 - 56
 - 57
 - 58
 - 59
 - 60
- Nash JE, Sutcliffe JV. 1970. River flow forecasting through conceptual models, a discussion of principles. *Journal of Hydrology* **10**: 282–290.

- Null SE, Viers JH. 2013. In bad waters: Water year classification in nonstationary climates. *Water Resources Research* **49**: 1137–1148. DOI: 10.1002/wrcr.20097
- Oudin L, Hervieu F, Michel C, Perrin C, Andréassian V, Anctil F, Loumagne C. 2005. Which potential evapotranspiration input for a lumped rainfall-runoff model? Part 2 – Towards a simple and efficient potential evapotranspiration model for rainfall-runoff modeling. *Journal of Hydrology* **303**: 290–306. DOI: 10.1016/j.jhydrol.2004.08.026
- Peel MC, Chiew FHS, Western AW, McMahon TA. 2000. Extension of unimpaired monthly streamflow data and regionalization of parameter values to estimate streamflow in ungauged catchments. In: *Australian Natural Resources*. Report prepared for the National Land and Water Resources Audit. Australia; 37.
- Perrin C, Michel C, Andréassian V. 2007. *Modèles hydrologiques du Génie Rural (GR)*. Cemagref UR Hydrosystèmes et Bioprocédés, Antony; 16.
- Rau P, Bourrel L, Labat D, Melo P, Dewitte B, Frappart F, Lavado W, Felipe O. 2017a. Regionalization of rainfall over the Peruvian Pacific slope and coast. *International Journal of Climatology* **37**(1): 143–158. DOI: 10.1002/joc.4693
- Rau P, Bourrel L, Labat D, Frappart F, Ruelland D, Lavado W, Dewitte B, Felipe O. 2017b. Hydroclimatic change disparity of Peruvian Pacific drainage catchments (in revision). *Theoretical and Applied Climatology*.
- Ruelland D, Ardoin-Bardin S, Collet L, Roucou P. 2012. Simulating future trends in hydrological regime of a large Sudano-Sahelian catchment under climate change. *Journal of Hydrology* **424–425**: 207–216. DOI: 10.1016/j.jhydrol.2012.01.002

Ruelland D, Dezetter A, Hublart P. 2014. Sensitivity analysis of hydrological modelling to climate forcing in a semi-arid mountainous catchment. In: *Hydrology in a changing world: environmental and human dimensions*. IAHS Publ. **363**: 145–150.

Ruelland D, Hublart P, Tramblay Y. 2015. Assessing uncertainties in climate change impacts on runoff in Western Mediterranean basins. In: *Hydrologic non-stationarity and extrapolating models to predict the future*. IAHS Publ. **371**: 75–81.

Seibert J, Beven KJ. 2009. Gauging the ungauged basin: how many discharge measurements are needed? *Hydrology and Earth System Sciences* **13**: 883–892. DOI: 10.5194/hess-13-883-2009

Seiller G, Anctil F, Perrin C. 2012. Multimodel evaluation of twenty lumped hydrological models under contrasted climate conditions. *Hydrology and Earth System Sciences* **16**: 1171–1189. DOI: 10.5194/hess-16-1171-2012

Seiller G, Hajji I, Anctil F. 2015. Improving the temporal transposability of lumped hydrological models on twenty diversified U.S. watersheds. *Journal of Hydrology Regional Studies* **3**: 379–399. DOI: 10.1016/j.ejrh.2015.02.012

Thirel G, Andréassian V, Perrin C, Audouy JN, Berthet L, Edwards P, Folton N, Furusho C, Kuentz A, Lerat J, Lindström G, Martin E, Mathevet T, Merz R, Parajka J, Ruelland D, Vaze J. 2015. Hydrology under change: an evaluation protocol to investigate how hydrological models deal with changing catchments. *Hydrological Sciences Journal* **60**(7–8): 1184–1199. DOI: 10.1080/02626667.2014.967248

Thompson SE, Sivapalan M, Harman CJ, Srinivasan V, Hipsey MR, Reed P, Montanari A, Blöschl G. 2013. Developing predictive insight into changing water systems: Use-

inspired hydrologic science for the anthropocene. *Hydrology and Earth System Sciences* **17**(12): 5013–5039. DOI: 10.5194/hess-17-5013-2013

Valéry A, Andréassian V, Perrin C. 2010. Regionalization of precipitation and air temperature over high-altitude catchments - learning from outliers. *Hydrological Sciences Journal* **55**(6): 928–940. DOI: 10.1080/02626667.2010.504676

Wale A, Rientjes THM, Gieske ASM, Getachew HA. 2009. Ungauged catchment contributions to Lake Tana's water balance. *Hydrological Processes* **23**: 3682–3693. DOI: 10.1002/hyp.7284

Wang H, Sankarasubramanian A, Ranjithan RS. 2015. Understanding the low-frequency variability in hydroclimatic attributes over the southeastern US. *Journal of Hydrology* **521**: 170–181. DOI: 10.1016/j.jhydrol.2014.09.081

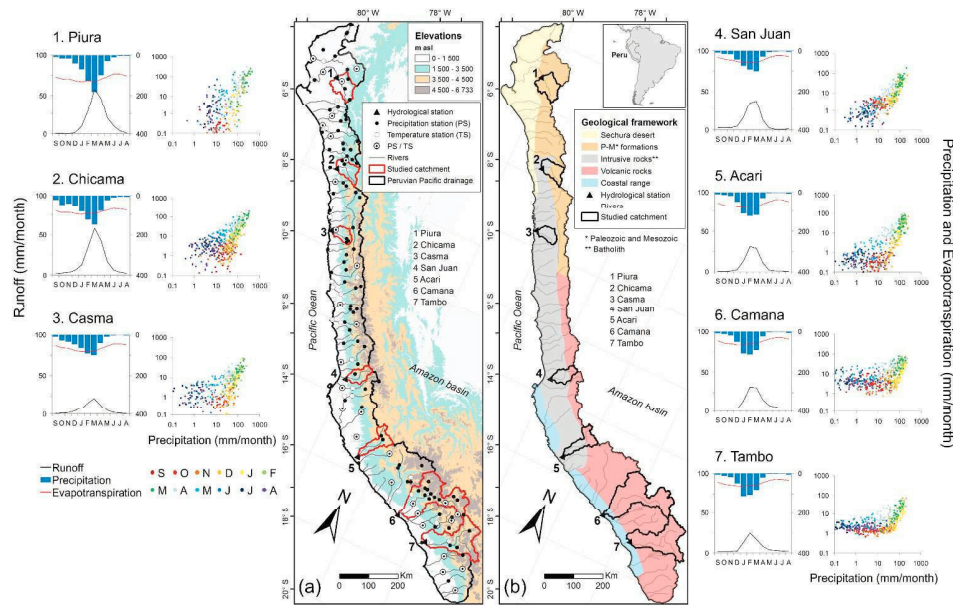


Figure 1. Spatial distribution of 7 studied catchments in the Pd. (a) Hydrometeorological stations and topography from SRTM digital elevation model; (b) Geological framework (Gilboa, 1971). Each catchment has a mean seasonal lumped runoff, precipitation and evapotranspiration (left) and presents a precipitation-runoff anticlockwise hysteresis plot in a bi-logarithmic scale of monthly data (right). Colour classification is scaled for a hydrological year (September - August).

239x150mm (300 x 300 DPI)

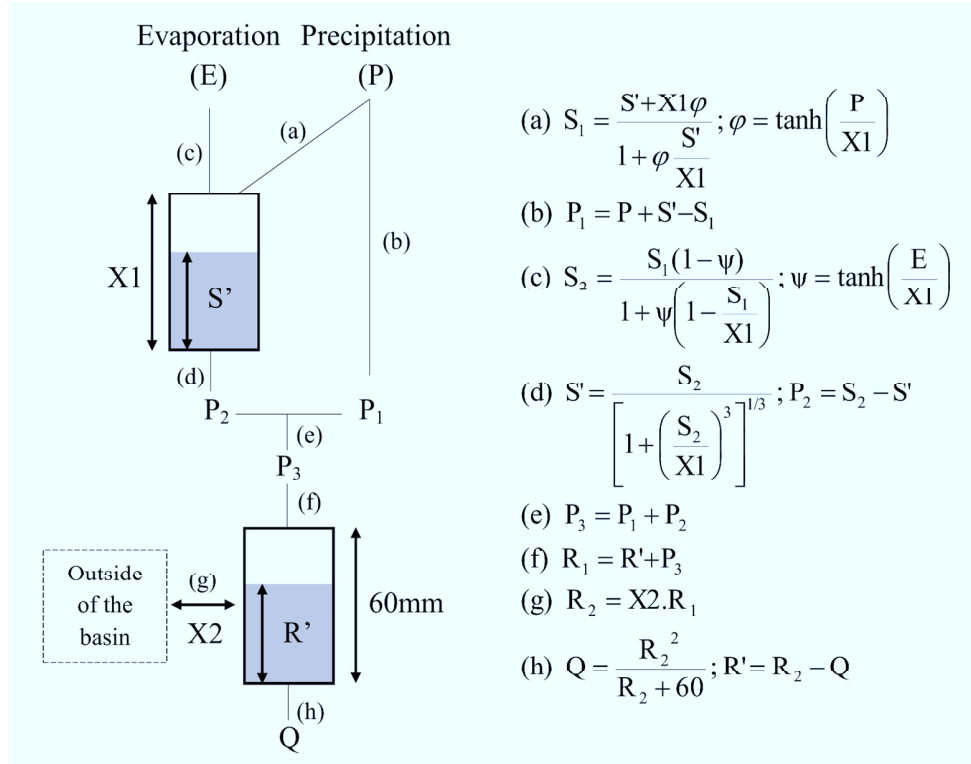


Figure 2. Scheme of the GR2M model with the parameters X1 and X2 (modified from Mouelhi et al., 2006a).

139x110mm (300 x 300 DPI)

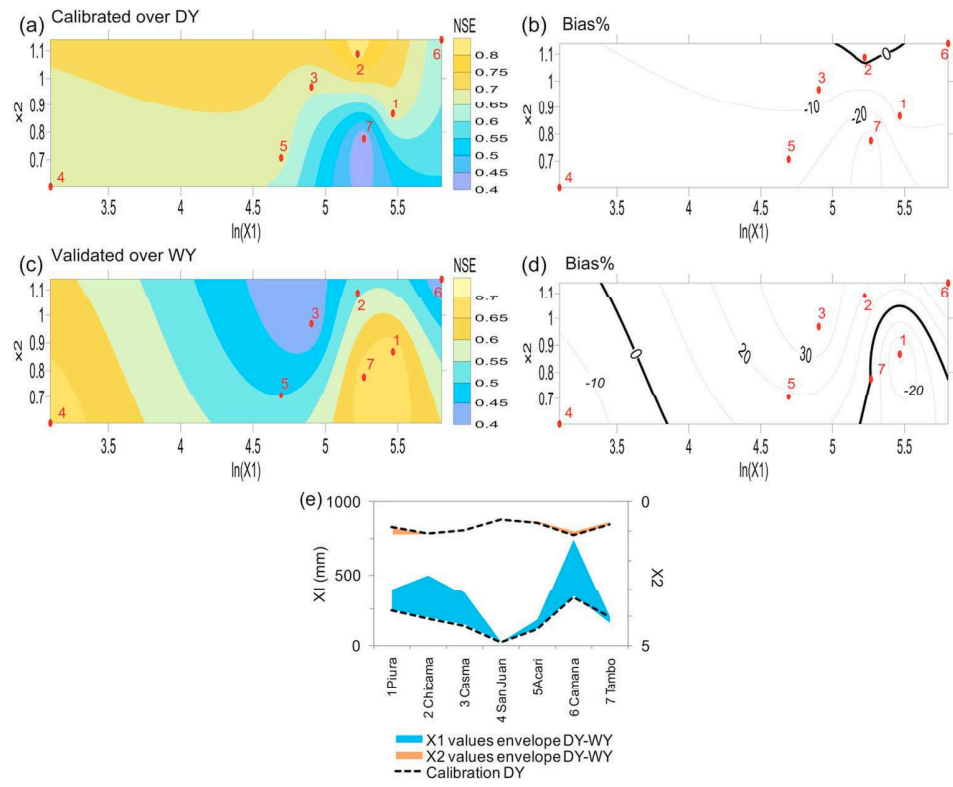


Figure 3. Evaluation of the performance of GR2M model (catchments in numbers) via parameter transposability (DSST). (a) NSE for the calibration over dry (DY) years. (b) Idem for the bias. (c) NSE for the validation over wet (WY) years. (d) Idem for the bias. (e) GR2M parameters values (X1 and X2) within the calibration envelope over DY and WY.

124x100mm (300 x 300 DPI)

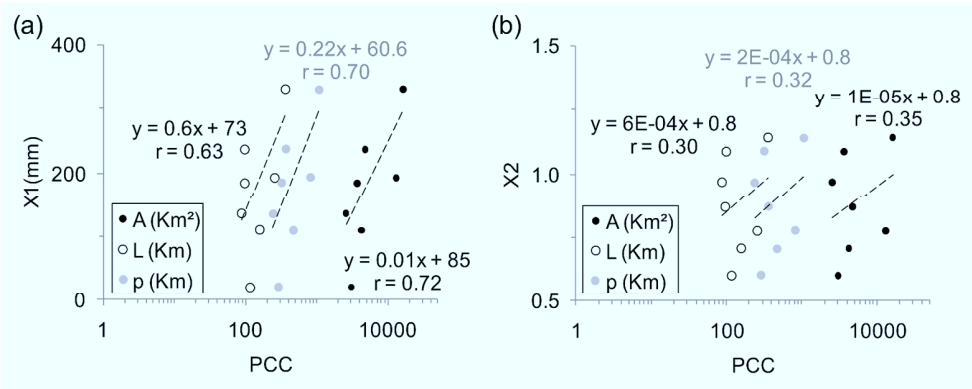


Figure 4. Linear associations between physical catchments characteristics (A: Area, L: Main channel length, p: Perimeter) using a natural bi-logarithmic scale (a) for the X1 parameter; (b) for the X2 parameter.

150x60mm (300 x 300 DPI)

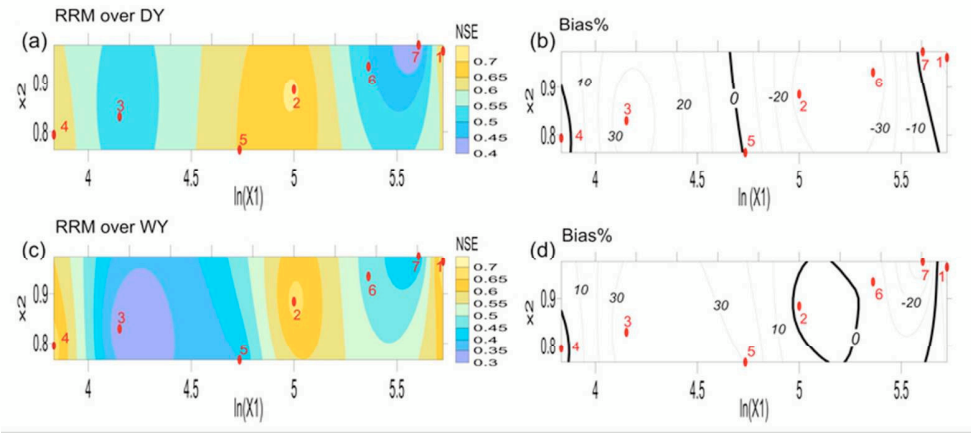


Figure 5. Performance of the Regional Runoff Model (catchments in numbers) via parameter transposability (DSST). (a) NSE for the calibration over dry years (DY). (b) Idem for the bias. (c) NSE for the validation over wet years (WY). (d) Idem for the bias.

70x31mm (300 x 300 DPI)

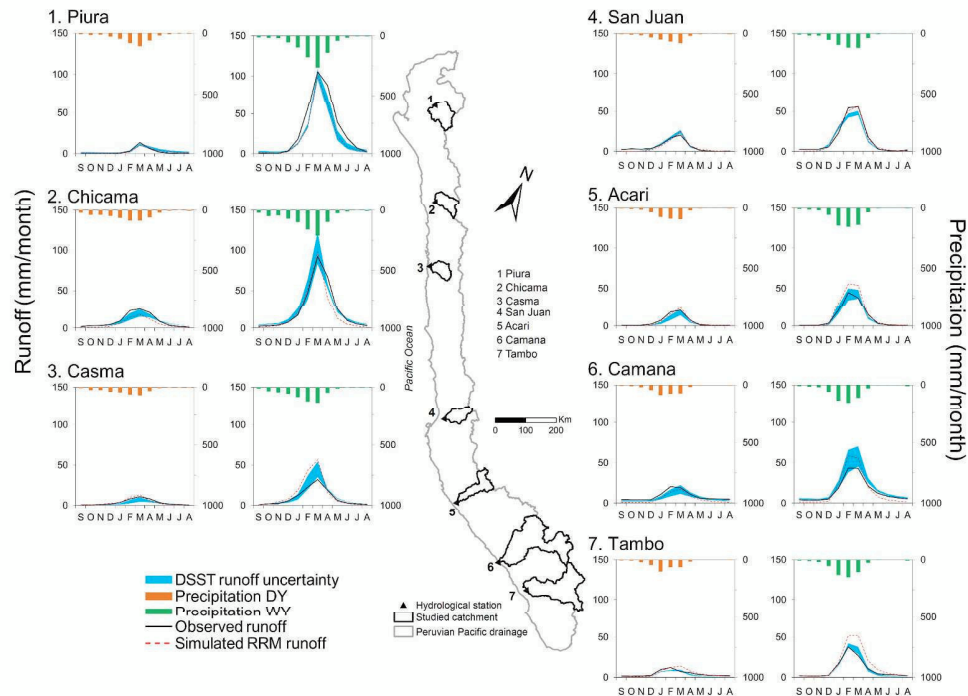


Figure 6. Mean seasonal runoff (observed, uncertainty by DSST, simulated by the regional runoff model) and precipitation over dry (DY) and wet (WY) years for each catchment. Calibration over DY and validation over WY considering a hydrological year (September to August).

189x139mm (300 x 300 DPI)

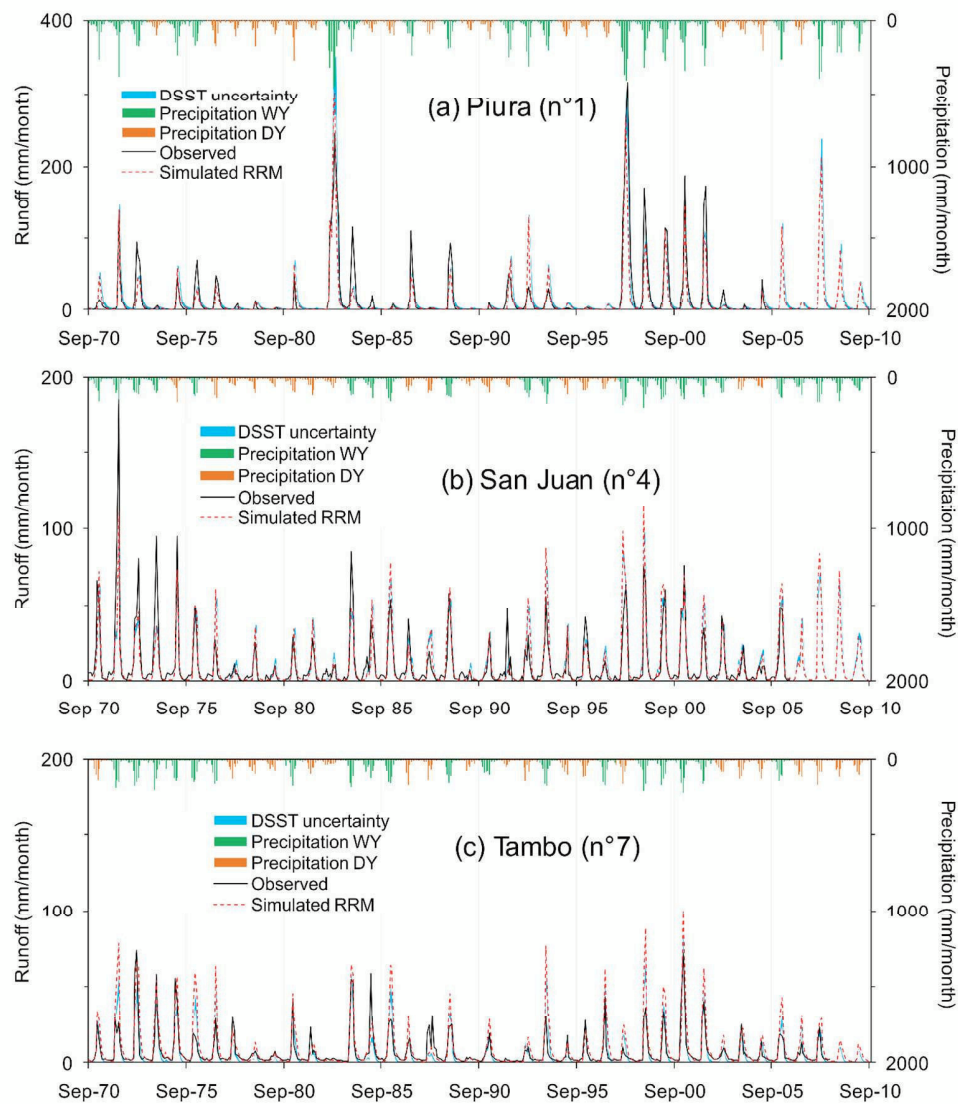


Figure 7. Runoff simulations along dry (DY) and wet (WY) years. Observed and simulated monthly runoff by GR2M and the regional runoff model. Runoff uncertainty via DSST.

129x150mm (300 x 300 DPI)

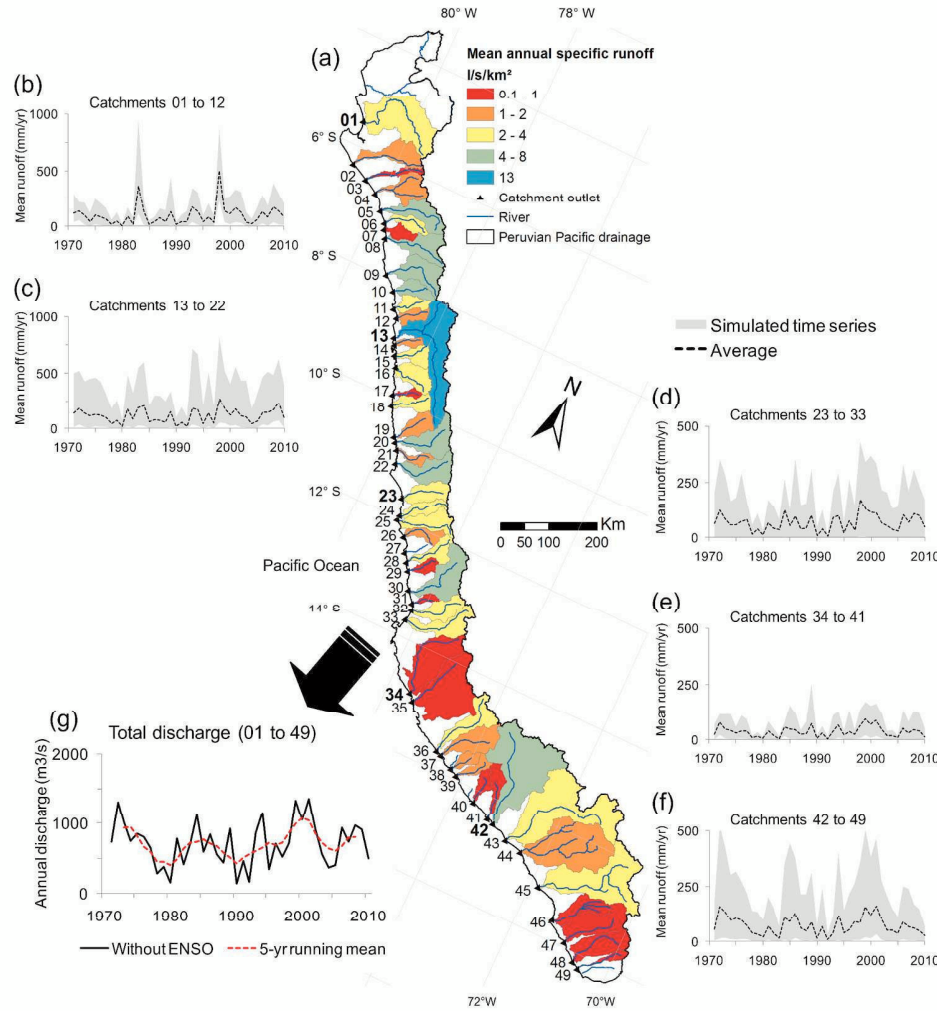


Figure 8. Spatial distribution of ungauged freshwater runoff (1970–2010) estimated by the RRM over 49 main catchments of the Pd: (a) Mean annual specific runoff by catchment. (b) to (f) Annual time series grouped in function of the regime characteristics. (g) Total annual discharge reaching 709 m³/s.

174x184mm (300 x 300 DPI)

Table 1. General characteristics of the 7 studied catchments at their outlets gauging stations for the indicated period (Min Alt: Minimum altitude; Max Alt: Maximum altitude; A: drainage area; L: main channel length; p: perimeter; S: mean slope; P: Mean annual precipitation; PET: Mean annual evapotranspiration; R: Mean annual runoff).

n°	Catchment	Gauging Station (data period)	Min Alt m asl	Max Alt m asl	A (km²)	L (km)	p (km)	S %	P mm/yr	PET mm/yr	R mm/yr
1	Piura	Pte. Nacara (1970–2005)	119	3526	4762	96	363	5.7	613	1376	181
2	Chicama	Salinar (1970–2008)	350	4217	3684	98	323	8.5	643	1013	211
3	Casma	S. Tutuma (1970–2005)	71	4769	2567	86	241	9.1	430	769	75
4	San Juan	Conta (1970–2006)	350	5049	3057	116	293	6.9	393	496	119
5	Acari	Bella Union (1970–2008)	70	4620	4242	158	471	6.1	486	715	92
6	Camana	Pte Camana (1970–2006)	122	6300	16238	360	1060	5.4	441	593	137
7	Tambo	Chucarapi (1970–2008)	281	5554	13063	254	820	5.0	418	566	82

Table 2. GR1A performance and mean annual runoff values for dry (DY) and wet (WY) years following the DSST scheme DY↔WY. Observed runoff at gauging station (R_{obs}); Simulated runoff (R_{sim}). Satisfactory results are shaded in grey rows.

n°	DY→WY						WY→DY					
	R_{obs} mm/yr		X	NSE (Bias%)		R_{sim} mm/yr		X	NSE (Bias%)		R_{sim} mm/yr	
	DY	WY		Calibration DY	Validation WY	DY	WY		Calibration WY	Validation DY	DY	WY
1	26	345	0.66	0.51 (20)	0.69 (-29)	31	247	0.46	0.86 (2)	-0.10 (12)	58	357
2	102	321	0.63	0.70 (2)	0.71 (-4)	101	303	0.57	0.73 (4)	0.58 (16)	114	330
3	40	109	0.74	0.50 (~0)	0.10 (40)	38	153	0.94	0.54 (3)	0.12 (-33)	26	112
4	65	173	0.81	0.20 (-3)	0.09 (4)	60	175	0.87	-0.20 (-3)	0.06 (-13)	54	163
5	57	127	0.84	0.61 (1)	0.10 (49)	58	179	1.15	0.22 (-1)	0.14 (-39)	5	21
6	99	175	0.58	0.46 (-2)	0.12 (45)	96	254	0.87	-0.19 (-3)	-0.30 (-44)	55	171
7	51	113	0.94	0.30 (-5)	0.21 (27)	48	142	1.13	0.60 (~0)	-0.19 (-30)	35	112

Table 3. GR2M parameters set and efficiencies over dry (DY) and wet (WY) years following the DSST scheme DY↔WY. Satisfactory results are shaded in grey rows.

n°	DY→WY				WY→DY			
	XI (mm)	X2	NSE (Bias%)		XI (mm)	X2	NSE (Bias%)	
			Calibration DY	Validation WY			Calibration WY	Validation DY
1	237	0.87	0.68 (-7)	0.68 (-33)	397	1.11	0.72 (-14)	0.60 (78)
2	185	1.09	0.82 (2)	0.54 (19)	494	1.08	0.73 (-7)	0.58 (-28)
3	135	0.97	0.66 (-6)	0.41 (40)	361	0.95	0.73 (-1)	0.33 (-51)
4	22	0.60	0.67 (-16)	0.68 (-19)	16	0.62	0.70 (-7)	0.63 (6)
5	109	0.71	0.67 (-16)	0.49 (18)	175	0.64	0.64 (-16)	0.53 (-50)
6	331	1.14	0.61 (-4)	0.40 (39)	739	0.99	0.71 (-1)	0.32 (-46)
7	194	0.78	0.41 (-36)	0.68 (~0)	143	0.66	0.73 (-19)	0.36 (-48)

Table 4. Mean monthly values of S' and R' reservoirs for dry (DY) and wet (WY) years following the DSST scheme DY↔WY. Valid results are shaded in grey rows according to Table 3.

n°	Catchment	DY→WY				WY→DY			
		S'		R'		S'		R'	
		(mm/month)		(mm/month)		(mm/month)		(mm/month)	
		DY	WY	DY	WY	DY	WY	DY	WY
1	Piura	20	39	7	16	44	86	12	20
2	Chicama	28	40	16	22	106	153	15	22
3	Casma	16	24	11	17	64	102	8	16
4	San Juan	~0	~0	9	13	~0	~0	11	14
5	Acari	13	19	8	13	30	42	6	11
6	Camana	81	114	16	22	199	274	13	21
7	Tambo	41	57	8	13	26	36	7	11

1
2
3
4
5
6
7
8
9
10
11
12
13
14
15
16
17
18
19
20
21
22
23
24
25
26
27
28
29
30
31
32
33
34
35
36
37
38
39
40
41
42
43
44
45
46
47
48
49
50
51
52
53
54
55
56
57
58
59
60

Table 5. Mean values of regional discharge (SD: Standard deviation)

Regional discharge	Including ENSO extreme years	Excluding ENSO extreme years
Mean (m ³ /s)	747	709
Minimal (m ³ /s)	136	136
Maximal (m ³ /s)	1876	1358
SD (m ³ /s)	375	322
Trend (m ³ /s/decade)	+58	+43

Annex A.4

Article published in Hydrological Processes

Low-frequency modulation and trend of the relationship between ENSO and precipitation along the northern to centre Peruvian Pacific coast.

Bourrel L, Rau P, Dewitte B, Labat D, Lavado W, Coutaud A, Vera A, Alvarado A, Ordoñez J.

Submitted in June 12, 2013

Accepted in May 15, 2014

Published in an issue in March 2, 2015

<http://dx.doi.org/10.1002/hyp.10247>

Low-frequency modulation and trend of the relationship between ENSO and precipitation along the northern to centre Peruvian Pacific coast

Luc Bourrel,^{1*} Pedro Rau,^{1,4} Boris Dewitte,² David Labat,¹ Waldo Lavado,³ Aude Coutaud,¹
Andrea Vera,¹ Abigail Alvarado¹ and Julio Ordoñez³

¹ UMR 5563 GET, Université de Toulouse – CNRS – IRD – OMP – CNES, Toulouse 31400, France

² UMR 5566 LEGOS, Université de Toulouse – CNRS – IRD – OMP – CNES, Toulouse 31400, France

³ SENAMHI, Lima 11, Peru

⁴ IMEFEN, Universidad Nacional de Ingeniería, Lima 25, Peru

Abstract:

The relationship between El Niño Southern Oscillation (ENSO) and precipitation along the Peruvian Pacific coast is investigated over 1964–2011 on the basis of a variety of indices accounting for the different types of El Niño events and atmospheric and oceanographic manifestations of the interannual variability in the tropical Pacific. We show the existence of fluctuations in the ENSO/precipitation relationship at decadal timescales that are associated with the ENSO property changes over the recent decades. Several indices are considered in order to discriminate the influence of the two types of El Niño, namely, the eastern Pacific El Niño and the central Pacific El Niño, as well as the influence of large-scale atmospheric variability associated to the Madden and Julian Oscillation, and of regional oceanic conditions.

Three main periods are identified that correspond to the interleave periods between the main climatic transitions over 1964–2011, i.e. the shifts of the 1970s and the 2000s, over which ENSO experiences significant changes in its characteristics. We show that the relationship between ENSO and precipitation along the western coast of Peru has experienced significant decadal change. Whereas El Niño events before 2000 lead to increased precipitation, in the 2000s, ENSO is associated to drier conditions. This is due to the change in the main ENSO pattern after 2000 that is associated to cooler oceanic conditions off Peru during warm events (i.e. central Pacific El Niño). Our analysis also indicates that the two extreme El Niño events of 1982/1983 and 1997/1998 have overshadowed actual trends in the relationship between interannual variability in the tropical Pacific and precipitation along the coast of Peru. Overall, our study stresses on the complexity of the hydrological cycle on the western side of the Andes with regard to its relationship with the interannual to decadal variability in the tropical Pacific. Copyright © 2014 John Wiley & Sons, Ltd.

KEY WORDS precipitation; ENSO; Modoki; decadal modulation; trend; Pacific coast; Peru

Received 12 June 2013; Accepted 15 May 2014

INTRODUCTION

El Niño in Peru is often associated with heavy rain along the coastal fringe of the country due to the intrusion of warm tropical waters along the coast that allows deep convection in a region where cold upwelled waters and semi-arid to arid climate usually prevail (Tapley and Waylen, 1990; Lagos and Buizer, 1992). Over the last decades, two extreme El Niño events (1982/1983 and 1997/1998) took place that had large socio-economical consequences because of the disasters caused by the floods and droughts. According to OPS (2000), direct

losses caused by the 1997/1998 event was estimated at \$1000m, of which \$800m were in the northern Pacific coast, as a result of heavy rains, and \$200m were in the southern Andes region, due to the effects of droughts. The economic impact of these disasters induced a 12% significant reduction of the GDP of Peru.

Considering the societal concern, recent studies have thus been devoted to inferring precipitation in Peru on the basis of seasonal forecast products from climate models (Lagos *et al.*, 2008). The approach consists in building a statistical model between local precipitation as inferred from observations and climate indices as derived from sea surface temperature (SST) of the tropical Pacific predicted by the seasonal forecast systems (e.g. NCEP). Lagos *et al.* (2008) showed that this can provide a useful approach for predicting extreme events at least, although some indices (i.e. NINO1 + 2) may not be as reliable as others (i.e.

*Correspondence to: Luc Bourrel, UMR 5563 GET, Université de Toulouse – CNRS – IRD – OMP – CNES, 14 Avenue Edouard Belin, Toulouse 31400, France.
E-mail: bourrel@get.obs-mip.fr

NINO3.4, NINO4) for precipitation predictions in Peru. The skill of the forecast system is also highly dependent on the selected predictors and statistical method. For instance, the linear assumption, often used for the statistical approach, is certainly not the most appropriate for predicting precipitation in Peru, because El Niño Southern Oscillation (ENSO) has a strong positive asymmetry (evidenced by the extreme warm events) reflecting the nonlinearity in the system (An and Jin, 2004). Recent studies have revealed that there are also different types of El Niño events that have distinct characteristics in terms of atmospheric teleconnections (Yeh *et al.*, 2009), frequency (Kim and Yu, 2012) and oceanographic manifestations off Peru (Dewitte *et al.*, 2012). Two types of El Niño events have been documented so far in the literature (Ashok *et al.*, 2007; Kug *et al.*, 2009): the so-called Cold Tongue El Niño or eastern Pacific El Niño (hereafter EP El Niño) that corresponds to extreme warm events developing strong SST anomalies in the eastern equatorial Pacific and the Warm Pool El Niño or central Pacific El Niño (hereafter CP El Niño) that corresponds to standing warm SST anomaly development in the central equatorial Pacific, within the so-called Warm Pool region. In a recent study, Takahashi *et al.* (2011) suggest that the dominant mode of variability in the equatorial Pacific is in fact associated to a regime that encompasses the CP El Niño and that the EP El Niño events are extreme events, which are by definition much rarer than CP El Niño events. This view has of course implications for the study of the ENSO teleconnection pattern over Peru for precipitation because CP El Niño events are characterized by weak anomalous SST conditions off Peru compared with EP El Niño (Dewitte *et al.*, 2012).

In addition, ENSO is a non-stationary phenomenon (Boucharel *et al.*, 2009) having a significant modulation of its characteristics (amplitude, frequency and asymmetry) at decadal timescales (Guilderson and Schrag, 1998; Torrence and Compo, 1998). For instance, there has been a climate shift in the 1970s from when EP El Niño events became stronger (Miller *et al.*, 1994). The 1980s and 1990s are in fact the decades over which the relationship between ENSO and hydrology (precipitations and discharges) in Peru (Lagos *et al.*, 2008; Lavado *et al.*, 2013), in Chile (Montecinos and Aceituno, 2003) and in Ecuador (Bourrel *et al.*, 2010; 2011) is the most significant because of the strong signature on the regional circulation of the two extreme events of 1982/1983 and 1997/1998. Over the last two decades, the CP El Niño has however become more frequent relatively to the EP El Niño (Yeh *et al.*, 2009; Lee and McPhaden, 2010; Takahashi *et al.*, 2011). Such change in the ENSO characteristics has been shown to modify features of the equatorial oceanic and atmospheric circulation in the

Pacific, i.e. the oceanic equatorial Kelvin waves (Dewitte *et al.*, 2012) and the intraseasonal atmospheric variability (Gushchina and Dewitte, 2012) including the Madden and Julian Oscillation (MJO) (Madden and Julian, 1972).

All these aspects of the change in ENSO properties have been somewhat overlooked in studies addressing the impact of ENSO on the precipitations along the coast of Peru, although they can provide guidances for refining current forecasting strategies aimed at improving resource management (agriculture and water resources).

In this paper, our motivation is to revisit the relationship between ENSO and precipitations along the coast of Peru, taking into account different aspects of its manifestations on SST and in the atmosphere in the tropical Pacific, as well as its low-frequency property changes, in particular the increased occurrence of CP El Niño in recent decades (Lee and McPhaden, 2010; Takahashi *et al.*, 2011). In that sense, our study extends the ones by Lagos *et al.* (2008) and Lavado *et al.* (2013). Because of the interplay between large-scale and regional oceanic conditions, such relationship is thought to result from the nonlinear interaction between local and remote influences, which a study based on a diversity of indices may help to disentangle. For instance, precipitation events in the Piura region (5°S) are associated to SST warm episodes along the coast that are not necessary related to EP El Niño events (Woodman, 1985). Simply, former studies have focused on extreme El Niño events that caused large economic losses for Peru, but little has been said on moderate events. In a context of climate change, there is also a clear need to better understand the natural low frequency of the teleconnection pattern. Here, we take advantage of a long-term data record and a revisited interpretation of the ENSO variability over the last five decades, where ENSO is viewed as two distinct and independent regimes, one associated to extreme events, i.e. the case of the 1982/1983 and 1997/1998 strong El Niño events, and the other one associated to moderate warm event and La Niña events (Takahashi *et al.*, 2011).

The paper is organized as follows. The data and methodology used in this study are described in the Data and Methodology sections. We provide the results in the Results section and the conclusions in the Conclusions section.

DATA

Digital elevation model

The digital elevation model is obtained from 90-m resolution SRTM data (Shuttle Radar Topography Mission, NASA-NGA, USA) and is available from <http://srtm.csi.cgiar.org/SELECTION/inputCoord.asp>. It allows delineating the major river watersheds from highlands limits between

Pacific and Amazon basins to the Pacific coast and also allows checking the location of the meteorological stations.

Precipitation data

Monthly rainfall data were provided by SENAMHI (National Service of Meteorology and Hydrology of Peru). The longest period available corresponds to 48 years from 1964 to 2011, but some rainfall stations present missing information. Therefore, our database includes 52 meteorological stations with a maximum of missing information

around 5% covering the whole Peruvian coast from northern to centre.

The stations are located along all the Pacific coast and their elevations vary from 1 (e.g. Puerto Pizarro station) to 4406 m asl (e.g. Choclococha station). Because of this latitudinal and altitudinal dispersion (Figure 1), we propose a standard process for data quality assessment, data completion and regionalization processes.

We defined regions for grouping stations into climatological homogeneous zones, on the basis of the regional

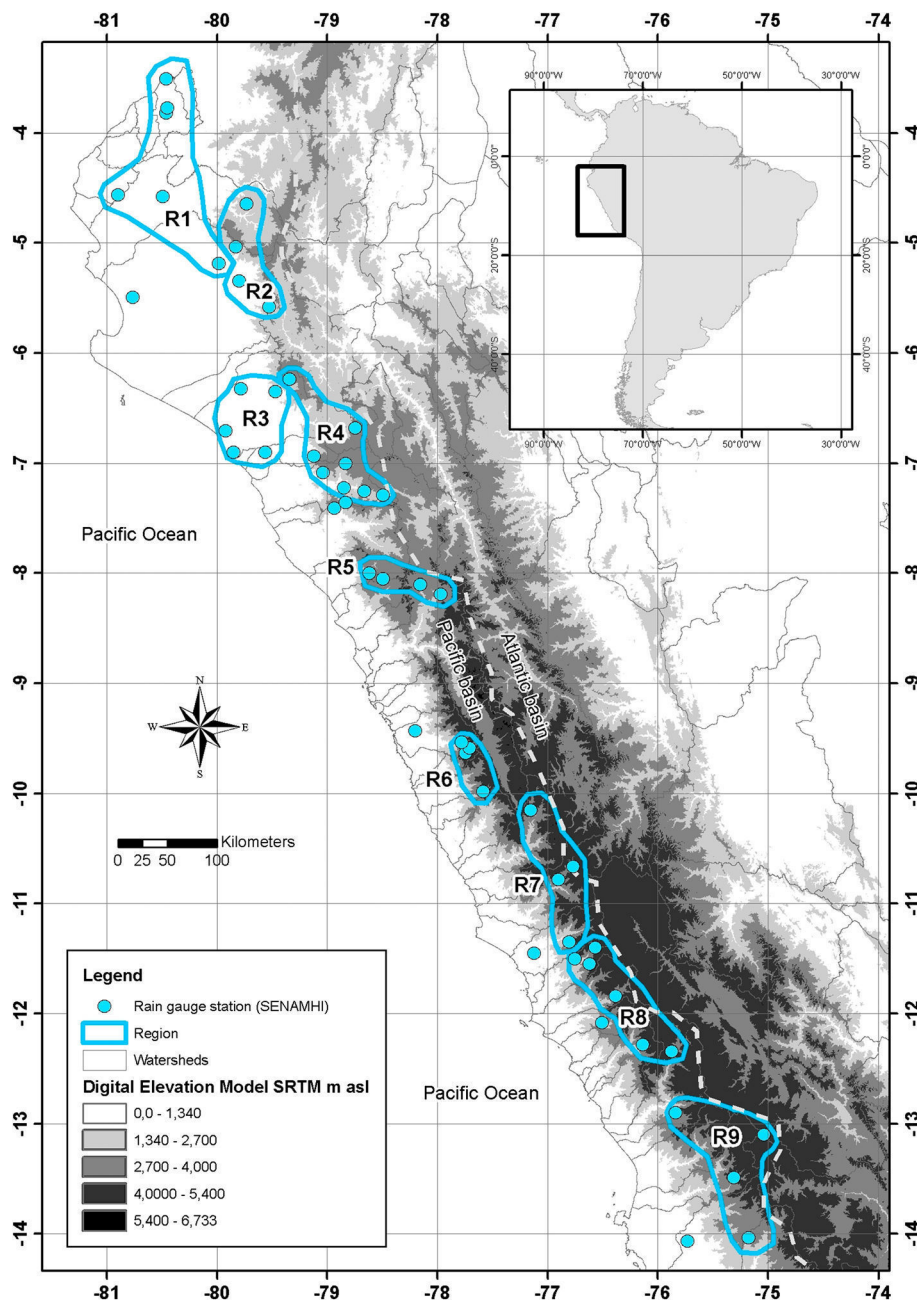


Figure 1. Altitude and location map of the meteorological stations (*in situ* data, SENAMHI). Location of the nine regions (cyan contours). The heights come from the digital elevation model SRTM with 90 m of resolution

vector methodology (Brunet-Moret, 1979), which consists in assuming that for the same climatic zone under the same rainfall regime, the total annual rainfall is pseudo proportional, with a little random variation due to rain distribution in the zone. Then, we complete our series and obtain for each region a representative time series. The algorithm is briefly described as follows:

1. Identification of regional vectors by considering the statistical and hydrographic criteria (elevation, watershed boundaries and latitude). Here, we use a linear correlation between the regional vector obtained and the series of months to complete.
2. If a significant correlation is not reached, we conducted an analysis of linear correlation between the stations of a region for a given month.
3. If a significant correlation is not reached at level 2, we compared monthly hyetographs between neighbouring stations of a region and complete the missing monthly data.
4. Finally, in the case of a normal event (i.e. not El Niño event), we reconstructed the series replacing each monthly precipitation value by the corresponding interannual mean monthly value calculated for all the periods (including an arbitrary small noise on the mean and standard deviation of the value).
5. Otherwise, it is not recommended to complete the missing months.

Once the data completion process is validated, we estimated the average monthly precipitation for each region for the entire period of 48 years, using classical interpolation methods such as Thiessen, inverse distance and Kriging. To present our results, we used the Kriging technique, which leads to the most accurate estimates (von Storch and Zwiers, 2003).

For all our study, we used the yearly averaged precipitation data, which correspond to the annual hydrological cycle spanning from September to August.

ENSO indices

We use classical monthly ENSO indices (Kiem and Franks, 2001) derived from databases of the NOAA (Climate Prediction Center): SST 1 + 2 (NINO 1 + 2), SST 3 (NINO 3), SST 4 (NINO 4), SST 3.4 (NINO 3.4) and Southern Oscillation Index (SOI). We used non-standardized monthly anomalies.

The preliminary stage is to identify periods of extreme ENSO events (El Niño and La Niña), using the distribution of positive or negative values of each of conventional indices used to characterize ENSO (SOI and SST); in the same way, we also identified these periods from excesses and deficits of precipitation on each region.

Former studies show that there is a close relationship between the development of El Niño and a SOI fall (negative values) and an increase (positive values) of SST indices (Lagos and Buizer, 1992; Lagos *et al.*, 2008; Lavado *et al.*, 2013). Kiem and Franks (2001) mention two methods for identifying ENSO events. The first method consists in identifying the years when the SOI is above or below its average value for a minimum period of 5 months consecutive. The second method is the same as the first method but using indices based on SST anomalies instead of the SOI index.

Whereas these indices are commonly used for ENSO impact studies, they are not completely appropriate for characterizing the different types of El Niño that have been documented in recent years (Ashok *et al.*, 2007; Kug *et al.*, 2009). In our study, in the aim to select the ENSO indices that best explain the precipitation, we performed the principal component analysis (PCA) method (see more details on the PCA method in the Principal Component Analysis section). It is illustrated in Figure 2 that most indices have a large projection on SST3 (i.e. the angle between the indices and SST3 is less than 45°), which indicates that they are all highly correlated. Only the SST1+2 index that accounts for extreme and/or coastal El Niño has a weak projection on the SST4 index (i.e. the two indices are almost orthogonal).

In a recent study (Takahashi *et al.*, 2011), two new indices were proposed, the so-called E and C indices that can describe two regimes of variability accounting for extreme warm events (or EP El Niño) and moderate events (La Niña and CP El Niño), respectively. These

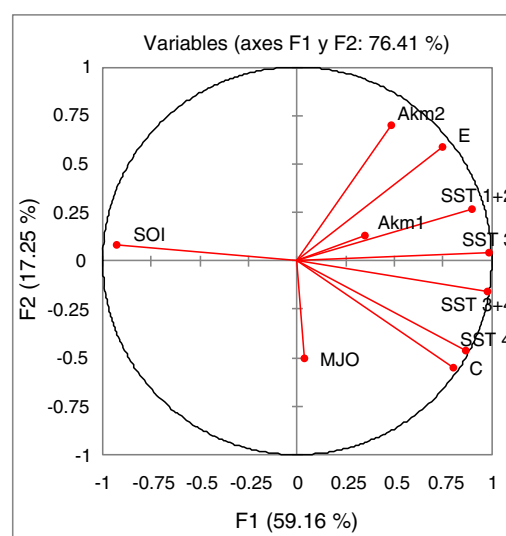


Figure 2. Projection of El Niño Southern Oscillation indices into a principal component analysis (PCA). Note that the E and C indices are by construction orthogonal on the basis of the monthly averaged data. For the PCA, averaged data from September to February were used

indices are by construction independent (orthogonal). They are comparable with the SST1 + 2 and SST4 indices respectively (Figure 2). The E index accounts for the SST variability in the far eastern Pacific and captures very clearly the two strong El Niño over the data record used in this study, namely, the 1982/1983 and 1997/98 El Niño. Therefore, correlation analysis using this index will emphasize the relationship for extreme events. By construction, the C index is orthogonal to the E index, the correlation analysis using this index will emphasize the relationship between precipitation variability and moderate El Niño and La Niña events. Note that the E and C indices were calculated from monthly mean values and we considered the mean over SONDJF for the PCA (Figure 2), so that they do not appear strictly orthogonal.

MJO and equatorial ocean Kelvin wave activity indices

The motivation for using such indices lies in part to the possibility that different regimes of atmospheric circulation may take place over the different regions because of their distinct elevation. In particular, the western coast of Peru is embedded in the large-scale subsidence zone corresponding to the descending branch of the Walker circulation, leading a shallow marine boundary layer propitious to the development of low-level clouds. Thus, conversely to the region over the Andes where deep convection and advection of humidity from the Amazon basin can take place, the coastal region is characterized by a relatively stable air column, implying dry mean conditions. Still, at 2000 m asl, deep convection associated to large-scale disturbances (e.g. MJO) or/and orographic-induced circulation can take place, which is associated to precipitation. On the other hand, where SST near the coast reaches a threshold from which deep convection can occur, local precipitation events can be generated. Such events may be thus triggered by SST anomalies induced by the crossing of equatorial Kelvin waves.

MJO activity index. Atmospheric circulation in the region of Peru is also influenced by atmospheric conditions not necessarily directly related to ENSO but to local ocean conditions in the central-western Pacific. The MJO (Madden and Julian, 1972) is a tropical global scale atmospheric disturbance and the dominant tropical intraseasonal mode. It is a key source of untapped predictability in both the tropics and extratropics (Wheeler and Kiladis, 1999; Wheeler and Weickmann, 2001; Waliser *et al.*, 2003; Waliser, 2005; Gottschalk and Higgins, 2008). The MJO can propagate from the western Pacific to the South American continent, which can alter the tropospheric circulation all over the tropical band, with a potential impact on precipitation over the South American continent. Because MJO is a circumnavigating wave, it can modify the regional

atmospheric circulation in northern Peru by altering the well-stratified air above a shallow inversion zone in this region due to the coastal upwelling. In particular, the inversion zone near the coast lies around the 900 hPa isobar below which low clouds (stratocumulus) generally develop. MJO-related variability is also found in the mid-latitudes of the Southern Hemisphere and modulates the South-Pacific anticyclone, which variability is influential on the atmospheric circulation off central Peru (Dewitte *et al.*, 2011a, b). At last, MJO is tightly linked to ENSO (Roundy and Kiladis, 2006), and its activity may also reflect ENSO property changes (Gushchina and Dewitte, 2012).

In this study, we use an MJO activity index following the method by Wheeler and Kiladis (1999), which consists in extracting the energy bivariate space–time spectral analysis (Hayashi, 1982) of outgoing longwave radiation in the frequency-space domain of the MJO over the tropical belt. The MJO-filtered time series is then used to define an MJO activity index by taking the variance over a 3-month running window and averaging over the region where its variability peaks. Typically, an MJO activity index is defined by averaging over the western central Pacific along the equator (5°S–5°N; 120°–180°E) (McPhaden *et al.*, 2006; Gushchina and Dewitte, 2012). We choose here to remove the annual cycle by a wavelet multiresolution filtering (Labat *et al.*, 2000). Summarizing the MJO activity index used in the paper accounts for the periods when there is an enhanced or reduced variability of the MJO. When this index is larger than usual (positive anomaly), this means that more high-frequency fluctuations of tropical Pacific origin may reach the Peru coast and lead to precipitation anomalies on average along the coast.

Oceanic regional indices. The MJO is also associated to the formation of Westerly Wind Burst (Vecchi and Harrison, 2000) in the equatorial western central Pacific that can trigger planetary oceanic waves, called equatorial Kelvin wave. The energy of these planetary oceanic waves is within the intraseasonal frequency band, i.e. $\sim [2\text{--}120] \text{ days}^{-1}$ (Dewitte *et al.*, 2008). We will refer to these intraseasonal Kelvin waves as intraEKW hereafter. They should not be confused with the interannual Kelvin waves that are forced when El Niño develops, i.e. when the atmospheric circulation in the tropics interacts with the warm SST anomalies, leading to energetic westerlies at interannual timescales. The interannual Kelvin waves, named interEKW hereafter, are tightly linked to ENSO in the tropical Pacific and therefore do not convey more information than say the E and C indices. The intraEKW is active also during ENSO but presents a seasonal modulation depending on the nature of ENSO (Gushchina and Dewitte, 2012). It propagates from the central Pacific to the coast of Ecuador and locally can modify the

oceanographic conditions along the coast of Peru (Dewitte *et al.*, 2012). For instance, a downwelling intraEKW (i.e. which deepens the thermocline) can produce a warming event along the coast of Peru (see Mosquera *et al.* (2013) for the 2002 El Niño), which in turn may favour local convection leading to intense rainfall events (Woodman, 1985). Therefore, change in intraEKW activity can be reflected in the precipitation fluctuations at interannual timescales through its impacts on coastal SST. The intraEKW may be associated to episodic warm/cold events along the coast that are not related in a straight-forward manner to ENSO. In this study, we define an intraEKW cumulative index that is aimed at quantifying the integrated effect of an intraEKW along the coast. The concept is similar to cumulative upwelling index defined by Bograd *et al.* (2009) but for the oceanic Kelvin wave is based on the idea that, whereas a downwelling intraEKW will favour a warming along the coast, the opposite phase (upwelling) will induce cooler conditions along the coast, not favourable for precipitation. Over a year, the cumulative effect of the intraEKW can be estimated by considering the integration of the skewness of the intraEKW over the period that encompasses the Austral summer season (i.e. when intraEKW activity usually peaks, cf. Dewitte *et al.* (2011a, b)). This index is therefore defined as

$$C_{EKW}^n(y) = \int_{D-6}^{D+6} (\text{IntraEKW}^n(x = 90^\circ W, t))^3 \cdot dt \quad (1)$$

where D is the month of December of the year y , t is in days and n refers to the type of the waves. Two types of waves will be considered here that differ from their vertical structure and phase speeds along the equator. These waves, which are the most energetic in the equatorial Pacific, will

be referred to as $n=1$ or $n=2$ waves (i.e. EKW1 and EKW2). Note that the C_{EKW}^1 (hereafter Akm1) and C_{EKW}^2 (hereafter Akm2) indices also reflect the ENSO amplitude and evolution at basin scale because intraEKW is linked to ENSO (Hendon *et al.*, 2007; Gushchina and Dewitte, 2012).

The intraEKWs are derived from an oceanic reanalysis (SODA) over the period 1958–2008. The method consists in projecting the zonal current and pressure anomaly field on the theoretical wave structures as estimated from the mean stratification of the oceanic reanalysis. Details on the method can be found in Dewitte *et al.* (2008).

We worked with the ten indices described earlier (see Table I for a summary). However, considering the inter-relationship between indices, we will focus on five indices that exhibit significant correlation with precipitation fluctuations. Please note that all the results presented in this paper correspond to the yearly averaged data, from September to February for the ENSO indices.

METHODOLOGY

Principal component analysis

The selection of ENSO indices that best explain rainfall indices was performed using the PCA, a factorial method of data analysis, which explores the connections between variables to be studied as a whole, to highlight possible correlations (Lagarde, 1983; von Storch and Zwiers, 2003).

The wavelets and coherence analysis

To study the periodicity of the series (ENSO indices and precipitation), we used wavelet analysis. For a more extensive review of wavelet theory and applications, the reader is referred to Labat *et al.* (2000) or Labat (2005).

Table I. List of indices used in the paper

Name	Methods	Aims	Data sources	References
SST1 + 2 SST3 SST3.4 SST4 SOI	Averaged SST over tropical Pacific sectors Based on pressure level differences between Tahiti and Darwin locations in the tropical Pacific.	Characterizing the El Niño with classical indices Characterizing the El Niño canonical	ERSST.V3B NOAA	Kiem A. and Franks S (2001) Rasmusson and Carpenter (1982)
E/C	Based on the first two EOF modes of SST in the tropical Pacific	Characterizing the two types of El Niño	HadiSST	Takahashi <i>et al.</i> (2011)
MJO	Wavelength–frequency (w-k) decomposition and recomposition in the MJO w-k domain	Characterizing regional atmospheric circulations related to MJO	NCEP/NCAR reanalysis	Wheeler and Kiladis (1999)
Akm1/Akm2	Two baroclinic modes, Akm1 and Akm2 are considered as the most energetic Kelvin waves	Characterizing oceanographic conditions related to El Niño and coastal SST anomalous conditions	Simple Ocean Data Assimilation (SODA) reanalysis	Dewitte <i>et al.</i> (2008)

The basic aim of wavelet analyses is both to determine the frequency (or scale) content of a signal and to assess and determine the temporal variation of this frequency content (Heil and Walnut, 1989). Therefore, the wavelet transform is the tool of choice when signals are characterized by localized high-frequency events or when signals are characterized by a large number of scale-variable processes. Because of its localization properties in both time and scale, the wavelet transform allows for tracking the time evolution of processes at different scales in the signal. This time-scale wavelet transformation $C_{\psi}^x(a, \tau)$ is defined in the case of a continuous time signal as

$$C_{\psi}^x(a, \tau) = \frac{1}{\sqrt{a}} \int_{-\infty}^{+\infty} x(t) \cdot \psi^* \left(\frac{t - \tau}{a} \right) dt \quad (2)$$

where $*$ corresponds to the complex conjugate. The function $\psi(t)$, which can be real or complex, plays the role of a convolution kernel and is called a wavelet.

The parameters a and τ are used to adjust the shape and location of the wavelets respectively in scale and time domains. Changing t , e.g. allows for moving the centre of the wavelet. Then, the wavelet transform is a sort of microscope with magnification $1/a$ and location given by the parameter τ .

Then, another concept is also used: the wavelet coherence. Classically, the notion of coherence in signal processing consists of a measure of the correlation between two signals or between two representations of these signals.

Here, we will use the wavelet coherence of two signals defined by Torrence and Webster (1999). They propose to determine wavelet coherence between two signals $X(t)$ and $Y(t)$ using a smooth estimate of the wavelet spectrum and to define a smooth wavelet spectrum and cross spectrum, respectively noted $SW_{XX}(a, \tau)$ and $SW_{XY}(a, \tau)$

$$SW_{XX}(a, \tau) = \int_{t-\delta/2}^{t+\delta/2} W_{XX}^*(a, \tau) W_{XX}(a, \tau) da d\tau \quad (3)$$

$$SW_{XY}(a, \tau) = \int_{t-\delta/2}^{t+\delta/2} W_{XX}^*(a, \tau) W_{YY}(a, \tau) da d\tau \quad (4)$$

The scalar δ represents the size of the two-dimensional filter, used for time and scale averaging as a necessary step for coherence calculation. The wavelet coherence WC can then be defined by analogy with Fourier coherence as

$$WC(a, \tau) = \frac{|SW_{XY}(a, \tau)|}{\sqrt{[|SW_{XX}(a, \tau)| \cdot |SW_{YY}(a, \tau)|]}} \quad (5)$$

A temporal mean of the wavelet coherence can also be relevant in order help to identify ENSO indices that have a major influence on precipitation variability from a global point of view.

Correlation analysis

The correlation analysis is used to estimate the ENSO–precipitation relationship. The significance of the correlation coefficients was estimated using a t -test.

Correlation analysis was first performed for the monthly averaged anomalies relative to the mean seasonal cycle over the whole record. Because the rainy season for the coastal regions is concomitant with the periods when precipitation anomalies are the strongest, the results are similar if the correlation analysis is performed for the yearly averaged data, which corresponds to the annual hydrological cycle spanning from September to August. ENSO indices were averaged over September to February, which corresponds to the ENSO extended peak phase. The results of the correlation analysis presented in this paper correspond to the yearly averaged data, respectively from September to August for precipitation and from September to February for the ENSO indices.

RESULTS

Regionalization of precipitations

The basin's mean altitude levels vary from the sea level up to more than 4000 m (Andes). In some cases, there are glaciers and peaks above 6000 m. Hydrological year covers the period from September to August for all the watersheds and does not change with latitude.

Using the regional vector methodology, nine climatically homogeneous regions (R1 to R9) are identified. We can note that there are five rainfall gauge stations along the coast (northern to centre) that do not belong to any of nine regions identified with the regional vector because they present a strong intermittent regime. Anyway, we have taken into account these five stations in Figure 3b to complete our downstream dataset along the coast. In the rest of the study, these five isolated rainfall gauges are not considered. We only work with the nine identified regions.

According to Figure 1 and Table II, each region is characterized by an uninterrupted series of mean monthly precipitation considering the full set including the years of strong El Niño events, namely, 1982/1983 and 1997/1998. Table II shows two series (including and excluding the strong ENSO episodes) of the yearly averaged data over 1964–2011 period, and we show on Figure 3a the mean monthly rainfall distribution for the nine regions not considering ENSO events.

In Figure 3b, we can see that the nine regions are distributed in two groups of regions corresponding to downstream regions (R1 and R3 and remaining stations, located along the coast region) and upstream regions (R2, R4 to R9 located in the Andean slopes) from north to south. Downstream (upstream) regions are located below (above) an altitudinal level around 1500 m asl (Table II)

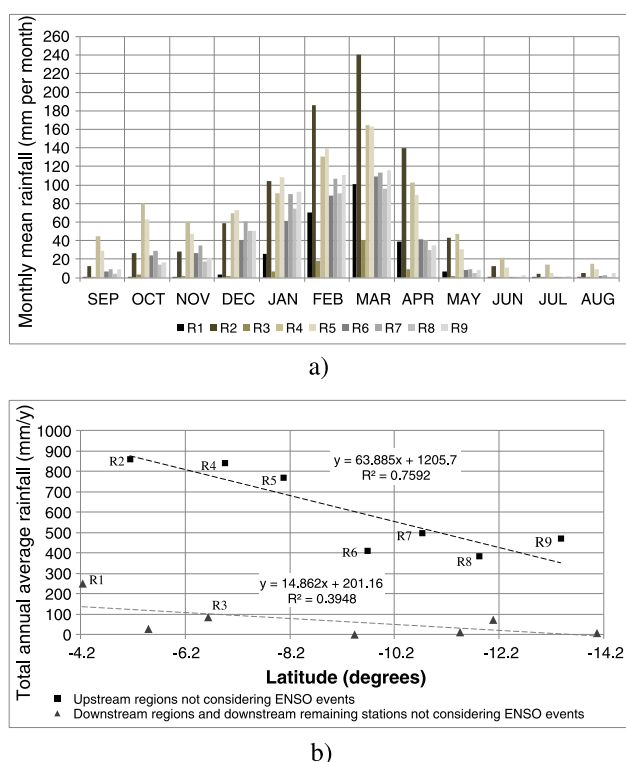


Figure 3. a) Mean monthly rainfall values for the nine regions not considering strong El Niño events (1982/1983 and 1997/1998). b) Total annual rainfall versus latitude (not considering El Niño Southern Oscillation events) showing two groups clearly defined coinciding with upstream and downstream areas

and characterized by a yearly average rainfall below (above) 300 mm/year (Figure 3b).

Figure 3b illustrates too that the annual precipitation increases with the altitude (Table II) and decreases with latitude (from north to centre).

Coherence between ENSO indices and precipitation series

Wavelet analysis for precipitation series (from R1 to R5) through the scale band between 2 and 16 years has allowed identifying clearly the strong events over the

period 1964–2011, which are the 1982/1983 and 1997/1998 El Niño events (see Figure 4a for R1). Without considering these strong events, we can identify events of lower intensity and higher frequency (see Figure 4b for R1). We also note that the influence of these strong events is not clear from R6 to R9 (see Figure 4c for R6). For all nine regions, the major peaks are located in the period bands of 2–4, 4–8 and 8–16 years. We implement the classical statistical significance estimation based on comparison with red noise (Torrence and Webster, 1999). We choose here an 80% statistical significance based on the relative shortness of the data. For example, similar statistical significances were used by Labat (2006). The 80% threshold was chosen here in order to get statistical significance on all the three peaks mentioned (2–4, 4–8 and 8–1 years).

In the same way, the ten ENSO indices for the period 1964–2011 show that ENSO events are also associated to periods in the range of 2–4, 4–8 and 8–16 years. These results are consistent with those of other authors (Diaz and Markgraf, 2000), which showed that the ENSO periodicity has three dominant modes of frequency variation: quasi-biennial, quasi-quadrennial and quasi-decadal (see Figure 4d for E index). That also confirms that the quasi-biennial and quasi-quadrennial modes are dominant in the Intertropical Convergence Zone (Lagos and Buizer, 1992).

The wavelet analyses suffer here from the classical ‘cone influence issue’, i.e. the region of the wavelet spectrum in which edge effects become important and make questionable the possible interpretation of the wavelet analysis. Then, the wavelet analysis gives only unquestionable results on the 1977–2000 interval for scales larger than 16 years. Therefore, even though if the validity of the presence of the 16-year oscillation may be questionable, the absence of discontinuity in the 16-year spectral band on the time intervals corresponding to the cone of influence suggests that this oscillation is present over all the 1964–2011 time interval.

Table II. Description of the nine climatically homogeneous regions

Region	Mean latitude (south)	Minimal elevation (m asl)	Maximal elevation (m asl)	River watershed	Total annual rainfall including El Niño years (mm)	Total annual rainfall excluding El Niño years (mm)
R1	4.23°	1	440	Tumbes-Piura	386.8	250.5
R2	5.15°	480	2740	Chira-Piura upstream	924.6	862.0
R3	6.63°	18	500	Chancay	130.4	86.7
R4	6.96°	850	3030	Motupe-Jequetepeque	861.7	841.3
R5	8.08	2580	3460	Moche-Nord Santa	779.9	769.1
R6	9.68	2285	3570	Casma-Huarmey	420.4	409.2
R7	10.74°	2333	3950	Pativilca-Huaral	498.7	498.5
R8	11.82°	2479	3875	Chillon-Cañete upstream	384.1	384.5
R9	13.38°	2533	4406	Cañete-Ica	467.6	470.7

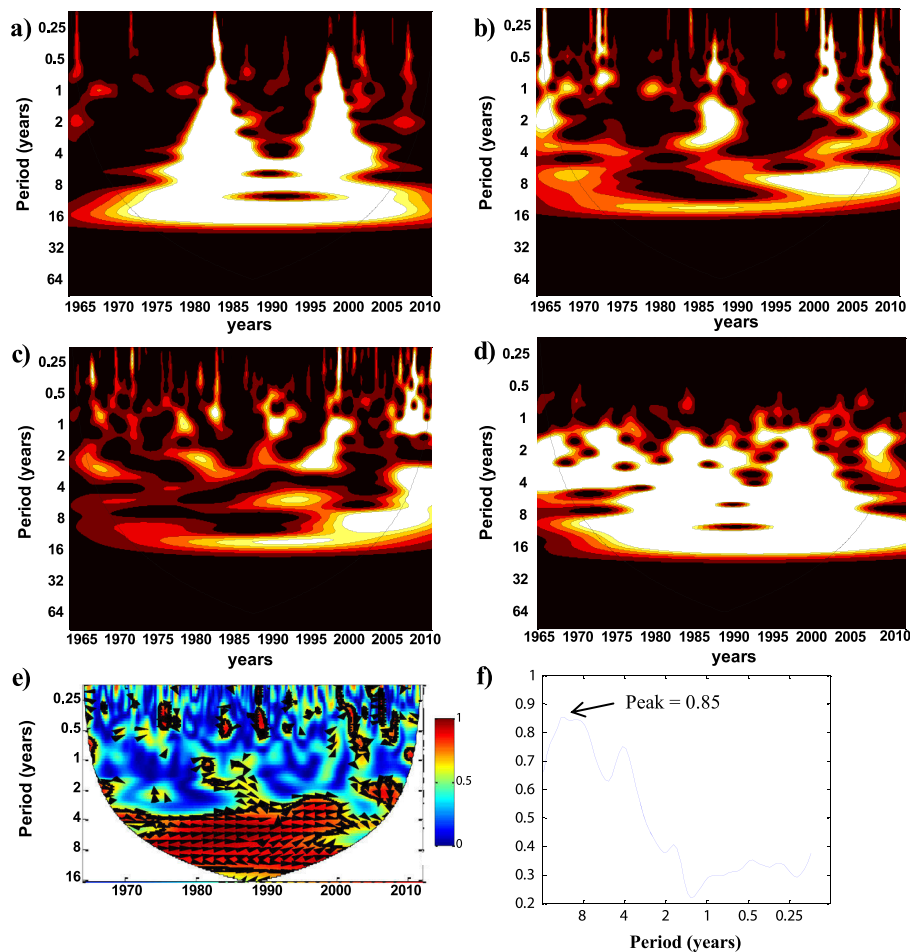


Figure 4. a) Wavelet of R1 precipitation, b) wavelet of R1 precipitation not considering strong El Niño events, c) wavelet of R6 precipitation, d) wavelet of E index, e) wavelet coherence between E index and R1 precipitation and f) mean coherence peaks for wavelet coherence between E index and R1

The wavelet coherence analysis between ENSO indices and precipitation series allowed us to quantify the relation between an ENSO index and precipitation over a region. The vectors in black on Figure 4e indicate the values of the phase shift between two time series. Thus, a vector pointing to the right shows a direct relation, whereas a vector pointing left indicates an inverse relation (negative correlation). Figure 4e displays the wavelet coherence of R1 precipitation and E index, which shows a strong coherence (red coloration); the average maximum coherences are above 0.8 for periods of 4–16 years (Figure 4f), for quasi-decadal and quasi-quadrennial periods with a change of phase (change of direction of the arrows) in periods of 8–16 years.

Table III provided the values of maximal coherence for all regions. Interestingly, all maximal coherences are found at the decadal frequency, which indicate that the low-frequency ENSO modulation is the most influential on precipitation along the coast of Peru. This justifies the selection of sub-periods for the correlation analysis (refer to succeeding text). The results also indicate that some

indices are more relevant for the northern part of Peru (SST 1 + 2, SST 3), whereas others are more relevant for regions of central Peru (SST4, SST 3.4). Not surprisingly, the E index exhibits a large coherence from north to centre (R1 to R5) because it accounts for extreme warm events. For MJO, the values of highest coherence are located on the upstream basins (R2, R4, R5 and R6, values between 0.62 and 0.79) consistent with the expectation that MJO is influential at relatively high altitudes. For oceanic indices, the Akm1 index is more influential in the north and in the basins downstream of R1 and R3, whereas the Akm2 index has the largest coherence with R1 and R2. Coherence values for the region R9 are not significant for any index: they are lower than 0.50, and the highest is that of the MJO (0.49).

Low-frequency modulation of ENSO and precipitation regime

The two main climate shifts in the tropical Pacific over the last five decades include the 1976/1977 climate shift (Miller *et al.*, 1994; others) and, more recently documented,

Table III. Summary of maximal coherences for each region (in all cases, coherences correspond to quasi-decadal frequency)

Latitude °sur	Region	Wavelet coherence ENSO indices with maximal coherences (c)
4.23°	R1	SST 1 + 2 (c = 0.84), SST 3 (c = 0.69), SST 4 (c = 0.61), SST 3.4 (c = 0.65), MJO (c = 0.55), SOI (c = 0.58), E (c = 0.85), C (c = 0.73), Akm1 (c = 0.68), Akm2 (c = 0.70)
5.15°	R2	SST 1 + 2 (c = 0.62), SST 4 (c = 0.58), MJO (c = 0.72), E (c = 0.83), C (c = 0.68), Akm2 (c = 0.54)
6.63°	R3	SST 1 + 2 (c = 0.54), SST 4 (c = 0.53), MJO (c = 0.66), E (c = 0.79), C (c = 0.65), Akm1 (c = 0.60)
6.96°	R4	SST 4 (c = 0.55), SST3.4 (c = 0.50), MJO (c = 0.69), E (c = 0.59), C (c = 0.50)
8.08	R5	MJO (c = 0.62), E (c = 0.66)
9.68	R6	MJO (c = 0.79), E (c = 0.48)
10.74°	R7	SST 4 (c = 0.58), SST3.4 (c = 0.55), C (0.51)
11.82°	R8	SST 4 (c = 0.50), E (c = 0.71), C (c = 0.52)
13.38°	R9	SST 1 + 2 (c = 0.40), SST 4 (c = 0.40), MJO (c = 0.49)

the 2000 shift when the mean state became cooler (Tsonis *et al.*, 2007; Luo *et al.*, 2012; McPhaden, 2012; Xiang *et al.*, 2012; Hong *et al.*, 2013). Change in mean SST is influential on the teleconnection pattern and may impact precipitation at the regional scale. Here, as a first step, we consider three periods corresponding to these two transitions: P1 (1964–1976), P2 (1978–1999) and P3 (2000–2011). Instantaneous correlation analyses are carried out between the five indices (Table I) and the nine regions (Ri; $i = 1, 2, \dots, 9$). We retain results for the E, C, Akm1, Akm2 and MJO indices considering that the E and C indices grasp the behaviour of other indices based on SST through linear combination (Takahashi *et al.*, 2011) and that the other ones account for specific oceanographic and atmospheric processes (see section on Data). Figure 5 displays the results. For the P2 period, we provide statistics with and without extreme events, which indicates that the known relationship between precipitation and ENSO over northern Peru (Lagos *et al.*, 2008) is mostly the result of the influence of the two El Niño events of 1982/1983 and 1997/1998. For instance, the correlation over the regions R1 to R3 is above 0.7 for the E index and the Akm2 index when these events are considered (Figure 5a). These correlations remain hardly significant when the events are not considered (Figure 5b – middle). Interestingly, the MJO index is almost insensitive to the consideration of extreme events with correlation value above the significance level for all Ri except R1, whereas the C index exhibits a relatively large correlation (significant) in some regions when the influence of extreme events is removed.

Another interesting feature arising from the results of Figure 5 is the significant change in correlation according to the period under consideration for some indices. In particular, the C index and Akm1 index become more influential on precipitation during P3 on average over the regions. The C index exhibits a large correlation with precipitation over the regions R6 to R9 during P3. On the other hand, the MJO index exhibits a reduced correlation with precipitation over P3 compared with P2. Besides the low-frequency modulation of the correlation, a large latitudinal variability is also observed, which is difficult to interpret.

Regarding the oceanic Kelvin waves, first of all, from Figure 2, Akm1 and Akm2 indices have a comparable behaviour than the SST 1 + 2 and E indices, verifying their influence on coastal conditions changes. In particular, when we consider the strong El Niño events of 1982/1983 and 1997/1998 (Figure 5a), the Akm2 index has a comparable relationship with precipitation than the E index, i.e. large correlation in the northern part of Peru that decreases southward. The Akm2 index captures well the peak of strong El Niño (Dewitte *et al.*, 2012) where the Akm1 index is more relevant for intraseasonal Kelvin activity prior to the development of strong El Niño (Gushchina and Dewitte, 2012), which may explain its low correlation with precipitation over the period 1977–1999 dominated by strong El Niño activity. On the other hand, the influence of the first mode Kelvin wave (Akm1) on precipitation increases over the 2001–2011 period (Figure 5b) characterized by both occurrences of central Pacific El Niño and La Niña events. Its influence on precipitation is the largest for the southernmost regions (R6 to R9) and is comparable with the C index that grasps the central Pacific variability.

Considering the significant decadal variability in the relationship between ENSO and precipitation evidenced earlier, we now investigate if a long-term trend in this relationship can be observed in some regions. We consider here the E and C indices. The 11-year running correlation between these two indices and precipitations is presented in Figure 6a, b and c (this leads to a loss of 5 years in the beginning and at the end of the period). Here, again, we will consider the analysis without the 1982/1983 and 1997/1998 extreme events in order to highlight the change in teleconnection pattern associated to moderate warm events. This results in computing the correlation from nine points instead of 11 points over the periods that encompass the 1982/1983 and 1997/1998 El Niño events. Figure 6a indicates that no clear trend can be detected in most regions with a large meridional and temporal variability of the correlation. The E index accounts for SST variability in the far eastern Pacific that can be associated to intraseasonal

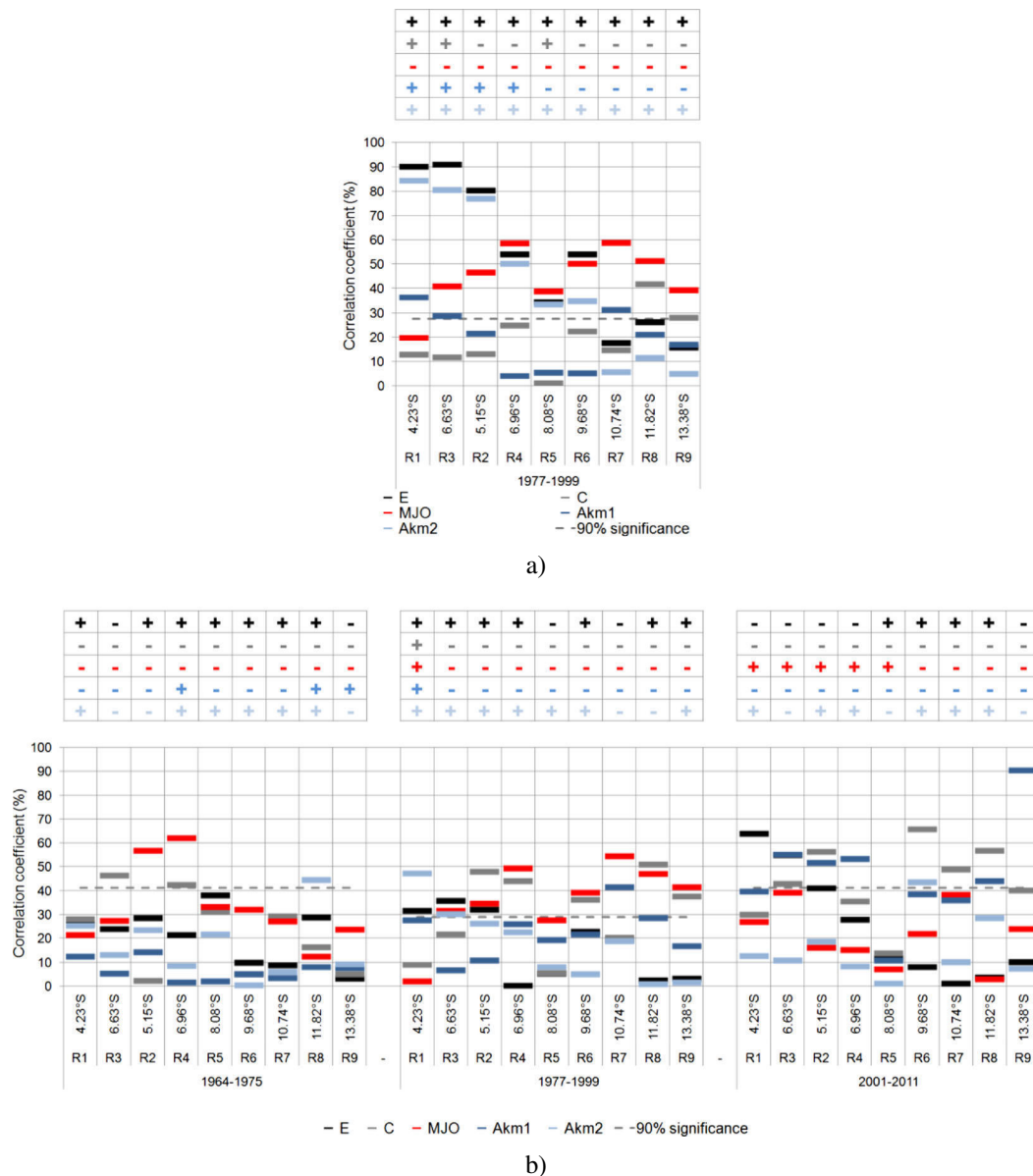


Figure 5. a) Correlation coefficients in absolute value expressed in % for the 1977–1999 period along latitude and b) *idem* for 1964–1975, 1977–1999 and 2001–2011 periods, but not considering strong El Niño events (1982/1983 and 1997/1998). The horizontal grey line indicates the significance level at 90%. For Akm1 and Akm2, data only extend until 2008. Absolute values of the correlation are considered to highlight variations as a function of periods. The sign of the correlation is indicated on top of each panel

Kelvin activity and the development of extreme El Niño events such as the 1982/1983 and 1997/1998 El Niño events. Because they are not taken into account in the calculation of Figure 6a, the variable correlation traduces local effects of the either intraseasonal Kelvin waves on SST or local atmospheric perturbations that modify SST along the coast. In order to illustrate the impact of the two extreme El Niño events, a figure similar to Figure 6a is presented to take them into account (Figure 6b). It clearly shows that statistics are completely changed when these events are considered, with a very high correlation between

the E index and precipitation all over the coast over the period encompassing these events. The central Pacific El Niño, accounted by the C index, is also characterized by a warming in the eastern Pacific but at a different time in the year (in Austral winter rather than in Austral summer) and with a much less amplitude characterized by a warming in the central Pacific (Dewitte *et al.*, 2011a, b). This warming in the eastern Pacific usually disappears after a few months, and cooling conditions develop (Dewitte *et al.*, 2012). Figure 6c displays the 11-year mean correlation between the C index and precipitation. It indicates a more

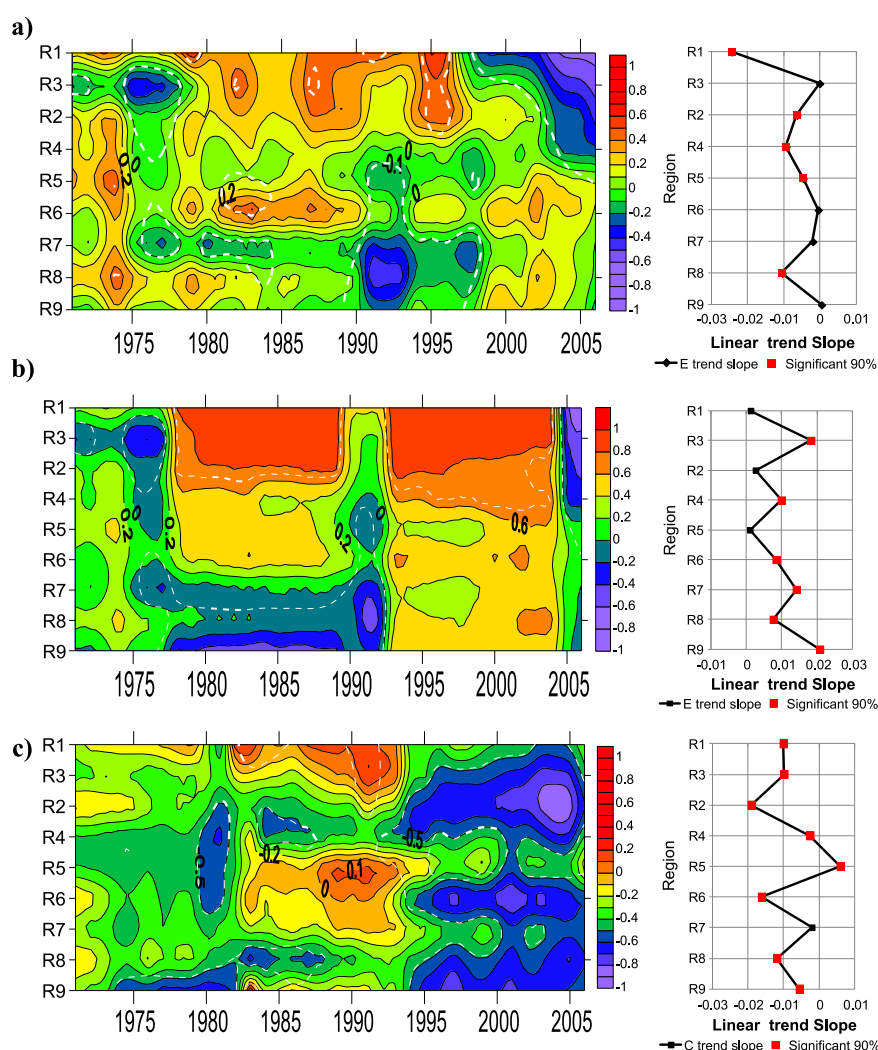


Figure 6. a) Eleven-year running correlation coefficients between the E index and precipitations within each region (R1 to R9) not considering the El Niño Southern Oscillation (ENSO) strong events of 1982/1983 and 1997/1998. The plot on the right hand side displays the slope of the linear trend of the running correlation (red dots indicate that the trend is significant at the 90% level using a student *t*-test). The white dashed lines indicate the significance level of the correlation at the 75% level. b) *Idem* for E index but considering the ENSO strong events of 1982/1983 and 1997/1998 and c) *idem* for C index not considering the ENSO strong events of 1982/1983 and 1997/1998

contrasted behaviour compared with the E index, with in particular a more clearer decadal modulation of the ENSO–precipitation relationship. In addition, the correlation is mostly negative indicating that central Pacific El Niño activity is associated to drier conditions along the coast of Peru. This situation is emphasized from the 1990s in particular for the regions R2, R6 and R9, with a marked negative trend of the running correlation. The strongest negative correlations and trends are found for the northern region R2 during the 2000s, which corresponds to the period of occurrence of only CP El Niño events.

Our aforementioned interpretation of the low-frequency changes in the relationship between the E and C indices and precipitation relies on the assumption that precipitation along the coast of Peru can be influenced by some aspects of the intraseasonal tropical variability both in the

ocean and the atmosphere. As a consistency check, we provide comparable analysis than Figure 6 but for the Akml and MJO indices (Figure 7). The results indicate that there is also a low-frequency modulation of correlation between the indices and precipitation. The negative trend is obvious for the Akml index because of the decrease in correlation from the 1990s in the central and southern regions. This is consistent with the interpretation that intraseasonal downwelling Kelvin wave activity during central Pacific El Niño (Gushchina and Dewitte, 2012) is enhanced, whereas the SST along the coast is reduced from the 1990s. Here, it is not possible to conclude if it is the La-Niña-like mean conditions (leading to cool conditions off Peru) from the 1990s or the coastal cooling associated to central Pacific El Niño that produce the decreased precipitation during

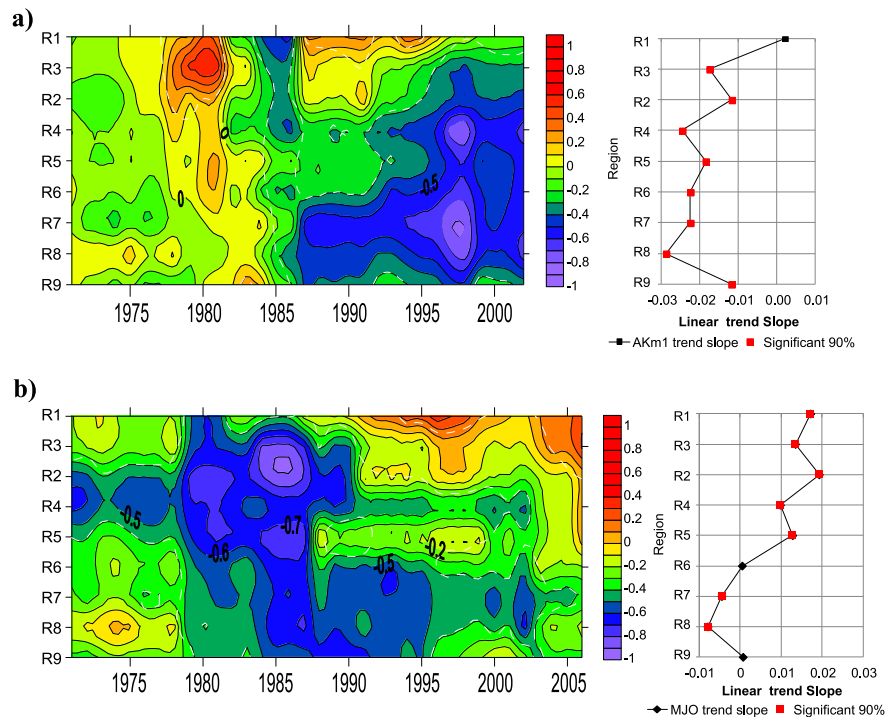


Figure 7. a) Eleven-year running correlation coefficients between the Akm1 index and precipitations within each region (R1 to R9) not considering the El Niño Southern Oscillation strong events of 1982/1983 and 1997/1998. The plot on the right hand side displays the slope of the linear trend of the running correlation (red dots indicate that the trend is significant at the 90% level using a student *t*-test). The white dashed lines indicate the significance level of the correlation at the 75% level. b) *Idem* for Madden and Julian Oscillation index

interannual events. Interestingly, the relationship between precipitation and the MJO index has an opposite trend (i.e. positive), which suggests that the MJO activity leads to increased precipitation in recent years, in particular in the northern regions.

CONCLUSIONS

In this paper, we used precipitation records from a network of 52 rainfall gauge stations located between 3.5°S and 14°S and from 0 to 4000 m from northern to centre of Peruvian Pacific coast over the period 1964–2011. A climate homogenization procedure, based on the regional vector methodology, allows inferring nine regions with monthly precipitation time series, estimated by Kriging interpolation, that exhibit a marked latitudinal variability in terms of mean precipitation. In particular, increased mean is observed in the northern regions compared with the central Peru regions, which is consistent with the larger oceanic influence on precipitation. Such meridional anisotropy is also found for the relationship between precipitation and ENSO consistent with previous studies (Lagos *et al.*, 2008; Lavado *et al.*, 2013). It is here shown that the strong positive relationship between precipitation and ENSO over the entire records results mostly from the

influence of the strong events of 1982/1983 and 1997/1998. Without considering these extreme events, the relationship between ENSO and precipitation exhibits a significant decadal modulation with the larger ENSO impact over the 1990s and afterwards. In particular, in the 2000s, the relationship between ENSO variability and precipitation reverses compared with the previous decade, i.e. El Niño occurrence is associated to reduced precipitation. This period is also associated to the occurrence of only CP El Niño events that are associated with neutral to cool SST anomalies along the coast of Peru.

A variety of ENSO indices, including the C and E indices recently defined by Takahashi *et al.* (2011), are used to estimate trends in the ENSO–precipitation relationship. We also use indices derived from equatorial oceanic Kelvin wave estimates in order to take into account oceanic influences not directly related to the interannual variability over the entire tropical Pacific. Oceanic Kelvin wave at intraseasonal timescales can in particular impact SST along the coast and modify the mixing in the marine boundary layer along the coast leading to either increased convection (mostly in the northern part of Peru) or increased stability under upwelling events (all along the coast). Our analysis indicates that in the recent decades, the ENSO influence on precipitation along the coast is characterized by an

inverse relationship, which results from both the increased occurrence of CP El Niño events that lead to cooler SST conditions off Peru (Dewitte *et al.*, 2012) and from the influence of La Niña events and upwelling events. The mean SST off Peru has cooled in the recent decades (Gutierrez *et al.*, 2011; Dewitte *et al.*, 2012). A shift towards cooler conditions in the 1990s is also observed in the mean state of the tropical Pacific (Hong *et al.*, 2013) that is suggested to be concomitant to the increased occurrence of CP El Niño (Chung and Li, 2013). So, both changes in mean upwelling and in upwelling variability may contribute to strengthen the inverse relationship between ENSO and precipitation along the coast of Peru over the recent decades.

Overall, our results suggest a significant change in the ENSO–precipitation relationship along the coast of Peru due to the predominance of CP El Niño type in recent decades. It calls for better understanding the oceanic influence on the marine boundary layer considering cooler SST along the coast tends to stabilize the marine boundary layer and lead to drier conditions near-shore. On the other hand, most of the regions considered here are located at a 2000 m elevation, which is above the marine boundary layer, so that precipitation changes may be influenced by non-local processes. A better understanding of the regional atmospheric circulation in this region is required, which will help in better identifying key indices that can be related to precipitation variability at different altitude along the coast. This can be addressed from the experimentation with a regional high-resolution atmospheric model, which is planned for future work.

In the same way, the use of the ten ENSO indices associated with different facets of ENSO (ENSO canonical vs ENSO Modoki) improves our understanding of the complex relationship between precipitation and ENSO in Peru (from northern to centre of Pacific coast). We plan to extend this type of studies at regional scale to help improve climate and hydrological forecasts for the most affected countries of the Pacific coast of South America (Peru and Ecuador).

ACKNOWLEDGEMENTS

We thank Prof. Dacha Gushchina (University of Moscow) for carrying the MJO index calculation from NCEP/NCAR reanalysis. The three anonymous reviewers are thanked for their constructive comments.

REFERENCES

- An S-I, Jin F-F. 2004. Nonlinearity and asymmetry of ENSO. *Journal of Climate* **17**: 2399–2412.
- Ashok K, Behera SK, Rao SA, Weng H, Yamagata T. 2007. El Niño Modoki and its possible teleconnection. *Journal of Geophysical Research* **112**: C11007.
- Bograd SJ, Schroeder I, Sarkar N, Qiu X, Sydeman WJ, Schwing FB. 2009. The phenology of coastal upwelling in the California Current. *Geophysical Research Letters* **36**: L01602. DOI: 10.1029/2008GL035933.
- Boucharel J, Dewitte B, Garel B, duPenhoat Y. 2009. ENSO's non-stationary and non-Gaussian character: the role of climate shifts. *Nonlinear Processes in Geophysics* **16**: 453–473.
- Bourrel L, Labat D, Vera A, Coutaud A, Ronchail J, Guyot JL, Armijos E, Pombosa R. 2010. Correlation between the climatic indices of the ENSO phenomenon (El Niño - La Niña) and the rains and discharges indices on the Pacific coast of South America: Esmeraldas river basin. *International Workshop on ENSO, Decadal Variability and CC in South America*, October 12–14, 2010: Guayaquil, Ecuador.
- Bourrel L, Melo P, Vera A, Pombosa R, Guyot JL. 2011. Study of the erosion risks of the Ecuadorian Pacific coast under the influence of ENSO phenomenon: case of the Esmeraldas and Guayas basins. *World's Large Rivers Conference 2011*, International Conference on the Status and Future of the World's Large Rivers. April 11–14, 2011: Vienna, Austria.
- Brunet-Moret Y. 1979. Homogénéisation des précipitations. *Cahiers ORSTOM, sér. Hydro-biologie* **XVI**(3–4): 147–170.
- Chung P-H, Li T. 2013. Interdecadal relationship between the state and El Niño types. *Journal of Climate* **26**(2): 361–379.
- Dewitte B, Purca S, Illig SL, Renault L, Giese B. 2008. Low frequency modulation of the intraseasonal equatorial Kelvin wave activity in the Pacific Ocean from SODA: 1958–2008. *Journal of Climate* **21**: 6060–6069.
- Dewitte B, Illig S, Renault L, Goubanova K, Takahashi K, Gushchina D, Mosquera K, Purca S. 2011a. Modes of covariability between sea surface temperature and wind stress intraseasonal anomalies along the coast of Peru from satellite observations (2000–2008). *Journal of Geophysical Research* **116**: C04028. DOI: 10.1029/2010JC006495.
- Dewitte B, Choi J, An S-I, Thual S. 2011b. Vertical structure variability and equatorial waves during Central Pacific and Eastern Pacific El Niño in a coupled general circulation model. *Climate Dynamics* DOI: 10.1007/s00382-011-1215-x.
- Dewitte B, Vazquez-Cuervo J, Goubanova K, Illig S, Takahashi K, Cambon G, Purca S, Correa D, Gutierrez D, Sifeddine A, Ortlieb L. 2012. Change in El Niño flavours over 1958–2008: implications for the long-term trend of the upwelling off Peru. *Deep Sea Research II*. DOI: 10.1016/j.dsr2.2012.04.011.
- Diaz H, Markgraf V. 2000. *El Niño and the southern oscillation: multiscale variability and global and regional impacts*. Cambridge University Press: Cambridge; 496.
- Gottschalk J, Higgins W. 2008. Madden Julian oscillation impacts. *NOAA/NWS/NCEP Climate Prediction Center*.
- Guilderson TP, Schrag DP. 1998. Abrupt shift in subsurface temperatures in the tropical Pacific associated with changes in El Niño. *Science* **281**: 240–243.
- Gutiérrez D, Bertrand A, Wosnitz-Mendo C, Dewitte B, Purca S, Peña C, Chaigneau A, Tam J, Graco M, Echevin V, Grados C, Fréon P, Guevara-Carrasco R. 2011. Sensibilidad del sistema de afloramiento costero del Perú al cambio climático e implicancias ecológicas. *RPGA SENAMHI* **3**: 1–24.
- Gushchina D, Dewitte B. 2012. Intraseasonal tropical atmospheric variability associated to the two flavors of El Niño. *Monthly Weather Review* **140**(11): 3669–3681.
- Hayashi Y. 1982. Space-time spectral analysis and its applications to atmospheric waves. *Journal of the Meteorological Society of Japan* **60**: 156–171.
- Heil C, Walnut D. 1989. Continuous and discrete wavelet transforms. *SIAM Review* **31**: 628–666.
- Hendon HH, Wheeler MC, Zhang C. 2007. Seasonal dependence of the MJO-ENSO relationship. *Journal of Climate* **20**: 531–543.
- Hong C-C, Wu Y-K, Li T, Chang C-C. 2013. The climate regime shift over the Pacific during 1996/1997. *Climate Dynamics*. DOI: 10.1007/s00382-013-1867-9.
- Kiem A, Franks S. 2001. On the identification of ENSO-induced rainfall and runoff variability: a comparison of methods and indices. *Hydrological Sciences* **46**(5): 715–727.
- Kim ST, Yu J-Y. 2012. The two types of ENSO in CMIP5 models. *Geophysical Research Letters* **39**: L11704. DOI: 10.1029/2012GL052006.
- Kug JS, Jin F-F, An S-I. 2009. Two types of El Niño events: cold tongue El Niño and warm pool El Niño. *Journal of Climate* **22**: 1499–1515.

- Labat D, Ababou R, Mangin A. 2000. Rainfall–runoff relations for karstic springs. Part II: continuous wavelet and discrete orthogonal multiresolution analyses. *Journal of Hydrology* **238**(3): 149–178.
- Labat D. 2005. Recent advances in wavelet analyses: part 1. A review of concepts. *Journal of Hydrology* **314**–1: 275–288.
- Labat D. 2006. Oscillations in land surface hydrological cycle. *Earth and Planetary Science Letters* **242**(1): 143–154.
- Lagarde J. 1983. Initiation à l'analyse des données, BORDAS (eds), Paris, 157p.
- Lagos P, Buizer J. 1992. El Niño and Peru interannual climate variability, *Natural and Technological Disasters*. Chapter 17. The Pennsylvania Academy of Science.
- Lagos P, Silva Y, Nickl E, Mosquera K. 2008. El Niño – related precipitation variability in Peru. *Advances in Geosciences* **14**: 231–237.
- Lavado W, Silvestre E, Felipe O, Bourrel L. 2013. ENSO impact on hydrology in Peru. *Advances in Geosciences* **11**: 1–7.
- Lee T, McPhaden M. 2010. Increasing intensity of El Niño in the central equatorial Pacific. *Geophysical Research Letters* **37**: L14603. DOI: 10.1029/2010GL044007.
- Luo JJ, Sasaki W, Masumoto Y. 2012. Indian Ocean warming modulates Pacific climate change. *Proceedings of the National Academy of Sciences of the United States of America* **109**: 18701–18706.
- Madden R, Julian P. 1972. Description of global-scale circulation cells in the tropics with a 40–50 day period. *Journal of the Atmospheric Sciences* **29**: 1109–1123.
- McPhaden MJ, Zhang X, Hendon HH, Wheeler MC 2006. Large scale dynamics and MJO forcing of ENSO variability. *Geophysical Research Letters* **33**(16): L16702. DOI: 10.1029/2006GL026786.
- McPhaden MJ. 2012. A 21st century shift in the relationship between ENSO SST and warm water volume anomalies. *Geophysical Research Letters* **39**: L09706. DOI: 10.1029/2012GL051826.
- Miller A, Cayan D, Barnett T, Graham N, Oberhuber J. 1994. The 1976–77 climate shift of the Pacific Ocean. *Oceanography* **7**: 21–26.
- Montecinos, A, P Aceituno, 2003. Seasonality of the ENSO-related rainfall variability in central Chile and associated circulation anomalies. *Journal of Climate* **16**: 281–296.
- Mosquera K, Dewitte B, Illig S, Takahashi K, Garric G. 2013. The 2002/03 El Niño: equatorial wave sequence and their impact on sea surface temperature. *Journal of Geophysical Research: Oceans* **118**: 1–12.
- OPS. 2000. Perú: Fenómeno El Niño, 1997–1998. Organización Panamericana de la Salud. Fenómeno El Niño, 1997–1998, Washington D.C.
- Rasmusson E, Carpenter T. 1982. Variations in tropical sea surface temperatures and wind fields associated with the southern oscillation/El Niño. *Monthly Weather Review* **110**: 354–384.
- Roundy PE, Kiladis GN 2006. Observed relationship between oceanic Kelvin waves and atmospheric forcing. *Journal of Climate* **19**: 5253–5272.
- Takahashi K, Montecinos A, Goubanova K, Dewitte B. 2011. ENSO regimes: reinterpreting the canonical and Modoki Niño. *Geophysical Research Letters* **38**: L10704.
- Tapley T, Waylen P. 1990. Spatial variability of annual precipitation and ENSO events in western Peru. *Hydrological Sciences Journal* **35**: 4, 429–446.
- Torrence C, Compo G. 1998. A practical guide to wavelet analysis. *The Bulletin of the American Meteorological Society* **79**: 61–78.
- Torrence C, Webster PJ. 1999. Interdecadal changes in the ENSO–monsoon system. *Journal of Climate* **12**: 2679–2690.
- Tsonis A, Swanson K, Kravtsov S. 2007. A new dynamical mechanism for major climate shifts. *Geophysical Research Letters* **34**: 113705.
- Vecchi GA, Harrison DE 2000. Tropical Pacific sea surface temperature anomalies, El Niño and equatorial westerly wind events. *Journal of Climate* **13**(11): 1814–1830.
- von Storch H, Zwiers F. 2003. *Statistical Analysis in Climate Research*. Cambridge University Press: Cambridge; 495.
- Waliser DE, Lau KM, Stern W, Jones C 2003. Potential predictability of the Madden-Julian Oscillation. *Bulletin of the American Meteorological Society* **84**: 33–50.
- Waliser DE 2005. Predictability and forecasting. In *Intraseasonal Variability of the Atmosphere–Ocean Climate System*, Lau WKM, Waliser DE (eds). Springer Heidelberg: Germany.
- Wheeler M, Kiladis G. 1999. Convectively coupled equatorial waves. Analysis of clouds and temperature in the wavenumber–frequency domain. *Journal of the Atmospheric Sciences* **56**: 374–399.
- Wheeler M, Weickmann KM. 2001. Real-time monitoring and prediction of modes of coherent synoptic to intraseasonal tropical variability. *Monthly Weather Review* **129**: 2677–2694.
- Woodman R. 1985. Recurrencia del Fenómeno El Niño con intensidad comparable a la del Niño 1982–1983. *Concejo Nacional de Ciencia y Tecnología (CONCYTEC)*, Lima; 301–332.
- Xiang B, Wang B, Li T. 2012. A new paradigm for the predominance of standing Central Pacific Warming after the late 1990s. *Climate Dynamics*. DOI: 10.1007/s00382-012-1427-8.
- Yeh SW, Kug SJ, Dewitte B, Kwon M, Kirtman B, Jin F 2009. El Niño in a changing climate. *Nature* **461**: 511–514.